HEALING IN BITUMEN

TOWARDS A PRAGMATIC APPROACH TO QUANTIFY HEALING ABILITY IN ASPHALT BINDERS

GREET LEEGWATER

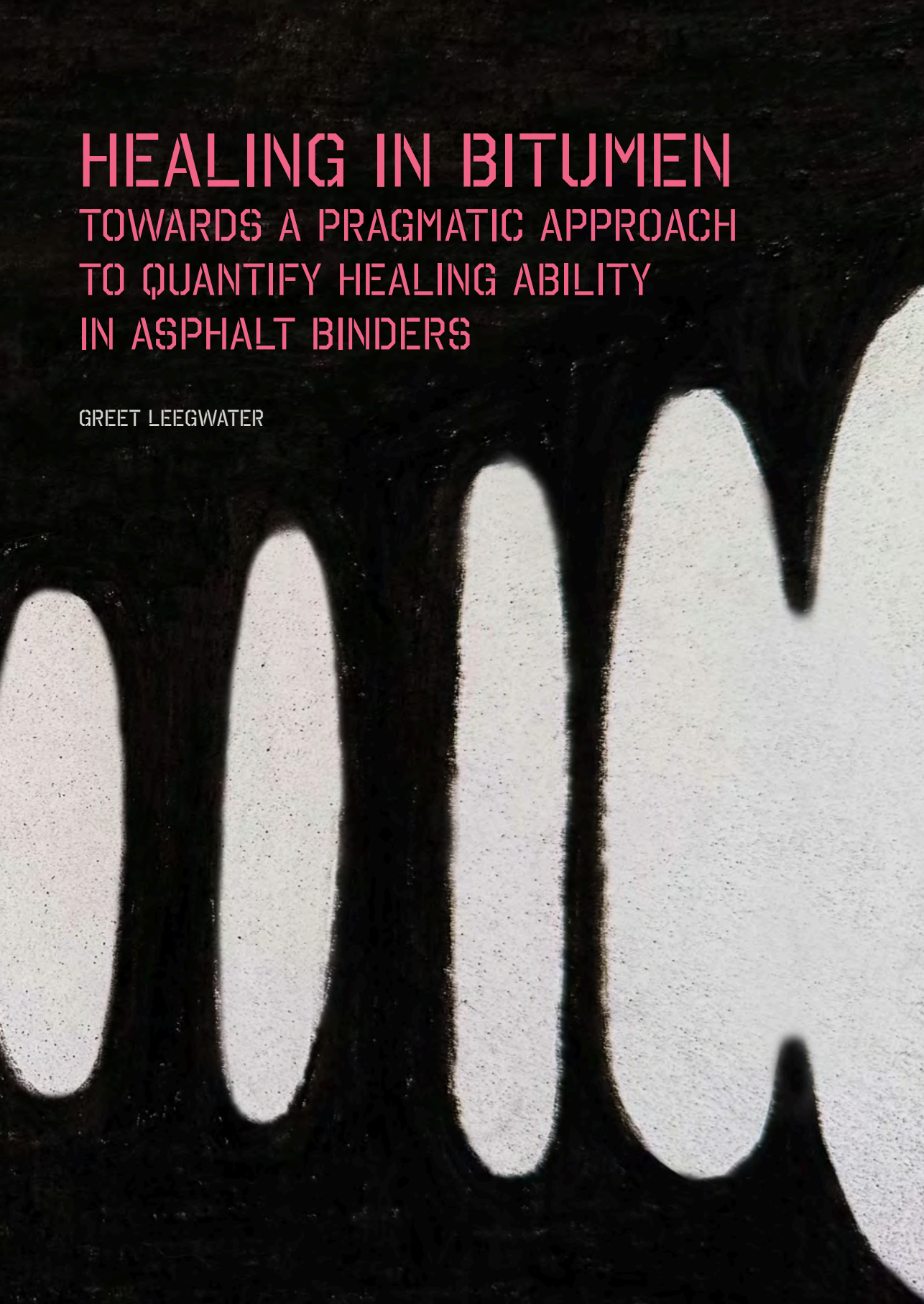

HEALING IN BITUMEN
TOWARDS A PRAGMATIC APPROACH TO QUANTIFY HEALING ABILITY IN ASPHALT BINDERS

Dissertation

for the purpose of obtaining the degree of doctor
at Delft University of Technology
by the authority of the Rector Magnificus Prof.dr.ir. H. Bijl;
Chair of the Board for Doctorates
to be defended publicly on
Thursday April 23rd 2026 at 12:30

By

Greetje Aletta LEEGWATER

This Dissertation has been approved by the promotors.

Composition of the doctoral committee

Rector Magnificus	chairperson
Prof.dr.ir. S.M.J.G. Erkens	Delft University of Technology, promotor
Dr. A. Varveri	Delft University of Technology, promotor

Independent members

Prof.dr. M.J. Santofimia Navarro	Delft University of Technology
Prof.dr. A. Chabot	Université Gustave Eiffel, France
Prof.dr. C. Raab	EMPA, Switzerland / CU, Canada
Dr. H. Soenen	Nynas, Sweden / U. of Antwerp, Belgium
Dr.ir. M.M. Villani	Rijkswaterstaat
Prof.dr.ir. H.E.J.G. Schlangen	Delft University of Technology, *reserve member*

Printed by Ridderprint
Cover & lay-out design Maaike Disco, proefschriftopmaak.nl
ISBN 978-94-6384-945-6

This thesis was executed with financial support of InfraQuest, a collaborative program between TU Delft, TNO funded by Rijkswaterstaat.

An electronic version of this dissertation is available at: http://repository.tudelft.nl

TABLE OF CONTENTS

SAMENVATTING

Het healinggedrag van asfaltmengsels en bindmiddelen is cruciaal voor de prestaties van asfaltverhardingen en als gevolg hiervan hun levensduur. Hoewel het al jaren bekend is dat bitumineuze materialen zelfherstellend gedrag vertonen na rustperiodes, wordt het onderliggende mechanisme nog niet goed begrepen. Dit gebrek aan inzicht vormt vooral een probleem bij de introductie van innovatieve, duurzame materialen, waarvan het healinggedrag onbekend is. Om risico's te beperken bij toepassing van innovatieve materialen, mogen bij deze materialen de voordelen van healinggedrag niet worden meegenomen in de ontwerpberekeningen. Deze conservatievere aanpak resulteert in dikkere asfaltlagen bij toepassing van innovatieve materialen, wat de milieuwinst van duurzamere asfaltmengsels teniet doet, en de transitie naar duurzamer asfalt terecht of onterecht belemmert. Het hoofddoel van dit onderzoek was het inzicht in het healinggedrag van bitumen verdiepen en een betrouwbare testmethode ontwikkelen die het healend vermogen van traditionele en innovatieve bindmiddelen kan bepalen.

Om voort te kunnen bouwen op bestaande kennis, is gestart met een grondige literatuurstudie. Hieruit kwam naar voren dat healinggedrag onder andere moeilijk te kwantificeren is, omdat de experimentele aanpak zich richt op het meten van herstel van schade, terwijl in asfalt juist een eenduidige definitie van schade ontbreekt. Als gevolg hiervan is het startpunt van een healingtest niet exact bekend, wat doorwerkt in onzekerheid in de uitkomst. Deze onzekerheid draagt hoogstwaarschijnlijk bij aan de testafhankelijkheid van healingonderzoek. Uit het literatuuronderzoek kwam ook naar voren dat er een breed geaccepteerd, conceptueel model voor healing van asfalt en bitumen bestaat. Ondanks de brede acceptatie, is dit model afkomstig uit de polymeerwetenschap, nog in weinig detail uitgewerkt of gevalideerd voor bitumineuze materialen.

Om dit bestaande model verder uit te breiden en te valideren, is een nieuwe Two-piece healing test ontwikkeld met behulp van een Dynamic Shear Rheometer (DSR) in trekmodus. Een belangrijke innovatie in deze opstelling, is de mogelijkheid om de contactdruk op het healingoppervlak te beheersen. Het literatuuronderzoek liet namelijk zien dat dit een belangrijke parameter is voor het healinggedrag. Daarnaast maakt de opstelling gebruik van een artificiële schade, wat zorgt voor een goed gedefinieerd startpunt van de healingtest. Met behulp van deze opstelling is het mogelijk om healingtesten uit te voeren met hele korte en lange rustperiodes; van minder dan een minuut tot meer dan een week.

Met behulp van deze nieuwe opstelling is vastgesteld dat minstens de helft van het strekteherstel kan worden toegeschreven aan adhesie van het healingoppervlak. Omdat de hoeveelheid adhesie rechtstreeks afhankelijk is van de hoeveelheid oppervlak dat in contact is, welke op haar beurt afhangt van de krachten die het healingoppervlak samenbrengen, is geconcludeerd dat healingmetingen beter geïnterpreteerd kunnen worden als de krachten nabij het contactoppervlak bekend zijn. Daarnaast is opgemerkt dat adhesie direct sterkte oplevert, waardoor het sterkteherstel gelijk opgaat met de groei van het contactoppervlak.

Uit metingen na verschillende healingperioden, blijkt dat het sterkteherstel in eerste instantie snel verloopt; in de eerste drie minuten treedt meer sterkteherstel op dan in de dertig minuten erna en zo verder. Significante verschillen in gedrag zijn dus goed vast te stellen na relatief korte healing periodes. In de praktijk zijn de rustperiodes ook kort, vanwege de grote vrachtwagenintensiteit in Nederland. Als gevolg hiervan wordt het passend geacht om, bij het ontwerp van een healingtest, te kiezen voor een relatief korte healing periode. De, in dit onderzoek ontwikkelde, two-piece healing-opstelling sluit hier goed bij aan met een herhaalbaar testresultaat na een relatief korte healingperiode. Daarnaast is de test uit te voeren op een DSR, welke beschikbaar is in meerdere laboratoria in Nederland. De Two-piece healing test lijkt daarom een interessante optie voor een snelle en praktische beoordeling van het healingvermogen van een bindmiddel. Er is echter nog wel meer validatieonderzoek naar onderscheidend vermogen en relatie met gedrag in de praktijk.

Een andere belangrijke bevinding uit het onderzoek is dat de sterkte sneller herstelt dan de taaiheid van het materiaal. Dit terwijl een afname van taaiheid juist de vermoeiingsweerstand aanzienlijk kan verminderen en deze een cruciale rol speelt in de ontwerpberekening van de levensduur. Het relatief trage herstel van taaiheid en de verwachtte negatieve invloed op de vermoeiingslevensduur van asfalt vereisen nader onderzoek.

In het onderzoek is het healinggedrag van drie traditionele bindmiddelen met vergelijkbare penetratiegraad bekeken. Deze bindmiddelen vertoonden onderling een vergelijkbaar healinggedrag. Daarnaast trad, zoals verwacht, het herstel van prestaties in deze bindmiddelen sneller op in vergelijking met hardere bindmiddelen. Aanvullend onderzoek is nodig om te bepalen of deze trend ook geldt voor innovatieve bindmiddelen met een vergelijkbare penetratiegraad.

Het in de literatuur beschreven healingmodel, dat healing beschrijft als het samenspel van contactvorming en sterkteontwikkeling, is in dit onderzoek uitgebreid met de parameters contactdruk, oppervlakteruwheid en oppervlakte-energie. Verdere validatie van deze uitbreiding van het healingmodel vereist metingen van deze parameters in combinatie met healingtesten.

Samengevat verdiept de thesis het inzicht in het healinggedrag van bindmiddelen, met name door de belangrijke rol van adhesie aan te tonen en daarmee de noodzaak om contactdruk tijdens healingonderzoek explicietmeet mee te nemen. Dit inzicht is cruciaal voor het interpreteren en verfijnen van testmethoden, en voor het kiezen van de meest voorspellende test voor praktijkprestaties.

Er zijn ook een aantal fundamentele onderzoeksrichtingen geïdentificeerd die kunnen bijdragen aan meer begrip van healinggedrag. De twee belangrijkste zijn een diepgaander onderzoek naar de invloed van oppervlakte-eigenschappen op healing, en een nadere studie van moleculaire dynamiek in en om het healingoppervlak om het proces van homogeniseren en het herstel van taaiheid beter te begrijpen.

SUMMARY

Healing behaviour of bituminous binders and consequently asphalt concrete is critical to the performance and longevity of asphalt pavements. While asphalt concrete is known to exhibit self-healing properties during rest periods between traffic loads, the mechanism behind this healing is not well understood. This lack of understanding becomes particularly problematic when innovative, sustainable binders are introduced to the market, for which healing behaviour is unknown. To limit risks with respect to performance, this lack of knowledge is currently translated in a conservative pavement design, resulting in thicker pavements. Offsetting environmental gain from using more sustainable asphalt mixtures and hindering the adoption of innovative binders. Therefore, the main goal of the executed work was to improve the understanding of healing in bitumen and to develop a reliable test method that is able to assess healing performance of traditional and innovative asphalt binders.

To ensure the research builds on existing knowledge, the first step was a thorough review of the state of the art. Literature shows that healing in asphalt is difficult to quantify, as tests are focussed on the assessment of damage restoration, while the definition of damage in asphalt is still under debate. As a result, the extent of damage at the start of healing tests is often unknown, likely contributing to the highly test-specific healing results reported over time. Literature has also shown that there is a well-established conceptual model for healing in asphalt concrete and bitumen, derived from polymer science. However, this model remains underdeveloped and has seen only limited validation for bituminous materials.

With the aim to further expand and validate this healing model, a novel two-piece healing test has been developed using a Dynamic Shear Rheometer (DSR) in tensile mode. A key innovation in this setup is its ability to precisely control not only temperature and healing time, but also contact pressure at the healing interface. This pressure is a major factor in contact development, as highlighted by the healing model presented in literature. In addition, the setup uses synthetic damage, allowing for a well-defined starting point in healing tests. It supports a wide range of healing durations; from under a minute to over a week, enabling detailed study of both short-term and long-term healing behaviour.

Using this setup, it was found that at least half of strength restoration stems from adhesion at the healing interface. Since adhesion depends directly on the amount of contact formed, and contact is influenced by interface stresses, this highlights the critical need to know and control stresses at the contact area during healing assessments. As adhesion does not require time to develop this also implies that this part of the restoration occurs just as fast as the restoration of contact.

As healing was monitored at various time-steps it could be determined that healing occurs rapidly at first; more restoration is observed in the first 3 minutes than in the next 30. Rest periods on our highly trafficked road network are also relatively short. The

combination of these two observations points toward the option that a short duration healing test, is likely to capture the most relevant aspect of healing in practice. If this can be proven, it opens up the route to use a short healing period in the novel test set-up to serve as a practical and fast healing assessment. The relatively wide availability of DSR-equipment in Netherlands will enable wider adoption of the test method.

Another important finding from the research is that the material strength recovers quicker compared than the toughness. A reduction in toughness can significantly impair fatigue resistance. This is important for pavement design, as the fatigue performance of asphalt concrete plays a critical role in service life predictions. Therefore, this issue requires further investigation, especially if the industry intends to adopt a rapid healing test approach.

The research also compared the healing behaviour of three traditional binders with similar penetration grades. Results showed that these binders exhibited comparable healing performance, while healing occurred notably faster compared to healing behaviour of harder binders. Further investigation is needed to determine if hardness of binder is also an indicator for healing behaviour for innovative binders.

The existing healing model, that presents healing as the convolution of contact area regeneration and strength development of this contact, is augmented within this research with the parameters; normal force at the healing interface, surface roughness and surface energy. This augmented healing model requires further validation as these additional parameters should be assessed in combination with healing performance.

The thesis deepens the perspective on binder healing, particularly by demonstrating the significant role of adhesion and emphasizing the need to account for interfacial stresses during healing tests. This insight is not only crucial for interpreting test results and refining test methods, but also for selecting the healing test that has the most predictive power for real-world pavement performance.

Next to this several fundamental research directions are outlined to further advance our understanding of healing. Two key areas are highlighted: first, a deeper investigation into the influence of surface characteristics on healing; and second, a closer study of molecular dynamics at the binder surface to better understand the homogenization processes at the healing interface and the restoration of ductility.

PREFACE

This thesis set out to gather knowledge that could guide the Dutch road sector towards a substantiated approach for incorporating healing in the Dutch design approach. At the time that I started this PhD adventure, this sounded like an ideal challenge for my PhD thesis, as it was both fundamentally challenging and relevant for practice. I have learned so much since then. Not only as more than 13 years have passed since then, but also as the research advanced my insights into asphaltic materials and humbled me into the realization that our material is so complex, that a PhD research can only advance us some steps. As a result, I must admit that I was able to provide less answers than I had hoped and expected to deliver. I therefore truly hope that there are other people out there, who are brave enough to try and bring this topic further. And if so, please let me know if you think I can be assistance, as I do believe that with joint efforts we can bring more relevant pieces of the healing puzzle together.

At this moment, I am immensely proud that I have been able to wrap up this research and by that have been able to add contribute to the understanding of healing of bitumen. But, as when raising a child, I must admit “it took a village” to shape my initial thoughts and bring them to their full potential as presented in this book. I owe a great deal of thanks to my village. If it were not for them, this book would not exist. I will try and acknowledge the most important helpers below, however I realize that it is most likely that I will not do justice to all people that have been supportive.

First of all, I must thank InfraQuest for providing me the chance to do a PhD. As studying this topic as a PhD candidate, gave me so much opportunity to really dive into the subject and learn so much about healing and asphalt materials in general. I also owe gratitude to my Promoters Sandra Erkens and Katerina Varveri for their guidance while executing the work. And even though Katerina was only involved in the last years, her help was essential to pick up the pace and push towards completion, for which I am very grateful. From the academic staff of the TU Delft I also want to particularly mention Martin van de Ven. When I had troubles to see the light at the end of tunnel, your kind and motivating feedback helped me to regain confidence and inspired me to keep on going. As I did laboratory work, I also need and want to acknowledge Macro Poot and Michèle van Aggelen, our lab technicians at the TU Delft. Without their support it would have been impossible to get anything done in the lab. Thanks for the lunch crew, consisting of Rita, Maria, Sayeda, Alieh and Francesco, who were there to specifically not talk about work during our breaks,. I also want to express my gratitude towards the two Master students that were under my supervision as part of this work; Simone Dijkhuis en Elena Daniele. I enjoyed their company and the scientific interaction when working on the thesis, and they made the journey a little less lonely. Next to this, Elena has also contributed to the reported results as she executed one of the test series on 70/100 bitumen reported in Chapter 5.

I also owe gratitude to TNO for supporting me during this adventure, as I have been affiliated with TNO throughout this project. As the time period was long and the management structure of TNO involves a wide range of people that have been of support, it is impossible to mention all people. But I at least should mention Martijn Stamm en Adri Vervuurt, who were essential in setting up this project. Next, I also want to mention the “Roadies”, as they feel like my TNO family, always offering a listening ear or a helping hand when I needed it. And of course, my manager Mirjam Steins (and all the managers before her) in acknowledging the relevance of this project and motivating me to finish it.

I also want to acknowledge all the help from friends and family as they have been very supportive, showing interest in me and my project, offering a helping hand or just listing to me nag about it. A special thanks to Viola, Marieke and Marieke and off course all the others for your attention and support. When I needed to get the work back into flow, my oncle Gijsbert was extremely hospital by providing a working sanctuary, including a large private office and a full week lodging away from all my everyday responsibilities. And a really big shout out goes to my mother, for the countless times that she took care of our children allowing me time to write. While I should also not forget my dad, as he took over babysitting whenever my mother had other obligations.

And last but not least, I really need to thank my partner Bram and our kids. As I did the final part of the work in my own time, there were numerous weekends that I spend behind the computer. I need to thank (or offer my apologies) to my children, Cas, Jacob and Ellen, for accepting that their mum wasn’t around in many weekends to do stuff. Their existence was also very valuable to put the PhD-work into perspective; showing that even though it needed to be done, this thesis wasn’t the most important thing in the world. I also am very grateful to my partner Bram for taking care of our children and managing the household while I was locked away upstairs. Sometimes even taking the family to his parents for the whole weekend, providing me with an empty house without distractions. He wouldn’t nag about this, but just ask: “How much more time do you need?”. Finally there the answer is: “No more!!”

1

INTRODUCTION

1.1 HEALING OF BITUMINOUS MATERIALS IN PAVEMENTS

1.1.1 Bituminous materials have a natural healing ability

Asphalt has the remarkable ability to restore damage. The recovery of damage in asphaltic materials is observed both in the laboratory (Bazin and Saunier 1967; Bonnaure, Huibers, and Boonders 1982; Qiu, Molenaar, van de Ven, and Wu 2012; Little, Bhasin, and Darabi 2015) and in the field (Groenendijk 1998; D. Williams 2001). For example, tests performed by Groenendijk in the LINTRACK (an accelerated pavement testing facility at TU Delft) indicated a stiffness recovery of a pavement section after a weekend without loading (Groenendijk 1998). In pavement engineering this recovery of performance is called healing. Since pavements are not loaded continuously, this healing ability increases the service life and is therefore taken into account in pavement design methods (Van den Bergh 2011), including the Dutch design approach (Rijkswaterstaat 2011). The impact of healing ability on the predicted service life is very substantial and has a significant influence on the calculated pavement thickness (Sandra Erkens, Arthur van Dommelen, Dave van Vliet, and Leegwater 2012).

1.1.2 Fatigue is the governing damage mechanism in pavement design

Fatigue damage is the primary failure mechanism in the structural design of pavements. Rather than failing from a single overload, the structure deteriorates due to the cumulative effect of numerous loads. Each load causes micro-damage, which accumulates over time, ultimately leading to pavement failure. A pavement undergoes numerous load repetitions over its lifetime due to heavy vehicle traffic, which are different for each road section. Structural design accounts for expected vehicle passes, as each axle load induces bending and tensile strain at the pavement's bottom. Key design parameters include magnitude and frequency of the expected axle loads during the pavements lifetime, and the resistance of the asphalt concrete against fatigue loading.

1.1.3 Impact of healing on fatigue performance

The resistance of asphalt concrete to fatigue differs per asphalt mix and therefore has to be assessed in the laboratory. Fatigue tests, requiring around 1 million load cycles, are time-consuming. To accelerate testing, loads are applied using a continuous sinusoidal signal. In the European standard (EN-12697-24), five different methods are allowed to assess the fatigue resistance, which are all based on a (haver)sine load. A continuous load signal differs from real pavement loading, where rest periods occur between axle loads and trucks due to spacing and wheel positioning. As said bituminous materials heal, therefore these pauses in the load present in practice, allow the asphalt to restore its performance, making damage progression faster in laboratory tests than in actual pavements. The design approach must account for asphalt's enhanced healing potential in real-world conditions.s.

1.2 HEALING OF ASPHALT IS PAVEMENT DESIGN

1.2.1 A specific healing factor for each design method

Asphalt concrete pavements became widespread in the early 20th century, with designs varying by country due to local conditions. As healing had a strong influence on the performance in practice most design methods tried to determine a healing factor through extensive study and test programs, comparing fatigue test results with and without rest periods (Claessen, Edwards, Sommer, and Uge 1977) (Company 1978) (Verstraeten, Veverka, and Francken 1982) (Westera 1993).

However, these programs revealed that healing behaviour is highly test-specific. More healing is observed in stress controlled tests compared to strain controlled tests (Bonnaure, Huibers, and Boonders 1982; Francken 1998). The mode of loading also influences the observed healing, with two-point bending promoting the most recovery, followed by three-point bending, while four-point bending results in the least healing (Westera 1993). Despite a thorough analyses of some of these results, no plausible explanation for the observed differences has been presented (Westera 1994). This results in the inevitability that the prescribed test method for fatigue influences the observed healing, making healing design method specific. Next, these programs also demonstrated that assessing healing was very time-consuming, with high variation in results and uncomprehensible differences. Since full understanding seemed unattainable, all design approaches adopted a fixed constant to account for discrepancies between laboratory conditions and real-world practice, including healing (Van den Bergh 2011), this constant is often referred to as the healing factor, however as mentioned, it actually comprises also other unexplained differences between laboratory and practice. This factor adjusts the number of axles a pavement endures in the laboratory to estimate its real-world load capacity. Since rest periods improve performance in practice, the factor is always greater than 1.

1.2.2 Healing factor in the Dutch design guidelines

Dutch pavement design guidelines for highways, Ontwerpinstrumentarium Asfaltverhardingen (OIA) (Rijkswaterstaat 2011) use a maximum healing factor of 4, which is adopted from the Shell Pavement Design Manual (Company 1978). This factor is reduced for binders with a low penetration grade and mixtures with a low binder content. The reduction due to penetration grade is based on a broad fatigue and healing study performed in a large scale testing machine (De La Roche, Odeon, Simoncelli, and Spernol 1994). This research found no healing in very hard binders with a 10/20 penetration grade. Earlier research had already demonstrated that asphalt concrete made with a higher binder content has better healing performance (Bonnaure, Huibers, and Boonders 1982). The correction factors for the healing factor can be found in Table 1.1. The table interpolates between knowledge that traditional Dutch pavements made with 50/70 binder heal well, and French findings that asphalt with a 10/20 binder shows minimal healing and adds the influence of binder content.

Table 1.1 Value of the healing factor dependent on both bitumen content of the asphalt mixture and penetration grade of the binder (Rijkswaterstaat 2011).

		Penetration (0.1mm)					
		10/20	15/25	20/30	30/45	40/60	50/70 and up
Bitumen content (% m/m) in asphalt mixture	4	1.1	1.3	1.5	2.4	3.8	
	4.5	1.2	1.3	1.6	2.6	4.0	
	5	1.2	1.4	1.6	2.7		
	5.5	1.2	1.4	1.7	2.9		
	6	1.2	1.5	1.8	3.1		

1.3 CURRENT HEALING APPROACH HAMPERS THE USE OF NEW MATERIALS

In the current time frame there is a strong drive to develop materials that are more sustainable to meet climate goals as formulated in the Paris Agreement (Climate 2015). Nowadays, there are already many materials available on the market that have a lower environmental impact, for instance high recycling percentages and low production temperatures (Bizarro et al. 2021) (Jahanbakhsh, Karimi, Naseri, and Nejad 2020), but also biobased binders are making their way to our pavements (Mensink et al. 2024). However, the healing ability of these new materials is unknown and could therefore introduce large risks with respect to the service life performance. Therefore in Netherlands it isn't allowed to use Table 1.1 to calculate the healing factor for these innovative mixtures. Dutch road owners take a cautious approach, reducing chances of early failures and increased maintenance cost, by applying a healing factor of 1 to all asphalt mixtures with innovative binders. While this minimizes the risk of shorter pavement lifespan due to a possible lack of healing, it necessitates thicker pavement designs, increasing costs and environmental impact. As a result, the environmental benefits of a more sustainable asphalt product are lost by the required additional thickness. This impedes actual application of these new materials, elongating the path towards more sustainable pavements.

If risks with respect to healing ability of these innovative binders can be quantified, a higher healing factor could be allowed, without increasing costs and risks for the road owner. This will increase their application which will contribute to more sustainable and costeffective pavements. However, in spite of many additional research efforts into healing since the formulation of the design guidelines, the healing mechanism is still poorly understood (Sun et al. 2018). And there is no consensus on how to characterize the healing potential of an asphaltic material (Baaj 2025).

1.4 RESEARCH APPROACH

1.4.1 Research gap

Despite extensive research, the scientific community has yet to develop a proven healing test or model capable of delivering reliable predictions that convince researchers, practitioners and asset managers. Fundamental insight in the physical and chemical mechanisms behind healing behaviour of asphaltic materials is still missing.

1.4.2 Scope of the research

Asphalt concrete consists of a mixture of bitumen, gravel, sand and filler. Bitumen is the binder that glues the gravel, sand and filler, or aggregates together. While the aggregates provide stiffness which is needed for load bearing capacity. Due to this divers composition, asphalt concrete a heterogenic material, which complicates behaviour prediction due to intricate bitumen-aggregate interactions. As healing has proven to be challenging to understand, it is decided for this thesis to focus on the healing behaviour of bitumen. Bitumen flows slowly, enabling it to close microcracks, which fundamentally explains its healing capability, while under the conditions in pavements, aggregates are not expected to heal. In a later stage the understanding of healing of bitumen should be translated into healing behaviour of asphalt mixtures.

Damage is required to study healing. Damage in asphalt can be induced in many ways. Fatigue damage is commonly used as the starting point for healing tests, given its impact on fatigue resistance in design. However, this approach presents two key challenges: fatigue resistance measurements often show significant variability, with performance differences between specimens reaching a factor of two within a single test series. Additionally, there is ongoing debate about defining an appropriate failure criterion in fatigue damage (Di Benedetto 2004). Using a fatigue-damaged specimen as the starting point for a healing test complicates interpretation, as the exact damage level remains undefined. Therefore, this study will not be based on fatigue damage, but starts with a clearly defined damage.

1.4.3 Aim of the thesis

This thesis aims to enhance understanding of bitumen healing mechanisms and develop a test and a model to support practical assessment tools, facilitating broader use of innovative materials. In order to achieve this the following Research Questions (RQ) will be addressed:

RQ1. What is known and unknown about healing behaviour of asphalt and binders?

RQ2. How can a test method be designed to further increase our understanding of healing?

RQ3. How does the creation of contact impact healing of bituminous binders?

RQ4. How does time influence the healing behaviour of an asphalt binder?

RQ5. Are there more insights from the more general field of material science that can increase our understanding of healing of asphalt binders?

RQ6. How can a more accurate material model be developed to describe the processes governing the healing behaviour of bitumen addressing both mechanical and physicochemical aspects?

1.5 OUTLINE OF THE THESIS

In order to realize the aim and answer the research questions, several steps are taken in this thesis, resulting in an outline which is schematically presented in Figure 1.1.

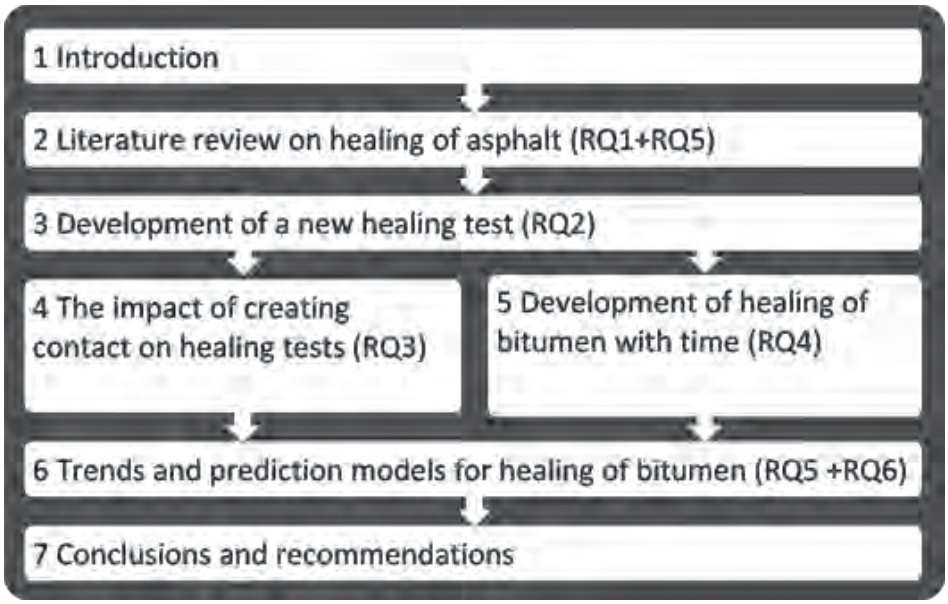

Figure 1.1 Set-up of the thesis.

To address Research Question 1, a literature review is executed on healing of asphaltic materials in Chapter 2. In this chapter, measured healing behaviour and hypotheses on healing mechanisms are described. This chapter also addresses more general aspects from material science, which are relevant for the healing of asphaltic materials, addressing RQ5. Chapter 3 introduces a new test setup designed to explore previously unstudied healing aspects, with that addressing Research Question 2. In Chapter 4, Research Question 3 is addressed by reporting on a test program investigating contact

formation and its role in healing. Chapter 5 presents findings on healing progression over time, answering Research Question 4. Chapter 6 integrates insights from the research program with existing literature and material science theories (Research Question 5) to refine healing models (Research Question 6). The thesis closes in Chapter 7 with key findings and recommendations.

2

LITERATURE REVIEW ON HEALING OF ASPHALT

LITERATURE REVIEW ON HEALING OF ASPHALT

The restoration of damage in asphalt materials, in the form of healing of asphalt, has been studied for more than halve a century. This chapter aims to provide an overview of all past research to provide an answer to the first Research Question from Chapter 1: "What is known and unknown about healing behaviour of asphalt and binders?". The answer to this question helps to further detail the research gap and forms the basis for the other Research Questions that have been introduced in Section 1.4.3.

The first section provides a more elaborate description on what behaviour is considered when the term healing is used and what this implies when the behaviour is studied. Section 2.2 gives a description of the different test approaches used to assess healing performance of a material. In Section 2.3, a summary is given of healing tests conducted over the years in order to identify influencing parameters. Section 2.4 discusses the mechanism that play a role in healing, in this section material models that have developed to describe healing will also be presented. Section 2.5 presents an introduction to general material properties of bitumen and asphalt which are relevant for the healing mechanism of healing. In Section 2.6 the parameters associated with the regeneration of contact area at the healing interface are discussed. Next, Section 2.7 explains the physics behind the attraction of surfaces, demonstrating how adhesion contributes to healing. The processes driving the homogenization of the material that is brought into contact at the healing interface are addressed in Section 2.8. The chapter closes in Section 2.9 by providing a condensed overview on the existing body and by that answering RQ1. Next to this, based on the literature review, the research gaps are presented. Based on these research gaps Research Questions 2 to 6, from Chapter 0 are formulated, including an outlook on when they will be addressed in the remaining chapters of the thesis.

2.1 STUDYING HEALING IN BITUMINOUS MATERIALS

2.1.1 Healing in bituminous materials

The healing ability of asphalt has been first systematically reported by Bazin and Saunier (1967). The authors stored specimens after loading and retested them after different rest periods. They found that under the right conditions a significant restoration of properties could be observed. These authors named this behaviour "healing". Since then a substantial amount of research has been done into this phenomenon, as will become clear from this chapter. However the mechanisms behind healing of asphalt are still not fully understood and observed trends remain unexplained (Qiu 2012; Ayar, Moreno-Navarro, and Rubio-Gámez 2016; Sun et al. 2018). In this chapter an overview is

[1] In pavement engineering 'adhesion' is typically used for interaction between binder and aggregates, while 'cohesion' is used for interaction between the binder itself. In this thesis however the term adhesion refers to the interaction between two surfaces, which can also be of the same material.

presented of relevant insights in healing behaviour that have been reported in literature. This section also presents a recent set of definitions on healing of asphaltic materials and addresses terminology used within this thesis.

2.1.1 Healing versus self-healing

More recently, restoration of the performance of a material during its service life has been identified as a relevant research topic for materials in general. White et al. (2001) kick-started this research topic by designing materials that are able to repair damage autonomously. They call the materials with restoration ability self-healing materials and have identified asphalt as one of these materials (Zwaag 2008). This implies that *healing* and *self-healing* are slightly different terms for the same phenomenon; the terms merely originate from different research areas.

In order to discern between materials that by nature already have the ability to restore properties and materials with added features to improve healing performance, the following definitions are recently developed within the pavement research community (Leegwater et al. 2020).

> **Intrinsic Self-healing**: Aspect of the self-healing behaviour that is inherent to the material used.
>
> **Extrinsic Self-healing**: Aspect of the self-healing behaviour that can be attributed to an added phase or action that is specifically used to improve self-healing capabilities, to trigger crack-healing or prevent crack propagation.

This thesis is focussed on the natural healing ability of asphaltic materials. Following the definitions described above this means that this thesis focusses on *intrinsic self-healing*. As the whole of this thesis addresses this specific type of healing, the for the ease of reading the word 'Healing' is used in the remainder of text, except when a specific different type of self-healing is addressed. In Section 2.3.7 of literature review some attention is paid to research on extrinsic self-healing, as insights obtained when improving the self-healing behaviour also contribute to the understanding of intrinsic self- healing.

2.1.2 Definition of damage with respect to healing

This study aims to increase the insight in healing of bituminous materials. When studying healing it is important to note that in order for healing to take place, some sort of damage is required. However, if damage is defined as anything that leads to a change in the initial material properties, there are many different types of damage in bituminous materials, e.g. changes in material properties with time (ageing), the loss of stiffness or adhesion due to the ingress of water, the loss of integrity due to (micro-) cracking. The damage that is relevant with respect to healing is the loss of the resistance to a mechanical load as a result of loading. Therefore, in order to focus the efforts of this study, damage is defined

as the loss of mechanical properties, i.e. the strength or the stiffness, due to the initiation, coalescence and propagation of micro-cracks within the material as a result of loading.

2.2 HEALING ASSESSMENT OF ASPHALTIC MATERIALS IN THE LABORATORY

2.2.1 Damage development during fatigue testing

This section provides an introduction to fatigue damage in asphalt concrete. Fatigue damage is an important damage mechanism for asphalt. Healing can be seen as a mechanism that restores fatigue damage, therefore healing tests are often developed as a variant of a fatigue test. It is important to note that the exact nature of fatigue damage in asphaltic materials is still an active topic of research and debate (Di Benedetto 2004; Moreno-Navarro and Rubio-Gámez 2016). This section provides a condensed overview on the current understanding of fatigue damage and its relevance for healing tests.

Fatigue damage is the weakening of a material as a result of cyclic loading at load levels lower than the material strength (Paris, Tada, and Donald 1999). The concept behind fatigue damage is that microscopic cracks start to develop at locations with high local stress. Localization points where cracks nucleate are holes, discontinuities in the material or internal interfaces. With each load repetition these micro-cracks can grow and eventually coalescence to a macro-crack that leads to failure. As there are multiple factors that determine if locally there is a stress concentration, the development of damage can vary strongly from test specimen to test specimen. Consequently the number of cycles that lead to failure show a relatively large variation. If two similar asphalt concrete specimens are tested, the number of loads to failure can easily differ with a factor of 2 (Di Benedetto 2004).

The main feature of a fatigue test for pavements is a large number of load repetitions (around 1 million) at a relatively low strain level. In a fatigue test, the load can be applied in a variety of configurations and using test specimens with different geometries, resulting in different stress states in the sample. In asphalt testing, known configurations include uniaxial tension-compression, indirect tension, two point bending, three point bending, four point bending (EN-12697-24 2012; Di Benedetto 2004). At this point in time, there is no international consensus on what is the best approach for fatigue testing of asphalt, each approach has its own advantages and disadvantages. As a result, the standard test used to determine fatigue resistance of asphalt mixtures differs from country to country even within Europe; in the Netherlands the four point bending test is used, while for instance France the two point bending test is used. Next to these differences in test configuration, tests can be performed either force or displacement controlled. In general, in all cases a higher stress or larger displacement (resulting in a larger strain) during loading will result in a lower number of cycles until failure (Di Benedetto 2004).

The main output of a single fatigue test is the change of stiffness (*S*) as a result of the number of load cycles (*N*), a so called S-N curve. Figure 2.1 shows a typical S-N curve for an asphalt mixture. In the graph three main damage phases can be distinguished:

Phase 1 Initial stiffness reduction;

Phase 2 Linear stiffness reduction with the number of loads;

Phase 3 Accelerated stiffness reduction.

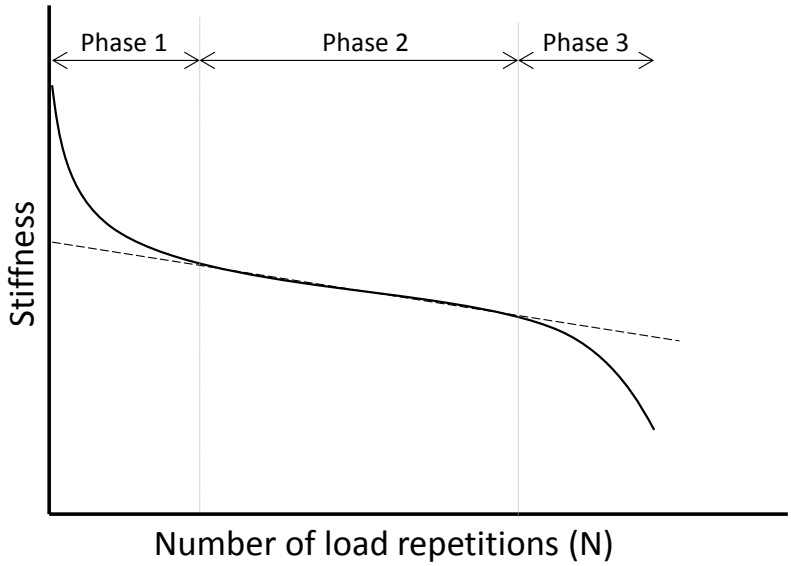

Figure 2.1 Typical stiffness reduction under the influence of load for an asphalt mixture

The outcome of a fatigue test is the number of loads that can be sustained until the specimen fails. In asphalt fatigue there are multiple definitions for the moment of failure (Di Benedetto 2004). One definition of failure is the transition point between phase 2 and 3, as this can be interpreted as the moment that the crack growth rate accelerates and micro cracks transform into macro cracks. However, it is not evident to determine this moment exactly, as (contrary to the image presented in Figure 2.1) phase 2 is never purely linear and a real S-N curve is not perfectly smooth. Consequently, if this analysis is automated, data artefacts can substantially impact the calculated number of loads to failure. Therefore while theoretically sound, this criterion is less suitable for practical application due to these potential distortions. In order to address this ambiguity, often a more straightforward and more practical failure criterion is used, namely a certain reduction in stiffness compared to the original value. For asphalt a stiffness reduction of 50% is often used (Molenaar 2018). This criterion is practical as there is no ambiguity to determine it. It is also clear that when 50% of the stiffness is lost, the bearing capacity

of the material has changed dramatically, which is expected to influence the structural behaviour of the pavement. However, the downside is that this criterion is not based on the shape of the curve and therefore is not related to the damage level of the specimen. It is therefore possible that the material has met this specific failure criterion, while damage development is limited and the curve is still in phase 1.

It is therefore desired to formulate a failure criterion, which incorporates a deeper understanding of the mechanism behind the observed stiffness loss in a fatigue test. Therefore, recent research into fatigue damage has focused on the origin of the observed stiffness reduction. Unlike steel, where fatigue results from the initiation and propagation of cracks (Wöhler 1870), the reduction in stiffness of asphaltic materials is not solely due to cracks. In fact there are a multitude of processes contributing to the stiffness reduction observed in a fatigue test. Four processes are named that together result in the total stiffness reduction of an asphalt sample tested in fatigue (Di Benedetto, Nguyen, and Sauzéat 2011; Mangiafico et al. 2015; Isailović, Wistuba, and Falchetto 2017). These processes are nonlinearity, heating, thixotropy and micro damage. Below the mechanism behind these four processes are explained in more detail.

Nonlinearity: For low strain levels it has been shown that bitumen behaves Linear Visco Elastic, however above a certain strain level this linear relation is lost (Delgadillo, Cho, and Bahia 2006). The threshold for the strain level for linear viscoelastic behaviour is not easy to establish for asphalt mixtures. This is caused by the fact that inside an asphalt mixture, the local strain in the binder can become much larger than the globally applied strain (Kose, Guler, Bahia, and Masad 2000). In a fatigue test this nonlinear behaviour can be interpreted as damage overestimating the total amount of damage (Gauthier, Bodin, Chailleux, and Gallet 2010). During the first cycles of loading, the loading signal is often not applied accurately by the testing machine, resulting in a lower initial strain level. Due to non-linearity in the response, this lower strain level results in a higher initial stiffness detection. When the specimen is at the desired strain level a lower stiffness will be detected while no damage is present in the specimen.

Heating: During a fatigue test, specimens are deformed as a result of loading. For viscous materials like asphalt, not all deformation is elastic, part of the energy invested in deformation will be transferred into heat. As a result the temperature of the specimen increases during the fatigue test (Lundström, Ekblad, and Isacsson 2004). As the response of asphalt is temperature dependent, this increase in temperature will result in a reduction of observed the stiffness. In order to assess the extent of this effect two studies have placed thermocouples inside a test specimen and both observed a temperature increase of around 0,9 °C (Mangiafico et al. 2015; Isailović, Wistuba, and Falchetto 2017). These studies also showed that this heat was lost relatively quickly when loading was stopped. Isailović, Wistuba, and Falchetto (2017) report that this effect is not present anymore 2500 s (~40 minutes) after the test is stopped.

Thixotropy: A material is thixotropic if loading results in a decrease in viscosity, which is not immediately recovered when the loading is stopped. This loss of viscosity restores with time if the material is left to rest (Mewis and Wagner 2009). The popular example of this behaviour is ketchup; you need to shake the bottle to get the ketchup to flow. Thixotropy finds its origin at the molecular level. Molecules need time to organize themselves in an energetically favourable manner. Due to loading the level of organization of molecules is disturbed. As a result distances between molecules increase and consequently, the amount of interaction forces will be less, which in turn reduces the stiffness. This behaviour is reversible, indicating that the stiffness will increase again after the shear load is removed and molecules have time to reorient themselves more energy favourable, increasing their molecular interaction and consequently the macroscopic stiffness.

Micro damage: As a result of inhomogeneity's, stress concentrations will occur which will initiate cracks which will lead to stress redistribution and with time in crack growth.

The first three effects described above (non-linearity, heating and thixotropy) impact the observed stiffness of the specimen, while they are not indicative of damage; non-linearity is an artifact influencing the test result but not the material; heating and thixotropy are fully reversible. These three effects are therefore named biasing effects (Baaj, Di Benedetto, and Chaverot 2005; Di Benedetto, Nguyen, and Sauzéat 2011; Mangiafico et al. 2015). In order to have clear definitions on what is considered damage and healing, recently some additional definitions have been proposed (Leegwater et al. 2020), that are reproduced below and illustrated in Figure 2.2.

> **Damage**: loss of original mechanical properties, i.e. the strength or the stiffness, due to the initiation, coalescence and propagation of micro-cracks within the material.
>
> **Restoration**: The total observed change in mechanical properties after a period of rest.
>
> **Recovery**: Component of the restoration that can be attributed to changes in response resulting from cyclic loading, more specifically heating and thixotropy.
>
> **Self-healing**: Component of the restoration that can be attributed to the closure and repair of (micro) cracks.

Mangiafico et al. (2015) conducted various tests on six different types of mixtures. In their work they varied the strain between 50 to 110 μm/m and the temperature between 8 and 14 °C, while loading at 10 Hz. Tests on mixtures were performed in tension/compression configuration on cylindrical samples (150 mm high, 75 mm in diameter). Temperature was measured inside and on the surface of the specimen using thermocouples. Five load

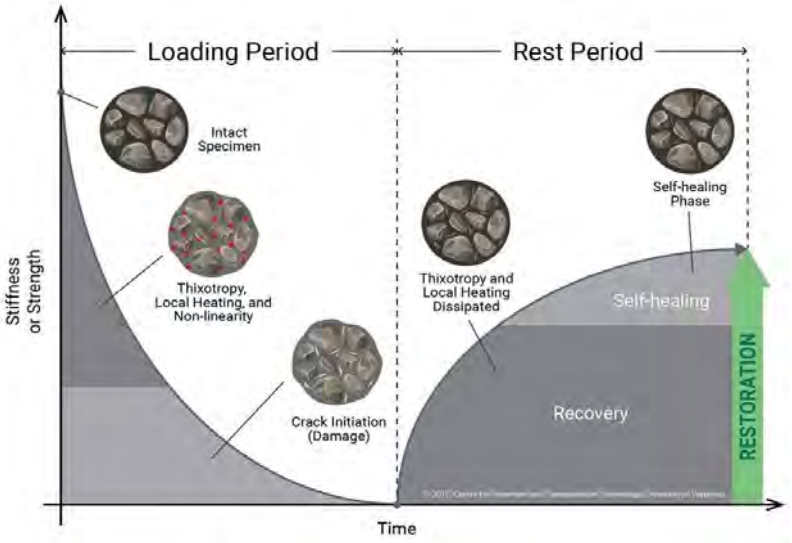

Figure 2.2 Schematic overview of contributions to the restoration of performance of different phenomena (Leegwater et al. 2020)

cycles of 100.000 load repetitions each were applied with 24 hours of rest in between, see Figure 2.3. The recovery detected in each cycle was assigned to one of the four processes, illustrated in Figure 2.4. This is done using the following approach. The effect of non-linearity is assessed by extrapolating the response at different strain levels to an imaginary stiffness at a strain level of "0 μm/m" (~19.300 MPa in this example) and using this as a base level. Next, the loss that remained after a rest period of 24h was assigned to damage as a result of microcrack formation. The amount of stiffness loss caused by heating was assessed by measuring temperature difference inside the specimen and relate it to the temperature sensitively of the specimen. Lastly the remainder of the recoverable loss observed was assigned to thixotropy, essentially unifying thixotropy with unexplained biasing effects. The relative contribution of during each loading cycle is shown in Figure 2.5. This figure shows that biasing effects make up 80 to 90% of the stiffness loss. It should be noted that in this approach all restoration occurring in the rest period of 24 hours is seen as recovery, while during this period healing could also take place. Next to this, it is not clear what the real damage level was inside the specimen at the moments the restoration was measured.

Next to the biasing effects, research into fatigue damage has also shown that the fatigue resistance is test configuration dependent (Di Benedetto 2004; Westera 2002). From this observation, the conclusion can be drawn that the measured fatigue resistance is, for the existing tests, not a material parameter, but a test parameter.

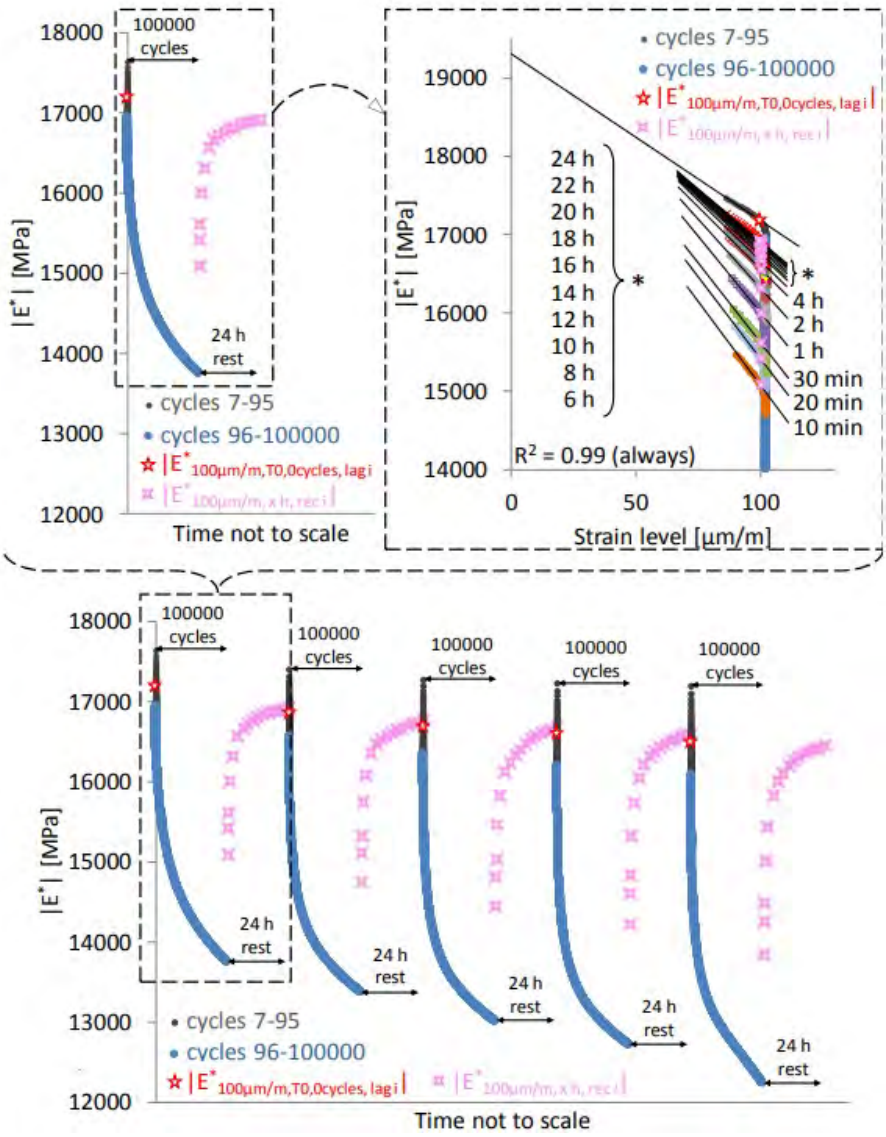

Figure 2.3 Stiffness development during 5 load and rest cycles (Mangiafico et al. 2016)

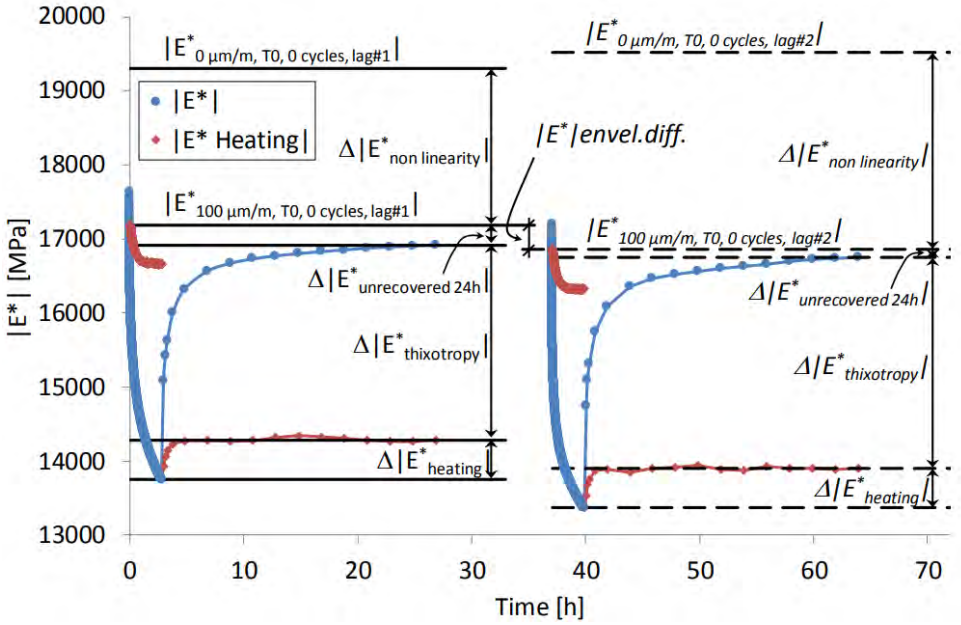

Figure 2.4 Estimation of biasing effects and unrecovered |E*| variations during the first two loading cycles of for mix 35/50 B + 20% RAP (Mangiafico et al. 2016)

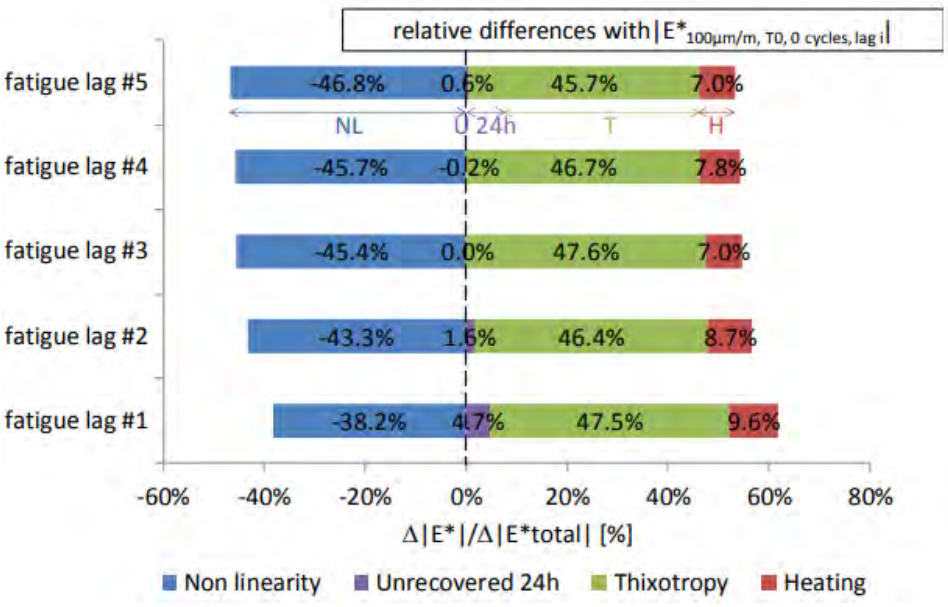

Figure 2.5 Relative contribution of biasing effects to stiffness reduction (Mangiafico et al. 2016)

2.2.2 Damage based on a single crack

Compared to fatigue damage a more clear expression of damage is a crack in a specimen (Qiu, van de Ven, and Molenaar 2013). If a specimen is loaded until it fails, a failure strength can be obtained, which provides an ideal reference value when retesting the specimen. This is for instance done by performing a direct tensile test (Qiu, van de Ven, and Molenaar 2013) or a three point bending test (García 2012). Although such an approach is very straightforward and provides a very clear reference for a healing test, this approach has been used only incidentally in the past. This is most likely related to the fact that ultimate strength tests are not a part of the framework used in designing pavements to meet service life requirements. There is no straightforward approach available to translate ultimate strength test results into fatigue performance, making a translation to practice challenging.

2.2.3 Test approaches for determining the healing capacity of a material

With time, many test set-ups have been presented to assess the healing capacity of asphaltic materials. In this section a classification of the test types is provided, as this can help to interpret the different results that have been published over the years. Various test methods have been developed to assess healing across all scales of asphaltic materials, including bitumen, mastic, mortar, and asphalt concrete. Additionally, methods exist to evaluate healing in full pavement structures. One way to classify these healing test methods is by examining how rest periods are introduced. There are two primary approaches. The first approach involves subjecting a damaged specimen to a single extended rest period, allowing it to heal. Since the specimen is typically stored during this time, this method is known as “storage healing.” The second approach incorporates short rest periods after each loading cycle in a fatigue test, enabling gradual healing throughout the process. This method is referred to as “intermittent healing.” Both test approaches will be discussed in greater detail in this section, and as combinations of these approaches have also been used to assess healing, combinations will be discussed afterwards.

2.2.3.1 *Storage healing tests*

The first step in a storage healing test is to introduce (micro) cracks in a specimen in a controlled manner, to create damage which can heal. The damage introduced in the sample can be of any kind; from invisible micro cracking induced by fatigue loading to a fully cracked specimen with two fully separated crack interfaces. Next, the damaged specimen is allowed to rest under specific conditions; e.g. a certain temperature, a fixed time, a stress state for a predetermined period of time. After the rest period has ended the specimen is loaded in the same way the damage was created, to assess its properties. Usually the performance after loading is compared to the original performance, however it can also be compared to specimens that have healed under different conditions.

An example of a healing test of the storage type is presented in Figure 2.6. This graph shows an S-N curve of a fatigue test which includes a rest period. The test starts with the induction of damage by means of a fatigue load, the black line shows the reduction of stiffness as a result of the load. After 20.000 load repetitions at a loading frequency of 10 Hz the loading is stopped and the specimen is subjected to a rest period of 30.000 s (8,3 hours), indicated by RP in the graph. During this period the specimen is kept inside the machine however no data is captured. After the rest period the fatigue loading is restarted and the detected stiffness is shown by the red line. It can be seen from the graph that the stiffness immediately after the rest period is almost as high as the initial stiffness. However, if the black and the red curve are compared, it can be seen that the inclination of the red line in the second phase of the fatigue curve seems to be a bit steeper compared to the black line. A stronger inclination of this second phase could be interpreted as an indication that due to remaining damage in the specimen after the healing period, the resistance to fatigue loading has declined.

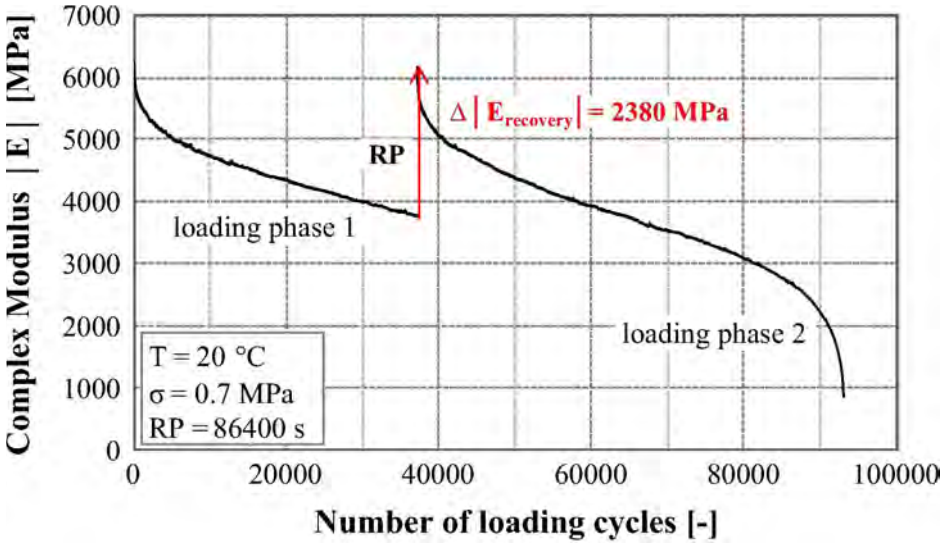

Figure 2.6 S-N curve of a uniaxial tension-compression fatigue test, with a rest period of 30.000 s (Isailović, Wistuba, and Falchetto 2017)

There are two approaches to determine the healing performance from storage healing tests. For a specimen that has no remaining strength after the initial damage phase, the healing is defined as the ratio between the performance of a healed sample, and the original undamaged performance, as presented in Equation 2.1.

$$Healing\ ratio = \frac{f_{healed}}{f_{original}} \times 100\% \qquad (2.1)$$

In this case the healing ratio ranges from 0 to 1, with 0 indicating no recovery after a healing period and 1 indicating full recovery. This approach can be taken for different performance parameters, for instance strength, stiffness, fracture toughness, etc.

This approach is less applicable for healing tests that start with fatigue damage, like the example shown in Figure 2.6. In the case of fatigue loading the resistance to failure is defined as the number of loads (*N*) until a specimen fails, therefore for these cases it would be better to have a healing ratio based on the ratio between the number of loads to failure with and without healing, see Equation 2.2.

$$H = \frac{N'_f}{N_f} \qquad (2.2)$$

With

N'_f = numbers of loads to failure with healing period

N_f = number of loads to failure without healing period

This means that in the first place a reference value for the number of load to failure without rest period needs to be available, which requires additional testing. As there is a large spread in fatigue results, at least six tests are required to come up with a reasonable average healing performance and the same number of specimens is also be required for the healings tests.

It should be noted that the value of the healing factor calculated with Equation 2.1 results into a distinctly different factor. In Equation 2.1 a healing ratio of 1 indicates that the full performance has been restored during healing. While if the healing factor in Equation 2.2 has a value of 1, this indicates that the number of loads to failure has not increased during the healing period, implying that no healing has taken place.

The recovery of the stiffness in fatigue test can be used as a parameter in Equation 2.1. In a fatigue test this stiffness recovery is available as an output of the original specimen without additional testing. As the stiffness can be measured non-destructively, it is also possible to monitor healing progress with time during a rest period, as is shown in Figure 2.3. However, due to all the biasing effects in the loss of stiffness, see Section 2.2.1, the correlation between stiffness recovery and real crack healing behaviour is not straight forward.

2.2.3.2 *Intermittent healing tests*

The second approach to measure healing is to create a loading pattern that matches loading events in practice more closely. This is done by introducing a rest period after each loading period, this type of healing test is called intermittent healing (Raithby and

Sterling 1970; Bonnaure, Huibers, and Boonders 1982; Van Dijk and Visser 1977). This type of healing test is by definition a variation of a fatigue test. The rest period can be selected freely, but is usually a multitude of the loading period, 2 to 20 times the period of a loading cycle (Raithby and Sterling 1970; Van Dijk and Visser 1977; Francken 1979; Bonnaure, Huibers, and Boonders 1982).

The healing performance determined using the intermittent healing test approach is usually defined as the ratio between the number of loads to failure with and without rest periods as already presented in Equation 2.2. As a result the healing ratio ranges from 1 to 20 or even more (Van den Bergh 2011; Bonnaure, Huibers, and Boonders 1982).

An advantage of the intermittent approach is it directly connects to the current pavement design methods, as the healing factor from Equation 2.2 can immediately be used in the design calculation as a correction factor as also introduced in Section 1.2.1. There are however also disadvantages of this approach. A first challenge is the ability of the test machine to actually apply the intended load signal during a test. This issue is not elaborately discussed in literature, however most fatigue testing equipment requires a few loading cycles to achieve the desired load signal. This issue was already discussed in Section 2.2.1, when non-linearity was introduced as biasing effect. This points out that it testing equipment is not able to apply a single load signal followed by a period of not loading in a controlled manner. Next to this, it is also possible that the initiation or the termination of a load signal introduces higher stress peaks compared to a smooth harmonic loading signal. Therefore, when using this test approach, it is essential to check if the intended load signal is actually realized by the testing machine. Another important drawback of this type of healing test is that it is very time consuming. A regular fatigue test in Netherlands already takes more than 9 hours ; $1*10^6$ repetitions, at 30 Hz (Rijkswaterstaat 2011), which then also has to be repeated six times for each of the three strain levels to obtain a reliable outcome. If for an intermittent healing test, a rest to load ratio of 10 is chosen, the total test duration is already 10 times longer in the case that the material doesn't show any healing. In the more likely case that healing is observed, the test time can be four times longer, resulting in a test period of 4 to 16 days for a single healing test. As a result, these types of intermittent healing tests are too time consuming for application in practice.

2.2.3.3 *Hybrid healing tests*

In the literature there are also research approaches presented that combine storage healing with intermittent healing (Kim et al. 2002; Lu, Soenen, and Redelius 2003; Bahia, Zhai, Onnetti, and Kose 1999; Van den Bergh 2012) and many others, these will be referred to as hybrid healing tests in this thesis. In general these protocols include

[2] Fatigue testing needs to be done at three different strain levels according to EN 12695-24, the Dutch standard requires at least one strain level below and one above the strain at which the material can take 1x106 load repetitions, so that this property can be determined through interpolation rather than extrapolation

multiple loading cycles, followed by multiple rest cycles. In some cases a hybrid loading regime is selected as test equipment cannot realize intermittent loading with sufficient accuracy as already explained in Paragraph 2.2.3.2.For example, based on observations on the actual load signal, Van den Bergh (2012) selected a protocol with 30 load cycles followed by 90 rest cycles, resulting in a rest to load ratio of 3. Another variation on the healing test approach is taken by Kim, Little, and Lytton (2003). They chose to introduce 10 rest periods of 2 minutes during a fatigue test. The advantage of such an approach is that the presumed damage level at the start of each rest period is slightly larger. Palvadi, Bhasin, and Little (2012) used this assumption to study the impact of the damage level on healing. However, it should be considered that due to many influencing factors on damage (see 2.2.1), the actual damage level in an asphaltic specimen always is a point of debate. As a result, there are many approaches to assess the level of damage in a specimen which will be discussed in the next section.

2.2.4 Assessment of damage level in fatigue and healing tests

The previous section demonstrated the importance of having a clear definition of damage at the start of a healing period. When a specimen is fully broken, resulting in two separate pieces, the extent of damage is evident. However, in case of fatigue damage, as discussed in Section 2.2.1, it is hard to assess the damage level in a specimen based on the observed stiffness due to biasing effects. As a result many scientists have tried to come up with approaches to extract which part of the stiffness loss can be attributed to the formation and the healing of micro-cracks.

2.2.4.1 *Damage criteria based on stiffness evolution and the number of load cycles*

A possible failure criterion for fatigue damage is based on the total number of cycles and the measured stiffness in relation to the original stiffness; in this case the number of cycles is multiplied by the measured stiffness and divided by the initial stiffness; $nE^*/E^*_{initial}$ (Cocurullo, Airey, Collop, and Sangiorgi 2008). The maximum of this value is taken as the moment of failure. In Figure 2.7 the result of this failure criterion for stress controlled, 2-point bending tests is shown by the green dot. In the figure the criterion is compared to a stiffness reduction of 50% (in blue) and 90% (in red). It was found that the proposed criterion of Cocurullo and al. (2008) was more conservative compared to the 90% stiffness reduction criterion, however depending on test conditions it was either more or less conservative compared to the 50% criterion. The advantage of this criterion is that it produces a clearer transition between phase 2 and phase 3 compared to the infliction point shown in Figure 2.1, as the equation results in a maximum value instead of an turning point in the stiffness curve. However, it can also be seen from the image, that the chosen method to determine the maximum influences the determined number of loads to failure, as in this graph the green dot is not the highest measured value; apparently outliers are excluded from the analyses.

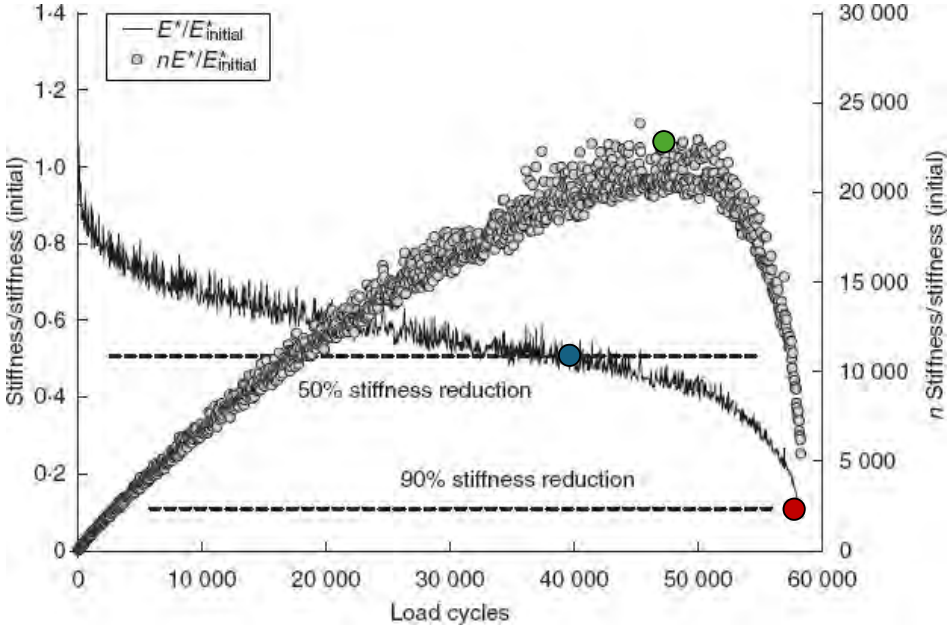

Figure 2.7 $nE^*/E^*_{initial}$ as failure criterion (in green) in comparison to 50 (in blue) and 90% (in red) stiffness reduction (Cocurullo, Airey, Collop, and Sangiorgi 2008)

2.2.4.2 *Damage criteria based on energy dissipation*

When a purely elastic material is deformed all energy that is needed to deform the material is stored as elastic energy and fully released once the material is allowed to go back to its original shape. This behaviour is illustrated by the stress strain curve shown in the left graph in Figure 2.8. Characteristic for a viscoelastic material, is that energy is lost during deformation of the material. The energy that is not stored as elastic energy is transformed into different types of energy, for instance material flow or the creation of cracks. This is illustrated by the stress strain curve in the right graph of Figure 2.8. In this figure the amount of energy lost as a result of the loading and unloading is shown as the grey area. The amount of lost energy can be calculated by summing up the amount of work done. The amount of work can be calculated, by integrating the force over the displacement (or stress over strain).

When an asphaltic material is subjected to cyclic loading, a small amount of energy is lost in each loading cycle. With time different theories have been posed on how the amount of energy dissipated during loading can be related to fatigue damage in the material. An overview of the most cited methods in literature is presented below. However, it should be noted that that there are even more variants presented in literature and as the debate on fatigue damage continuous, new approaches are still being developed, often adding more details to existing approaches.

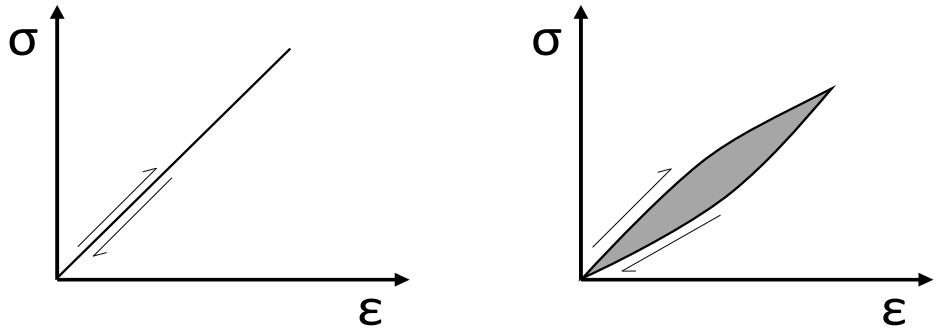

Figure 2.8 On the left an elastic stress strain curve on the right a viscoelastic stress strain curve with in grey the energy lost in the deformation.

The first theory on analysing dissipated energy to assess damage was proposed by Van Dijk, Moreaud, Quedeville, and Uge (1972). They proposed that the total energy lost in a fatigue test is the same for both stress and strain controlled tests. Building on this idea it was hypothesized that the amount of energy lost per cycle in a similar fatigue test was related to the fatigue life (Van Dijk 1975; Pronk and Hopman 1991). However, during further exploration of this hypothesis it became clear that not all energy dissipated in a loading cycle is related to the creation of damage, as there are processes that absorb energy that are not damage (see also the biasing effects in Section 2.2.1). The theory was refined to propose that only changes in dissipated energy relate to damage (Kim, Little, and Benson 1990; Carpenter and Jansen 1997). Biasing effects are strongest at the start of loading, but after a certain period of loading biasing effects result in a constant amount of energy loss per cycle. Any additional energy loss beyond this baseline can then be attributed to real physical damage, specifically the formation of (micro)cracks. This means that damage in the specimen is correlated to excess energy loss above the level that can be attributed to biasing effects.

It is assumed that the biasing effects are strong at the start of loading and when a steady state is achieved result in a constant energy loss. Only the additional energy losses on top of the constant loss are assumed to be related to the creation of damage or (micro) cracks. This implies that there is a correlation between additional energy loss, once an equilibrium has been established, and the level of damage in a specimen.

Carpenter and Shen (2006) further optimized this concept and proposed a model that assumes that the energy loss in a fatigue test corresponds to the 3 phases that are present in the S-N curve, see Figure 2.1. Their model assumes that the ratio of dissipated energy change (*RDEC*) is different for each phase. During phase I, at that at the start of the fatigue test, the energy dissipation per cycle is high, as during this phase the biasing effects have a large effect on the loss of stiffness. During phase II there is a relatively constant level of energy dissipation per cycle, which is assumed to be related to the amount of micro damage which develops. Finally at phase III there is a large increase in

energy dissipation, which is associated to the large deformations that are present during the actual failure of the specimen. The amount of energy loss during phase II is the so called Plateau Value (*PV*).

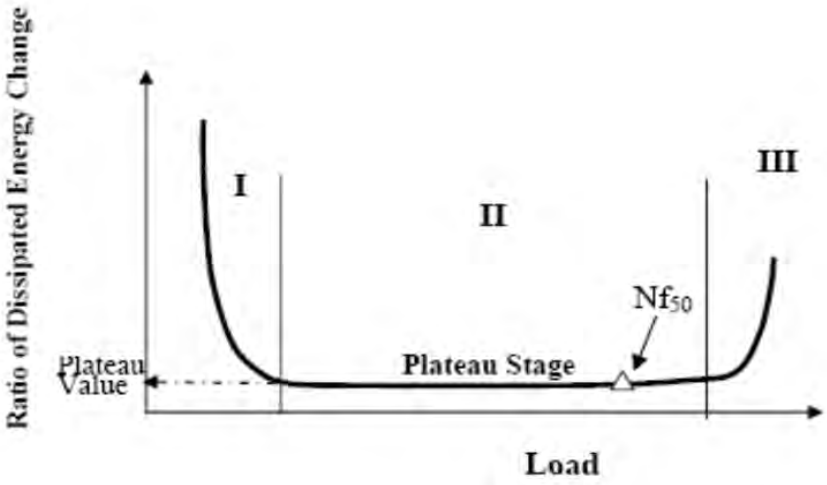

Figure 2.9 Model for ratio of dissipated energy change for different phases of a fatigue curve (Carpenter, Ghuzlan, and Shen 2003)

This *RDEC-ratio* is calculated following Equation 2.3. The ratio is based on the dissipated energy change between a consecutive group of cycles *a* and *b*. In this equation the average of a group of cycles is used as there is a large variation present in the energy loss in each individual cycle. Usually the difference between *a* and *b* is a 100 cycles.

$$RDEC = \frac{DE_b - DE_a}{DE_a(b-a)} \qquad (2.3)$$

With

DE_a=Dissipated energy in cycle a

DE_b=Dissipated energy in cycle b

Figure 2.10 shows an example of the result of an RDEC-ratio calculation for an actual fatigue test. From this figure the large variation in the obtained value for the energy loss also becomes clear. It can also be seen that the transitions between the phases are in practice much less clear compared to the schematic image presented as Figure 2.9.

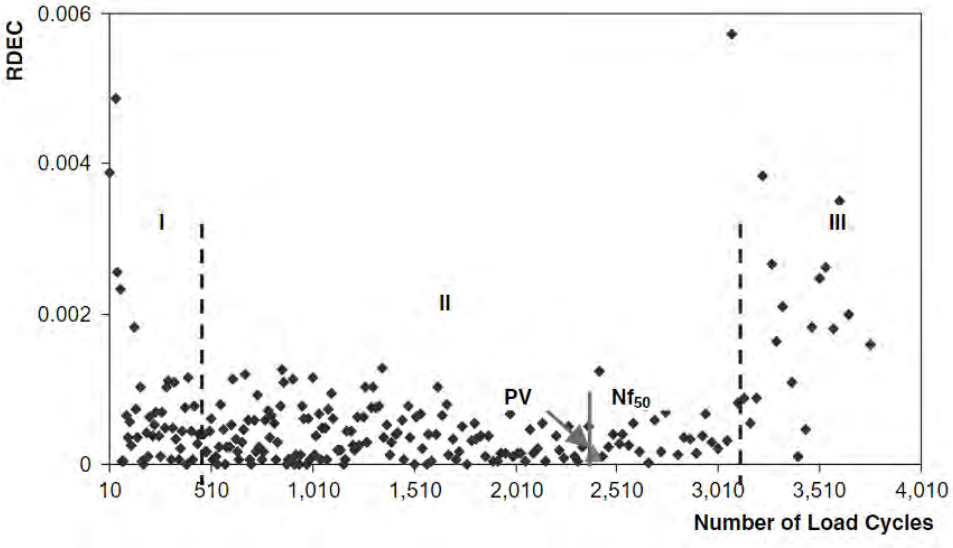

Figure 2.10 RDEC plot, showing the change in ratio of dissipated energy over the three phases of a fatigue test (Carpenter and Shen 2006)

The Plateau Value (*PV*) is interpreted as an indicator that predicts fatigue life. The researchers hypothesize that a lower *PV* corresponds to a longer fatigue life as there is less damage inflicted per cycle. Within this study, specimens were also subjected to intermittent fatigue tests. They found, when plotted on a log-log scale, a linear relationship between the length of the rest period and *PV*. Indicating that longer rest periods lead to a lower *PV*, indicating a longer fatigue life.

Kim, Little, and Benson (1990) also use the concept of changes in energy dissipation, by introducing the concept of pseudo strain. Their analysis is based on the use of the correspondence principle introduced by (Schapery 1984). By using the so called creep compliance, the part of the strain that is 'non-damaging' is removed, transforming strains into pseudo strains. The pseudo energy density can now be calculated by multiplying the pseudo stress with the pseudo strain. It is assumed that all the biasing effects are not affecting the pseudo strain density and therefore this energy can directly be related to the formation of microcracks. This transformation also has the advantage that the remaining pseudo response is elastic, which makes it possible to use the more simple elastic calculation methods for a viscoelastic material.

Based on the pseudo energy density also a healing index can be calculated. It is assumed that the pseudo energy density increases as a result of healing during the rest period. The resulting ratio is calculated by subtracting the pseudo energy density in the last cycles before a rest period from the pseudo energy density in the first loading cycles after the rest period and dividing this over the pseudo energy density in the first loading cycle after the rest period, this is written as Equation 2.4. Again the average of a series of cycles is

usually taken, as also these energy densities show a variation. NB. For the calculation only the tension part of the stress strain curve is used, which makes this approach not useful for 4PB or ITT fatigue tests.

$$H = \frac{\emptyset_A^R - \emptyset_B^R}{\emptyset_A^R} \quad (2.4)$$

With:

$\emptyset_A^R$= the pseudo energy density after rest

$\emptyset_B^R$= the pseudo energy density before rest

The concept to assess damage and healing based on energy dissipation using pseudo strain has been further developed (Lee and Kim 1998; Daniel and Kim 2001). The resulting Visco Elastic Continuum Damage (VECD) model claims to predict damage and healing under complex combinations of cyclic loading.

These models for analysing fatigue and healing based on energy dissipation are popular, as the proposed relation of damage with irreversible dissipated energy sound logical and therefore acceptable. However, many researchers have also reported inconsistencies, when they tried to apply the proposed equation and models to their own data (Bhasin, Castelo Branco, Masad, and Little 2009; Sandra Erkens, Arthur van Dommelen, Dave van Vliet, and Leegwater 2012; Stegeman 2020). Bhasin, Castelo Branco, Masad, and Little (2009) used a variety of energy based models on his own data set. This comparative study demonstrated that by analysing data using an energy approach, the difference in measured fatigue performance between constant strain and constant stress tests mode is reduced, however it is still present. He did confirm that de PV value was correlated to the fatigue performance of a mix, although the *RDEC*value did show very high variability making this approach inaccurate, which jeopardizes its discriminative power. Sandra Erkens, Arthur van Dommelen, Dave van Vliet, and Leegwater (2012) were not able to find the three phases in their data using the RDEC approach, also reporting a high amount of noise on the data. Stegeman (2020) evaluated several energy approaches in a large study on fatigue and found limited added value of evaluating energy dissipation compared to more direct analyses of the stiffness loss in the fatigue curves, following methods to determine the transition from phase 2 to 3 as described in paragraph 2.2.4.1.

2.3 INSIGHTS ON HEALING BEHAVIOUR BASED ON HEALING TESTS

2.3.1 Introduction

Since the 1960's of the previous century research has been conducted into the phenomenon healing. As explained in Section 1.2, healing is important for pavement

design methods. Therefore several countries executed large research programs to come up with healing factors matching their pavement design procedures (Raithby and Sterling 1970; Francken 1979; Bonnaure, Huibers, and Boonders 1982; Van Dijk 1975; Westera 1993). These tests showed that healing depends on the test method. As a result, established healing factors vary significantly between methods, see Table 2.1 (Van den Bergh 2011). This table presents the variation in shift factors between design methods. Some methods, apply a general shift factor, while others break it down into individual factors for healing, crack propagation, and traffic wander. The crack propagation factor accounts for the fact that pavement does not fail immediately upon the first crack, while the wander factor takes into account the positive effect that the exact location of the tire changes per vehicle.

Table 2.1 Healing and general shift factors according to different design procedures (Van den Bergh 2012)

References	Type of test	Load mode *	Individual factors			General shift
			Healing	Crack propagation	Traffic wander	
Asphalt Institute						13
Nottingham - Pell	Rotating Bending	F	5	20	1	100
Nottingham - Brown (critical conditions)	Rotating Bending	F	20	20	1,1	440
NRA Dublin Golden 1988	Rotating Bending	F				230
SHELL SPDM 1978	Variable	D	2 - 10	1	2,5	10 - 20
LCPC	2 point bending	D				1,6 – 3,7
SHRP A-003 Von Quintus 1994						10 - 13
BRRC Verstraeten 1974	2 point bending	F	7,1	3	1 – 2,5	7,1
DWW 1998 Groenendijk et al	4 point bending	D	4			

* F = Force controlled; D = Displacement controlled

Since then scientist have tried to unravelled the mystery, resulting in an extensive amount of literature, including several overviews (Qiu 2012; Moreno-Navarro, Sol-Sánchez, and Rubio-Gámez 2015; Sun et al. 2018; Ayar, Moreno-Navarro, and Rubio-Gámez 2016). The overview papers share most of their conclusions, although there are also some differences in focus. Qiu was the first one to stress the importance of research on different scales, looking at bitumen, mastic and asphalt. Both Ayar et al. and Sun et al. stress the importance of an holistic view, and suggest addressing healing from both a chemical and a mechanical perspective to improve insight. Ayar et al. (2016) point out that especially the use of new materials requires better understanding of healing and point to the importance of validation of the occurrence of healing in practice. Sun et al. (2018) pay more attention to provide an overview of extrinsic healing approaches. As there are already many overviews available, the aim of this section is not to provide an additional, extensive overview of the literature on healing, its aim is to provide an overview on the used test methods and the established correlations between healing performance and other parameters.

2.3.2 Initial observations on healing of asphalt mixtures

In the first period of structured healing research from 1960 to 1980 healing is mostly studied as a part of research on fatigue (Raithby and Sterling 1970; Van Dijk, Moreaud, Quedeville, and Uge 1972; Van Dijk and Visser 1977; Francken 1979; Verstraeten, Veverka, and Francken 1982). This research consequently concluded that when intermittent loading was used instead of cyclic loading, a higher number of loads to failure was observed.

Bonnaure, Huibers, and Boonders (1982) created the first overview on healing research on asphalt mixtures. They summarized trends, showing that longer healing periods resulted in more healing. They also concluded that all but one research reported more healing at higher healing temperatures. The exception was observed by Raithby and Sterling (1970) where the observed healing at 40 ˚C, was less compared to healing at 10 and 25 ˚C.

Bonnaure, Huibers, and Boonders (1982) also reported that it was not possible to really compare test results, as all tests were executed on different asphalt mixtures, while mixture type influences the healing behaviour. Therefore they also executed their own healing research, using an intermittent healing test protocol and a three point bending apparatus. They varied the ratio of rest to load periods, using the ratios; 0, 3, 5, 10 and 25. Test samples were made of dense asphalt concrete using 45/60 and 80/100 pen grade bitumen. Measurements where performed under constant stress and constant strain. Test were executed at a frequency was 40 Hz and at three temperatures; 5, 20 and 25 °C. Their results confirmed the positive influence of temperature and rest to load ratio. From their results they added the observation that asphalt mixtures with a lower stiffness (S_{mix}), usually caused by a softer binder, exhibit a higher healing capacity (N_i/

N_c). A graph to demonstrate this effect is presented as Figure 2.11. The lines in the graph are the fatigue lines corresponding to different load to rest ratios (*i*). The squares are reproduced data originating from research reported by Van Dijk and Visser (1977). It is concluded by the researchers that at longer rest periods (ratio of 10 and 25), the dense asphalt concrete studied by Bonnaure, Huibers, and Boonders (1982) showed similar behaviour compared to the results obtained on a base course mix as reported by Van Dijk and Visser (1977), while at lower load to rest ratios the healing was more extensive in the work of Bonnaure, Huibers, and Boonders (1982).

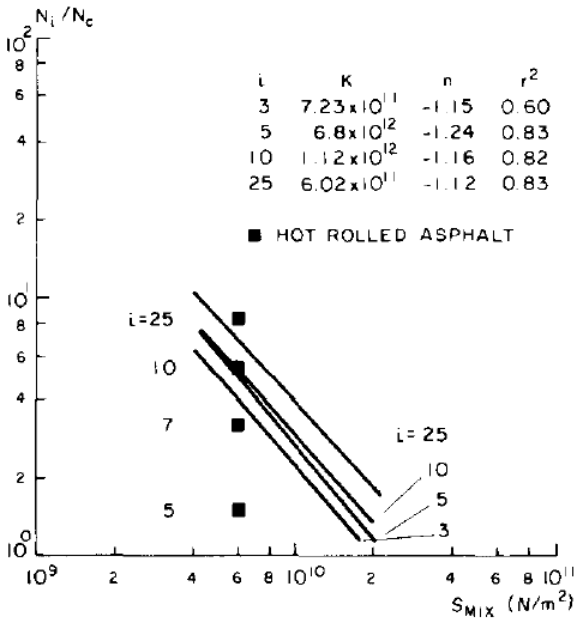

Figure 2.11 Life Ratio (Ni/Nc) as a function of the stiffness modulus of the Mix (Smix) for varying lengths of rest periods (i) (Bonnaure, Huibers, and Boonders 1982).

Concluding, Bonnaure, Huibers, and Boonders (1982) report the following trends:

- A higher number of loads to failure is observed when rest periods are introduced in between loading periods. All studies showed a significant amount of healing in intermittent healing tests when load to rest ratios were introduced from 1,5 up till 20.
- Healing ratios (determined according to Equation 2.2.) vary between 2 to 20 depending on test conditions.
- Healing increases with increasing resting time. At low rest to load ratios a little bit more rest time has a large impact on the healing. However, as the load to rest ratio

increases, there seems less impact of additional healing time resulting in an upper limit of the number of loads to failure.

- The amount of healing detected increases as the temperature increases, with one exception for the 40 ˚C test series reported by Raithby and Sterling (1970), see also Figure 2.12.
- Intermittent healing tests performed under stress controlled conditions show more healing compared to healing tests under strain controlled conditions.
- No general quantitative correlations can be found to relate the amount of healing to the loading conditions and/or materials used.

The trends of number of loads to failure compared to rest to load ratio using intermittent tests of all research mentioned in this section is very nicely summarized by a figure created by Qiu (2012), which is reproduced here as Figure 2.12.

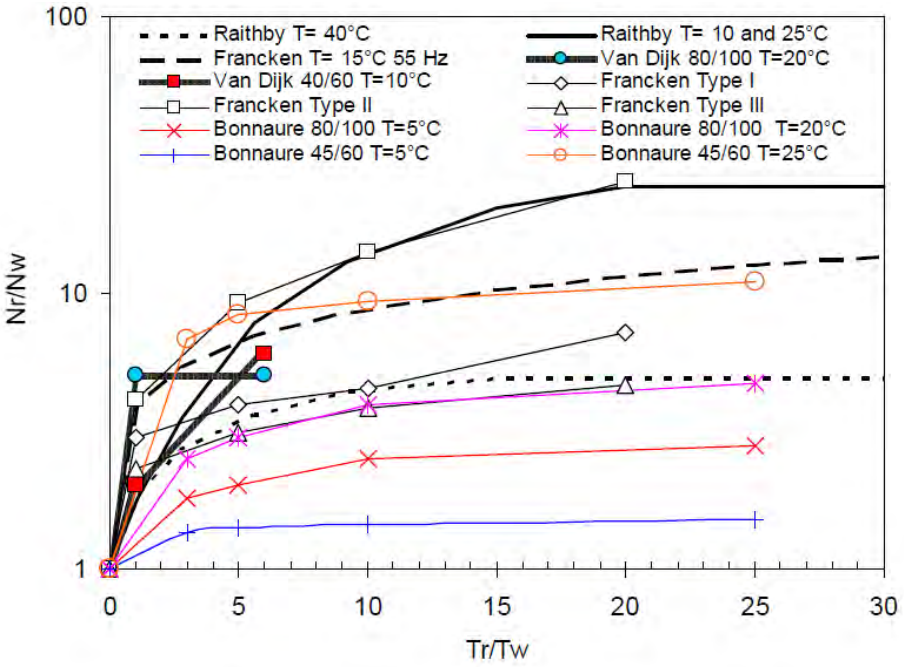

Figure 2.12 Overview of reported intermittent healing results from 1970 to 1982 (Qiu 2012)

On the horizontal axis, *Tr*/*T*w is the ratio between rest to load periods. On the vertical axis, *N*r/*N*w is the ratio of the fatigue life with rest periods to fatigue life without rest periods. This figure does not provide all details or results, however it does show that all intermittent healing research points towards an upper limit for the rest to load ratio. This overview implies that in intermittent healing tests, for rest to load ratios higher than 20, the additional healing is expected to be very limited.

2.3.3 Intermittent healing research on Dutch mixtures

In the Netherlands a substantial amount of research has been conducted starting at the end of the 1980's and the beginning of the 1990's. The aim of this research was to incorporate the state of the art of healing into the Dutch design regulations (Westera 1993, 1994; Westera 2002). Within this research four different asphalt types were studied, however most tests were performed on one type of asphalt mixture (GAB 0/16 type 57, 4,5% bitumen pen grade 45/60). In order to assess the impact of the test method used, different tests methods were used to assess the healing potential of the same mixture. All tests were conducted comparing the number of loads to failure, using continuous cyclic loading and intermittent loading, calculating the healing according to Equation 2.2. Test were conducted in both force and displacement controlled mode with 2, 3 and 4 point bending test set-ups. This required tests to be executed in different laboratories in both the Netherlands and Belgium. An overview of the results is presented in Table 2.2.

Table 2.2 Measured healing based on Nf (50% S_0) force and displacement controlled of GAB 0/16 4,5% bitumen 45/60, T = 15 ˚C t_{rest}/t_{load} = 10 (Westera 1993)

N_f -ε		4point	(freq)	3point	(freq)	2point	(freq)
Displacement	H_μ	1,0	(29)	2,8	(29)	4,2	(56)
	σ	0,7		1,1		0,8	
Force	H_μ	4,5	(55)	3,9	(29)	7,6	(56)
	σ	1,1		1,4		2,2	
	H_μ	4,3	(29)				
	σ	1,2					

Table 2.2 reports the average healing factors (H_μ) with their standard deviation (σ), for different test setups, in displacement and force controlled mode. From the table it becomes clear that more healing is detected in force controlled tests, which is in line with earlier observations (Bonnaure, Huibers, and Boonders 1982). A second conclusion is the amount of healing detected also depends on the type of test set-up used; most healing is observed in 2-point bending tests, followed by 3-point bending tests and finally 4point bending tests. These results confirm earlier observations stating that the amount of healing detected depends on the test method used. The researchers suggest it would be best to select the test method which is closest to loading in practice to determine a healing factor for a pavement design method. However, they remark that it is not known which of the set-ups resembles loading in practice most and therefore more research is needed.

The results reported in Table 2.2, were all executed with a rest to load time ratio of 10. Next to this, some tests were conducted with a rest to load time ratio of 20. In case of

force controlled, 4point bending, longer rest periods (ratio 20) resulted in a significantly higher healing factor of around 10, compared to a healing factor of 4,3 for a load to rest ratio of 10. This confirms the trend reported in Figure 2.12.

This research revealed that healing correlates with the rest-to-load period ratio rather than absolute rest time. This can be deduced from two data points presented in Table 2.2. The force controlled 4point bending test is performed at two frequencies. The absolute healing time at a frequency of 29 Hz is twice as long compared to the healing time when the test is performed at 55 Hz, while the measured healing is roughly the same.

This research also demonstrated the positive influence of bitumen content on healing ability. The resulting fatigue lines are reported in Figure 2.13. In the graph it can be seen that mixture C with the highest bitumen percentage (5%) has the best healing performance at all strain levels, while mixture A with the lowest bitumen percentage (4%) has the lowest healing ratio. The other two mixtures with the intermediate bitumen content (4,5%) are in between of A and C.

In order to try and explain why the used test method had such a large influence on the observed healing, the test results were analysed while looking at different parameters

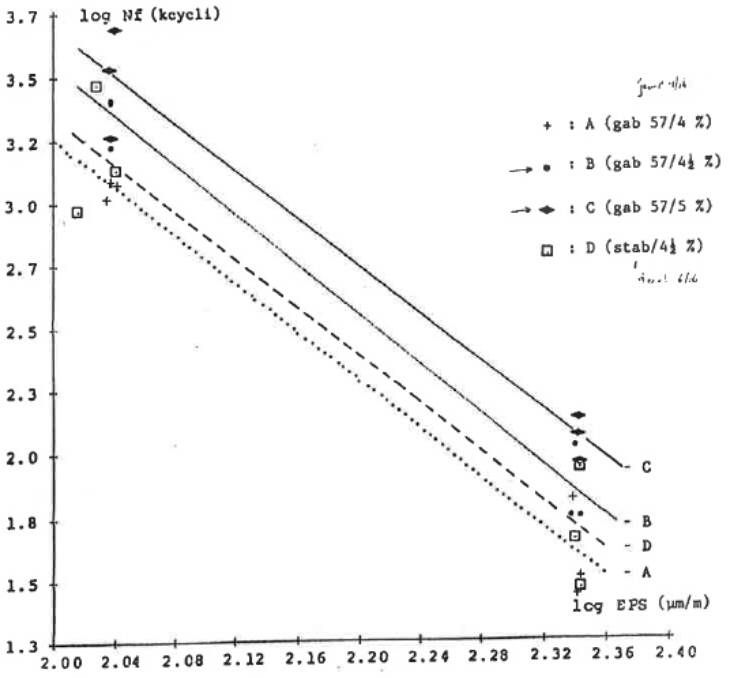

Figure 2.13 Healing factor in relation to strain level in strain controlled 4-point bending tests (Westera 1993)

more specifically strain level, initial stiffness modulus, initial pseudo stiffness, phase angle, energy dissipation per loading cycle, initial energy dissipation per cycle, ratio between the initial energy per load cycle and the average energy per load cycle. However, in all these analyses no strong correlations between any of these parameters were found, again pointing out the challenge to correlate energy dissipation to physical damage, as also pointed out in paragraph 2.2.4.2.

(Westera 1994) poses an interesting, but unverified hypothesis to explain the better healing performance observed in the two point bending test. It is suggested that the compressive force at the healing interface, present in the two-point bending test due to the self-weight of the specimen's top part, see Figure 2.14, enhances the healing performance. Bazin and Saunier (1967) demonstrated that healing is more effective when there is a small compressive force present at the healing interface, which is the case for a two point bending set-up. However, in the 3 and 4point bending test set-ups, damage develops in the vertical plane, resulting in a vertical healing interface, that consequently is not loaded by the self-weight of the specimen with no normal force present during the healing period. This theory does not explain the difference between the observed healing in the 3 and the 4point bending test, nor the difference between force and displacement controlled tests.

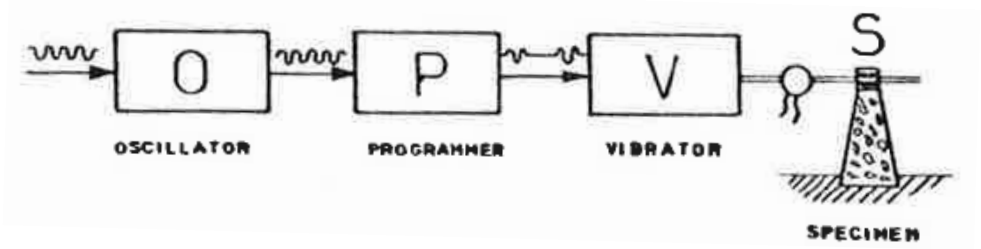

Figure 2.14 Orientation of a two point bending test specimen during loading (Bazin and Saunier 1967)

2.3.4 Observations on healing tests executed on pure binders using a crack healing approach

Hammoum, de La Roche, Piau, and Stefani (2002) and Maillard, de La Roche, Hammoum, Such, and Piau (2004) have studied healing at the binder level using their own developed Local Fracture Test. This set-up mimics the fracture and healing of thin films of bitumen between two aggregates subjected to a tensile load. The binder is held between two hemispheric steel protuberances, simulating two aggregates in the bituminous mix, see Figure 2.15 a. After a crack is introduced, the specimen is left to heal for various time periods, before it is retested to assess the healed strength. Using this test approach, the steps of loading until failure, followed by a rest period and testing the healed strength, can be repeated several times to assess the impact of previous damage. As there is no cyclic load involved, this test method can be classified as a storage healing test, see

Section 2.2.3. During the rest period, the sample is brought back to its original geometry by applying a compressive force of 50 N (or 5 daN, as shown in the image). The extend of healing of the binder film assessed in two ways. The first approach uses damage assessment by ultrasonic waves. In the second approach force displacement curves are evaluated for initial failure and the failure after one or more rest periods, see Figure 2.15

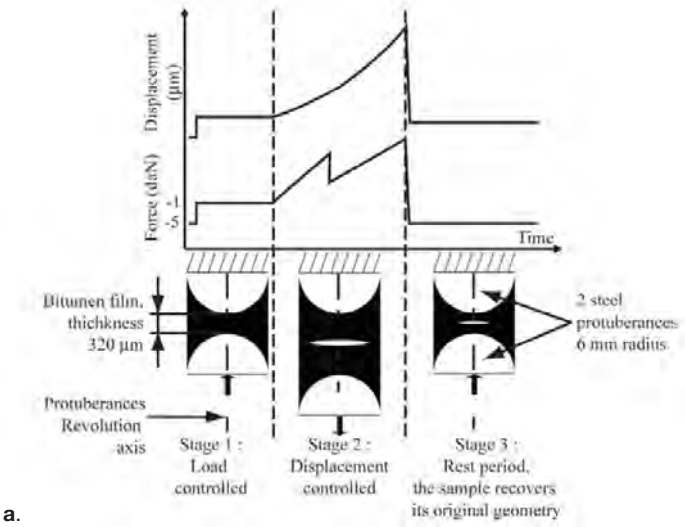

a.

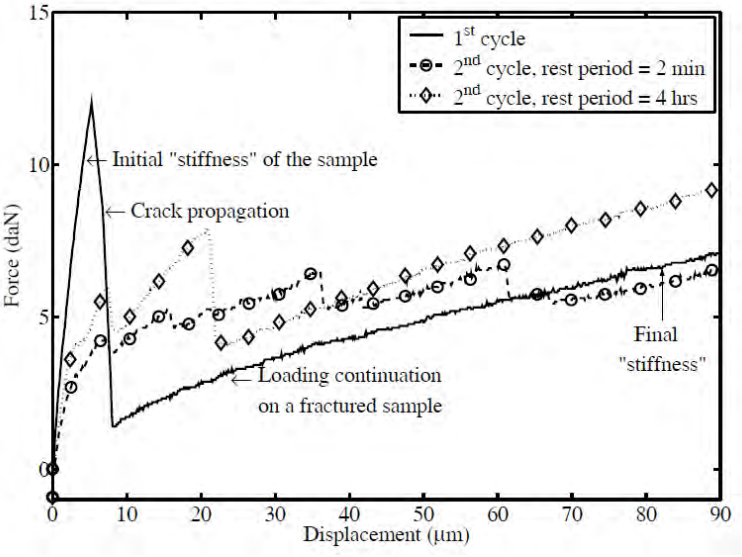

b.

Figure 2.15 a. Visualization of the local fracture test. **b.** Test result presenting the force displacement curves of the initial test and after two different healing periods (Maillard, de La Roche, Hammoum, Such, and Piau 2004; Maillard, de La Roche, Hammoum, Gaillet, and Such 2004)

The results obtained with this set-up are evaluated by comparing the peak strength and the final stiffness of the virgin specimen to the healed specimen. The results show more recovery of both parameters at higher temperatures. Next to this, it was observed that healing could already be detected at a temperature of -5 °C. It was also observed that longer rest times result in more healing. This is also visible in Figure 2.15 b where the peak stiffness and the final stiffness are higher for a specimen that has healed for 4 hours compared to a specimen that rested for 2 minutes. Finally it was observed that the extend of healing decreases with the number of load and healing cycles.

2.3.5 Observations on healing of bitumen using fatigue tests

Santagata, Baglieri, Dalmazzo, and Tsantilis (2009) and Sun et al. (2016) related stiffness recovery of binders in Dynamic Shear Rheometer (DSR) fatigue tests to, amongst others, a Saturates, Aromatics, Resins and Asphaltenes (SARA) analysis, see paragraph 2.5.3.2 for an explanation on the analyses of bitumen using SARA fractions. Santagata, Baglieri, Dalmazzo, and Tsantilis (2009) used a storage healing approach. They use a DSR to execute a stress controlled time sweep test at an equivalent binder stiffness level and introduce rest periods of 2 hour. An example of a response curve is plotted as Figure 2.16. They base their healing index on the number of additional loads to failure after a rest period, divided by rest time multiplied with the loading frequency during testing. They show that their proposed healing index correlates with the Saturates/Aromatics ratio (for more details on Saturates and Aromatics see 2.5.3.2) and argue that this aligns with the physical nature of the material, as a higher amount of saturates will increase the total molecular mobility in the material. However, their reported healing index is not verified by any other means and the found correlation is not very strong. It is therefore concluded that this research indicates that it is interesting to look at these type of indices, while it is plausible that the observed correlation does not exist for other materials or other test approaches.

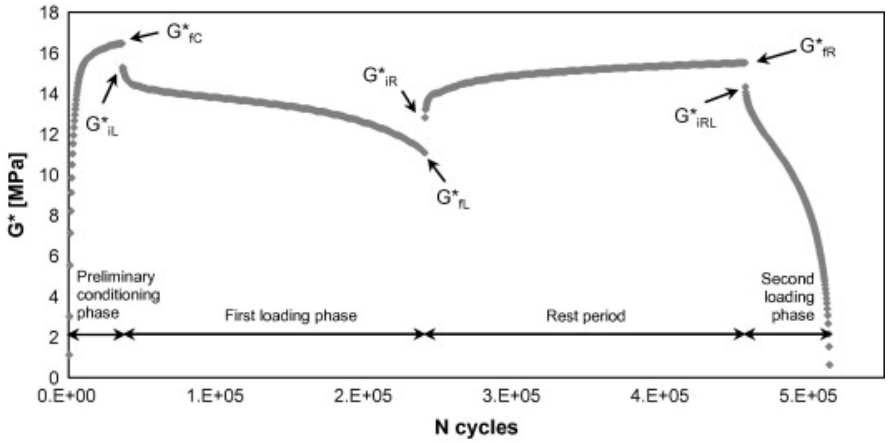

Figure 2.16 Typical result of a time sweep test on a bituminous binder using a DSR apparatus (Santagata, Baglieri, Tsantilis, and Dalmazzo 2013)

More recently a comparative study has been executed, within the RILEM Technical committee 278 CHA, to assess predictive power of different binder healing test approaches (Baglieri et al. 2022). They compared the healing ability of three binders using a Time Sweep test with a Single Rest Period (TSSRP), which is a similar approach as used in the previous section, a Time Sweep test with Multiple Rest Periods (TS-MRP) and a Linear Amplitude Sweep test with a single Healing or rest period (LASH). In the LAS (H) test approach, the amplitude of the loading signal is linearly increased during the test. The consequence is a very fast test, however the applied strain levels are well outside the linear elastic domain, making them harder to interpret and also less aligned practice. The comparison is presented as Figure 2.17, demonstrates a different ranking in healing ability was found, when different test approaches were compared. Similar results were found by Peng (2024). Again showing that the test used has a stronger influence on the observed healing compared to the influence of the material itself.

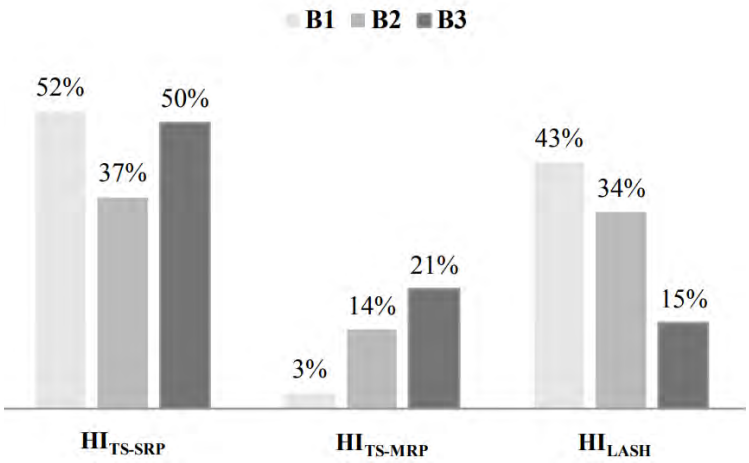

Figure 2.17 Healing indicators of three different binders using three different test methods, B1 and B2 are neat binders, B3 is a polymer modified binder.

2.3.6 Impact of damage intensity on healing

In several healing studies it has been shown that the size of the crack has impact on the ability of cracks to heal (Kim et al. 2002; Song, Little, Masad, and Lytton 2005; Qiu 2012). Kim et al. (2002) damaged specimens using a Dynamic Mechanical Analyzer (DMA) to evaluate healing of sand asphalt specimens. They found that if the damage in the specimen, assessed by a larger loss in stiffness, was more intense the additional number of loads to failure was less. Song, Little, Masad, and Lytton (2005) analysed damage in asphalt mastics (binder and filler) by using a DMA to damage specimens, while using a X-ray CT scanner to assess damage in specimens by assessing the amount of voids. Their results indicate that more voids as a result of repeated mechanical loading, result

in less healing. Qiu (2012) executed Direct Tension Tests (DTT) on asphalt mastics at low temperature. Using microscopy images Qiu (2012) verified that the crack width within his specimen increased as the applied displacement increased. He varied the amount of displacement applied and looked for correlations with the amount of healing detected. An example of the results is shown in Figure 2.18. In the graphs it can be seen that when a large displacement is applied to the specimen and consequently the crack width within the specimens increased, the specimens required a longer time to heal or did not fully heal. From the graphs it can be seen that especially large cracks require more time to heal.

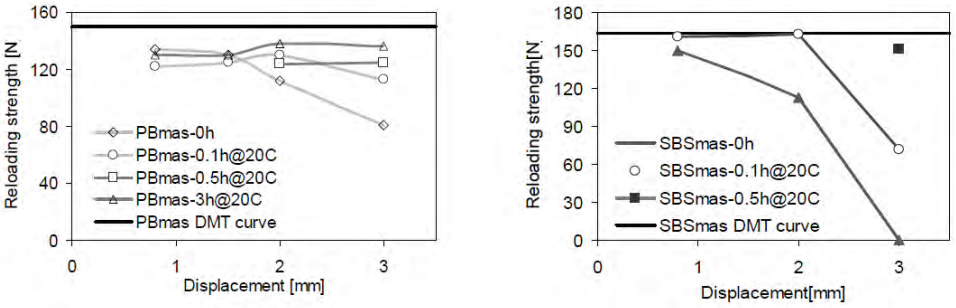

Figure 2.18 Strength recovery of specimens subjected to different elongations during testing corresponding to larger crack size and the effect of healing time for mastic made with Penetration grade Bitumen (PB) on the left and SBS modified bitumen on the right (Qiu 2012).

2.3.7 Extrinsic self-healing in asphalt

Extrinsic self-healing materials are specifically designed to have an improved self-healing performance. Extrinsic self-healing is not the focus of this research, however during research on extrinsic healing some observations have been done, which shed some light on intrinsic healing, these findings are therefore reported in this section.

One concept to improve the healing capacity of asphalt builds on the addition of conductive material to the asphalt mix, to allow for easy heating of the pavement during its service life, with the aim to heal cracks. As research into asphalt healing has shown that healing proceeds faster at higher temperatures (see Section 2.3.2), it was hypothesized that cracks in a pavement could be healed by heating the pavement (García, Schlangen, van de Ven, and Liu 2009). Adding steel fibres to the asphalt mix combined with the use of induction heating was identified as a practical method to heat a pavement to serve as a form of maintenance. One of the perceived risks in this approach is that the bitumen can be damaged due to overheating. However, research has demonstrated that if the temperature during healing does not exceed 85 °C the bitumen is not damaged or significantly aged by the heating process (Liu, Schlangen, van de Ven, and García 2010).

This approach has been demonstrated in the laboratory (García, Schlangen, and Van de Ven 2011) and subsequently test sections have been constructed (Liu, Schlangen, and Van Bochove 2013). During the project HEALROAD (Healroad 2018) an important discovery was done. It was noticed that the maximum temperature realized during a healing action did not correlated with the amount of healing observed, instead the temperature increase that was realized per second (*K*s*) correlated to the healing observed. It is therefore hypothesised that it is not the temperature itself that triggers the flow that enables healing, instead it could be rate of thermal expansion of the bitumen, which is the driving mechanism behind that flow that closes cracks (Grossegger and Garcia 2019). If the material expands before stresses are relaxed crack surfaces are brought together actively allowing for more healing.

2.4 HEALING MECHANISM

2.4.1 Introduction

Previous sections described healing based on test observations. However, to understand and predict healing behaviour, a theory of how healing works describing the underlying mechanisms is essential. Such a model can also serve as the foundation for a predictive healing model. This section reports on the most dominant healing mechanism reported in literature and models based upon this theory.

2.4.2 A healing theory adopted from polymer science

2.4.2.1 *Description of the healing mechanism in polymers*

Kim, Little, and Benson (1990) connect their work on healing to healing described in polymers (Wool and O' Connor 1981). In this paper Wool and O' Connor (1981) propose a healing theory which is based on the idea that in order to transfer load, surfaces need to be in contact. This material model is based on the concept that healing of asphalt is the convolution of the area of cracked surface that has regained contact (wetting) and the load that can be transferred by this regained contact (intrinsic healing). At a later stage in time a nice visual representation of this model has been drafted, see Figure 2.19. In the paper the concept is introduced and equations are proposed on regeneration of contact and rearrangement of molecules. They support their theory by showing that experimental results on healing of soft polymers match their equations.

2.4.2.2 *Polymer healing model*

Their key mathematical model describes healing as the convolution of two processes that occur simultaneously: the wetting of surfaces (creating a load transfer area, *A*) and the intrinsic healing of the wetted area (load bearing capacity of areas in contact R_h). The convolution integral that is able to combine the effect of both processes is given in Equation 2.5.

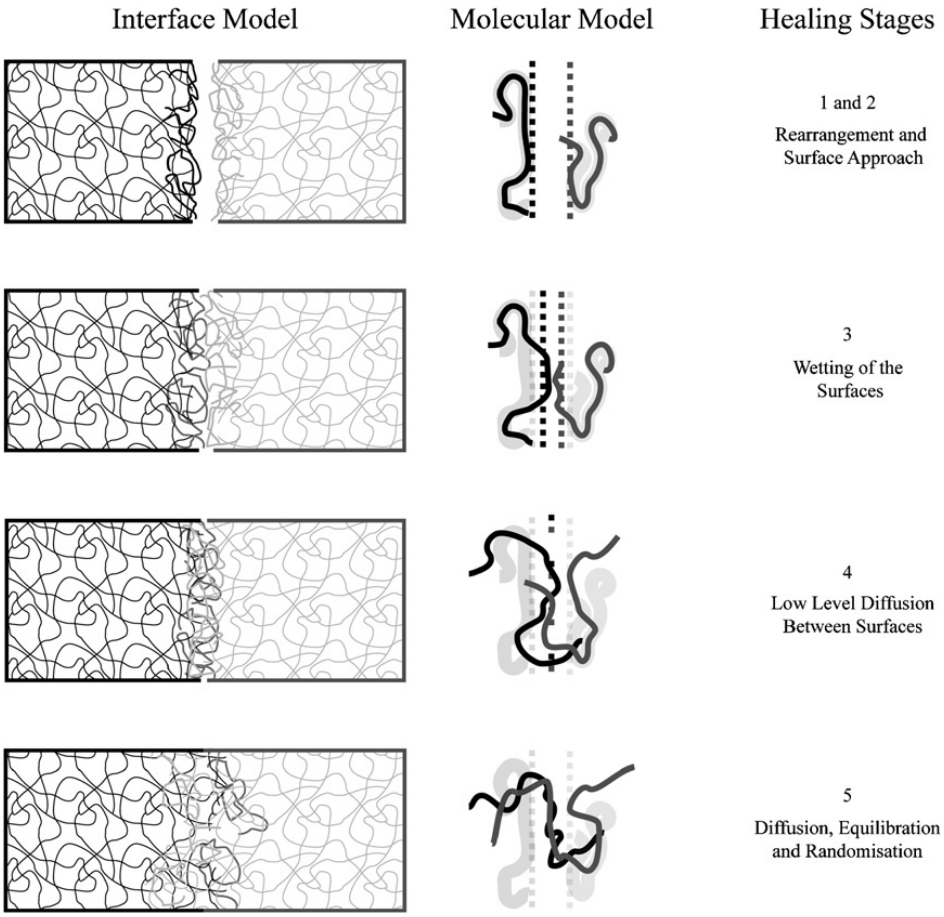

Figure 2.19 Step wise model on healing of polymers (Wu, Meure, and Solomon 2008).

$$\boldsymbol{R = \int_{\tau=0}^{\tau=t} R_h(t-\tau)\frac{dA(\tau)}{d\tau}d\tau} \qquad (2.5)$$

R is the ratio of the healed performance compared to the original performance, by definition this value ranges from 0 to 1; 0 indicating no recovery and 1 indicating full recovery, aligning with the earlier introduced Equation 2.1. The creation of molecular contact is represented by $A(\tau)$, this parameter also ranges from 0 to 1. Finally $R_h(t)$ is the equation describing the relative performance of the contact area, again ranging from 0 to 1. τ is a second variable running on the time axis. As the formula uses only relative performance values (values of 0 to 1), it is so generic that it can be used to describe the recovery of a wide range of material properties, e.g. stiffness or strength.

2.4.3 Experimental validation of the polymer healing model for asphaltic materials

In the work of Wool and O' Connor (1981) molecular chain length was an important parameter influencing the healing of polymers. Kim, Little, and Benson (1990) adopt this parameter and hypothesize that as molecules diffuse over the healing interface, longer chain lengths will create a stronger bridge between the surfaces, ultimately resulting in higher healing levels. Next to this they also assume that in case molecules have the same size, molecules that consist of long chains are more mobile compared to molecules that have a more compact structure, therefore resulting in faster homogenization of damaged areas and consequently as faster healing. Within their research Kim, Little, and Benson (1990) examine the healing performance of three asphalt mixtures that are produced with three different types of bitumen and correlate the observed healing to structural parameters of the bitumen. The healing index is determined on an asphalt beam loaded using a normal force in a displacement controlled mode. The extend of healing is determined by taking the difference between the pseudo strain energy (see paragraph 2.2.4.2). They take the energy before and after a rest period and divide this over the pseudo strain energy after the rest period (see Equation 2.4).

Several analyses have been done to assess chemical parameters of the bitumen to correlate the amount of healing with. Both aim to look at the structure of the molecules and identify long aliphatic chains, as long molecular chains were a key element in the healing model for polymers. Their first approach is based on Nuclear Magnetic Resonance (NMR) measurements which result in a ratio between methylene (CH_2) to methyl (CH_3). This ratio goes down as the chains get longer. The second approach is based on a chemical analyses called Fourier Transform Infrared (FTIR), which is able to identify chemical groups present in the binder. Using this technique a ratio can be identified by counting the total amount of hydrogen atoms in methylene and methyl group and dividing this over the total amount of carbon atoms in both groups, this parameter is called the MMHC-ratio. Contrary to the previous parameter, the ratio goes up as the chains get longer. For both ratios the value is taken of the saturate fraction, as it is argued that this group by definition contains the largest amount of long chains. They concluded that longer aliphatic chains present in bitumen increase healing potential.

Based on the research executed and reported in 1990 some of the original authors, made a new version of the graph presenting the found correlations between the two chemical parameters and the healing index (Little, Bhasin, and Darabi 2015), see Figure 2.20. In this figure the healing index is plotted against the MMHC ratio, while the CH_2/CH_3 ratio written in red alongside the graph, both parameters are based only on the 'Saturate' fraction of the binder (for a description of a saturate fraction see paragraph 2.5.3.2). From the graph it can be seen that for these three bitumen, if the saturate fraction contained molecules with longer chain lengths more healing was observed. However, looking closely at the graph is should be noted that these correlations are not that strong. The

healing index for bitumen S-20 en F-20 are quite similar, while they have a different branching and chain length factor. The fact that they confirm the trend is only based on the values for W-40. It should also be noted that 3 binders is a very small group to validate this theory and it does not become clear how this trend stretches to more extreme values. However, an interesting alternative validation for this theory is provided by Bhasin, Bommavaram, Greenfield, and Little (2011) who have studied the diffusivity of artificially designed bitumen using molecular dynamic simulations. The model results showed that there is a good correlation between the chain length parameters and the observed bitumen mobility. It is therefore concluded that chain length in the binder is a possible indicator for its healing potential.

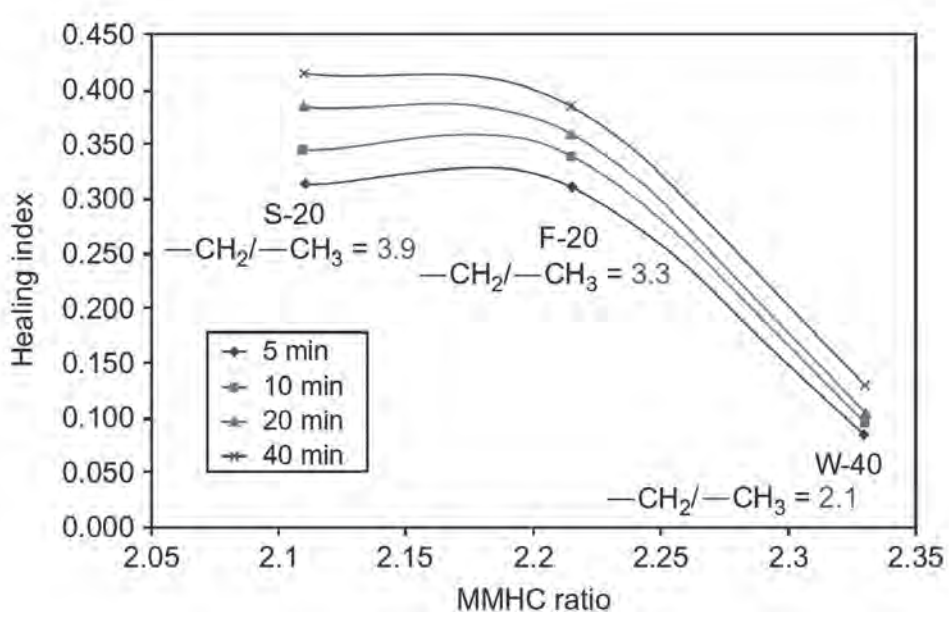

Figure 2.20 Correlation of MMHC ratio and healing index (Little, Bhasin, and Darabi 2015)

Relating differences in healing of binders to chemical properties has also been investigated using the two-piece healing method (Bhasin, Little, Bommavaram, and Vasconcelos 2008; Bommavaram, Bhasin, and Little 2009). In this work a crack is mimicked by two separate pieces of bitumen which are pushed together using a Dynamic Shear Rheometer (DSR) at the start of a frequency sweep test. The used specimens are 25 mm in diameter and have a thickness of 3,5 mm. One specimen is placed at the top spindle and one at the bottom. Next, the top spindle is slowly brought down in a displacement controlled mode, pushing the surfaces of the bitumen pieces firmly together until the assembled specimen has a height of 5 mm. As a result of the assembly procedure excess material is pushed out between the plates; the excess material is removed before starting the test. Next, the

machine readjusts the gap to ensure that the normal force is 0,4 ±0,1 N. The response of the assembled specimen is compared to a single specimen of the same material with the same thickness of 5 mm. Both the assembly procedure and the test are executed at 23 °C. When interpreting the results, it is assumed that the surface of these two pieces of bitumen are instantly in full contact as a result of the assembly procedure. Therefore the instant part of the strength is assumed to be related to the surface energy of the bitumen. The time dependent part is related to the homogenisation of the contact area and therefore related to self-diffusion ability of the material. The following equation is proposed to describe the observed healing in the two piece healing test (Bommavaram, Bhasin, and Little 2009):

$$I_h(t) = I_0 + (1 - I_0)(1 - e^{-qt^r}) \quad (2.6)$$

$I_h(t)$ = healed strength (value of 0 to 1 compared to original strength)

I_0 = instant healing strength

t = time

q = fitting parameter

r = fitting parameter

In the ARC quarterly report of April to June 2008 (FHWA 2008) a graph is presented showing the measured healing of five different SHARP bitumen using this method, see Figure 2.21. In this specific graph $I_h(t)$ was referred to as $R_h(t)$, but the two parameters are the same.

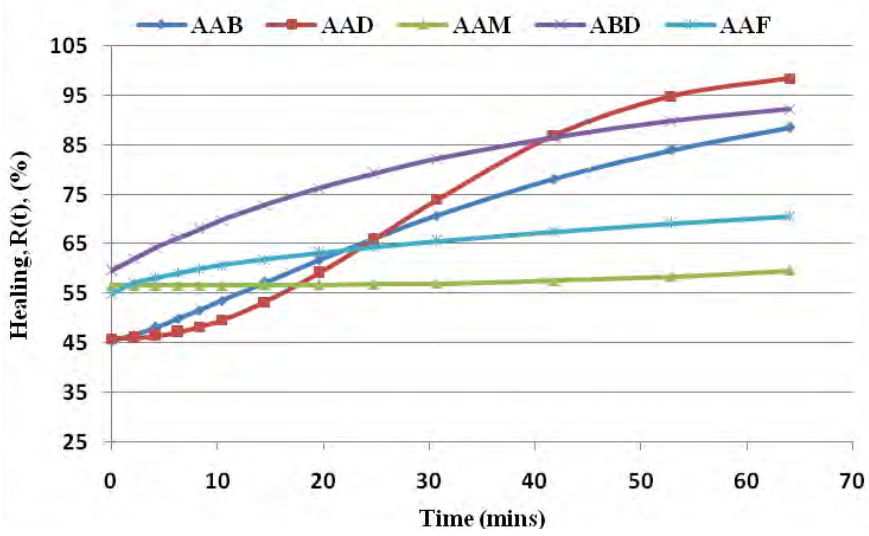

Figure 2.21 Healing measured with two piece healing methods (FHWA 2008)

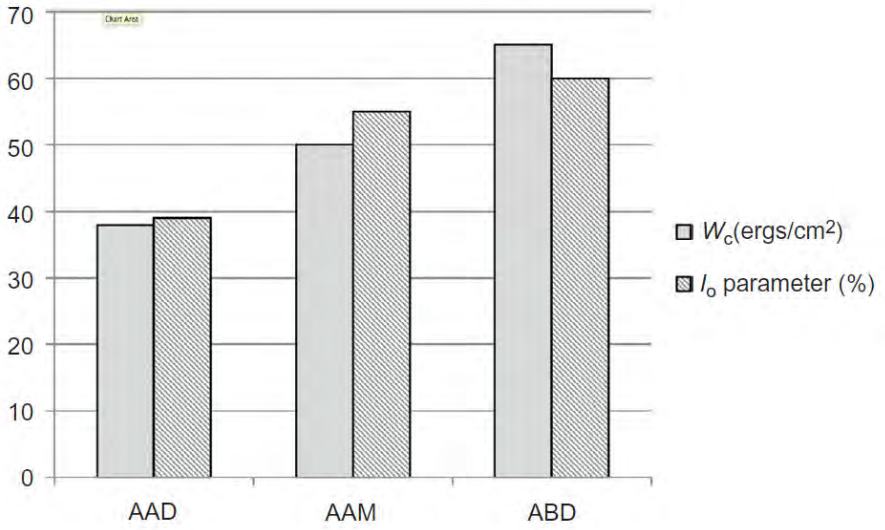

Figure 2.22 Values reported for surface energy (Wc) and the initial healing (I0)

The parameter I_0 in Equation 2.6 represents the instant healing based on the surface energy of the material. A good correlation between I_0 levels and surface energy as determined by the Wilhelmy Plate Method is reported (Little, Bhasin, and Darabi 2015), see Figure 2.22. Although it should be noted that this is only reported for three binders.

Qiu (2012) has also performed tests using the two-piece healing method. He found a strong dependence of healing and the gap width and the amount of pressure applied at the healing interface. When the distance between the plates is kept constant, there is a very small increase in stiffness modulus with healing the healing period, while the normal force reduces. While when the conditions of (Bommavaram, Bhasin, and Little 2009) are used and the normal force is kept constant during the healing period there is a clear increase in stiffness modulus during the healing period, while the gap reduced quite significantly. Qiu (2012) therefore concludes that many factors influence the amount of healing detected in the test setup as proposed by (Bommavaram, Bhasin, and Little 2009) and more research is needed to formulate a reliable and reproducible test. The need for further refinement of the test is also shared by the authors, as they indicate the need to further develop the test method to be able to lower the normal force level to 0,1 N (Bommavaram, Bhasin, and Little 2009).

The positive effect of normal force on healing in the two-piece test may stem from incomplete initial surface contact. Atomic Force Microscopy (AFM) images reveal a nanoscale surface texture in bitumen (~50 nm) that can delay contact development and introduce the possibility of the influence of friction at the healing interface (Soenen et al. 2014; Nahar, Schmets, Scarpas, and Schitter 2013), which is discussed in more detail in Paragraph 2.6.2.4. An increase in normal force will result in more contact, while a higher normal force will also result in more friction. The observed influence of normal

force on the healing performance, could be an indication that the surface contact is still developing during the healing period. Some conclusions from (Little, Bhasin, and Darabi 2015) assume that all healing over time observed in the two piece healing test, results from molecular diffusion across the interface. However, if surface contact at the healing interface is still developing, this assumption does not hold and the conclusions might be incorrect.

2.4.4 Multistep healing mechanism for healing of asphalt

Another model which further elaborates on the healing concept proposed by Kim, Little, and Benson (1990) is the multistep fatigue and healing model (Phillips 1998). This conceptual model connects the processes described by Kim, Little, and Benson (1990) and translates them into macroscopic behaviour of asphalt concrete. In the model the process of healing is the inverse of cracking, which both have a step wise impact on asphalt performance, see Figure 2.23. Healing starts with the closing of cracks, made possible by flow of material. When as a result of the flow of material there is no physical distance between the two surfaces, the interface can regain contact through the process of wetting, which is driven by surface energy. This restoration of contact between the surfaces results in restoration of the stiffness of the material and part of the strength. However, in order to regenerate all of the original strength, selfdiffusion is required to homogenise the interface. What is remarkable about this model is that there is asymmetry, namely during cracking, stiffness deteriorates before strength, whereas in the restoration phase, stiffness recovers first, followed by strength. This behaviour aligns with practical observations from fatigue testing, in which stiffness typically decreases and recovers more readily than strength. No experimental verification of this model has been presented (Phillips 1998).

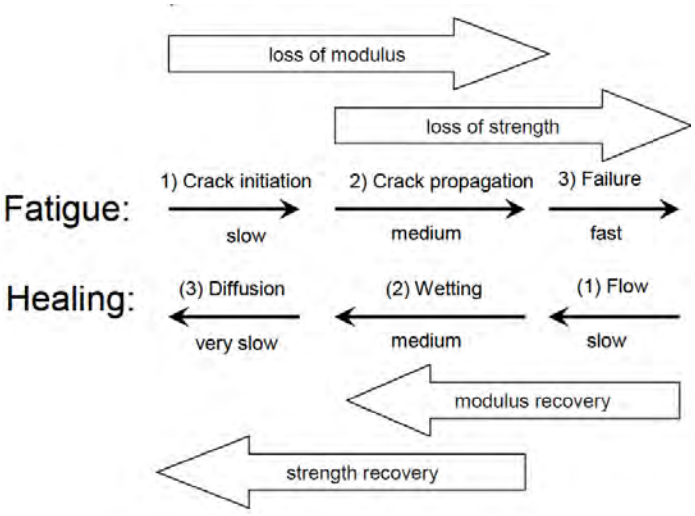

Figure 2.23 Schematic model on fatigue and healing (Phillips 1998)

2.5 MATERIAL PROPERTIES OF BITUMINOUS MATERIALS IN THE CONTEXT OF HEALING

2.5.1 Introduction

The previous section on material models for healing introduces the processes of adhesion and diffusion. In order to better understand these processes, some additional knowledge about physical and chemical nature of bitumen are relevant to address within this literature review.

2.5.2 Classification of bitumen

For the use in pavements, bitumen is usually classified using rheological properties. In Europe very simple and quite old tests are used for classification. The penetration test (EN 1426) is used to classify bitumen as a certain penetration grade, by measuring the hardness of a binder. In this test, the penetration depth of a needle with a specified weight of 100 gram is determined in dmm, after being placed on the surface of a cup of bitumen, after a period of 5 seconds. Most asphalt base layers in the Netherlands are constructed using bitumen with a pen grade of 40/60. Next to this penetration grade, the bitumen is also classified on its temperature sensitivity. For this aspect the Ring and Ball test (EN 1427) is used. In this test a metal ball is placed on a sheet of bitumen which is placed on a metal ring. The total set-up is place in a beaker glass with water which is heated in a controlled manner. As discussed in section 2.3, several studies on healing show that a higher penetration value, or a softer bitumen, results in more healing.

2.5.3 Chemistry of bitumen

2.5.3.1 *Bitumen production*

The chemical composition of a material is of interest as it determines which type of molecular interactions will take place within the material. As the type of molecular bonds and other molecular interactions have a large influence on the material behaviour, understanding the chemical composition of a material can provide insight in the mechanisms that play a role in its behaviour.

In order to explain the chemical composition of bitumen, it is insightful to start with the production process of bitumen. Bitumen is a by-product of the oil industry. Fuels are produced by subjecting crude oil to (vacuum) distillation and other kinds of separation techniques. Figure 2.24 provides an impression of the most simple process possible called fractional distillation. In this process bitumen is the residue that remains after fuels have evaporated from the crude oil. Incidentally, this residual stream is directly used as bitumen and therefore called straight run bitumen. However, in the current bitumen market many other blends are also sold. These can be blends that contain different streams from the refinery process, however there are also other recycling streams which are blended with the residue, for instance the residue of recycled oil from different origins.

By blending and/or undergoing post-processing a bitumen is created that meets the required specifications. In this it is important to realize that bitumen is a rather low cost bulk material in which material streams can be integrated that have a low or even negative market value. From this it can be concluded that bitumen is not a carefully engineered material with a designed composition. Bitumen is actually an arbitrary combination of heavy molecules present in crude oil, which remain after the extraction of more valuable production streams. Next to this, bitumen can also be blended with other oil rich streams like recycled waste oils. As bitumen composition varies widely, and material performance originates from molecular interactions, it is consequently also assumed that healing performance varies between asphalt binders.

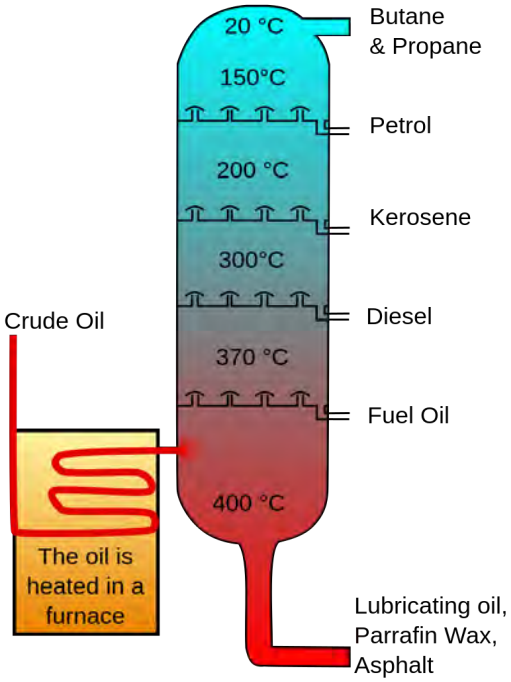

Figure 2.24. Schematic representation of the distillation of crude oil and the resulting products [Crude_Oil_Distillation-Psarianos, Theresa knott, CC BY-SA]

2.5.3.2 *Chemical composition of bitumen*

As a results of its production process, bitumen consists of an endless variety of molecules, therefore full chemical determination of bitumen is practically impossible (Speight 2014). Hence, the chemical analyses of bitumen focusses on aspects which can be determined, like the element or bond types present in the material (functional groups), the size of the molecules and interactions with specific chemicals. Through these types of analyses some general information can be obtained on the chemical composition of bitumen.

Bitumen consists mainly of large hydrocarbons supplemented by very small fractions of other chemical substances. The following mass percentages of elements are present in bitumen: Carbon (C) 82-88%; Hydrogen (H) 8-11%; Sulphur (S) 0-6%; Oxygen (O) 0-1,5%; Nitrogen (N) 01% and traces of the following metals Vanadium (V), Nickel (N), Iron (Fe) (Read and Whiteoak 2003). Sulphur, Oxygen and Nitrogen are usually present as part of a functional group within a hydrocarbon. These functional groups will affect the polarity of the material. It is sometimes suggested that the polarity of a material affects healing see Section 2.5.4.

The size of molecules in a material affect its behaviour, therefore the sizes of bitumen molecules will be discussed. The size of the molecules in a material have a strong influence on the mobility of molecules and, as mobility is needed for healing, the size of molecules is also important for healing. The smallest size of a molecule in bitumen is a direct result of the applied distillation conditions and is usually around 300 atomic mass units (amu). The size of the largest molecules present in bitumen is not well defined at this moment in time, even though there are a variety of methods available to assess the size of molecules in a material. The lack of clear value for the largest molecule size in bitumen is caused by the fact that it has been shown that this is dependent on the analyses method used (Groenzin and Mullins 1999). The sizes of the largest molecules reported range from 500 to 30.000 amu, indicating a difference of almost two orders of magnitude. Groenzin and Mullins (1999) also show that the observations of extremely large molecules are most probably related to clusters of molecules instead of single molecules. In their paper they claim that the largest individual molecules in bitumen are 500 to 1000 amu. This can be translated in a size of the largest molecule of around 2 nm. Therefore the material behaviour and its internal mobility is influenced by the size of the molecules, but also by their tendency to form clusters, as also suggested in (Schmets et al. 2009).

Another separation technique, which separates fractions based on their polarity, is also popular to characterize bitumen. By applying specific separation techniques, based on solubility, bitumen is divided in four specific groups of hydrocarbons, which are called Saturates, Aromatics, Resins and Asphaltenes or in short “SARA fractions” (Read and Whiteoak 2003; Lesueur 2009). It should be noted that the use of separation techniques to obtain these fractions also should be taken into account when using these fractions to explain bitumen behaviour. There are slight differences between commonly used separation techniques, which influence the exact boundaries between the fractions and therefore their exact size and behaviour (Redelius and Soenen 2015). The resulting four groups demonstrate different behaviour and also have specific chemical characteristics. The four fractions can be described as follows. **Saturates** are non-polar and chemically relatively inert, and at least a part of this fraction can crystalize at room temperature.

[3] Atomic Mass Units or AMU is a unit used in chemistry to quantify masses of atoms and molecules, 1 AMU=1/12 of the mass of an unbound carbon-12 atom

Aromatics are unsaturated hydrocarbons, containing one or more aromatic rings. **Resins** are saturated hydrocarbons containing ring structures. **Asphaltenes** are the largest molecules containing a multitude of organic rings and polar groups, making them chemically reactive but more importantly providing more options for complex molecular interactions. Based on the volume of each SARA fraction, researchers formulate predictions on the expected performance. For instance a colloidal stability index has been proposed (Gaestel, Smadja, and Lamminan 1971). They demonstrate that a bitumen is more stable and will therefore perform better if the ratio of Asphaltenes and Saturates over Resins and Aromatics is smaller. Santagata, Baglieri, Dalmazzo, and Tsantilis (2009) reported that bitumen with a higher Saturate over Aromatic index showed more healing (see 2.3.5), concluding that the long saturates chains contribute to the healing capacity of a binder.

2.5.4 Material characteristics based on physical-chemical nature of bitumen

2.5.4.1 *Introduction*

As discussed in Chapter 1, healing is an important factor in the design of pavement structures, as it strongly influences the fatigue performance in the laboratory. However, research on fatigue damage (as discussed in Section 2.2.1) and healing (as discussed in Section 2.3), have shown that processes occurring at a smaller scale, like crack formation, material flow, adhesion and diffusion, play an important role when understanding the mechanism of healing. Therefore within this section some fundamental physical-chemical principles behind the material behaviour of bitumen are described.

2.5.4.2 *Molecular interaction in bitumen*

At the molecular scale, material behaviour is determined by interactions between molecules. Chemist that studied bitumen point out that strength and stiffness of bitumen are mainly determined by intermolecular forces (Petersen et al. 1994; Redelius and Soenen 2015). Intermolecular forces (or Van der Waals forces) are so called short range forces (Kendall 2001), meaning that they are relatively strong when molecules are very close together, however they diminish fast as distance between molecules become larger; at a distance of a few nano meters the forces are already hardly detectable. There are many types of intermolecular forces, however Redelius and Soenen (2015) argue that, for bitumen London dispersive forces are most dominant. Next to the London dispersive forces, they also indicate the relevance of polar, hydrogen bonds and pi-pi interactions. These specific interactions are introduced below, with a short description for their relevance to bitumen.

The **London Dispersive forces** find their origin in temporary differences in electrical charges of molecules. The electrical charge around molecules is not constant but fluctuates in time. These fluctuations cause an electric field that affects charge distribution in nearby molecules, as a result instant dipoles are created that lead to attraction. Generally larger

molecules are more easy to polarize, so the larger the molecules the larger the London dispersive forces. As introduced in paragraph 2.5.3.2, bitumen consist of very large molecules, therefore it is logical to assume that these forces play an important role in the behaviour of bitumen.

Polar interactions (or Keesom interaction) originate from small differences in electrical charge in part of a molecule due to electrical charges of specific atoms. As a consequence the molecules are locally positive or negatively charged and positive regions of one molecule will attract negative charges of another molecule. Oxygen, Nitrogen and to a lesser extent Sulphur have a high electro negatively and will introduce a local electronegative charge in a molecule. This type of polarity can also induce polarity in molecules that are normally not charged, triggering molecular interactions, which is called **Debye forces**.

Pi-pi interactions are related to the stacking of clusters of aromatic rings. Especially asphaltenes contain these type of clusters of aromatic rings. Schmets (2009) has demonstrated that it is likely that these kind of interactions actually take place in bitumen and might provide an explanation why asphaltenes have such a large impact on bitumen viscosity.

In explaining bitumen behaviour, the relative importance of the molecular interactions described above is still a point of debate. As mentioned Redelius and Soenen (2015) claim that the London dispersive forces dominate the behaviour. In their paper they substantiate this by presenting calculations on the magnitude of these forces and compare them to the estimated magnitude of polar forces. They state that polar interactions, while present in bitumen are too small to dominate over the dispersive forces, due to the limited amount of polar groups in bitumen. However, other scientist argue that polar interactions are dominant as they describe correlations between adhesion, healing and polarity (Little, Bhasin, and Darabi 2015; Little, Allen, and Bhasin 2018; Petersen et al. 1994).

2.5.4.3 *Impact of intermolecular forces and chemical structure on bitumen behaviour*

These intermolecular forces can be used to explain some of the basic behaviour that is observed in bitumen which is relevant for healing, like temperature susceptibility, diffusion and adhesion. Below this is explained in some more detail.

Temperature influences the vibration of molecules. The higher the temperature, the larger the vibrations. When the vibrations increase beyond a certain point, these vibrations can result in a translational movement, making it possible for an individual molecule to move around in a random way, so called Brownian motion. This explains the driving mechanism behind diffusion.

At very low temperatures bitumen becomes very stiff, the temperature at which this occurs is called the glass transition temperature (T_g). The exact temperature at which this occurs

differs per bitumen, for bitumen commonly used in pavement engineering it is around -20 °C (Read and Whiteoak 2003). Below the glass transition temperature, bitumen molecules are immobilized by strong intermolecular forces, preventing translational motion. As a result, the material stiffness is governed by the molecular bonds within the bitumen molecules. Therefore the shear stiffness of bitumen below the glass transition temperature is in the order of magnitude of 1 GPa, which is the stiffness of the bonds in bitumen molecules (Gibson 2016). Consequently damage occurring below the glass transition temperature originates in breaking of molecular bonds and not separation of the molecules. As breaking of molecular bonds is brittle in nature, this explains why the observed damage in bitumen below the T_g is also brittle.

As the temperature increases above the T_g molecules gain more vibration energy resulting in larger distances between molecules and consequently lower interaction forces. Consequently, bitumen will become less stiff and molecules exhibit translational movement. However, as the molecules are large the van der Waals forces will remain rather strong, preventing the material from becoming a real fluid at ambient temperatures. In this state there is room for molecules to slide over each other when subjected to a load. This sliding actions result in the large deformation capacity for which bitumen is known. This concept of sliding movement also provides an explanation for the sensitivity of the response to loading speed. The movement of large hooked molecules like asphaltenes is hindered by their neighbouring molecules, due to interlocking of their protuberances. If the material is loaded fast, this interlocking prevents sliding action, consequently the observed stiffness is high. However, if the loading speed is low, due to the vibration energy, the molecules can wiggle themselves past protrusions of surrounding molecules, allowing for ductile deformation. As the temperature increases, the room for sliding increases, and the material becomes more ductile. until the point where molecules are fully free to move and the material becomes a liquid.

When two surfaces are brought very, very close together, the molecular forces at their surface will interact and attract each other. The molecules at the surface are in an energetically more favourable state if they have more interactions. All the interactions that are relevant when two surfaces come into contact will be discussed in more detail in Section 2.6.

2.6 ESTABLISHING CONTACT AT THE HEALING INTERFACE

2.6.1 Introduction

This section outlines material science insights on reestablishing surface contact, a fundamental first step in the proposed healing model from Section 2.4. This section is organized following the step wise healing steps described in Figure 2.19. In Section 2.6.2 surface roughness and resistance to deformation, are discussed which are governing

parameters with respect to surface approach. In Section 2.6.3 the concept of surface energy will be explained and the relevance for wetting of surfaces will be explained. In this section also some details will be provided on the surface energy measurement executed on bitumen. In Section 2.6.4 a mathematic representation will provided of the regeneration of contact area. Section 2.6.5 will discuss possibilities for experimentally the proposed model for the development of contact between two bitumen surfaces.

2.6.2 Physical aspects of the approach of two bituminous surfaces

2.6.2.1 *Theory on surface contact for elastic bodies*

Full contact is defined as molecular contact over the whole contact area. Material science describes the following influencing factors on contact creation when surfaces are brought together (Greenwood and Williamson 1966). All (semi) solid surfaces have some level of roughness, which impedes the creation of instant full contact. It has been shown that for elastic bodies, the amount of surface in molecular contact depends on the load applied perpendicular to the contact area. Therefore, a distinction is made between the apparent contact area A_0, which is the projection of the surfaces and the true contact area A_{true}, which is the area that is in full molecular contact. The development of contact under the influence of load is quite complex, as it is a combination of elastic and plastic deformation. However, it has been shown that for elastic bodies, the amount of true contact is linearly related to the applied force. Next to this, softer materials deform more easily, therefore when the same load is applied, more contact is created if the material is softer (Johnson, Kendall, and Roberts 1971). In the next sections, the parameters influencing of apparent and true contact will be explored in more detail for bitumen.

2.6.2.2 *Elastic versus viscous: effect of temperature and strain rate*

As stated before, the amount of contact created in a linear elastic material is proportional to the applied load. However, bitumen is not elastic, but viscoelastic, therefore the model prescribed above has to be modified for asphalt. Schapery (1989) states that when a viscoelastic body is loaded with a constant normal force, the instant amount of contact can be assumed to be proportional to the applied load. And if a material is stiffer (has a higher complex modulus) less contact will be created instantly compared to a softer material. Next to this, due to the viscous nature of the material, the amount of contact will grow with time, even at a constant load level. The speed at which the contact area grows with time depends on the viscosity of the material, a lower viscosity will lead to a faster increase of surface contact. As a part of the deformation in viscoelastic materials is permanent, part of the created contact will remain after unloading. This ability to permanently deform is clearly favourable for healing, as restoration of cracks due to an instant load can have a permanent effect on crack healing.

It is important to note that for bitumen the amount of viscous versus elastic deformation is strongly affected by temperature and loading speed. Below the glass transition

temperature (T_g) bitumen will behave like a solid and will only show elastic deformation. At high temperatures (140-170 °C) bitumen will behave like a liquid, having no elastic response but purely a viscous one. Next to temperature, the loading rate also strongly affects the ratio between elastic and plastic response in bitumen. At high loading rates, the material response has a large elastic component, while at low loading rates the material is more viscous. In this sense it is expected that, at the same temperature and load level, if there is a long healing period, the material can show flow like behaviour and can heal significantly, while in short periods flow is not expected to occur and very little healing is expected. This aligns with the observation of Qiu (2012), who conducted some tests that indicated that the time-temperature superposition principle (Monismith, Alexander, and Secor 1966) might also applicable for healing.

2.6.2.3 *Impact of load level*

The normal force is identified as an important parameter determining the amount of surface that is brought into contact in material science. If the load is larger, more contact is created. To some extent, the positive effect of a higher load has been demonstrated for bituminous materials in the laboratory (Bazin and Saunier 1967; Qiu 2012). However, in both cases there the application of a load was binary, either there was a load and healing was observed or there was no load and no or hardly any healing was observed. No study has been executed to the correlation between the load perpendicular to the healing interface and the amount of healing observed or the amount of contact created.

2.6.2.4 *Roughness of bitumen*

As stated in 2.6.2.1 surface roughness will influence the ease with which surfaces can come into true contact. Even though bitumen seems very smooth to the naked eye, AFM studies, first reported by Masson, Leblond, and Margeson (2006) have shown that bitumen can have micro roughness in the order of 50 nm. These local rough areas are the “bees” that appear in an AFM image. The roughness (height difference) over the bees is nicely illustrated in an image produced by Nahar (2016), which is reproduced as Figure 2.25. AFM inspections have also shown that bitumen is actually not a homogenous material, but a multiple phase system. Nahar, Schmets, Schitter, and Scarpas (2014) and Lyne, Wallqvist, and Birgisson (2013) suggest that at the surface the material is built up of two types of domains which they name the *catana* (the bees) and the *para* phase (material surrounding the bees). Probing of the surface shows that the catana phase is stiffer and less adhesive compared to the surrounding para phase. This higher stiffness is actually the cause of the manifestation of the bees, as the wrinkles making up the bees are caused by the local higher stiffness in combination with shrinkage during the cooling phase when the specimens are created (Lyne et al. 2013). There is still an active debate about the exact nature of these bees. Some researchers a connection to the content of asphaltenes (Pauli et al. 2001; Hofko et al. 2016), while others see more connection to the waxes (large saturates) (Das, Kringos, Wallqvist, and Birgisson 2013; Blom et al. 2018;

Blom, Soenen, and Van den Brande 2021; Pipintakos, Blom, and Soenen 2021) and it is also hypothesized that they consist of a combination of both asphaltenes and large saturates (Nahar 2016). AFM research has shown that the magnitude of the roughness depends strongly on the preparation of the specimens (Nahar, Schmets, Scarpas, and Schitter 2013). Next to this, it has also been observed in a qualitative manner that the roughness reduces, as the specimens age (Schmets et al. 2012; Nahar 2016). Although more recent research is less conclusive about the reduction of roughness with ageing (Pipintakos, Blom, and Soenen 2021). There is also no consistent evidence that the penetration grade is correlated with the roughness, as both larger and smaller roughness's have been observed with a higher penetration grade (Schmets et al. 2012; Ji et al. 2020). It has been shown that if bitumen does not contain wax, no significant microstructure is present and therefore the roughness is also significantly less (Soenen et al. 2014; Ji et al. 2020). So even though much remains unclear about the origin of the roughness it is unmistakably present at the surface of bitumen.

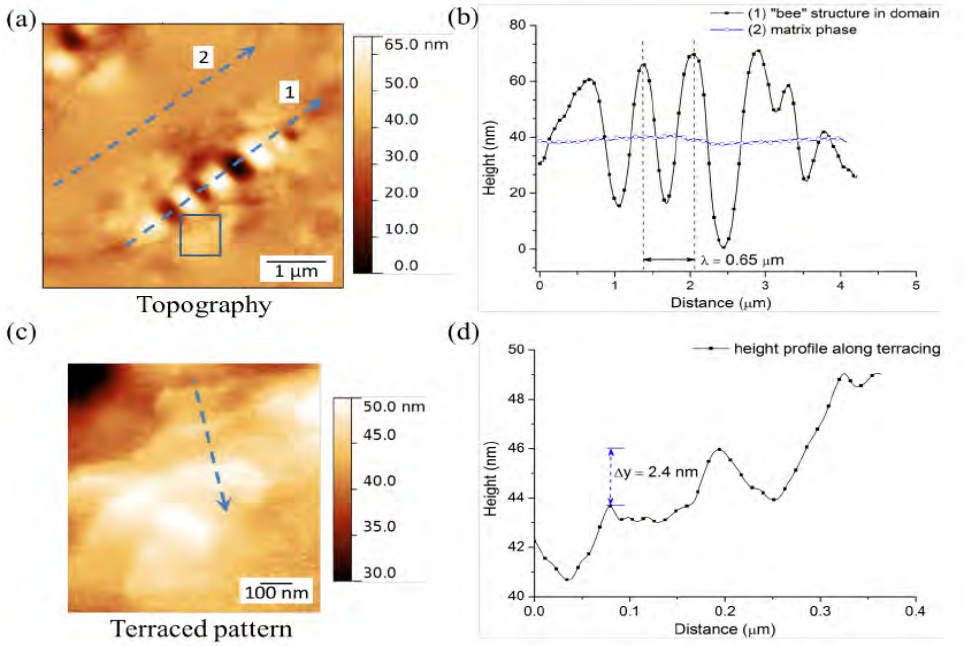

Figure 2.25 Characteristic features of bitumen microstructure. (a) AFM topography image of bitumen (PEN 70/100); b) height profiles along bee-structure and matrix phases; (c) terraced pattern and (d) step height along terraces. (Nahar 2016).

This local roughness will influence how bitumen surfaces can approach each other. As the two surfaces touch, there will be some initial contact points at the protrusions, while instant full contact is impeded, as schematically shown in Figure 2.26. The hindrance in a 3D plane is larger compared to this 2D image, as one protrusion can reduce contact

over a large area. This can be imaged from the 3D image of a bitumen surface shown in Figure 2.27. It is not possible to predict what exactly happens at the contact area, when surfaces are pushed together. However, as the catana phase is stiffer, it is possible that these domains will be pushed down into the softer surroundings, instead of deforming. If this happens, these domains can remain present at the contact area, as zones of limited contact for a certain period of time.

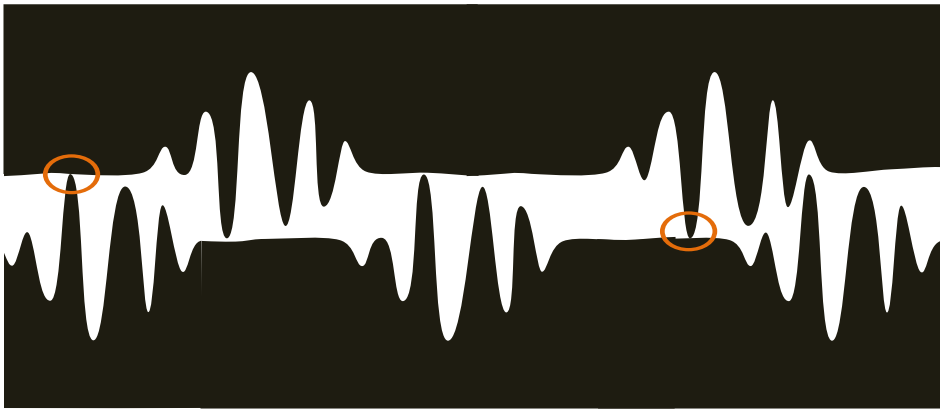

Figure 2.26 Distance between the largest part of the bitumen surface.

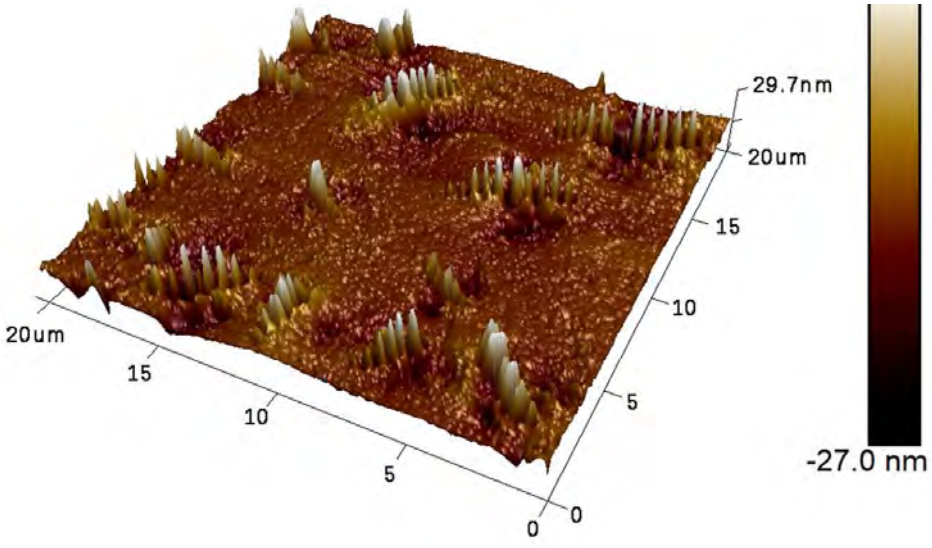

Figure 2.27 3D image of surface roughness of bitumen, bitumen type SK-70 (penetration 79), unaged, reproduced from (Ji et al. 2020)

The roughness presented above is the roughness that can be observed in air dried, pure bitumen surfaces and the shape and size of the bees is dependent on the exact method used when producing AFM specimen (Soenen et al. 2014). It has been shows that the roughness of a cracked bitumen surface is very different and will show no bees just after cracking, while bees will develop with time (Blom et al. 2018). From the images it can also be seen that if no bees are present, the surface is much smoother (roughness of +/1 nm), which will change the ease of surface approach significantly, while still impeding instant full contact.

2.6.3 Surface energy as driver for wetting

2.6.3.1 *Introduction*

There is a naturally present driving force in materials that can help to close cracks, as it is energetically more favourable for a molecule to have as much interactions with other molecules as possible, this driving force is called surface energy. The cracks we can observe in the outside world can be explained by the fact that, in many cases the forces keeping the surfaces of a crack apart are simply larger compared to this surface energy pulling the surfaces together. Surface energy is the driving mechanism for the wetting of surfaces which is required for surfaces to regenerate contact.

2.6.3.2 *The effect of surface energy at surfaces in close interaction*

The molecules at the surface of a material lack a part of their interactions and consequently have an energy potential called surface energy (Adamson and Gast 1967). The attraction exerted by surface energy has been demonstrated, by bringing two spheres of a soft rubber together using a small force (Johnson, Kendall, and Roberts 1971). These spheres are optically smooth (roughness or asperities are less than 20nm) and by using a material with a very low elastic modulus, the force required to flatten these asperities is less compared to the surface energy forces. In this experiment it was shown that the amount of observed contact area between the spheres is larger than would be expected from the externally applied force. This is illustrated in Figure 2.28. Here a_0 is the contact area that is expected based on the elastic deformation as a result of the external force, while a_1 is the contact area measured. The additional contact area observed in this experiment was related to the surface energy. Therefore showing that the amount of surface energy is directly related to the amount of interaction energy that the molecules at the interface are missing.

The amount of energy that can be gained through surface interaction differs per material, the consequences of this we observe in daily life. For example, plastics have a low surface energy, compared to water, while stones have the highest surface energy out of these three materials. As a result, when a drop of water is placed on a plastic surface it will not spread out and “wet” the surface, on the contrary the drop of water will try and minimize its surface and will try to form a sphere. The water molecules gain more

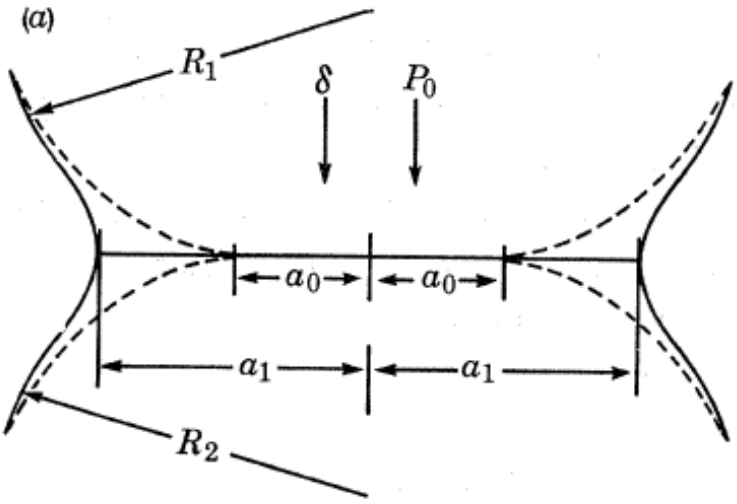

Figure 2.28 Contact area of spheres, with a_0 being the expected area in contact based on the externally applied force and a_1 being the actual measured contact area. The size of a_1 can be directly related to the surface energy of the material (Johnson, Kendall, and Roberts 1971)

energy by staying close to other water molecules, compared to the possible energy gain that they can acquire from interaction with plastic molecules. If the same drop of water is placed on a stone surface, the drop will immediately spread out on the surface, as much energy can be gained from interaction with a surface with a higher surface energy. As illustrated by this example, the potential for a liquid to wet another surface can be calculated if the surface energies are known (de Gennes, Brochard-Wyart, and Quere 2004). Surface interaction models are able to provide an estimate of the shape of a liquid on a surface based on their surface energies, as visualized in Figure 2.29. Depending of the surface energies of materials they will have the tendency to fully wet another surface or wet it only partially.

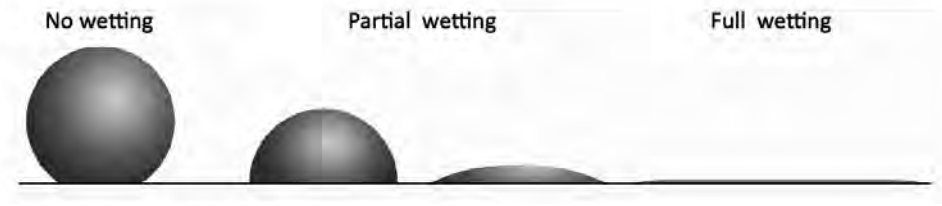

Figure 2.29 Possible interactions between a surface and a liquid. [By MesserWoland, https://commons.wikimedia.org/w/index.php?curid=1253800]

2.6.3.3 *Wetting of a crack*

In the case of a cohesive crack, the two resulting crack surfaces will have more or less the same surface energy as they are made up of the same material. Surface energy models indicate that in this case the surfaces will fully wet each other (de Gennes, Brochard-Wyart, and Quere 2004). However, the speed at which this full wetting occurs depends on the viscosity of the material (Kendall 2001). The wetting of a low viscosity material like water will be fast, as can be seen when two raindrops merge, for instance on the windscreen of a car. For a highly viscous material like bitumen, wetting at ambient temperatures will require much longer periods of time. As the wetting rate depends on viscosity, this indicates that wetting will progress faster for a softer bitumen (e.g. 70/100) as this has a much lower viscosity compared to harder bitumen (e.g. 10/20).

2.6.3.4 *Measuring surface energy in bitumen*

There are some challenges when measuring the surface energy of a material (de Gennes, Brochard-Wyart, and Quere 2004). In the first place because liquids require a different approach than solids and high energy surfaces (stones, metals) require a different technique than low energy surfaces (plastics). This is why there are many experimental approaches to measure the surface energy. Unfortunately, it has been shown that the used technique affects the measured surface energy, consequently making comparisons between different materials and conditions not fully possible. On top of these differences in experimental outcome, the determined surface energy also depends on the surface energy model used to analyse experimental data. Consequently, the determined surface energy is both dependant on the test method and the interpretation method, making it a complicated quantity to determine unambiguously.

This measurement challenge seems to be particularly important for bitumen. Van Lent (2014) has performed many types of surface energy measurements on a variety of bitumen types and aggregates. His measurements demonstrate that for bitumen the amount of surface energy detected strongly depends on both the measurement technique and the method used to analyse the data. For one single bitumen, he found surface energy values ranging from 13 to 58 mJ/m^2, depending on the measurement technique. This spread is very large when it is compared to the total variation he found between six different types of bitumen, which was 13 to 65 mJ/m^2. His work also showed that the relative ranking of observed surface energy for different bitumen types, varied with the used technique. This demonstrates that large conclusions based on single measurements for surface energy values for bitumen should be considered with care. These large varieties in surface energy measurements challenge the relevance of correlation presented between healing and surface energy, as for instance presented earlier in Figure 2.22, by (Little, Bhasin, and Darabi 2015). However, all the measurements indicate that bitumen has a lower surface energy compared to water which is around 72 mJ/m^2 at ca 20 °C. Indicating that water will always have a stronger interaction with aggregates compared to bitumen, highlighting the risk of stripping for asphalt when exposed to water.

2.6.3.5 *Artifacts in surface energy*

The surface energy that is observed is strongly dependent on the molecules that are present at the surface (Kendall 2001). This is why coatings or surface contaminations can result in large changes in the surface energy. This high impact of the type of molecules present at the surface on the surface energy is also relevant for bitumen. As already mentioned, bitumen consists of many different molecules. Following the surface energy theory, Cheng (2002) has proposed a theory that bitumen molecules will organize themselves to reduce the amount of energy lost at a surface. As a result of this, molecules with a lower surface energy will migrate to the surface and the actual surface energy detected there will be lower compared to what would be expected from the bitumen constituents. This theory is confirmed by the work of Van Lent (2014), as he showed that the surface energy of a bitumen surface was significantly different from the surface energy that could be measured at a surface that was in contact with a crystal. Also providing a possible explanation why the surface energies in bitumen vary so strongly, see 2.6.3.4. This reorganizing of molecules at the surface, will most likely also happen at crack interfaces, resulting in a lower surface energy of an old crack compared to a fresh crack. This would imply that wetting of a fresh crack progresses faster compared to an old crack. There is very limited literature available that can suggest a time scale for this process, making it unknown if these kinds of differences could play a role on the timescales relevant for healing. The work of Blom et al. (2018) shows that initial changes are visible after 15 minutes, however full homogenization of the surface will require longer time periods. As 15 minutes is a relevant time periods for healing, this indicates that there is a possibility that that reorganisation of surfaces could have a relevant effect on observed healing.

2.6.4 Conceptual model for regeneration of contact area

Wool and O' Connor (1981) have formulated a model for the regeneration of contact area in the healing of polymers, as discussed and presented in 2.4.1. Their model takes into account the effect of surface roughness described in paragraph 2.6.2.4, resulting in the development of contact starting from a number of asperities in the surface being the first point of contact. These initial contact areas, can subsequently grow as a result of wetting driven by surface adhesion (see paragraph 2.6.3.3) or another externally applied force. This model can be mathematically represented by modelling the contact points as nucleation points, from which the contact area grows with time in a radial direction. This process of nucleation and growth of contact area is schematically shown in Figure 2.30 a and b.

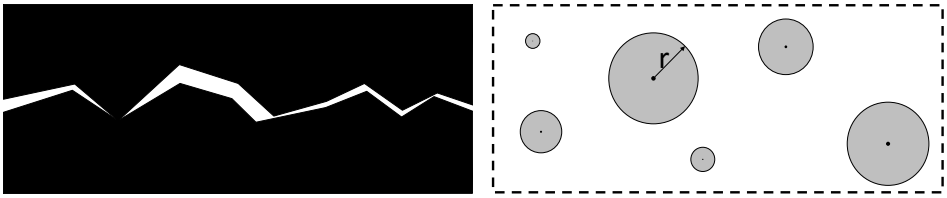

a. b.

Figure 2.30 Schematic representation of two surfaces approaching each other a. transverse cross-section of the healing interface, showing the impact of roughness, demonstrating that some points of the surface will come into contact first (nucleation points). b. Top view of the healing interface, where the black dots represent the nucleation points and the grey area the contact area which grows with time in the radial direction ***r***.

Their model assumes that separate contact areas, as shown in Figure 2.30b. grow with time and at some point start to overlap. The growth of contact area in this model can be described by an Avrami equation (Wool and O' Connor 1981). This type of equation results in values for the contact area ranging from 0, for no contact to 1, for full contact. Figure 2.31 shows the basic shape of the Avrami equation.

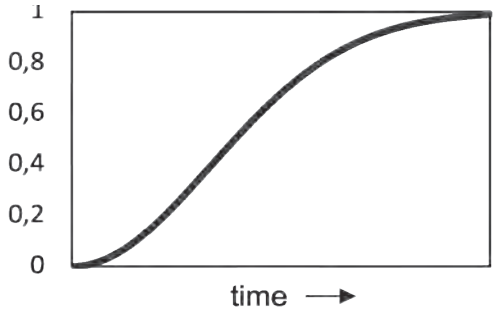

Figure 2.31. Development of surface area in contact with time, following an Avrami equation.

This equation results in differences in area growth rate over time. Initially the area growth rate is slow, resulting from the limited number of nucleation points. As the contact areas expand, the area growth rate becomes higher as the surface expands quadratically with radius. In the final stage, the growth rate goes down, as contact areas start to overlap. The general mathematical formula for the Avrami equation is given as Equation 2.7.

$$\varphi(t)=1\text{-}e^{\text{-}kt^m}) \qquad (2.7)$$

with

$\varphi(t)$ = the relative amount of area in contact

k = spreading parameter

m = nucleation parameter

t = time

In Equation 2.7 there are two constants. From the original theory of Avrami; constant '*m*' is related to the process of nucleation of contact areas and constant '*k*' is related to the speed at which the contact areas grow. The constant *m* is controlled by two effects; the number of nucleation points and the number of dimensions in which the nucleus can grow. For the case that healing occurs at an interface, the nucleation area is 2 dimensional, which implies that *m* should have a value of 2 (Avrami 1939; Wool and O' Connor 1981). The constant *k* is related to the speed at which the contact areas grow in the radial direction. For bitumen the growth rate it is that parameter *k* is related to the viscosity of the binder.

As mentioned in Section 2.6.2, the amount of instant true contact is related to the magnitude of the applied normal force perpendicular to the healing interface. This implies that when the healing period starts the amount of area in contact is more than 0. This means that t in Equation 2.7 is not the healing time. An additional time parameter is needed to account for the amount of contact created during the assembly of the surfaces. This can be done by introduction τ_0 as an initial value for *t* that corresponds to the amount of area that has already been brought into contact in combination with parameter τ that accounts the time that has passed since the start of the healing period, see Equation 2.8.

$$t = \tau_0 + \tau \qquad (2.8)$$

with

τ_0 = A value for *t* representing the contact area established before

healing begins.

τ = time since the start of the healing period

For some materials and/or situations Wool and O' Connor (1981) also suggest the model of instant wetting. In this case it is assumed that the whole surface is instantly in true contact. In this case, the area growth with time is a step function being either 0 or 1. The assumption of instant wetting, valid for water on stone, is less applicable to bitumen due to surface roughness (Paragraph 2.6.2.4). This roughness is expected to delays full contact development, requiring time to relax. In spite of this Bommavaram, Bhasin, and Little (2009) did also adopt this assumption in their work when using the two piece healing test. Which might explain the unexpected impact of normal force later found by (Qiu 2012) when he replicated their work, see also paragraph 2.4.3.

2.6.5 Measurement techniques to directly assess the amount of area in contact

The development of true contact is a small scale event. The difference in distance between no contact and contact is in the order of a nano meter. As a result, the creation of contact area is not a phenomenon that can easily be measured directly, as the measurement

requires high resolution while the contact area cannot be scanned directly. Very specialized equipment like an x-ray micro-tomograph, might have just enough resolution to capture the scale of the event. However, this technique has a specific challenge when measuring bitumen. Taking this measurement requires x-ray radiation to be send into the specimen, in order to create an image based on the radiation that is blocked and transmitted by the material, however this radiation also heats up the specimen. As the creation of contact is dependent on the viscosity (Section 2.6.3) and the viscosity of bitumen is temperature dependent, it is expected that creating an tomographic image will actually positively influence the development of contact.

In an exploratory effort to detect micro damage in mastic, Van den Bergh (2011) tried to capture cracks using the micro-tomograph scanner at the TU Delft. He started with several mortar specimen that were thought to have a significant amount of micro damage; the specimens were loaded in shear in the DSR until failure (about 10.000 cycles at 10 Hz). The specimen was taken in a cooled state (5 °C) to the scanner. The scan required 30 minutes, while the scan chamber was not temperature controlled. The resolution of the scan was 1µm. Only in one of the specimens, something was visible that could be a crack. It was concluded that, although the technique seems promising, an approach should be introduced to fix cracks or damage before the scan starts.

2.7 INSTANTANEOUS STRENGTH OF SURFACES IN CONTACT

2.7.1 Adhesion and cohesion in healing

The material healing model from Section 2.4 describes that the creation of surface contact results in an instant strength, as also described by Bommavaram, Bhasin, and Little (2009). The origin of this strength is adhesion between the two surfaces. When studying healing, the adhesion of two bitumen surfaces of the same material can also be seen as cohesion. However, as this thesis focusses on what happens at the contact development of surfaces, which can deviate from the bulk in both structure and chemical composition, it is decided to stick to the term adhesion, even though the surfaces are of more or less the same material.

The adhesive power of bitumen is quite clear for people who have worked with it. Bitumen tends to stick to anything it touches and consequently cleaning glasswork and tools can be a tough job. Therefore this sub-chapter tries to explain the physics behind the stickiness of bitumen and aims to relate this to the process of adhesion and healing.

2.7.2 Adhesion and surface energy

As already mentioned in Section 2.5.4 molecules are attracted to each other by intermolecular forces. These intermolecular forces also form the bases of adhesion (and cohesion). The magnitude of these intermolecular forces in adhesion depends on the surface energy and the distance between the surfaces. The concept of surface energy is already introduced in 2.6.3. The impact of distance will be illustrated below more

detail. Intermolecular forces are active at a very close range, which means that they become dominant on length scales smaller than 100 nm, however are not relevant when distances exceed 10 μm (Kendall 2001). This importance of close range can help to understand why materials with a high elastic modulus are not sticky. When two surfaces of a stiff material like steel are brought together, the inevitable roughness combined with the stiffness of the material, will result in a very limited number of small contact points at a molecular level, as illustrated in Figure 2.32. Consequently, the number of molecules that are close enough to experience molecular interaction is very limited, that together add up to a relatively small adhesion force that is not detectable on a macroscopic scale. If we pick up our coffee cup from the table, there is a molecular adhesion force present, however it is too small for us to notice in comparison to the self-weight of the cup.

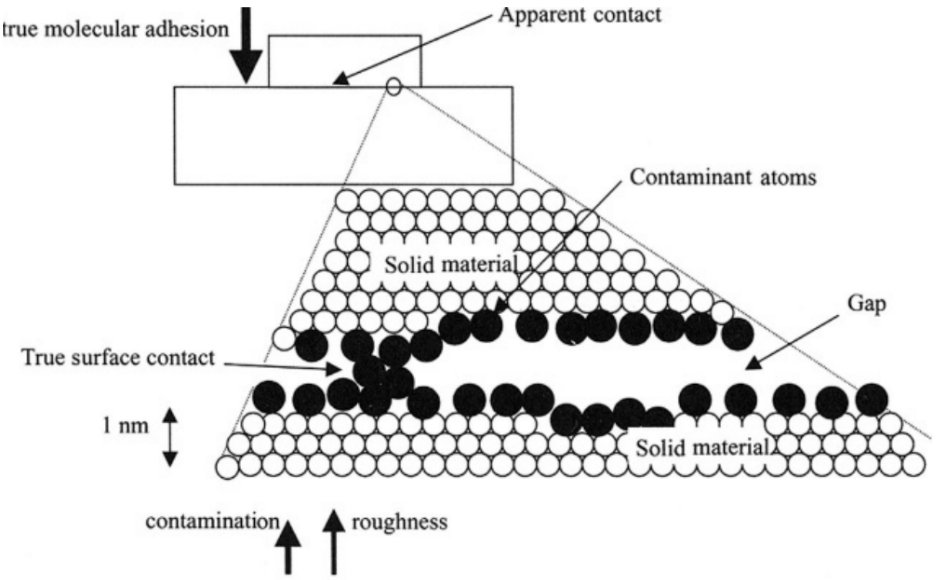

Figure 2.32 Apparent lack of adhesion due to limited contact between surfaces (Kendall 2001)

Bitumen is relatively soft at ambient temperatures and consequently low stress levels can already result in large deformations. Therefore in spite of a slight surface roughness, the amount of area that comes into close contact when a piece of bitumen is placed on a table is much larger compared to our coffee cup. In this case, the adhesive force could become large enough in comparison to the self-weight to experience stickiness. When the piece of bitumen is left overnight the bitumen has time to deform viscously under the influence of gravity and intermolecular forces, increasing the contact area and with that the adhesive force to a point where we simply cannot remove the bitumen from the table without a solvent. The ability of bitumen to deform viscous in relatively short time under relatively small loads is part of the explanation behind the adhesive power of bitumen; a

relatively large area of the bitumen can come into close enough range for intermolecular force to influence the macroscopic behaviour. This also provides an explanation why the stickiness of bitumen is so temperature dependent; a piece of bitumen at -10 °C is not sticky at all, as the material is will behave very elastic and stiff under these conditions; and will therefore not deform enough to generate significant intermolecular interactions with another surface.

2.7.3 From intermolecular forces to macroscopic adhesion

As introduced in the previous section, intermolecular forces form the basis for an adhesion force between two objects. However, even if surfaces are in full contact, surface energy does not translate directly into macroscopic adhesion, as local mechanisms influence how a microscopic surface energy translates in the macroscopic adhesion. One relevant case from Kendall (2001) will be paraphrased below to illustrate that there is much more to adhesion than surface energy alone.

> *Imagine a test set-up where a water droplet is placed on a glass sheet and a small plastic strip is placed on top of the droplet, see Figure 2.33. The so called peeling force can be measured to assess the amount of adhesion. In this set-up the force needed to peel the plastic film of the water is 1 mN for a strip with a width of 10 mm. This is in line with the force that can be calculated from the surface energy, which adds up to 0,72 mN. However, when the temperature is lowered below 0 °C and the drop of water freezes, the peeling force increases to 100 mN. The surface energies of the materials involved haven't changed significantly due to the temperature change as they are chemically the same, however the observed adhesion is a two orders of magnitude larger.*

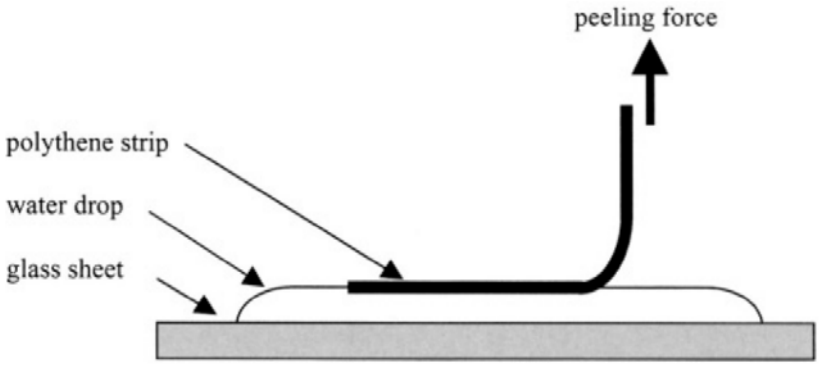

Figure 2.33 Peeling force needed to overcome adhesion of a poly ethylene strip (Kendall 2001)

> *The difference can be explained by the fact that at the moment the strip is in contact with ice, the damage mechanism changes from pure molecular adhesion to cracking. Cracking is an energy driven process, as a consequence we cannot*

simply look at the amount of area in contact and connect it to a strength per m^2, as can be done for a fluid surface. The work of adhesion of a cracking failure requires more parameters to evaluate than only the surface energy. As a result the macroscopic surface adhesion is not only dependent on surface energy, but also on stiffness and viscosity of the materials involved in the interaction. As a consequence the measured adhesion force can be orders of magnitude higher compared to the surface energy, as also demonstrated in this example.

For the case of bitumen, the viscosity also has a large effect on the amount of energy that has to be invested to break the adhesive connection. Therefore in adhesion not only surface energy and physical distance between the surfaces are influencing parameters, but also the stiffness and the viscosity of the bitumen. Due to these many influencing parameters, the absolute strength of the adhesion of bitumen is very hard to predict. This theory is the explanation why the macroscopic adhesion measured by (Little, Lytton, Williams, and Chen 2001) could not be converted into surface energies. However, general trends can be taken from the relations between the parameters in adhesion. For instance, if the surface energy is the same for two materials, the observed macroscopic adhesion is expected highest for the most viscous, or stiff, material as more energy is needed to deform this material.

2.8 HOMOGENISATION OF CONTACT AREAS

This section will explain how the healing interface homogenizes with time. As mentioned in Section 2.5.4, due to thermal energy a molecule has kinetic energy in the form of vibration, these vibrations cause collisions with other molecules resulting in rotations and translations. The resulting path that a molecule takes is random and called Brownian motion. The path that a molecule takes depends on its size and shape combined with the molecules that surround and the temperature. Molecules in solids remain largely fixed due to strong interactions, while those in liquids move much faster. Within a semi-solid like bitumen, molecular movement is slow but present.

The average speed at which molecules travel in a certain medium is defined as the diffusion coefficient D (m^2/s). The rate of movement of molecules within that material itself, is called selfdiffusion. Bitumen is a rather compact arrangement of large (300 amu) to very large molecules (1000 amu), see Section 2.5.4. When these large molecules move around, they will collide easily with other molecules or get stuck in between the branches of other large molecules. As a result, the speed of selfdiffusion in bitumen is rather slow compared to real liquids.

In case of concentration differences, molecular movements collectively drive net transport from high to low concentration (Einstein 1905). If there are concentration differences of certain type of molecules between the healing interface and the bulk, due to this transport phenomenon these will reduce with time. Fick's second law of diffusion

(Equation 2.9) can be used to calculate molecular concentration as a function of time and the (self-)diffusion coefficient. In Section 6.2.4 of, a plausible assumption is formulated for the self-diffusion coefficient of bitumen.

$$\frac{C_x}{C_0} = 1 - \mathrm{erf}\left(\frac{x}{2\sqrt{Dt}}\right) \tag{2.9}$$

With

t = time;

x = distance between the bulk area and the healing interface;

C_0 = concentration at the bulk;

C_x = concentration at location x;

D = diffusion coefficient.

Equation 2.9 implies that the process of homogenisation is driven by concentration differences between the healing interface and the bulk. As a result, the process of homogenisation will initially be fast when concentrations differences are largest and will slow done with time and approach an asymptotic value as the concentration difference diminishes over time.

2.9 CONCLUSIONS

2.9.1 Influencing factors on healing

Based on extensive experimental studies described in this chapter, several key parameters influencing healing have been identified, along with their specific effects. This provides the answer to the first part of RQ1; describing what is known about healing. A distinction is made between three types of parameters; external, material and damage related parameters. This distinction is made to create more clarity in the role they play in the healing mechanism.

2.9.1.1 *External parameters*

In past research the most consensus has been achieved on which external parameters influence the healing of asphalt. Most research concludes that both a longer **rest time** and a higher **temperature** result in more healing. Time and temperature are 2 fundamental physical quantities controlling physical processes. Experimentally, an upper limit to this positive effect of rest time and temperature is often reported, indicating that there is a limit to the positive impact of both rest period and temperature on healing.

There are a number of studies that report on the positive influence of a **compression force** perpendicular to the crack on healing performance, see Section 2.3.3 and 2.4.

This implies that the **stress state at the healing interface** should also be considered as a parameter. The impact of stress state might be related to the observation that when healing is studied using fatigue damage, **stress controlled** tests consequently result in more healing, compared to **strain controlled** tests.

2.9.1.2 *Material parameters*

Most material parameters that have been suggested to influence healing are related to the binder. Properties of the binder that influence healing capacity are **viscosity or binder hardness** (Section 2.3.2), **surface energy** (Section 2.4), **molecular mobility** interpreted as chain length (Section 2.4) and possibly **temperature expansion** of a binder (Section 2.3.7). A binder with a higher penetration value (lower viscosity) results in a higher level of healing. A binder with a higher surface energy is reported to result in a higher instant healing when cracked asphalt surfaces are brought into contact. A higher molecular mobility will also result in faster healing. Finally, it is also hypothesized that a binder that expands more when it is heated will result in more healing as this will result in more contact area at the healing interface.

Next to these binder properties it has also been shown that the volumetric design of the asphalt mix influences the healing capacity of the asphalt mix as a higher **binder content** will result in more healing (Section 2.3.2 and 2.3.3).

2.9.1.3 *Damage parameters*

It is also recognized that the extent and nature of the damage influences the level of healing that can be achieved (Section 2.3.2 and 2.3.6). **Micro damage** will heal to a large extent even at low temperatures and short healing times. **Fully cracked specimens** will only show significant healing under extremely favourable conditions.

2.9.2 Research gaps in healing research

The literature review has also answered the second part of RQ1; What is still unknown about healing? An overview of these unknowns are summarised here to fully answer RQ1. These unknowns are also used to formulate additional Research Questions, which that have already been presented in Section 1.4.3.

Under a wide range of conditions healing of asphalt is observed, proving that this phenomenon exists and is relevant for asphalt performance. However, research has also demonstrated that the quantitative determination of healing behaviour heavily depends on the test method used. Showing not only differences in observed healing, but also in ranking of material performance between test methods.

Literature shows that an important obstacle in understanding healing, stems from the lack of insight in the damage development under fatigue loading. When studying fatigue, there is still an ongoing debate on, which part of the performance loss can be attributed to real damage and which part is caused by biasing effects. This ambiguity in

our understanding of damage also results in multiple definitions of the moment of failure. As a healing test starts with damage, this vague definition of damage, blurs the starting point and consequently also the result of a healing test.

Over time, much effort has been invested in trying to understand why different test methods lead to different healing results, however up until now, no general accepted answers have been found. Many studies have examined healing performance by analysing energy loss during deformation cycles and its variation over time. However, methods identified as successful by one research group usually did not result in the same level of success in other groups, consequently researchers continue to refine and enhance these techniques through ongoing efforts.

Much of the debate on damage described above, originates from the fact that after a fatigue test, the stiffness recovers fast and almost fully during a period without loading, while the number of loads to failure is much less affected by a rest period. This poses an interesting dilemma on which parameter to focus on during healing research. Stiffness recovery can be measured easily, and also has the advantage that it can be tested not destructive. However, it seems to have a limited correlation with service life, in terms of the number of load to failure. The real recovery of performance with respect to service life requires much more intensive and complicated test programs, while also tools are lacking to verify the relevance of performance measured in the laboratory with the performance in practice. All these factors and limitations should be taken into consideration when setting up a healing research.

The lack of insight in damage level and appropriate analyses method demonstrates that current test methods are not addressing all relevant parameters of the healing mechanism. This implies that a new tests method that is designed with these challenges in mind, could result in more insight in the healing mechanism. This is addressed in RQ2: How can a test method be designed to further increase our understanding of healing? While answering this question, the insights on relevant parameters reported in Section 2.9.1 should also be integrated ensure that key parameters are taken into account when designing a new test set-up. The design and set-up of a new test set-up for healing will be addressed in Chapter 3.

2.9.3 Material model for healing of asphalt

A material model for healing has been introduced in Section 2.4.1, which provides a theory of the healing mechanism of a discrete crack in asphaltic material. This model interprets healing as the combined result of two key steps; first the contact between the two crack surfaces has to be restored, next this contact area needs to homogenize over time. The amount of evidence presented to validate this model is limited, only presenting a small number of tests, with limited variation in the parameters.

The literature review also attempted to present theoretical knowledge concerning the two proposed mechanisms from a material science perspective. This resulted in a first answer

to RQ5; Are there more insights from the more general field of material science that can increase our understanding of healing of asphalt binders? The literature has proven that the mechanisms provide a very plausible basis for the observed healing behaviour. However, also from this perspective many details from this model remain unknown and are challenging to measure and or quantify, especially for bituminous materials.

The new test method that will be described in Chapter 3, will be used in this thesis to examine the two research gaps related to the creation of contact and the development of this contact over time in more detail. The development of contact relates to RQ3; How does the creation of contact impact healing of bituminous binders?, which will be addressed in Chapter 4. RQ4 focusses on the development of contact over time and will be addressed in Chapter 5, where the healing test is used to study the impact of time in more detail.

The information obtained in Chapters 4 & 5 are used to augment the existing healing model answering RQ 6 in Chapter 6; How can a more accurate material model be developed to describe the processes governing the healing behaviour of bitumen addressing both mechanical and physicochemical aspects? As the insights obtained with the test program did not provide all necessary information, within this chapter some additional efforts were done to further answer RQ5 using more fundamental principles from material science.

3

DEVELOPMENT OF A NEW HEALING TEST

DEVELOPMENT OF A NEW HEALING TEST

The aim of this chapter is to describe the development of a test set-up that helps to further understand the phenomenon of healing of bituminous binders. In Chapter 2 the mechanisms of healing was described as the combination of bitumen surfaces regaining contact and the load bearing capacity this contact. To study the regeneration of contact area, requires an explicit definition of the area of the healing interface, which is not the case in fatigue tests. The requirements for a new test set up that can uncover more of this regeneration of contact area is presented in Section 3.1. This section also addresses other parameters that need to be controlled more specifically. Next, the test and specimen preparation methods are presented in detail in Section 3.2. Section 3.3 introduces a reference specimen that can be used to assess a healing ratio. In Section 3.4 the strength increase of the bitumen specimen after production is discussed. In Section 3.5 the impact of strain rate during the tensile test on the detected strength is reported. In Section 3.6 the impact of temperature on the healing test is discussed. Section 3.7 discusses artefacts that occur while using the test method and proposes how these should be addressed when analysing the results. Finally Section 3.8 closes the chapter by summing up how this new test method can help to analyse healing behaviour and provides recommendations for further improvement of the test method.

3.1 REQUIREMENTS FOR A NEW TEST METHOD

3.1.1 Identified parameters influencing healing

In Section 2.9.1 an overview is presented of the key parameters that influence healing. When designing a test set-up these should be kept in mind, therefore they are presented in Table 3.1.

The material parameters from Table 3.1 will not be addressed in the test design, as the test intend to compare healing performance of different materials. However, it should be kept in mind that if the influence of different material parameters on healing is studied, these parameters need to be determined.

From the external parameters temperature and healing period are off course essential to monitor in a healing test, as this is already standard practise this will not be discussed any further. The force perpendicular is more interesting as this is almost never measured. The new test set-up aims to discern itself from the existing methods, by explicitly controlling this parameter.

The next focus of the set-up is to explicitly control the extent of damage. Damage can be seen as the combination of an area or a volume that exhibits damage and an intensity of this damage. In a fatigue test the level of damage remains undefined (see Section 2.2).

Table 3.1 Overview of influencing parameters on healing (based on Section 2.9.1)

Type of parameter	Parameter
External	Time
	Temperature
	Force perpendicular to the healing plane
Damage	The size and extend of (micro-)cracks
	Area of the surface that is in contact
Material	Viscosity or binder hardness
	Surface energy
	Molecular mobility (Self-diffusion speed, chain length, molecular shape, etc.)
	Temperature expansion
	Binder content (only relevant for asphalt mixtures)

When a specimen is loaded until failure, the amount of damage is known, although the damaged area is often heavily deformed or very irregular shaped. A specimen damaged until failure will therefore not result in a well-defined surface that can serve as a clear starting point for a healing test. This issue can be solved by starting a healing test with an artificial damage, which allows for the creation of a clearly defined healing interface and damage intensity. In this case any measured restoration of material property can be quantified and attributed to a specific surface area.

As discussed in the previous section a known damage area results in a known healing area, allowing for a more quantitative healing measurement. This approach has already been proposed for bitumen by Bhasin, Little, Bommavaram, and Vasconcelos (2008), see Paragraph 2.4.3. After bringing the two pieces of bitumen together the stiffness of the material in response to shear loading is measured over time to assess the process of healing. This approach has three drawbacks. The first drawback is that the test does not explicitly monitor the surface approach, limiting its ability to study contact area formation and its impact on healing. The second drawback is that the restoration is measured using stiffness. As discussed in the literature review (Section 2.2), the stiffness recovery includes biassing effects which makes it a flawed indicator to asses healing of physical discontinuities in the material. Thirdly, as mentioned in Paragraph 2.4.3, Qiu (2012) has pointed out that the variation of the normal force during this test was quite intense, which had an effect on the observed healing. In order to address these draw-backs the test concept of Bhasin, Little, Bommavaram, and Vasconcelos (2008) is modified as will be discussed in the following sections.

3.1.2 Mode of loading

The stress state to assess the healed performance, after a healing period should be as simple as possible. This can be achieved by applying a single stress, perpendicular to

the healing interface. This stress needs to be applied in tension mode, as a compression force perpendicular to the healing interface would trigger more healing and therefore influence the result. Therefore the mode of loading selected for the test set-up is uni-axial tension. Next, it is decided not to focus on the stiffness gain as this is a flawed parameter to assess restoration, but to determine the recovery of strength. This implies that the performed healing test is destructive and therefore requires reference specimen that can be used to verify strength and stiffness of an undamaged specimen. This specimen should be produced and subjected to the same conditions as the healed specimen.

3.1.3 Conceptual design of the healing test

A flow chart of the test procedure is presented in Figure 3.1. The test set-up is based on two separate pieces of bitumen that will be brought together under controlled conditions. At the start of the test, the two pieces of bitumen are not in contact and consequently the healing strength is 0. The healing tests starts with the controlled assembly of the two flat bitumen samples, creating a healing interface where they make contact. This first step is called the assembly phase. Next the healing phase starts, where the assembled specimen is left to heal under controlled conditions. After a specific healing period the pieces of bitumen are pulled apart by means of a displacement controlled uniaxial tensile test. The strength measured during the tensile test is interpreted as healing at the artificial healing interface. When the measured healing strength is compared to the original material strength a healing ratio can be determined. During the whole test, the temperature and healing period should be controlled, making it possible to monitor strength development over time.

The author realizes that the selected test method described above is not really the same as the healing of (micro-)damage in asphalt. Therefore, the results of this type of test set-up cannot directly be related to healing observed in fatigue tests or full scale pavements. However, the approach can provide valuable insights in the fundamental understanding of the recovery of strength in bituminous contacts and could therefore also provide a tool that is able to rank the restoration ability of bituminous binders and with that the healing ability. The test could also be used for binders that have been aged and or rejuvenated, in order to assess the impact of ageing on healing. However, when interpreting the results it should be taken into consideration that there are important differences between this test and real damage. In the first place the artificial surface is different from a real cracked surface. Next to this, bitumen behaviour is different from an asphalt mixture which also contains filler and larger aggregates. Finally the exposure to oxygen or moisture will be different in real damage compared to this artificial situation. In the following sections the schematic healing test described above will be transformed into a real set-up, describing the test apparatus, the test specimen and the test procedure in detail.

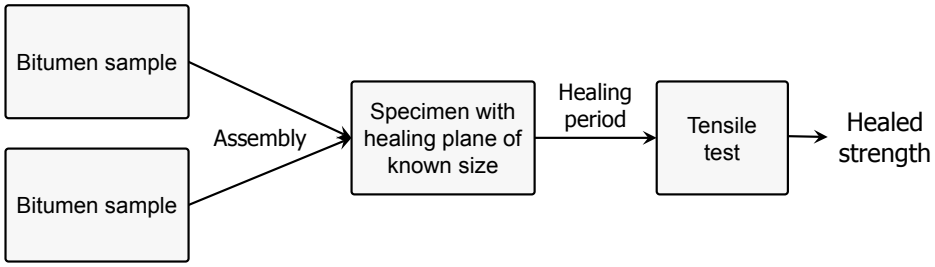

Figure 3.1 Flow chart of consecutive steps in healing test set-up.

3.2 DESIGN OF THE TEST METHOD

3.2.1 Test machine

Having control over temperature and healing time during assembly and loading is an important requirement for the test set-up. These requirements are met by the Anton Paar, EC Twist 502 which is shown in Figure 3.2. This machine is designed to load specimens in shear while measuring or applying a normal force, however if no shear force is applied this apparatus can also be used to focus on tension and compression loading. The test machine used at the pavement engineering section at the TU Delft has an CTD 180 oven which allows for high precision control (+/- 0,2 °C) of the temperature of the sample between -20 and 180 degrees Celsius. The software that is controlling the machine is flexible, allowing for the programming of several consecutive steps in a single test run. The machine has spindles that are designed to fix cylindrical specimens with a diameter of 6, 8 or 10 mm. These spindles are used to clamp the bitumen samples.

Figure 3.2 Anton Paar, EC Twist 502. Left: an overview of the machine, Right: with the oven open showing testing camber and clamps.

3.2.2 Specimen design

The half-specimens of bitumen are specifically designed to fit into the Anton Paar testing machine. This is done by integrating a stainless steel ring in the design, which can be used to clamp the half-specimen during testing in the machine, see Figure 3.3. The specimen design also aims to regulate the size of the healing interface by controlling amount of contact area that is created during the assembly phase. In the design of the specimen an elevated contact area is created with a diameter of Ø5,5 mm, resulting in a contact area of 23,8mm^2, the geometry of the half-specimen with the contact area is shown using a top view and cross section in Figure 3.3.

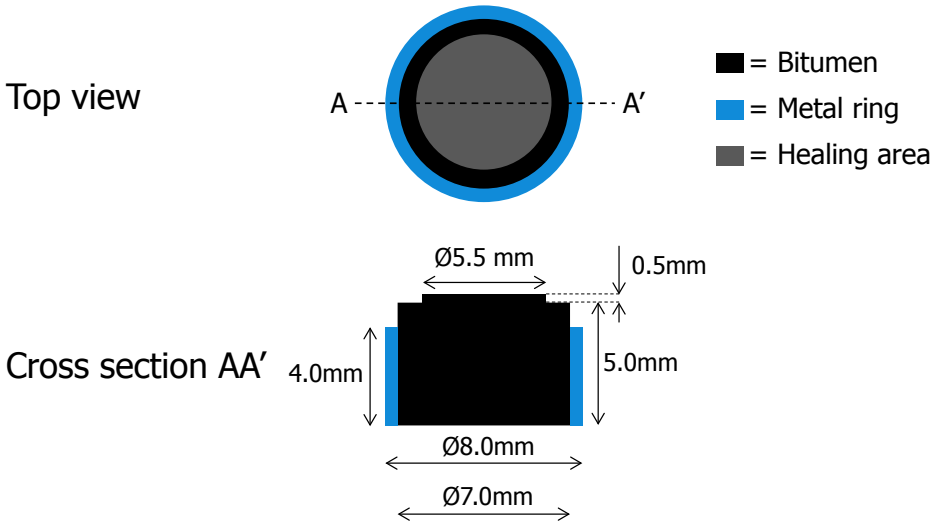

Figure 3.3 Top view and cross section of one half-specimen of bitumen, indicating dimensions and material use.

Appendix A is a laboratory protocol describing how these specimens can be made and what procedures should be used. Figure 3.4 shows a half-specimen made of bituminous binder using this protocol.

Figure 3.4 Photo of a single half-specimen.

3.2.3 Procedures for assembly and healing of half specimens

3.2.3.1 *General steps of assembly procedure*

A schematic impression of the assembly procedure is shown in Figure 3.5. Phase 1 represents the assembly phase where two bitumen half-specimens are brought together. This is done by applying a normal force as indicated by the arrows. During this step a round piece of silicon paper with a central hole of Ø5,5 mm is placed between the half-specimen to ensure that the contact area during assembly and healing remains limited to Ø5,5 mm, a photo of this piece of paper on a specimens is shown as Figure 3.6. Phase 2 is the healing phase where the surfaces are in contact and healing can take place over a prescribed period of time at a specific temperature. Phase 3 is the tensile phase where the degree of healing is tested by pulling the two half-specimens apart. This is done by a displacement controlled uniaxial tensile test.

There are two approaches worked out for the assembly procedure of the half-specimens into a complete specimen. In the first approach the specimens are assembled inside the testing machine. In the second approach the specimens are assembled by hand in a temperature controlled room. A general approach for both procedures and their characteristics is presented here. The details of both approaches can be found in **APPENDIX A.**

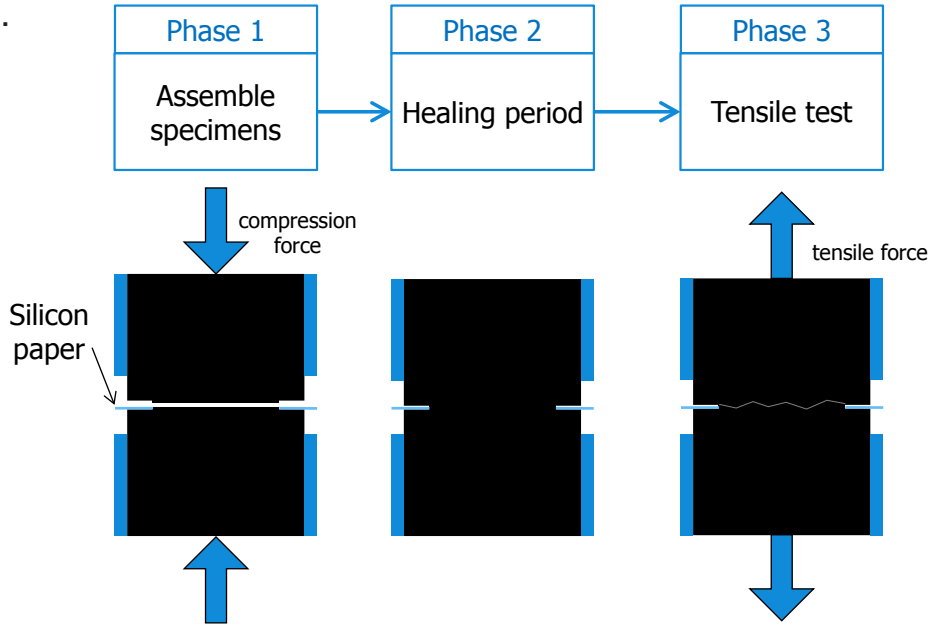

Figure 3.5 Schematic impression of assembly, healing and testing of specimens.

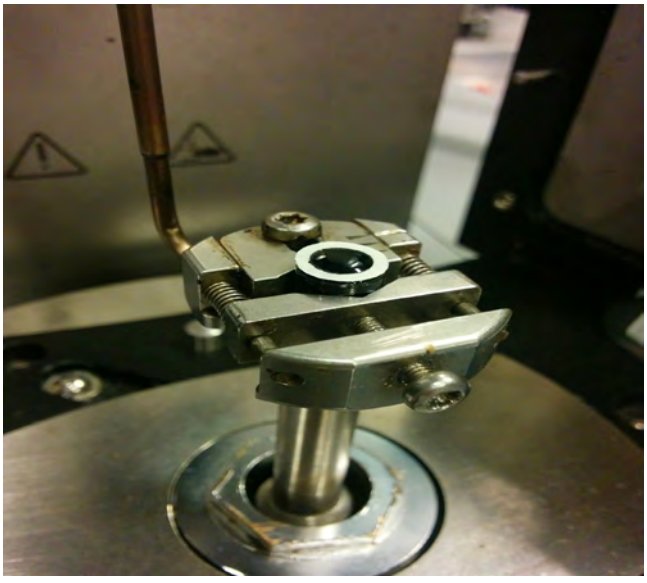

Figure 3.6 Silicon paper placed on a half specimen before assembly.

3.2.3.2 *Assembly phase inside the machine*

In case of assembly inside the testing machine, two half-specimen are brought together with a controlled displacement rate. Half specimens are placed both in the top and bottom clamp and are kept under temperature controlled conditions. When the two half specimens touch a normal force builds up, see Figure 3.7. The displacement stops when a predefined assembly force is reached, at this moment the assembly phase is completed. For the assembly reported in Figure 3.7, this is 1,8 N. During the consecutive healing phase, the distance between the half specimens is fixed. During this period any stress that been built in the specimen can relaxes, the rate at which this happens depends on the hardness of the binder. In the current test set-up this relaxation over time was not captured. For future research it would be interesting to verify with Anton Paar if it is possible to also store this information, as this relaxation time is also relevant when studying the creation of contact.

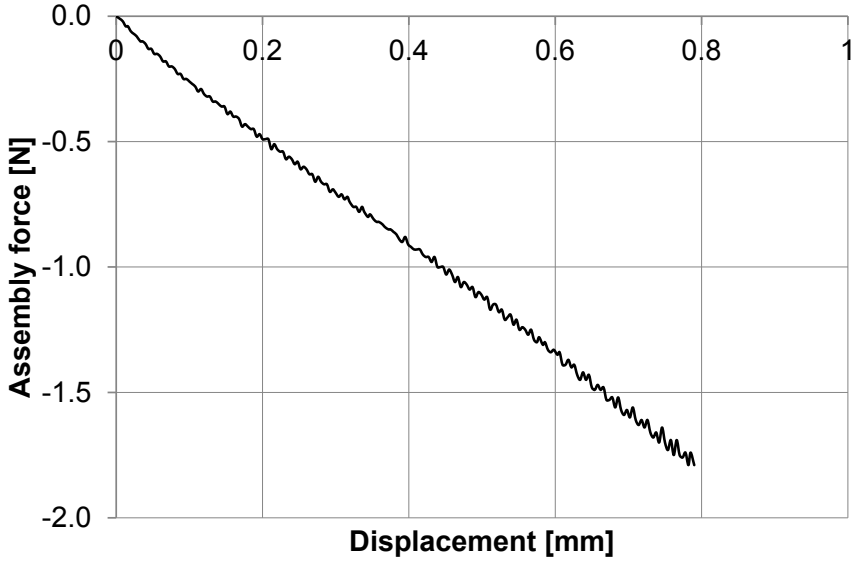

Figure 3.7 Characteristic assembly curve for a 70/100 bitumen sample assembled at a displacement speed of 0.04 mm/s until a force is reached of -1.8 N.

Due to the nature of the Anton Paar testing machine and accompanying software, there are only two parameters that can be varied during the assembly phase; the displacement rate that brings the halfspecimens together and the magnitude of the normal force that triggers the end of the assembly phase by stopping the displacement of the top spindle. These parameters are referred to as ‘assembly rate’ and ‘assembly force’, respectively. A characteristic force displacement curve for the assembly phase is already presented as

Figure 3.7, here the assembly rate was 0,04 mm/s and the assembly force was 1,8 N. The small “waves” in the curve indicate that the displacement is not uniformly applied, but step wise. The overall shape of the curve shows a linear relation between force and displacement.

In paragraph 2.6.2.1, it is stated that for linear elastic materials, the amount of contact created is linearly correlated with the applied normal force. As the assembly curve shows a more or less linear trend between force and displacement, it seems plausible to assume that the amount of contact area created during the assembly phase is also correlated to the applied assembly force for this viscoelastic material. However, even if there would be a linear correlation, as the complex modulus of each binder is different, a single assembly force will result a different amounts of contact area for different materials.

The moment that the surfaces of the two specimens first come into contact, is the moment that the healing process at the interface starts, indicating that healing already occurs during the assembly phase. The exact duration of the assembly phase depends on the assembly conditions. For example, the assembly phase for which the force displacement curve is shown in Figure 3.7, lasted 20 seconds. However, within the research slower assembly rates have also been applied resulting in an assembly phase of 800 seconds. After the assembly phase is completed, the transition of the testing machine between compressive and tensile mode, required to executed a tensile test, costs 10 seconds. Therefore, the shortest healing period that can be applied is not 0 seconds, but the total of the time from the moment the surfaces touch till the moment that the tensile test can start. For the example shown in Figure 3.7 this is 30 seconds.

Practical considerations limit the maximum healing period which can be applied using this approach; when the assembly phase is executed inside the machine, the machine remains occupied for the whole healing period and the tensile test. Within this research practical considerations, with respect to the availability of the testing machine has resulted in a maximum healing period of 200.000 s (~55 hours). The shortest and longest healing period that can reasonably be applied, in case of assembly inside the testing machine, are reported in Table 3.2. In this table the values matching the example from in Figure 3.7 are also presented.

Table 3.2 Overview of time periods required for each phase of the healing test when specimens are assembled inside the testing machine, including shortest and longest healing period.

	Test Phase			
	Assembly	**Transition**	**Shortes healing period**	**Longest healing period**
Time	1 – 3600 s	10 s	11 s	200.000 s
Time in example Figure 3.7	20 s	10 s	30 s	200.000 s

3.2.3.3 *Assembly phase in a temperature controlled room*

The assembly phase can also be executed in a temperature controlled room. In this case specimens are assembled in a stainless steel tube, with an inner diameter of 8,5mm. This tube envelopes the stainless steel rings of the two halfspecimens, ensuring vertical alignment during the assembly and healing phase. The inside of the tube is covered with silicon paper to prevent sticking of any excess bitumen to the tube. A photograph of the bottom half-specimen inside the alignment tube is presented in Figure 3.8. The healing period starts when the top specimen is placed in the tube.

Figure 3.8 A half-specimen in the alignment tube with the silicon paper controlling the contact area visible on top.

In this set-up the normal force perpendicular to the healing interface originates from gravity. This consist in the first place from the weight of the top half specimen (0,6 gram or 0,06 N). Next to this, small weights can be added on top of the combined specimen to increase the normal force, see Figure 3.9. The largest weight that fits on top of a specimen is 10 gram, resulting in a total load of 10,6 grams (or 0,11 N).

Figure 3.9 An assembled test specimen with a weight of 1 gram placed on top.

3.2.3.4 *Advantages and disadvantages of the two assembly techniques*

The biggest difference between the two assembly conditions is the stress at the healing interface during both the assembly and the healing phase. In case of assembly inside the test machine, the initial stress is large; 1 to 2 orders of magnitude higher compared to the stress used during storage healing. However, this stress is present for a very short time. In case of assembly inside the storage room, the stress at the healing interface is much smaller, however it remain present during the whole healing period. The force present at the healing interface during all phases of the test is schematically shown in Figure 3.10. The grey areas indicate during which periods the force and displacement are recorded during this research.

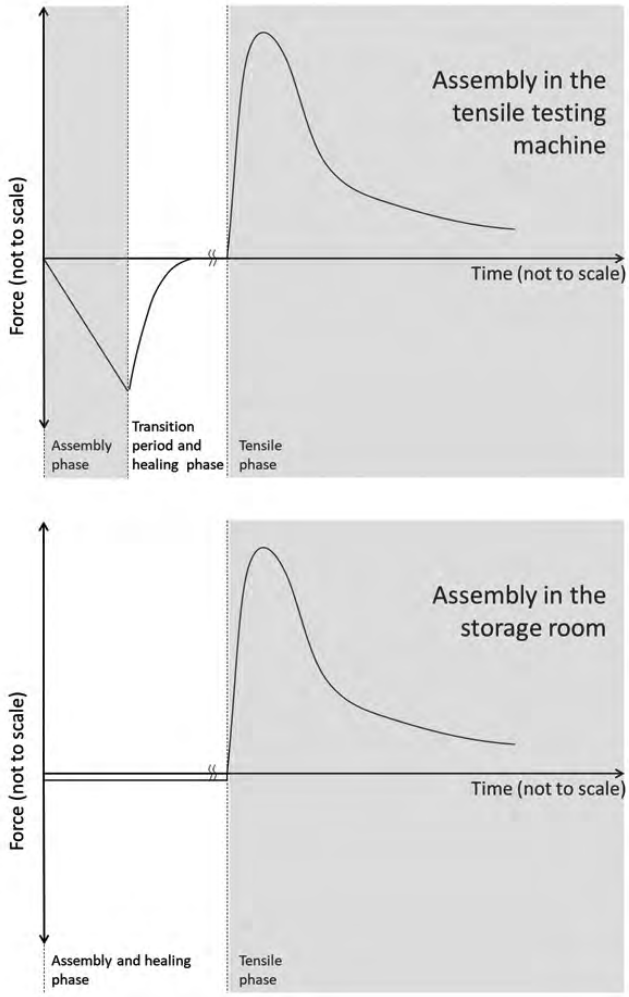

Figure 3.10 The normal force in the healing specimen, for the case of machine assembly (above) and storage room assembly (below), in grey the time period is indicated when forces and deformations are recorded.

Both methods have advantages and disadvantages, the preferred method depends on the aim of a study. Assembly inside the machine ensures precise control and enables short healing times, but limits test series size and maximum healing period. When storage room assembly is used, there is a larger risk of damage to specimen during transport and handling. This can be mitigated by making more spare specimens. Storage assembly also introduces a larger variation in test results, which are partly due to inherent larger measurement inaccuracies. Especially the determination of the distance between the steel rings, is inaccurate, see Figure 3.11. This distance is needed to determine the displacement rate that is required to ensure the desired strain rate. An error in the measured distance will affect the applied strain rate, and result in an error in the measured strength.

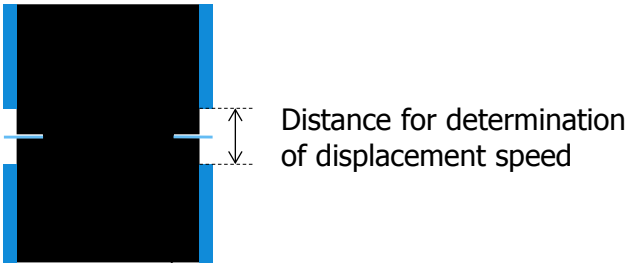

Figure 3.11 The distance between the rings in a specimen which needs to be measured.

3.2.4 Assessment of healing using a tension test

During the tensile test, the assembled specimens are pulled apart to assess the tensile strength of the healing interface. The tensile phase is quite similar for specimen that have been assembled inside the testing machine and in the temperature controlled room, however there are some small differences that will be discussed here.

The specimens assembled in the machine are already in place and at the right temperature just after the healing period ends. Next to this, the amount of displacement applied during the assembly phase is known, therefore the needed displacement rate during the tensile test is already known before the test starts. Consequently, the tensile test starts automatically after the prescribed healing period has finished. For specimens assembled inside the temperature controlled room some additional steps are needed before the tensile test can be executed. After removing the specimen from the alignment tube, its height has to be measured to determine the required displacement rate. Next, the specimen has to be placed and fixed in the testing machine. This starts with placing the specimen in the bottom clamp, next the top clamp is moved down slowly, until it encloses the top ring of the specimen and can be fixed. A partially mounted specimen is shown in Figure 3.12.

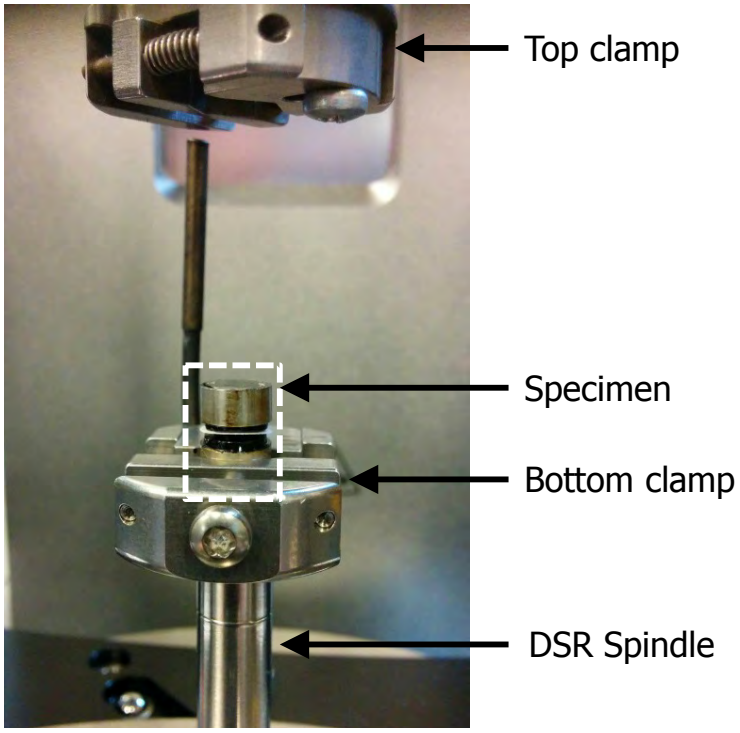

Figure 3.12 Specimen including silicone paper ring fixed in bottom clamp in DSR.

The results of the tensile tests can be presented using load-displacement curves. Figure 3.13 presents two tensile test results; specimens were assembled inside the testing machine and subjected to two different healing periods of 30 s and 20.000 s. The applied strain rate during the tensile test was 0,5 %/s, resulting in an execution time for the tensile test of around 10 minutes. The 30 s healing period, implies that the tensile test started immediately after assembly phase was finished. Both load-displacement curves show a ductile failure, where post-peak strength can be observed. The total applied deformation during the tensile test is 200 to 300% compared to the gap between the metal rings just after assembly. The test conditions used during this research were selected to ensure this type of failure, as the results are more reproducible compared to brittle failure.

The curves show two different possible scenarios for the end result of a tensile test. The specimen that has healed for 30 s loses all strength at an imposed displacement of ~ 4,5 mm, indicating that the two half-specimens are fully separated. When this specimen is studied after completion of the test it can be seen that both half-specimens have undergone a significant amount of deformation, see Figure 3.14.a. The specimen which has healed for 20.000 s is still in one piece at the end of the tensile test (see also Figure 3.14.b).

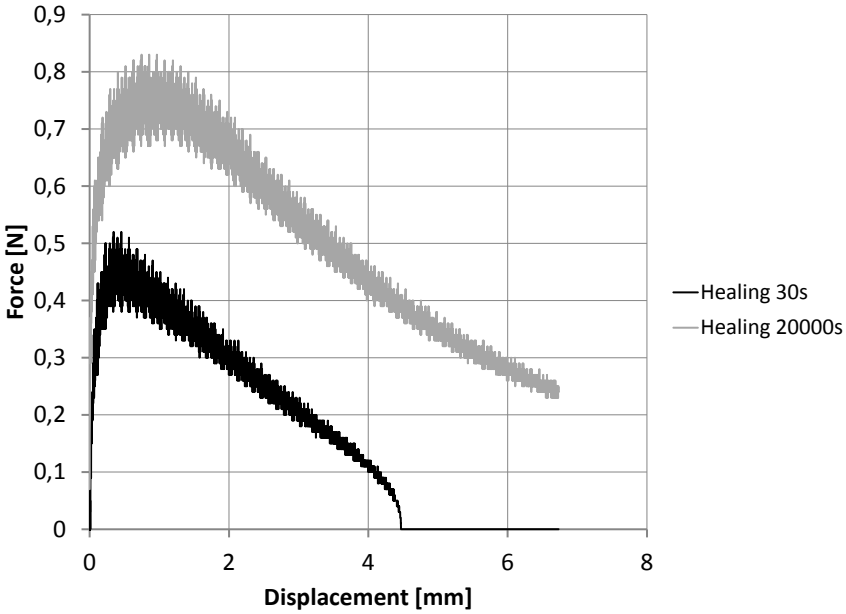

Figure 3.13 Characteristic force-displacement curve of a tensile test for a short and a longer healing period, for healing at 14°C.

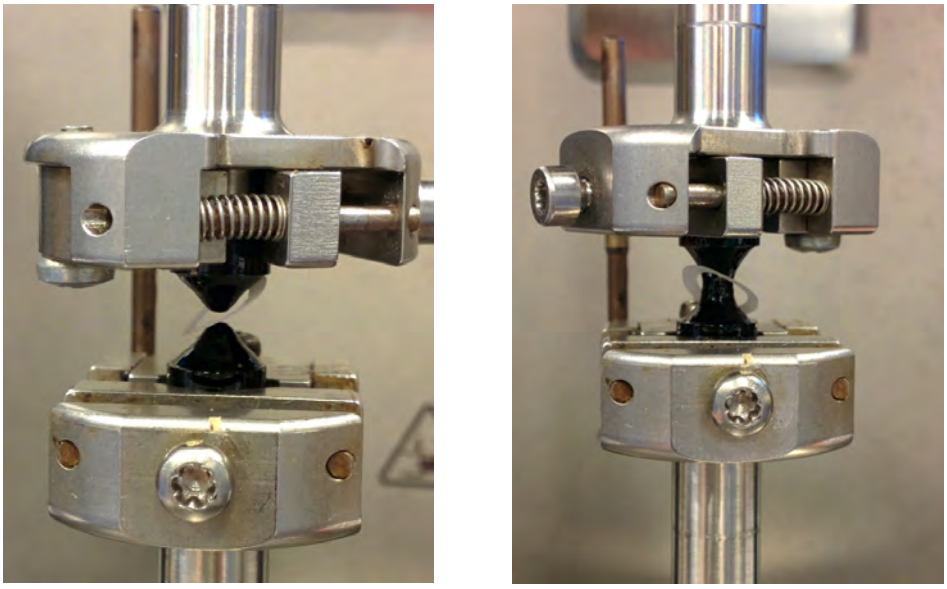

Figure 3.14 Pictures taken from healed specimens after a tensile test; a. specimen after a healing period of 30s, where the healing interface has come apart during the tensile test; b. specimen after a healing period of 20,000s where the specimen has remained in one piece.

Different aspects of the tensile test and the resulting force displacement curve can be used to assess the extent of healing. The most obvious parameter to assess healing is the peak force. However, it is also possible to use the initial stiffness, based on the slope of the force deformation curve before the peak. On the other hand the amount of work that is required for a certain amount of deformation can also be assessed. In this research the most used parameter was the peak force, although the amount of work has also been assessed for some analyses.

There is some noise visible in the data presented in Figure 3.13. It can be observed that the amount of force measured at a single strain varies quite significant resulting in a thick line in the graph. The data sampling frequency is chosen at a relatively high value of 10 data points per second. As also observed in the assembly phase (Section 3.2.3), the deformation seems to be applied in a somewhat stepwise motion by this specific machine. This can explain (part of) the noise in the measured tensile force. Smoother curves are preferred to create readable graphs and for data analyses purposes. In order to smoothen the curves, the running average is used. As a result the average value over a series of points is presented instead of the exact value measured. Figure 3.15 shows a visualisation of the same data as Figure 3.13, but now using a running average over 20 data points. The number of data points to calculate the running average is selected in such a way that the shape of the curve remains similar, while reducing the noise as much as possible. It should be realized that by manipulating the raw data, information can be lost, therefore for some parameters it is preferred to perform the data-analyses on the raw data. In this research the data is smoothened for the presentation in graphs and to capture the curvature of a line, for instance to assess the stiffness or the peak force.

3.2.5 Repeatability

As the presented test set-up is newly developed, it is important to verify the repeatability of the test. Both the repeatability of the assembly and the tension phase are evaluated. To verify the repeatability of the test, three results using one set of assembly conditions and one healing period are compared, for a bitumen with a 70/100 pen grade subjected to a healing time of 2000 s.

Figure 3.16 shows three force-displacement curves that were obtained during the assembly phase of three different specimens made from the same material. In all three cases the assembly force was 1,8 N and the assembly displacement speed was 0,04 mm/s. These conditions were selected to aim for a deformation during the assembly phase of 0,8 mm. The graph shows no data at the exact moment the assembly force reaches 1,8 N due to the data storage interval, which doesn't guarantee capturing that precise point. This is also the reason why the curves do not start at the origin. The results indicate that the same imposed deformation, results in slight differences in the measured force, which results in slight variation in the total amount of deformation applied during the assembly phase; specimen 2 and 3 show almost identical assembly curves, while

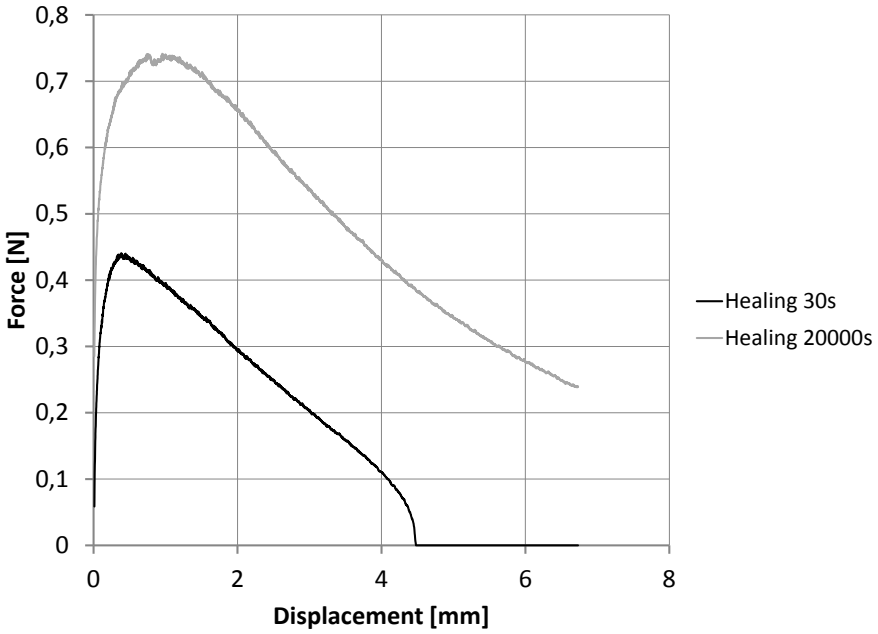

Figure 3.15 Force displacement curve using the same data as 4.15, with data smoothened by using a running average over 20 data points.

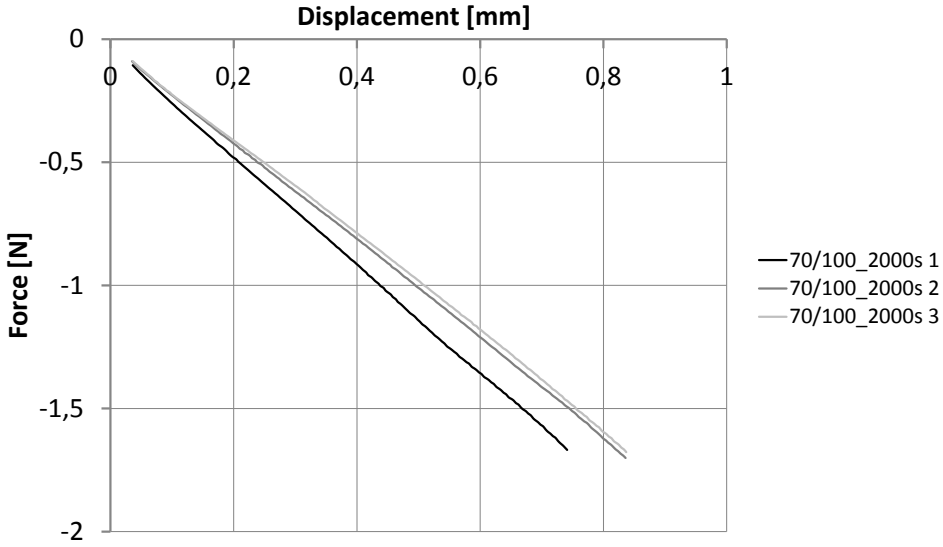

Figure 3.16 Force displacement curves corresponding to the assembly of three different half-specimens; a running average is used to smooth the curves.

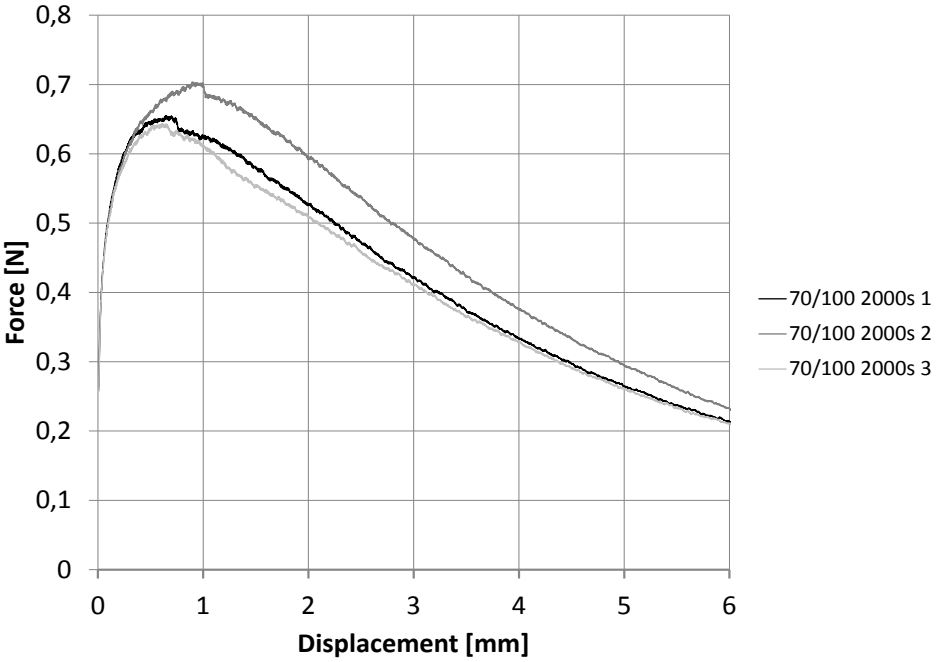

Figure 3.17 Force displacement curve showing the behaviour of a healed specimen during the tensile phase ; a running average is used to smooth the curves.

specimen 1 shows a slightly larger force when the same deformation is applied. The average recorded deformation was 0,84 mm; the largest deformation is 0,88 mm and the smallest is 0,78 mm, the standard deviation is 0,05 mm. As the standard deviation is less than 10% of the average value, it is concluded that the assembly phase of the test has a fair repeatability.

To demonstrate the repeatability of the tensile phase, the same specimens are used as in the evaluation of the assembly phase, described above and shown in Figure 3.16. The results of the tensile phase are presented as force-displacement curves in Figure 3.17. The tensile test was executed using a displacement rate of 11,25 µm/s for all three specimens. This displacement rate matches a strain rate of 0,5 %/s, which corresponds to an imposed displacement during the assembly phase of exactly 0,8 mm. However, in reality, as described above, there are slight differences in the amount of deformation applied for each specimen during the assembly phase. Consequently, the applied deformation rate of 11,25 µm/s, will not result in a strain rate of all specimens of 0,5 %/s, depending on the assembly phase the strain rate will be slightly higher or lower.

The highest detected value for the peak tensile force is in the tensile test is 0,80 N, while the lowest value is 0,73 N. The average value for the maximum tensile stress is 0,76 N. From these data a standard deviation can be determined of 0,029 N, resulting in a coefficient of variation of 0,047. As the standard deviation is less than 10% of the average value, it is concluded that the test has a fair repeatability.

What is also interesting to note from Figure 3.17 is that again two test results are very similar, more specifically those of specimen 1 and 3. This is remarkable as the assembly phase was actually slightly different for these specimens. Therefore, it is also concluded that the slight differences that were observed in the assembly phase do not seem to have a strong effect on the tensile phase.

The number of repetitions presented here is too limited to be statistically sound. Therefore it is recommended that the repeatability is verified using a larger number and also a wide range of tests.

3.3 REFERENCE VALUE TO ASSESS HEALING RATIO

3.3.1 Need for a reference value

Healing is the restoration of performance after damage, therefore healing is often expressed by a ratio that indicates which part of the undamaged performance has been restored. This can be done using Equation 3.1, that has already been introduced in chapter 2, and reproduced below. This equation requires a healed performance and an original performance. As the test set-up with the two separate pieces does not allow to determine an original performance, a reference specimen is required. The test design for a reference specimen is presented in this section.

$$Healing\ ratio = \frac{f_{healed}}{f_{original}} \times 100\% \qquad (3.1)$$

Equation 3.1 also implies that the healing ratio should have a value between 0 and 1; with a value of 0 indicates that there is no healing, a value of 1 indicating full healing, meaning that the specimen performs similar to an undamaged specimen.

3.3.2 Design of the reference specimens

When creating reference specimens it is important to realize that ageing is expected to affect the response of bituminous materials. Due to ageing a bituminous material becomes stiffer, stronger and less ductile over time. This process can be explained by both chemical and physical changes in the material (Jing 2019; Kliewer, Bell, and Sosnovske 1995). This ageing cannot be prevented, therefore when designing a test approach this impact of ageing has to be taken into account. The approach taken in this test design is to

ensure that the reference specimens have undergone a similar amount of ageing compared to the healing specimens. In order to guarantee this, both healing and reference specimens are produced with the same material, at the same time, while exposing them to the same temperature conditioning scheme before testing them at the same age.

Within a previous project at the pavement engineering section of TU Delft (Huurman, Mo, and Woldekidan 2010) the response of mastic is determined using small columns, see Figure 3.18. Their specimen design is adopted in this research for the reference specimen, as preliminary tests executed within this research demonstrated that this geometry is also effective to asses properties of bitumen. Consequently, the reference specimen are bitumen columns with a length of 12 mm and a diameter of 6 mm that have stainless steel rings at both ends, that allow for fixation inside the testing machine. The used rings are the same as the ones used for the healing half-specimen. A curve is added at the ring-column transition to reduce stress concentrations and prevent potential failure at the connection.

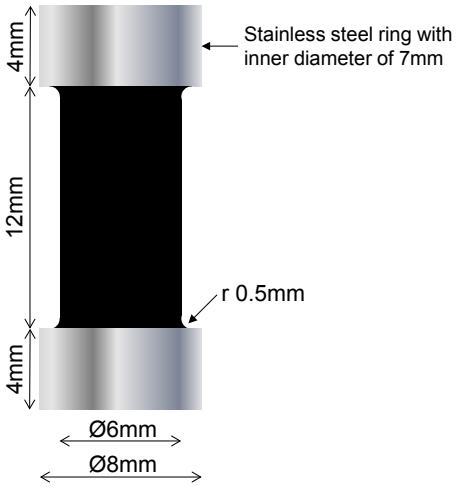

Figure 3.18 Shape and dimensions of reference specimen, consisting of a column of bitumen with stainless steel rings on the top and the bottom to be able to clamp the specimen in the testing machine.

3.3.3 Impact of the specimen height

The shape of the reference specimen (Figure 3.18) is different from the healing specimen (Figure 3.5); especially the height to diameter ratio both designs are different compared to the healing specimen. The reference specimen is higher, resulting in a larger part of the specimen with a constant cross-section. This leads to a more uniform stress distribution in the specimen during a tensile test, which could affect the detected tensile strength. In order to investigate the impact of the height of the reference specimen on the measured

tensile force, an additional test series has been performed. In order to investigate the impact of the height of the specimen, all specimens have the same diameter, but a varying height of 12 mm, 7 mm and 2 mm, see Figure 3.19. The 2 mm specimen has a height similar to the healing specimen.

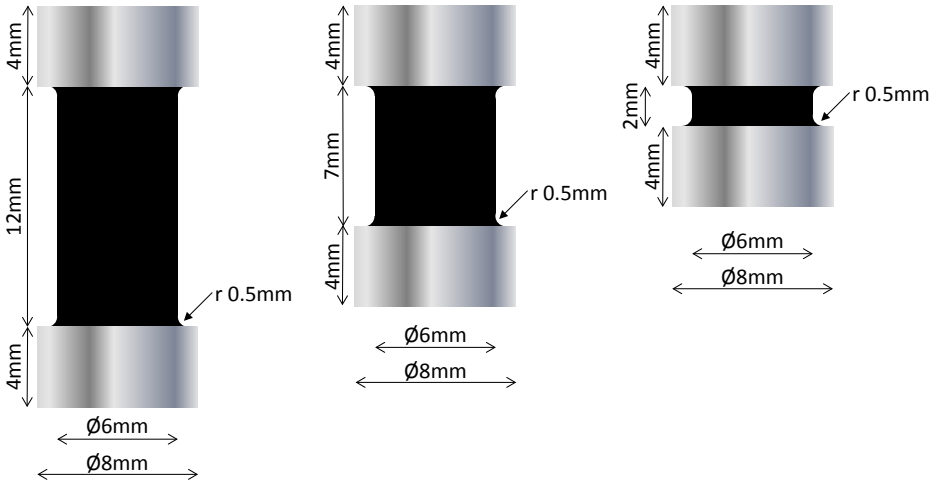

Figure 3.19 Specimens created to investigate the impact of sample height on assessed tensile strength

The tensile tests are repeated 3 times for each specimen size and the average result is presented. The strain rate for all tensile tests was 0,5 %/s. The average force-displacement curves for the tensile tests executed on the specimens with a different geometry are shown in Figure 3.20, to make them more comparable the results are also presented as force-strain curves in Figure 3.21. From Figure 3.20 and Figure 3.21 it can be seen that the height of the specimen has a slight impact on the peak load and the shape of the curve. The maximum force in relation to the specimen height is presented shown in Figure 3.22, the numerical values are given in Table 3.3. From the results it becomes clear that there is no clear correlation between the specimen height and the tensile strength. The specimens with a height of 7 mm show the highest tensile strength (average 1,40 N) followed by 12 mm and 2 mm (average 1,29 N). However, all results fall in the error bars of the 2 and 12 mm specimens, demonstrating that the height of the reference specimens does not significantly affect the observed maximum tensile strength. It is therefore concluded that the TU Delft column geometry is appropriate to serve as a reference specimen.

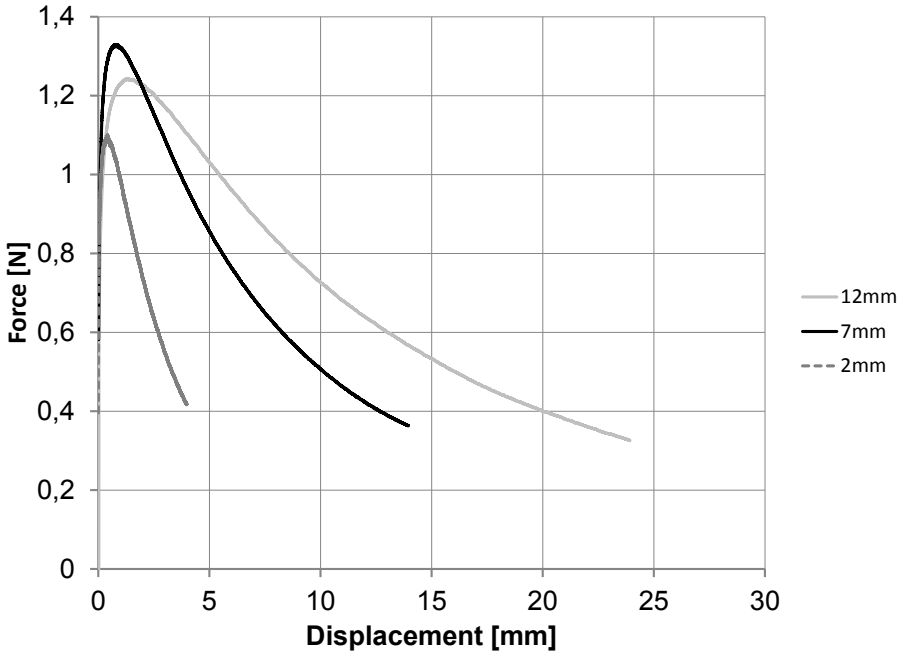

Figure 3.20 Average force-displacement curves for the tensile tests on reference samples with a height of 2, 7 and 12 mm at a strain rate 0,5 %/s.

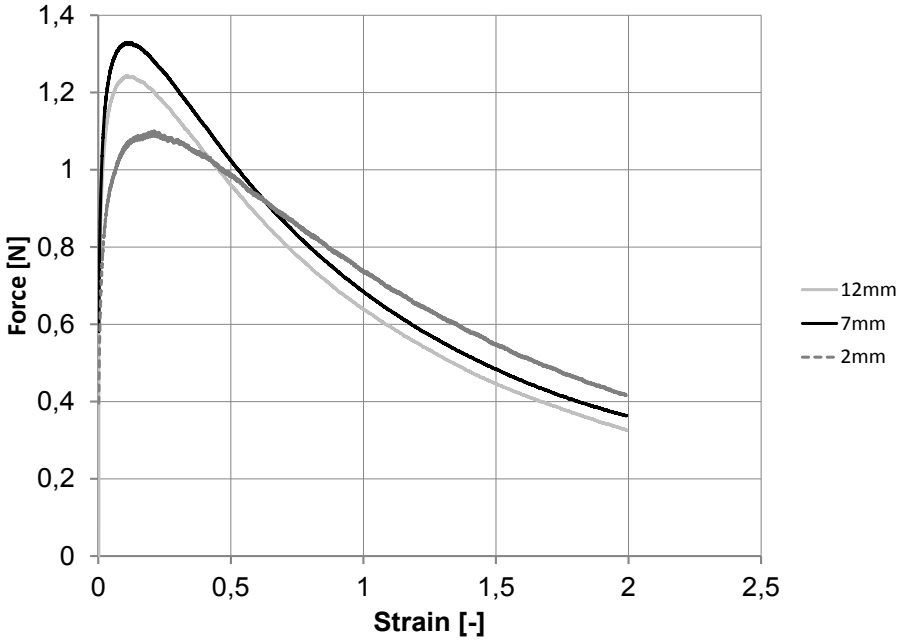

Figure 3.21 Average force-strain curves for the tensile tests on reference samples with a height of 2, 7 and 12 mm.

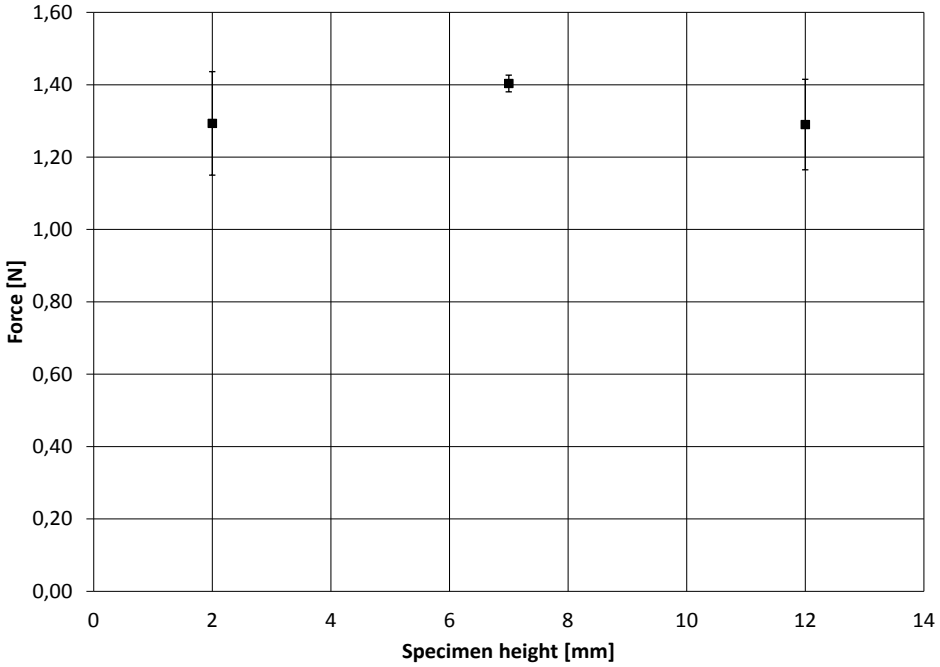

Figure 3.22 The measured maximum tensile strength (average and standard deviation) in relation to the specimen height

Table 3.3 Maximum tensile stresses in N observed for reference specimens with a different specimen height

	2 mm	7 mm	12 mm	Total population
Specimen_1 [N]	1,45	1,39	1,25	
Specimen_2 [N]	1,26	1,39	1,19	
Specimen_3 [N]	1,17	1,43	1,43	
Average [N]	1,29	1,40	1,29	1,33
Standard deviation	0,14	0,02	0,12	0,11
Coefficient of variation	0,11	0,02	0,10	0,08

3.4 STRENGTH INCREASE OF SPECIMENS DIRECTLY AFTER PRODUCTION

Initial tensile tests executed on the reference specimen indicated that the strength of the material is not constant over time, see Figure 3.23. Just after production the strength is lower, while the strength stabilizes after 24 hours. To limit the impact of this change in

material properties on the healing test executed in this research, all test specimen are left to rest after production in the temperature controlled room (14 °C +/-1 °C) for at least 48 hours and no longer than 7 days. A maximum resting time is set as it is plausible that after long resting periods a further increase in strength could be present.

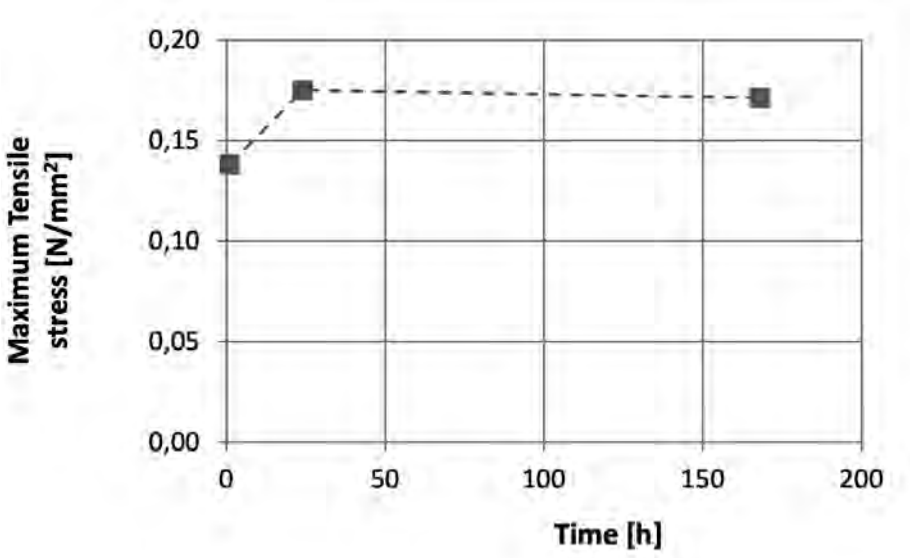

Figure 3.23 Strength development of reference samples stored at 14°C in relation to specimen age, test temperature 10 °C, strain rate 0,5 %/s.

3.5 INFLUENCE OF STRAIN RATE ON TENSILE STRENGTH

This section discussed the influence of strain rate on the detected tensile strength using this specific test set-up. As already discussed in the literature review, the response of bitumen is strain rate dependent. While executing the test program, specimens can be accidentally subjected to higher or lower strain rates than intended. By quantifying the correlation between strain rate and detected strength, it is possible to correct measured tensile force for a deviation in applied strain rate.

In order to investigate the impact of strain rate on the tensile strength, reference specimens with a specimen height of 12 mm have been loaded at three different strain rates; 0,5 %/s, 1,0 %/s and 1,5 %/s. The tests were executed at a temperature of 14 °C. Each test was repeated twice. The material tested was Q8 70/100 bitumen. The maximum tensile force is shown in Figure 3.24. The results presented show an almost linear relationship between strain rate and tensile strength for the strain rates assed. However, it should be noted that this specific linear relationship is only representative for the tested bitumen at the studied strain rates and will be different for other bitumen types or other strain rates.

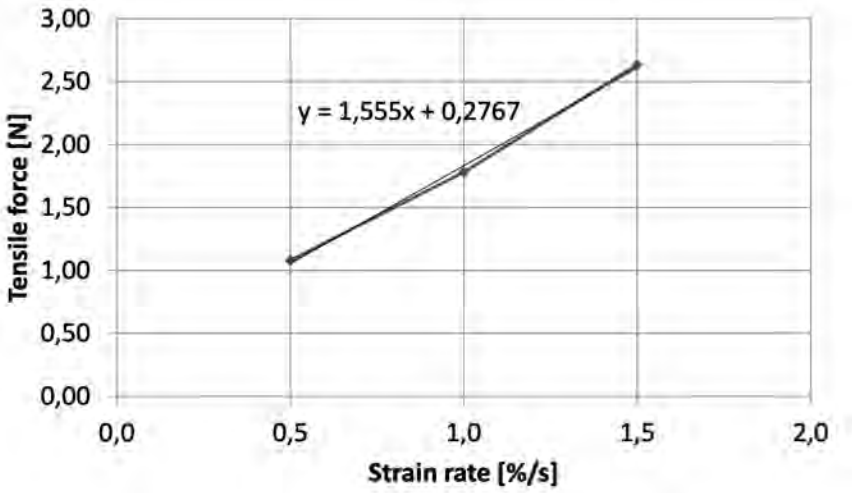

Figure 3.24 Influence of strain rate on measured tensile strength for reference samples of Q8 70/100 tested at 14 °C.

3.6 INFLUENCE OF TEMPERATURE ON THE HEALING TEST

Since healing is temperature-dependent, an initial test was conducted using the designed setup at a temperature 10 °C higher, being 24 °C to explore its effect and potentially accelerate the healing process. Q8 70/100 bitumen was used to produce specimens. Different healing periods were applied from 20 seconds up to 200.000 s (56 hours). The tests were repeated twice for the longest healing periods (20.000 s and 200.000 s) and 3 times for the short healing periods (20 s, 200 s and 2000 s). The specimens were assembled at an assembly rate of 0,04 mm/s and an assembly force of 0,2 N, resulting in an imposed displacement during assembly of 0,8 mm. The time required for the assembly phase was 20 s. The strain rate during the tensile test was 0,5 %/s.

The results of all tensile tests area presented in Figure 3.25. The graphs appear blocky, as the measured tensile strengths are so small they are near the load cell's resolution limit. As a result there is hardly any resolution in the results making it impossible to draw any conclusions.

Next to this, post-test observations showed that specimens subjected to long healing periods were severely deformed; at a healing period of 200.000 s the top half-specimen had almost fully dripped from the stainless steel ring. Specimen deformation was also observed for the reference specimen as their shape at the end of the test was slightly cone like, resulting loss of diameter at the top of the specimen. Therefore any quantitative results obtained in this test series should not be trusted. Considering the lack of resolution in the results, combined with the artifacts due the changes in geometry it is concluded that test method becomes unsuitable if the material gets too soft. Acceleration of the test can therefore not be done by a just increasing the test temperature.

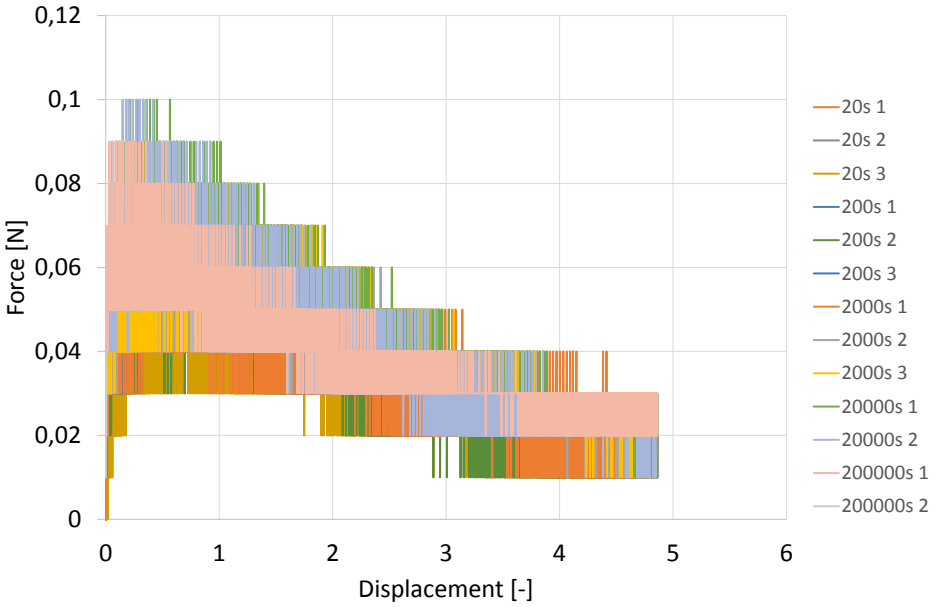

Figure 3.25 Stress-strain curves for all tensile tests executed at 24 °C when different healing periods are applied.

3.7 ARTEFACTS DURING TEST EXECUTION

3.7.1 Unexpected trends in healing development over time

The calculated healing ratio over time for first test series is presented in Figure 3.26. There are two remarkable aspects about the presented healing trend. The first observation is that the strength of the healed specimen at the longest healing period (100.000s ~ 28 hours) is larger compared to the reference value. As all material in this test series was treated similarly, they can be assumed to have the same aging degree. Therefore it is very unlikely that the higher strength observed in the healed specimens genuinely means that the healed material is stronger that the reference material. The higher strength of the healed material should therefore be interpreted as a artifact that is caused by other differences than the material. The second remarkable aspect of the graph is the strong increase in strength in the last healing time step of the healing period. An acceleration in healing behaviour does not align with the physical processes which are assumed to drive the healing process, as described in Chapter 2. All the described phenomena there result in a trend that moves towards a horizontal asymptote. The most plausible assumption is that the detected strength increase in the last and longest time step is not related to healing, but has another cause. There are two plausible explanations for an observed strength increase over time; the first one is an increase in material strength, the

second one being a change in geometry. The likeliness of both options will be discussed in the following sections. Based on this discussion a plausible explanation for these unexpected trends is formulated and a method to correct for these artefacts is proposed.

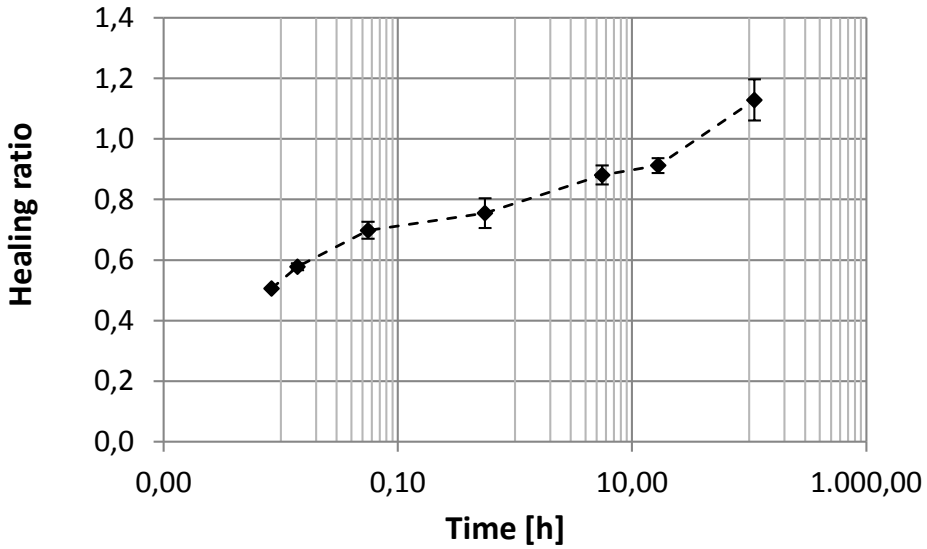

Figure 3.26 Healing ratio obtained by dividing healed strength with the reference strength for different healing times, using specimens made of Q8 70/100

3.7.2 Strength increase inside testing machine

A strength increase over time is often observed in bitumen, this is most likely related to a combination of steric hardening and ageing. In this particular research for instance, a strength increase in the hours after making specimens is the motivation to let the specimen rest before starting the healing experiment, see Section 3.4. It is hypothesized that the specific conditions inside the test chamber of the tensile test, where the healed specimen were held for 24 hours has attributed to the strength increase in the last time step. To assess the impact of specimens spending a long period inside the test machine, a control experiment has been executed on reference specimens. Four reference specimens were made and aged for 48 hours before testing. Two reference specimen were tested directly, while two other specimen were tested after they spend 48 hours inside the machine at 14,0 °C. There was no significant difference in strength observed between the specimens that were tested directly and the ones that were kept inside the chamber for an additional 48 hours. Therefore it is concluded that the higher observed strength in the last time step, is not related to a strength increase caused by accelerated aging of the material inside the test chamber.

3.7.3 Deviations in specimen geometry

3.7.3.1 *Effect of sagging on half specimen geometry*

A second reason for higher detected strength could be a change in specimen geometry. Variations in geometry can alter strain rate or cross-sectional area, both of which influence measured strength.

During production and testing, it was observed that the half-specimens tend to sag slightly during storage in the temperature-controlled room. This sagging has two geometrical effects which are illustrated in Figure 3.27. In the first place, the area that will be brought into contact during the assembly phase is slightly smaller, as the intended surface area has become smaller, next to this the surface has become slightly convex instead of perfectly flat. Secondly, the height of the half-specimen will be slightly less compared to the design. The extent to which this sagging occurs depends on various parameters, e.g. the temperature in the storage room or the type of binder. Hard binders (penetration grade 10/20) will hardly sag, while soft binders (penetration grade 70/100) will demonstrate sagging that can easily be detected with the naked eye. It has also been observed that even between binders with the same penetration grade more sagging can be observed, most probably due to differences in surface characteristic.

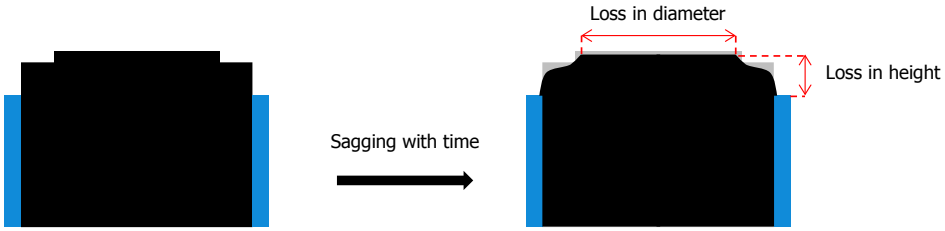

Figure 3.27 Schematic impression of sagging of the half-specimens

Short term effect of change in geometry

The immediate effects of these changes in geometry are as follows. In the first place, the area brought into contact during the assembly phase is smaller, due to the loss in diameter of the surface and the slight convex shape. As less contact is created, this change results in less healing. This means that this effect does not explain a higher strength after healing, it could only explain a lower strength. The second effect is the loss of specimen height. When the same deformation rate is applied to a shorter specimen, the strength is higher as the strain rate is higher, see Section 3.5. This phenomenon could therefore provide a plausible explanation for observed healing ratios higher than 1.

3.7.3.2 *Experimental investigation of the impact of sagging of half-specimens on healed strength*

Some experiments have been executed to assess if it is possible that the shape of the

specimen influences the amount of contact created. These tests were executed on Nynas bitumen with penetration grade 70/100 as it had been observed that sagging in specimens made with this specific binder was most distinct.

The two parameters that were varied were the size of the hole in the silicon paper controlling the contact area and the amount of deformation applied during assembly phase, see Section 3.2.3. Silicon papers were fabricated with a hole size of 5, 5,5 and 6 mm. The assembly force during the assembly phase was varied to result in vertical deformations of 0,4; 0,8 and 1,2 mm. Tensile tests were executed immediately after the assembly phase was completed and all tests have been performed twice.

The results of both test series are presented in Figure 3.28. In the graph the tensile force as detected is reported. The first observation that can be done from this graph is that a larger assembly force (or more vertical assembly displacement) results in a larger tensile force. The second observation is that the size of the hole in the silicon paper does not affect the detected tensile force when the assembly displacement is 0,4 and 0,8 mm. However, when a vertical displacement of 1,2 mm is applied, a larger hole results in a larger tensile force. It is therefore concluded that only when the vertical assembly displacement is 1,2 mm, the amount of contact created is controlled by the size of the hole in the silicon paper. This implies that when the vertical displacement during the assembly phase is less (0,4 mm or 0,8 mm), the amount of area that is brought into contact is smaller than the Ø5mm hole. This demonstrates that sagging can significantly influence the amount of area brought into contact and the observed “healing force”, especially when the amount of applied deformation during assembly is limited. For the Nynas specimens, assuming 5,5 mm² contact area leads to an overestimation of the actual contact area and an underestimation of the strength.

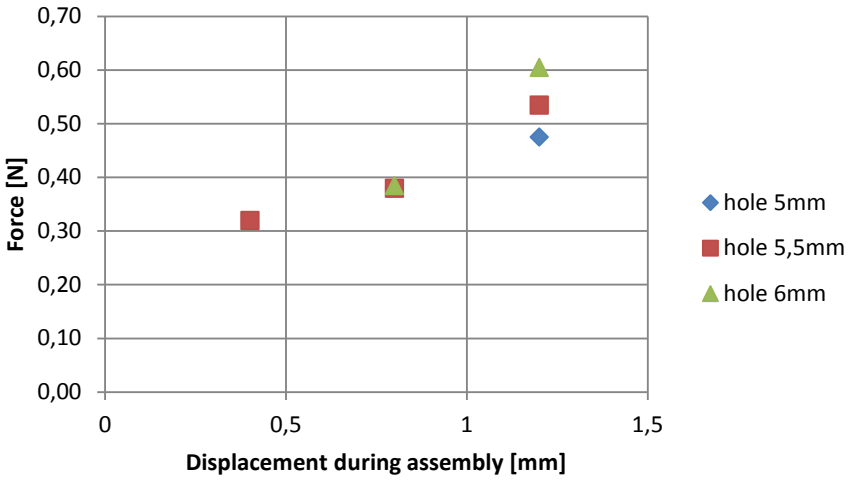

Figure 3.28 Impact of imposed displacement during assembly and hole size in silicon paper on the amount of tensile force detected immediately after assembly

3.7.3.3 *Changes in specimen geometry during test execution*

The sagging that occurs during specimen preparation, can also occur during the healing period. In the testing machine, the ring of the top half specimen is held at a fixed position. However, if the material within the ring is relatively soft, it can flow down under the influence of gravity. If the initial contact area is smaller than the hole in the silicon paper, as shown earlier, sagging during the healing period may cause the contact area to grow, see Figure 3.29. This effect is strongest in the longest time step, unless the full area of the hole in the paper is in already in contact before this moment. This mechanism could explain the unexpected upsweep in detected force that has been observed for the longest time step reported in Section 3.7.1.

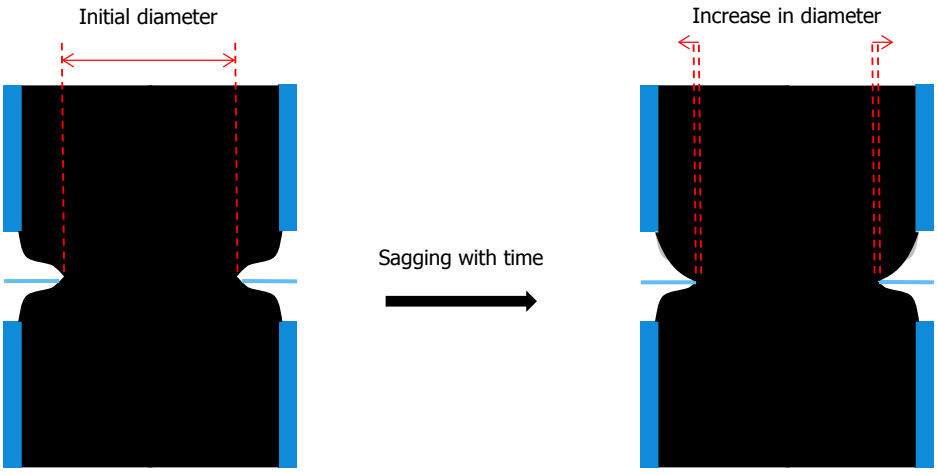

Figure 3.29 Schematic impression of sagging of specimens during healing

3.7.4 Approach to correct the calculated healing ratio for geometrical errors

3.7.4.1 *Expected healing development with time*

The healing model presented in Section 2.4.1 indicates that healing is the sum of two processes, first surfaces need to regenerate contact next this contact need to homogenize. Both processes can be described with an asymptotic curve, that approaches 1 as time progresses. Any combination of these curves will essentially have the same shape. Therefore, the development of healing over time is expected to have the general shape of an asymptote moving to a value of 1. In the following paragraphs the measured results will be corrected for the geometric artifacts discussed in Section 3.7.3. First, a correction for sagging during the healing period is proposed to align the trend with the expected asymptotic behaviour. Next a correction will be applied to ensure that the healing ratio does not exceed 1.

3.7.4.1 *Correction for sagging of the specimen during the healing experiment*

It has been hypothesized that the contact area increases during the healing experiment, as a result of sagging of the assembled specimen. To correct for this, it is assumed that the initial contact area just after assembly is Ø5 mm, with its radius increasing linearly over time during healing. This linear increase in radius corresponds to the model for area expansion of bitumen as presented in Section 2.6.4. As there is a serious upswing in tensile strength in the last time step, it is assumed that the specimen will have reached full contact (Ø5,5 mm) at around the duration of the last timestep, which is around 100 hours. The resulting area increase is graphically shown in Figure 3.30. When the results presented in Figure 3.26 are corrected for the effect of sagging during healing, by using an increasing contact area, a more realistic development of healing ratio over time is found, see Figure 3.31. It is recommended that further study will be done into this effect to, either prevent it from occurring or to be able to correct it using less assumptions.

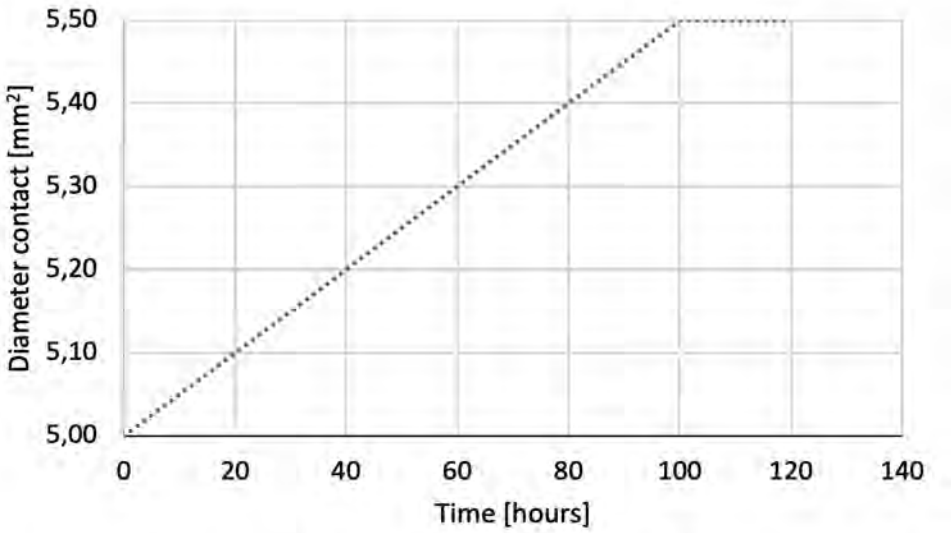

Figure 3.30 Assumption on development of contact area over time as a result of sagging of the specimen that is used to correct the strength development.

3.7.4.2 *Correction for the higher strain rate*

Another correction is needed to address the situation that the healing ratio should not exceed the value of 1. As discussed, the higher detected healing ratio could be caused by a higher strain rate in the healing specimen, caused by an overestimation of the specimen height due to sagging before assembly. The specimen height is not known, as this is not measured, therefore the error in applied strain rate cannot be calculated. The order of magnitude of the error is estimated using some assumptions. Assuming each halfspecimen sags by 0,1 mm, the total height loss is 0,2 mm. This is around 10% of the

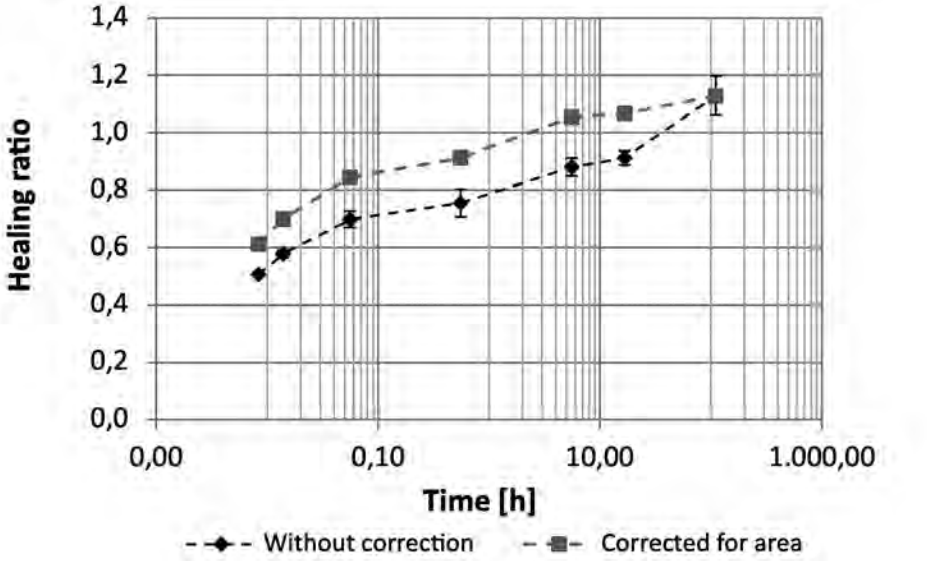

Figure 3.31 Graph for original healing ratio and corrected healing ratio which takes into account an increase in contact area due to sagging of the healing specimen during the healing period

specimen height (two half specimen (2x1,5 mm), minus 0,8 mm for deformation during assembly = 2,2mm). This results in a strain which is 10% higher than intended. The linear correlation presented in Figure 3.24 obtained for this material, implies that as a result of a 10% higher strain rate an increase in healing force of around 10% could be expected, which would result in a healing ratio of 1,1 instead of 1. If the asymptote is determined visually on the trend presented in Figure 3.31, a value of 1,18 seems reasonable. In order to normalize all healing values are divided by 1,18. The resulting normalized graph for the healing ratio is presented in Figure 3.32.

It is recognized that quite some assumptions were needed to arrive at the healing graph shown in Figure 3.32. As these assumptions could be challenged, some recommendations are given to ensure that in future research less assumptions need to be made. In the first place it is important to formulate an approach to assess the specimen height more accurately, resulting in a more accurate strain rate applied during the tensile test. Or alternatively to keep the half specimen in their mould until the moment of testing. Next to this attention needs to be paid to the amount of contact area created, either by optimizing the test method to ensure more control over the contact area or by formulating a method to measure the contact area in contact directly.

3.8 SUMMARY, CONCLUSIONS AND RECOMMENDATIONS

In this chapter a novel test method to assess healing of bituminous binders has been presented. In this method two pieces of bitumen are brought together under controlled

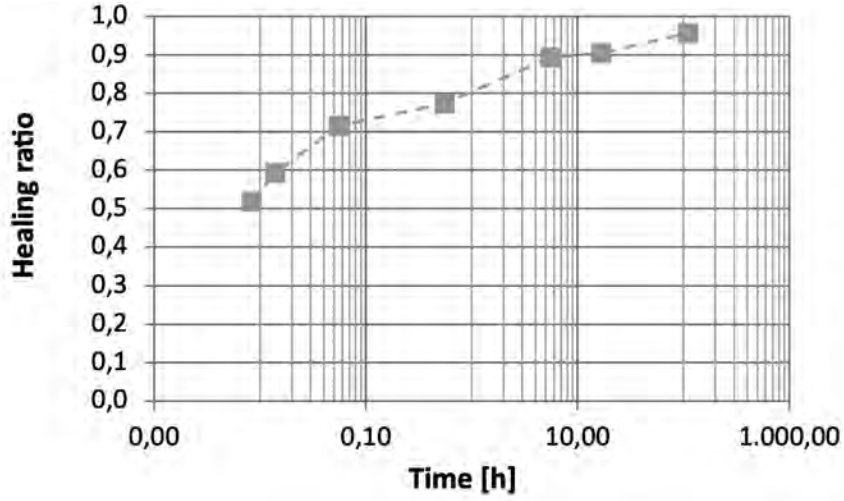

Figure 3.32 The development of healing of a binder over time, corrected for sagging and normalized

conditions creating a healing interface with a known surface area, mimicking two surfaces of a crack that are brought into contact again. The strength of this healing interface can be tested after different conditioning steps using an uniaxial tension test. The detected strength is an indication for the amount of healing.

The test is executed inside a rheometer, used in the tensile mode. In the chapter details are provided on how test specimens can be prepared. Two different approaches have been presented on how to assemble specimens; inside the testing machine and inside a temperature controlled room. The parameters that can be controlled during the healing test depend on the used assembly method. It was demonstrated that the developed test method has reasonable repeatability, with a standard deviation in detected healing of less than 10%. Finally, an approach to calculate the healing ratio, based on a reference specimen has been presented.

The recommended test conditions for the twopiece healing test in direct tension are:

- An assembly and healing temperature of 14 °C;
- A tensile rate of 0,5 %/s.

Other conditions depend on the material tested. In the next chapter more details will be presented on the optimal test approach.

The presented test method has demonstrated that it can be used to assess strength development in bitumen pieces that are brought together after different healing periods. By varying assembly conditions and healing periods, the RQ 4 and 5, as posed in Section 1.4.3 can be studied.

The test set-up does not provide a method to measure the size of the area brought into contact. As a result some assumptions are needed on the amount of area brought in

contact when interpreting the results. In order to be less dependent on assumptions, it is recommended that in further research an approach is sought to measure the amount of area in contact directly or at least have more control over this parameter during testing. Another aspect of the test that could be improved is the addition of a measurement technique to determine specimen height after preparation and assembly. As the specimens are easily deformable, a technique using laser light or an image scan are seen as the best options.

4

THE IMPACT OF CREATING CONTACT ON HEALING TESTS

THE IMPACT OF CREATING CONTACT ON HEALING TESTS

This chapter aims to investigate the impact of the process of creating contact between bituminous interfaces on the detected healing. The newly developed test set-up presented in Chapter 3 has created the opportunity to study the impact of the assembly conditions when two bituminous surfaces are brought together. The impact of the assembly process is studied for different binders with the aim to assess which trends hold for all binders and which characteristics are binder specific. The observations with respect to the impact of assembly conditions are combined with the state of the art on healing of bitumen (Chapter 2) and the formulated healing theory (Chapter 6) to expand the fundamental insight in healing of bituminous materials. Next to these fundamental insights, the observed impact of the assembly conditions is also used to formulate an assembly procedure for test series that focus on other aspects of healing, like the development of healing over time, which is studied in Chapter 5.

In Section 4.1 the possible variations that can be applied by the test machine during the assembly phase are presented. In Section 4.2 the test program that has been implemented is introduced and the results are presented in Section 4.3, 4.4 and 4.5, reporting on respectively bitumen with a penetration grade of 70/100, 40/60 and 10/20. The results are discussed in Section 4.6. In this section a subsection is dedicated to the formulation of an assembly procedure that can be used to study other aspects of healing. The chapter closes with conclusions in Section 4.7.

4.1 INTRODUCTION

4.1.1 Test method used

This part of the research focusses on the healing that can be observed immediately after the assembly phase has been completed. In this thesis, this part of the healing is referred to as ‘instant healing’. This short term process can be studied best if the half-specimens introduced in the previous chapter on the test method are assembled inside the test machine, as this method allows for testing using very short healing times. Therefore, all the test results presented in this chapter are obtained using the method where the assembly phase takes place inside the test machine.

4.1.2 Aim

The aim of the research presented in this chapter is to assess the relative contribution of instant healing to the total amount of healing that can be detected for bitumen. Therefore conditions were sought to almost instantly create good contact between two bitumen surfaces. These observations are also used to formulate a consistent and repeatable procedure for assembly phase that can be used to study other aspects of healing, like the relative healing capacity of binders or the impact of time on healing.

4.1.3 Variation in assembly conditions and its impact on healing

As mentioned in the previous chapter due to the nature of the Anton Paar testing machine and the software running on it, there are only two parameters that can be varied during assembly inside the machine; the assembly rate and the assembly force. In the case that the half-specimens were made of a purely elastic material and were perfectly flat, the assembly force would be linearly related to the amount of real contact created Paragraph 2.6.2.1. In line with this theory, a stiffer material requires a larger normal force to realize the same contact area. Due to the viscoelastic nature of bitumen, part of the assembly force will result in elastic deformation, while also a part will result in viscous deformation. Therefore, in case of bitumen no linear correlation is expected between the assembly force and the amount of contact created. However, it is expected that the applied assembly force does correlate to the amount of contact area created. It is relevant to note that contact that is created between surfaces as a result of viscous deformation will be sustained at least some time after the load has been removed and can even be permanent, while contact created through elastic deformation will be mostly lost after the load is removed. As healing is partly driven by the creation of surface contact, the longer present viscous deformation is expected to contribute more to healing compared to elastic deformation. Test parameters during the assembly phase will influence the degree to which the response of the bitumen is more elastic or viscous. For instance, at a lower assembly rate, the material will show more viscous deformation compared to elastic deformation. On the other hand, at a lower temperature the material will behave more elastic.

4.1.4 Healing period when studying instant healing

In this chapter, the focus is on instant healing, therefore the healing strength is tested immediately after the end of the assembly phase. However, it should be realized that this does not mean that the healing time is 0 seconds, as discussed in Chapter 3. All steps in the assembly phase require time and healing will start at the first moment the surfaces touch. The amount of time that the surfaces spend in contact during the assembly phase varies between tests, due to the variations in assembly conditions. This results in healing times for the test series presented in this chapter that range from 11 seconds to 25 minutes (1457 s).

4.2 TEST PROGRAM

4.2.1 Materials

The largest part of this test program is executed using a straight run 70/100 pengrade bitumen. 70/100 bitumen is the standard bitumen for Dutch Porous Asphalt surface layers that are present on most highways. It is assumed that this specific bitumen has good healing properties for two reasons. In the first place, relatively soft and soft binders

show good healing behaviour (Chapter 2). In the second place, the binder is the direct product of a vacuum distillation process (straight run), which means that it is expected to behave as a traditional well healing bitumen. Therefore this straight run, 70/100 binder serves as a good healing reference in this study. And it also provides a good starting point to investigate the impact of the assembly method on healing.

Additional tests have been executed using two harder binders, with a penetration grade of 40/60 and 10/20, respectively. Bitumen with a penetration grade of 40/60 is generally used for base layers in the Netherlands. Bitumen with a penetration grade of 10/20 is not regularly used for the construction of pavements. However, there are two reasons why 10/20 penetration grade is relevant for bases layers. In the first place when recycling the binder from the Reclaimed Asphalt Pavement (RAP) is harder and a maximum value for this is set at a penetration value of 10. Due to poor blending in recycling it is possible that this hard binder is still present as unblended fraction in the mix. Next to this, there is an innovative type of asphalt base layer made using 10/20 penetration grade binder called EME (Enrobé à Module Élevé), of which the healing properties are a topic of debate. All binders including the 70/100 originate from the same crude source and all are straight run bitumen. It is assumed that softer binders will show more healing, as this is indicated by the RWS guidelines Table 1.1 and is in line with literature Section 2.9.1. The aim of the variation in binder softness is to assess how binder grade affects the instant healing capacity.

4.2.2 Reference strength

In order to establish a healing ratio, reference specimen of 12 mm height are produced and tested twice to obtain a reference strength. The specimen were tested in tension, at a temperature of 14 °C, using a strain rate of 0,5 %/s.

4.2.3 Assembly conditions

In order to investigate the impact of the assembly conditions on healing, bitumen specimens were subjected to a variety of assembly rates and forces. The largest variation of assembly conditions is imposed on bitumen specimens made of 70/100 pengrade bitumen, as this the most relevant bitumen for the Dutch situation. In the first test series a constant assembly rate of 0,1 mm/s was used while the force at which the assembly phase was stopped varied using values of 1, 5, 10 and 20 N. In the second test series, the assembly rate was varied using values of 0,1; 0,02; 0,002 and 0,001 mm/s, while the assembly phase was stopped when a force of 1N was detected. The test series executed with the other two binders were significantly smaller. For the 40/60 binder the assembly force was set at 1 and 5 N, while an assembly rate of 0,005 mm/s was used. For the 10/20 binder the assembly force was initially set at 1 and 5 N, while using an assembly rate of 0,01 mm/s. However, as these conditions did not lead to any detectable healing this test series was not completed. Instead, the remaining half-specimens were assembled using an assembly force of 10 and 20 N, next to this a slower assembly rate of 0,00125 mm/s

was also used in combination with and assembly force of 20 N. An overview of the assembly conditions for all binders is presented in Table 4.1. The assembly phase of all tests were executed at a temperature of 14 °C. Each test was repeated two times.

Table 4.1 Overview imposed assembly conditions per type of binder

Binder	Assembly force [N]	Assembly rate [mm/s]	Assembly time [s]
70/100	1; 5; 10; 20	0,1	1,2; 4,4; 10,2; 13,8
70/100	1	0,1; 0,02; 0,002; 0,001	1,2; 11,6; 746; 1457
40/60	1; 5	0,005	30; 208
10/20	1; 5; 10; 20	0,01; 0,00125*	2; 5; 7; 8; 644*

*Only using an assembly force of 20N

4.2.4 Healing assessment using a tensile test

The tensile strength of the assembled specimens was tested directly after the assembly phase. During the tensile test, the specimens were subjected to a constant deformation speed of 0,015 mm/s. In retrospect it was a poor choice to subject the specimen to a constant deformation speed. The height of the healed specimens is affected by the assembly phase and by choosing a constant displacement speed, the specimens were subjected to a variation of strain rates. Due to the strain dependent response of bitumen, a variation in strain rate will also lead to a variation of detected tensile strength, as has been described in Section 3.5. Therefore when analysing the test results, the detected strength is corrected for the strain rate using the results presented Section 3.5. However, the required assumptions negatively affect the accuracy of the results. The tensile phase of all tests were executed at the same temperature of 14 °C.

4.2.5 Correction for variation of strain rate applied during the tensile test

During the execution of the test program it was noticed that there were a variety of factors that influenced the geometry of the specimens during the storage, assembly an healing phase, see also Section 3.7.3. Due to these effects the height of the combined specimen after healing was often shorter than intended, as a result the applied strain rate during the tensile tests was often higher than the intended 0,5 %/s. This error in measured strength, can be corrected when the correlation between strength and strain rate is known. The relation between strain rate and measured strength has been studied within this research for Q8 70/100 and has been reported in Section 3.5. Equation 4.1 is formulated, by applying a linear fit to the found correlation between strain rate and strength. This equation can be used to calculate the equivalent tensile strength at a strain rate of 0,5 %/s. This correlation is determined for strain rates ranging from 0,5% to 1,5%; which means that outside these ranges this formula should not be used.

$$\textbf{\textit{Tensile strength}}\ (0,5\%) = 0,055 * \textbf{\textit{tensile strain}} + 0,01 \qquad (4.1)$$

This correlation is only available for one type of 70/100 bitumen. However, as these type of corrections were needed for most of the test, this correlation is also used for the other 70/100 binders and the 40/60 bitumen. It was decided that it would be better to use the 70/100 correlation over not correcting for the difference in strain rate at all. However, for future research it is imported to recommended that the test program is set-up to ensure that these kind of corrections are not necessary.

4.3 TEST RESULTS 70/100 BITUMEN

4.3.1 Reference strength 70/100 specimen

The maximum observed tensile force obtained from the reference specimens is shown in Figure 4.1. The obtained maximum values were 1,82 N and 1,85 N, resulting in a strength of 0,064 N/mm^2 and 0,065 N/mm^2, when divided over the area of the reference specimen of 28,3 mm^2. The resulting average reference value for the tensile strength of the 70/100 bitumen of 0,065 N/mm^2.

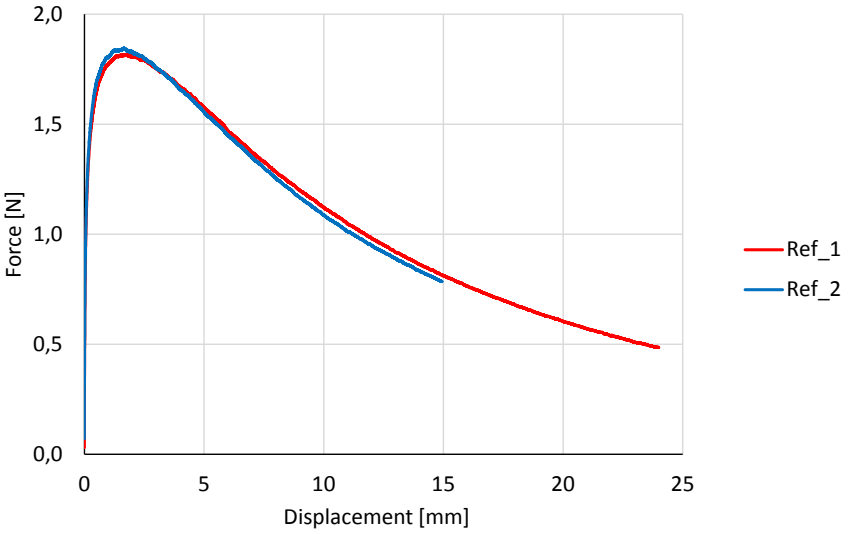

Figure 4.1 Tensile test of 70/100 reference specimen.

4.3.2 Assembly phase using different assembly forces on 70/100 bitumen

During the assembly phase both the applied force and the resulting deformation are measured continuously. The force - displacement curves for all specimens using a constant displacement speed of 0,1mm/s while varying the assembly force are presented in Figure 4.2. From the graph it can be seen that apart from the very small and very large displacements, there is a more or less linear relation between the applied deformation

and the detected assembly force, which can be interpreted as the stiffness of the material at this specific loading speed. The increase in slope after the deformation exceeds 1mm indicates an increase in stiffness. A possible explanation for this increase in detected stiffness is that at this amount of deformation, not only the small top (Ø5,5mm) of the half-specimen deforms, but a larger part of the cross-section (Ø8mm) is involved, which results in a higher stiffness. Due to this difference, the surface becomes about twice as large, which seems to coincide with the stiffness increase in the graph, which also doubles. An overview of the average displacement, the resulting strain speed during the tensile test and the time required for the assembly phase is provided in Table 4.2 per assembly condition.

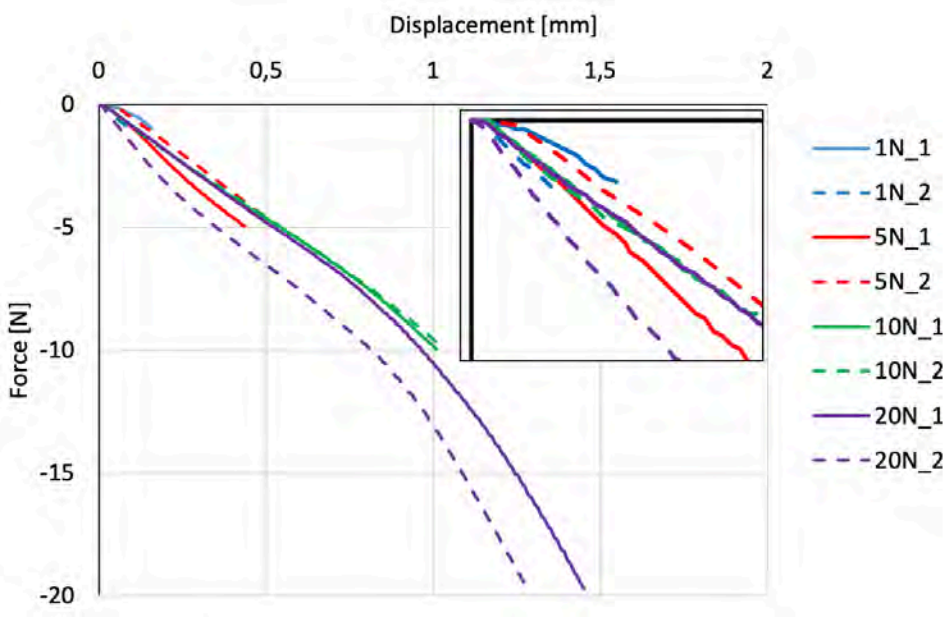

Figure 4.2 Force – displacement curves for the assembly phase of 70/100 bitumen using different assembly forces

4.3.3 Tensile strength of 70/100 specimen created using different assembly forces

All the results of the tensile tests with varying assembly forces from 1 to 20 N while using a constant displacement speed of 0,1 mm/s are plotted in Figure 4.3. A first observation that can be done, is that in some of the specimen there is compression force left in the specimens at the start of the tensile test. This residual force from the assembly phase is larger, as the applied assembly force was larger; it is not present for the specimens assembled with a force of 1 N, for the specimens assembled with 5 N it is -0,2 N at the start of the test, for specimens assembled at 20 N it is -0,8 N. It can also be seen that

Table 4.2 Deformation during force controlled assembly and resulting strain speeds during tensile test

Specimen	Assembly period [s]	Imposed displacement during assembly[mm]	Specimen height [mm]	Applied strain rate during tensile test [%/s]
1N_1	1,6	0,16	2,84	0,5
1N_2	0,9	0,09	2,91	0,5
5N_1	4,4	0,44	2,56	0,6
5N_2	4,9	0,49	2,51	0,6
10N_1	10,1	1,01	1,99	0,8
10N_2	10,3	1,03	1,97	0,8
20N_1	14,5	1,45	1,55	1,0
20N_2	12,9	1,29	1,71	0,9

during the tensile test, all tested specimen come apart fully during the tensile test as at some point the force becomes 0 in a step like fashion.

From the figure it can be seen that initially a higher assembly force results in a higher peak strength and more post-peak deformation. However, above an assembly force of 5 N no more strength is gained and above 10 N no more post peak deformation is gained. It could be concluded that for this binder an assembly force of 10 N results in the highest possible initial healing.

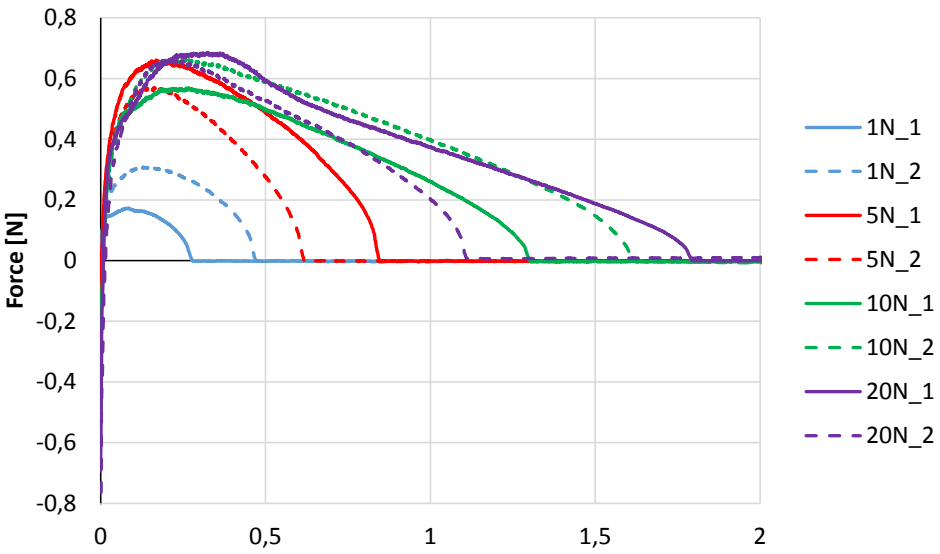

Figure 4.3 Force - displacement curves for all tensile tests with varying assembly forces and a constant assembly rate of 0,01 mm/s, curves are smoothed using a running average over 20 values.

The maximum detected tensile strengths are shown in Figure 4.4. In this figure the measured reference value for the tensile strength is also plotted. It can be seen that initially the impact of additional healing force is strong, however above 5 N additional force does not seem to result in additional strength. In the graph it can be seen that for assembly force values 5, 10 and 20 N the healed strength is it about 40% of the reference strength.

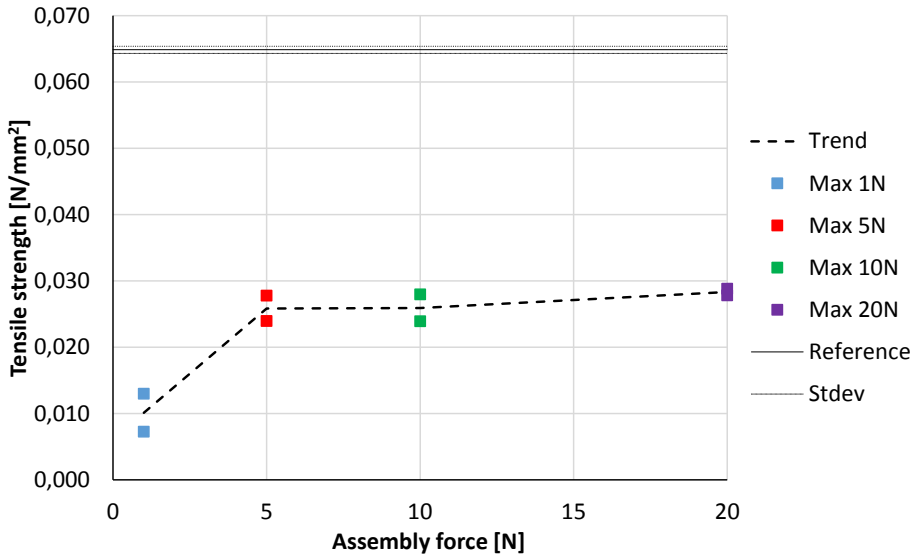

Figure 4.4 The determined healing strength and corrected healing strength for 70/100 specimens for varying assembly forces along with the reference strength of the material

4.3.4 Assembly phase using different assembly rate on 70/100 bitumen

During the assembly phase both the applied force and the resulting deformation are measured continuously. The force - displacement curves for all specimens that were assembled using a variation of assembly rates until an assembly force of 1N was reached are presented in Figure 4.5. The measurement interval was 0,1 s and to smooth the curves for the assembly rate of 0,02; 0,002 and 0,001 mm/s a running average for the force over 20 measuring points is used to create the graph. The blue lines in the graph are the same as the blue lines in Figure 4.2.

From the graph it can be seen that for each assembly rate there is similar relation between the applied deformation and the detected assembly force. This relation is more or less linear until a the deformation exceeds 1mm, as was also observed during the assembly process using different force levels (see Section 4.3.2). As could be expected from a strain rate dependent material like bitumen, the curves are steeper when a larger assembly rate is applied. From the graph it can be seen that the assembly phase of specimen 1 assembled at 0,002 mm/s was not completed. This was caused by an error in assembly settings.

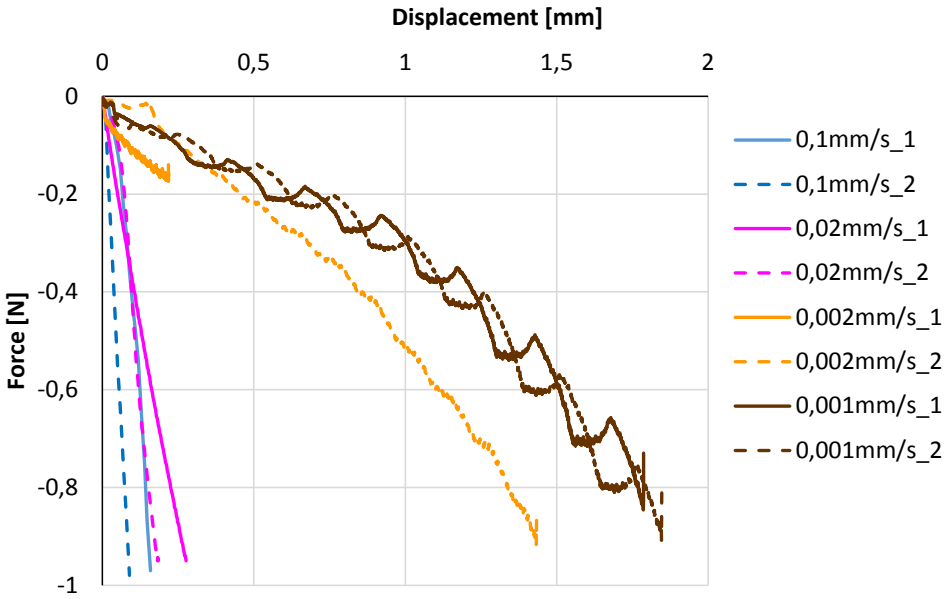

Figure 4.5 Force – displacement curves of the assembly phase for 70/100 bitumen using different assembly rates

In Figure 4.5 is can also been seen that for slow assembly rates, a large variation can be observed in the detected force at a similar displacement. At the slowest assembly rate of 0,001 mm/s, in spite of the running average, a wavy pattern even appears in the force – displacement curves (brown lines). Such a pattern can only be caused by artifacts in the steering mechanism of the machine, not by the material or the developing contact. Therefore it is concluded that with this specific machine an assembly rates of 0,002 mm/s or slower should not be used. From the graph it can also be seen that the assembly procedure of specimen 1 with an assembly rate of 0,002 mm/s was not completed, as the assembly force of 1 N was not realized. An overview of the average displacement, the time needed for the assembly and the resulting strain speed during the tensile test is provided in Table 4.3 per assembly condition.

4.3.5 Tensile strength of 70/100 specimen created using different assembly rates

All the results of the tensile tests while varying the assembly rate, from 0,001 to 0,1 mm/s using an assembly force of 1 N are presented in Figure 4.6. In one of the specimens, 0,02 mm/s_1, a slight residual force is still present from the assembly phase which is less than 0,1 N. It can also be seen that during the tensile test, all tested specimen come apart fully during the tensile test as at some point the force becomes 0 in a step like fashion.

Table 4.3 Deformation during displacement controlled assembly and resulting strain speeds during tensile test

Specimen	Assembly period [s]	Imposed displacement during assembly [mm]	Specimen height [mm]	Applied strain rate during tensile test [%/s]
0,1 mm/s_1	1,6	0,16	2,84	0,5
0,1 mm/s_2	0,9	0,09	2,91	0,5
0,02 mm/s_1	13,9	0,28	2,72	0,6
0,02 mm/s_2	9,3	0,18	2,82	0,5
~~0,002 mm/s_1~~*	~~117~~	~~0,22~~	~~2,78~~	~~0,5~~
0,002 mm/s_2	767	1,43	1,57	1,0
0,001 mm/s_1	1434	1,79	1,21	1,2
0,001 mm/s_2	1482	1,85	1,15	1,3

*Assembly procedure was not completed due to an error in the test settings.

From the figure it can be seen that up until an assembly rate of 0,002 mm/s, a slower assembly rate results in a higher peak strength and more post-peak deformation. Next to this for these specimens there is also a small peak is visible before the actual peak. A plausible explanation for this this peak, is that it caused by the bitumen coming loose from the silicon paper. These specimens have undergone an extremely large assembly deformation of 1,8 mm and as a result a significant amount of bitumen is pressed over the silicon paper.

In the graph, the result of specimen 1 assembled at 0,002 mm/s is also included, as the orange continuous line. The assembly phase of this specimen was not completed; the assembly force was only 0,3 N instead of the prescribed 1 N. If this result is compared to the spotted orange line, it can be seen that also in this case a higher assembly force results in a higher peak strength.

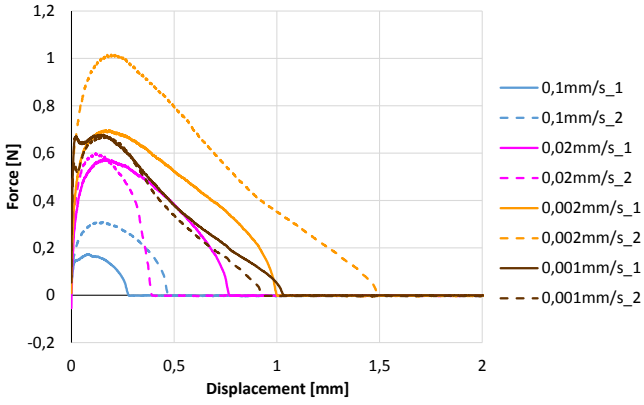

Figure 4.6 Force - displacement curves for all tensile tests with varying assembly rates and a constant assembly force of 1 N, curves are smoothed using a running average over 20 values.

Figure 4.7 shows the tensile strength versus the assembly rate. In the graph the reference strength is also plotted. From the graph it can been seen that a slower assembly rate, results in a higher tensile strength. This correlation is not linear. As mentioned, the tensile strength for the lowest assembly rate (0,001 mm/s) deviates from the expected trend. It is likely that the anomalies during assembly phase using this slow assembly rate, as described in Section 4.3.3. and shown in Figure 4.5, have affected the created contact and as such negatively influenced the healing strength. In order to assess the correlation the graph is also plotted using a logarithmic scale for assembly rate, see Figure 4.8. From the graph it can be seen that except for the slowest assembly rate, a logarithmic scale results in a straight line for the corrected healing strength. The detected instant healing when using an assembly rate of 0,002 mm/s is around 66% of the reference strength.

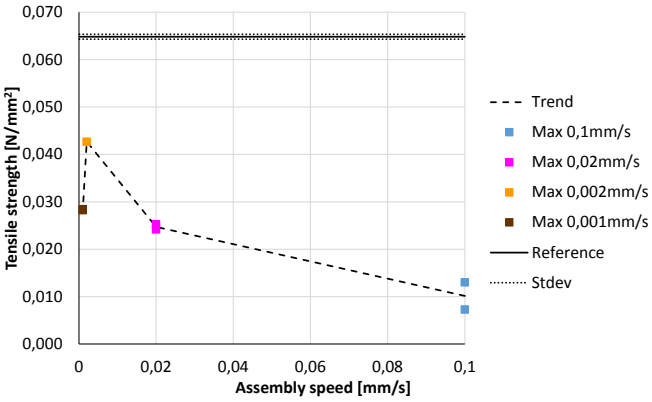

Figure 4.7 Reference, detected and corrected tensile strength for 70/100 healing specimens brought together using different assembly rates. NB. There is only one value for 0,002 mm/s.

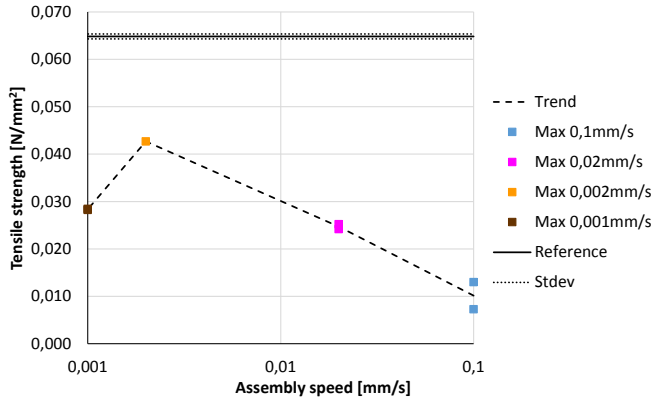

Figure 4.8 Reference, detected and corrected tensile strength for 70/100 healing specimens brought together using different assembly rates using a logarithmic scale for assembly rate.

4.3.6 Visual observations 70/100 specimens

All tensile tests executed in the 70/100 bitumen series reported in this section resulted in the surfaces of the half-specimens coming fully apart during the tensile test. A visual impression of the halfspecimens after testing is presented in Figure 4.9. When the surfaces of the half-specimen are inspected using a magnifying glass, the surfaces are still smooth and shiny, with no traces of any fibrils or anything being pulled from the surface. Therefore providing no visual indication that any material has transferred over the healing interface. Unfortunately there was no technical equipment available to take good micrographs demonstrating the smooth surfaces. The half specimens were more deformed when a larger area under the tensile graphs was observed, see Figure 4.3 and Figure 4.6.

Figure 4.9 Healed specimen after the completion of a tensile test

4.4 TEST RESULTS 40/60 BITUMEN

4.4.1 Reference strength 40/60 specimens

The maximum observed tensile force for the reference specimens was 7,74 N for Ref_1 and 7,70 N for Ref_2 (see Figure 4.10), resulting in a strength of 0,27 N/mm^2 and 0,27 N/mm^2 and an average reference value of the 40/60 bitumen of 0,27 N/mm^2.

4.4.2 Assembly phase using different assembly forces on 40/60 bitumen

During the assembly phase both the applied force and the resulting deformation are measured continuously. The force - displacement curves for the 40/60 specimen that were assembled using an assembly rate of 0,005 mm/s with an assembly force of 1 and 5 N are presented in Figure 4.11. As in this graph the assembly curves of the 1N

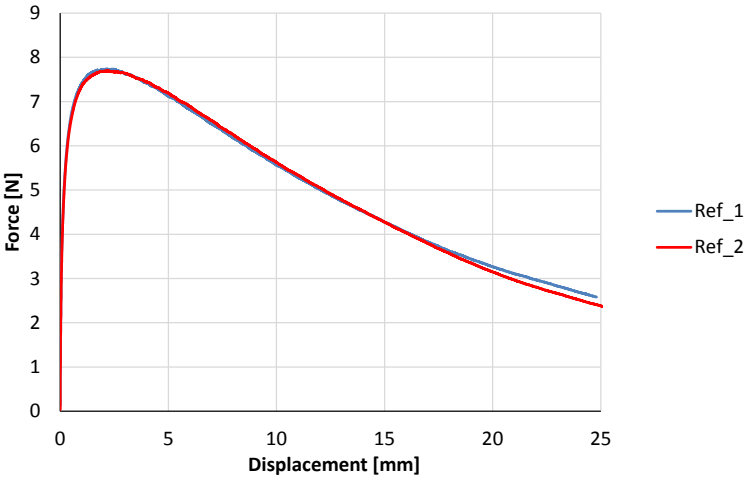

Figure 4.10 Tensile test of 40/60 reference specimen.

specimen are not that well visible, the force displacement curves for 1 N are presented in a separate graph, see Figure 4.12. Both test conditions have been repeated 4 times.

The relation between the force and the displacement for 1 N specimens is quite linear. However, the force displacement curves for 5 N are much less linear, also compared to the 70/100 specimens (Figure 4.2 and Figure 4.5). The higher stiffness at deformations around 1mm has also been observed in the 70/100 specimens. It has been hypothesized that this higher stiffness could be related to a larger portion of the specimen which is

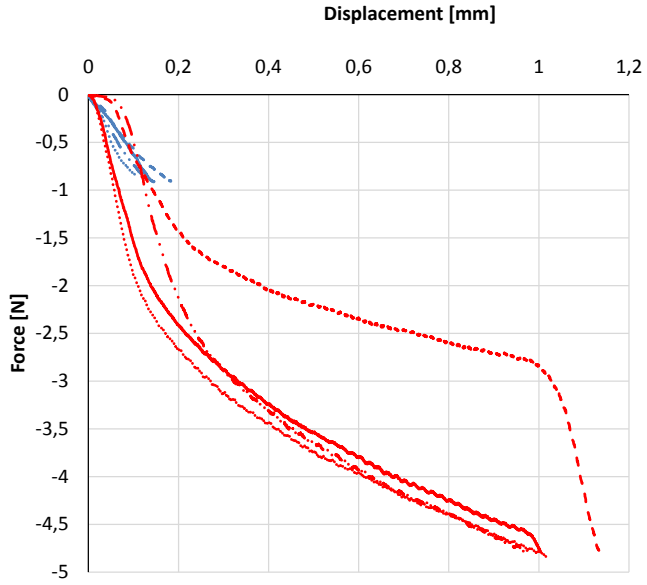

Figure 4.11 Force – displacement curve assembly phase with an assembly force of 1 and 5 N for 40/60 bitumen

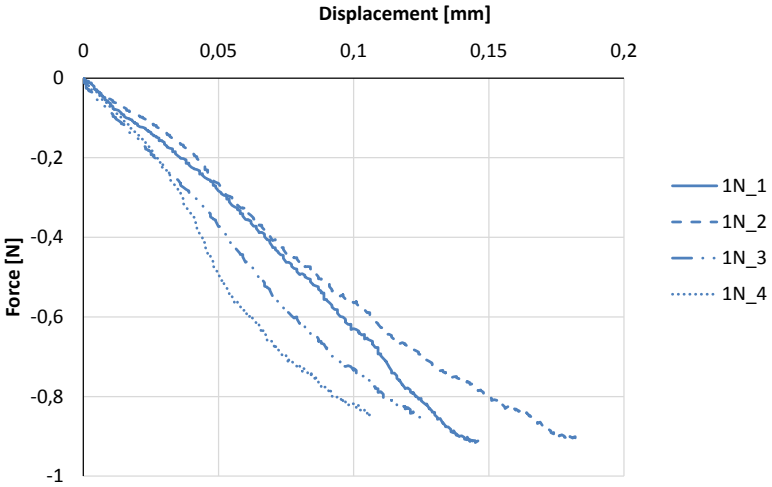

Figure 4.12 Force – displacement curve assembly phase with an assembly force of 1 N for 40/60 bitumen

deformed in this case, although the increase in stiffness here seems to be larger that could be expected based on the doubled amount of surface area. Based on the current insights no plausible explanation can be provided for the variations in the beginning of the assembly phase. An overview of the average displacement, the time needed for the assembly and the resulting strain rate during the tensile test is provided in Table 4.4 per assembly condition.

Table 4.4 Deformation during force controlled assembly, resulting strain rates during tensile tests and assembly times for different assembly conditions using 40/60 bitumen.

Specimen	Assembly period [s]	Imposed displacement during assembly [mm]	Specimen height [mm]	Applied strain rate during tensile test [%/s]
1N_1	30	0,15	2,85	0,5
1N_2	38	0,19	2,81	0,5
1N_3	27	0,13	2,87	0,5
1N_4	23	0,11	2,89	0,5
Average 1N	29,3	0,15	2,85	0,5
5N_1	197	1,01	1,99	0,8
5N_2	229	1,14	1,86	0,8
5N_3	193	0,96	2,04	0,7
5N_4	205	1,02	1,98	0,8
Average 5N	205,7	1,03	1,97	0,8

4.4.3 Tensile strength on 40/60 test specimen assembled under various conditions

All the results of the tensile tests executed on 40/60 specimen, with 1 and 5 N as assembly force are plotted in Figure 4.13. The result of specimen 3 assembled at 5 N is not plotted, as during the tensile test it was observed that the silicon paper was caught between the intended contact area jeopardizing the development of contact. As it is not measured how much of the contact area was affected, this result is left out as it cannot be interpreted with any certainty.

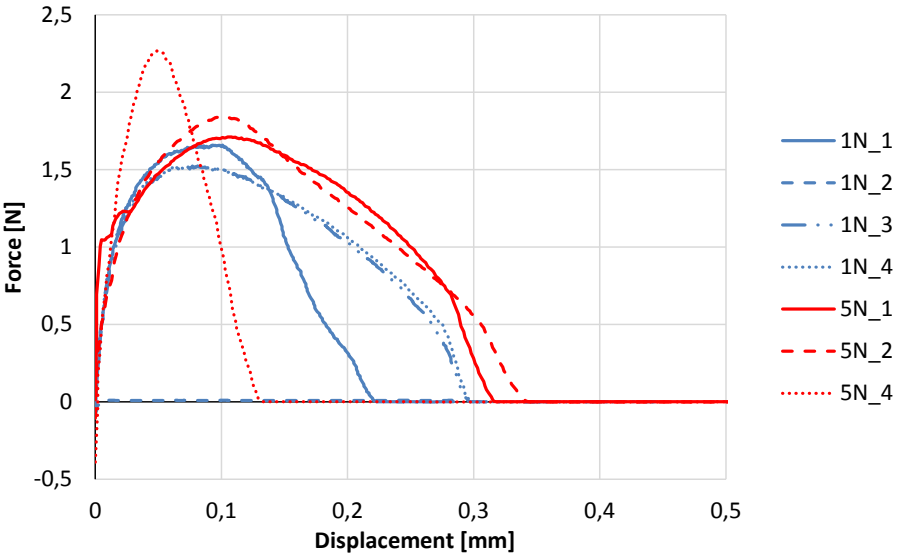

Figure 4.13 Force - displacement curves for all 40/60 specimens obtained from tensile tests following an assembly phase using an assembly force of either 1 or 5 N and a constant assembly rate of 0.005 mm/s.

The results of tensile strength tests reported in Figure 4.13 have actually been obtained while applying different strain rates during the tensile test. The obtained tensile strengths for the 5 N specimens are therefore judged to be less reliable compared to the 1 N specimens which were obtained at the desired strain rate. It is recommended that in future research aimed to study the impact of assembly conditions on healing, the strength – strain rate correlation should be part of the research. It can also be seen that during the tensile test, all tested specimen come apart fully during the tensile test as at some point the force becomes 0 in a step like fashion. Compared to the 70/100 specimen, the 40/60 specimen have much less post peak strength, with a maximum displacement of only 0,34 mm for 40/60 compared to values over 1 mm for 70/100.

The correlation between tensile strength and assembly force are reported in Figure 4.14. In this figure the reference value for the tensile strength is also plotted. If the corrected

value is representative for the determined tensile strength, it can be seen in the graph that an increase in assembly force, results in an increase in observed healing strength, although the impact of additional assembly force seems less for 40/60 compared to 70/100. The observed instant healing strength for 1 N is a little less than 20% of the original strength, while an assembly force of 5 N results in 30% recovery of the reference strength. This strength recovery is less compared to the 70/100 bitumen under similar conditions, which is in line with the expectations, as softer bitumen is considered to be a better healer.

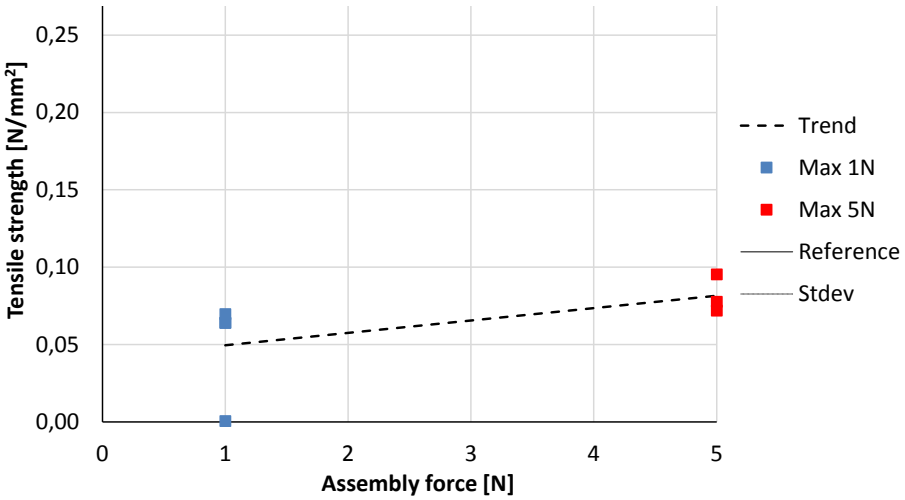

Figure 4.14 Detected and corrected tensile strength for 40/60 healing specimens brought together using and assembly rate of 0,005 mm/s and an assembly force of either 1 or 5 N along with the determined reference strength of the material.

4.5 TEST RESULTS 10/20 BITUMEN

4.5.1 Reference strength 10/20 specimens

For bitumen with a penetration grade of 10/20 three reference specimen were tested to determine the reference strength that is needed to calculate the healing ratio. The applied strain rate of 0,5 %/s resulted in brittle fracture near the rings of the specimen for all specimen, see Figure 4.15. There was a very large variation in test results, as can be seen see Figure 4.16. The three values for the maximum tensile force were 18,96 N, 0,34 N and 4,13 N. The resulting average reference value for the tensile stress is 0,28 N/mm^2 with a standard deviation of 0,28! The large standard deviation means the average value lacks numerical significance. Nevertheless, it's used to calculate a healing ratio to highlight trends in healing behaviour. This healing ratio should not be interpreted numerically, but rather as a tool to identify relative healing trends. .

Figure 4.15 Example of brittle fracture of reference specimen broken near the ring; at the right a schematic indication of the location of crack interface, at the left a photograph of both crack interfaces; at the top the side view of the column is shown, at the bottom the top view of the fracture interface is given with the metal ring visible.

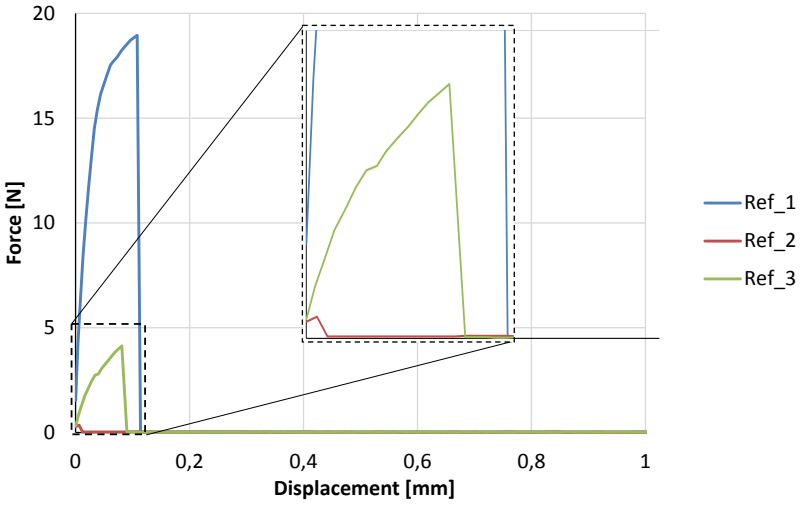

Figure 4.16 Force displacement graph for tensile tests of 10/20 reference specimen

4.5.2 Assembly phase using different assembly forces and speeds of 10/20 specimens

For the 10/20 specimen the assembly force used was 1, 5, 10 and 20 N, while the displacement rates were 0,01 mm/s and 0,00125 mm/s. During the assembly phase both the applied force and the resulting deformation are measured continuously. The force - displacement curves for 10/20 specimen variating the assembly forces are presented in

Figure 4.17, while in Figure 4.18 the curves are given for two displacement rates. Within this test series, the slow displacement rate is only used for the high assembly force. This was done as during the execution of the tests it was noticed that for low assembly forces no healing strength was detected. In response to this the initial test plan was changed to include higher assembly forces. To gain most insight from the little number of remaining specimen, the low assembly rate was only applied in combination with the large force of 20 N.

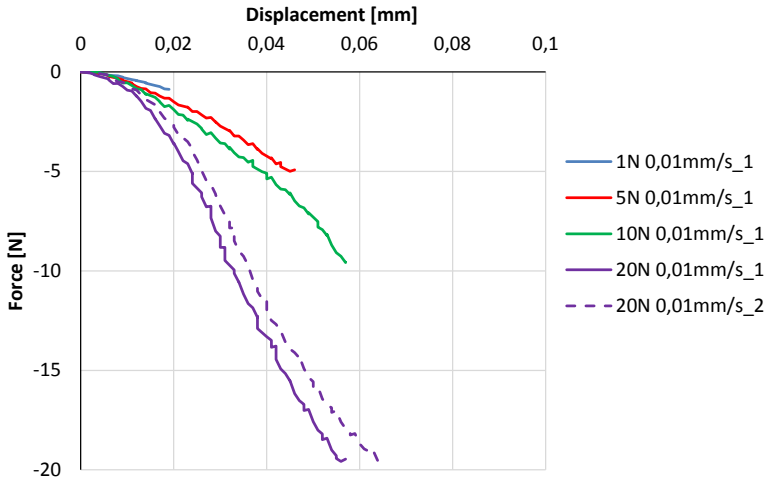

Figure 4.17 Force – displacement curve for the assembly phase of 10/20 bitumen showing multiple assembly forces at an assembly rate of 0.01mm/s.

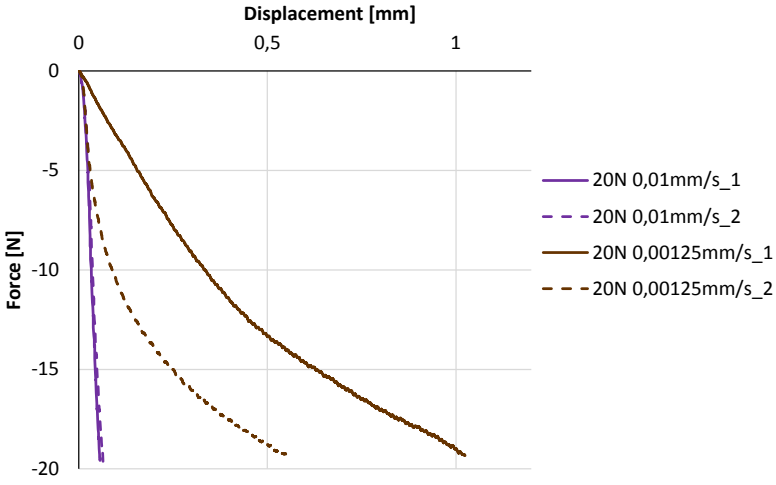

Figure 4.18 Force – displacement curve for the assembly phase of 10/20 bitumen showing two assembly rates at an assembly force of 20 N.

When evaluating the force - displacement curves of the assembly phase the following observations can be made. There is some variation between the deformation and the detected assembly force for half-specimens that were assembled using a speed of 0,01 mm/s. There seems to be an initiation phase, as initially the curves are less steep. A possible explanation could be that the initial stiffness is lower, due to presence of surface roughness, as for this hard binder, the imprint of the mould is still visible in the specimen. It is unexplained why a lower assembly force seems to result in a lower stiffness. For the specimen where an assembly rate of 0,01 mm/s is used, the total amount of deformation during the assembly phase is very limited; maximum of 0,07 mm for the largest force of 20 N. For these cases, the total displacement is an order of magnitude smaller compared to the 40/60 and the 70/100 binder. When the slow assembly rate is applied, the deformation during the assembly phase is not linear and decreases. An overview of the average displacement, the time needed for the assembly and the resulting strain rate during the tensile test is provided in Table 4.5, for each specimen.

Table 4.5 Deformation during force controlled assembly and resulting strain speeds during tensile test.

Specimen	Assembly period [s]	Imposed displacement during assembly [mm]	Specimen height [mm]	Applied strain rate during tensile test [%/s]
1N_0,01mm/s_1	2,0	0,02	2,98	0,5
5N_0,01mm/s_2	5,0	0,05	2,95	0,5
10N_0,01mm/s_1	6,5	0,06	2,94	0,5
20N_0,01mm/s_1	7,4	0,06	2,94	0,5
20N_0,01mm/s_2	8,1	0,07	2,94	0,5
20N_0,00125mm/s_1	831	1,02	1,98	0,8
20N_0,00125mm/s_2	457	0,55	2,45	0,6

4.5.3 Tensile strength on 10/20 test specimen assembled under various conditions

All the results of the tensile tests executed on assembled 10/20 specimen using various assembly conditions are plotted in Figure 4.19. Specimen 20N_0,00125mm/s was accidentally tested at a very different strain rate and is therefore not reported. If this figure is compared to Figure 4.3 and Figure 4.13 it can be seen that compared to the 70/100 and the 40/60 bitumen, the maximum tensile strength for healed specimen for 10/20 bitumen is highest. It can also be seen that when the specimens fails, the failure is completely brittle with no significant post peak tensile strength capacity. When the test starts, in some of the specimen there is still some compression stress in the specimen present from the assembly phase.

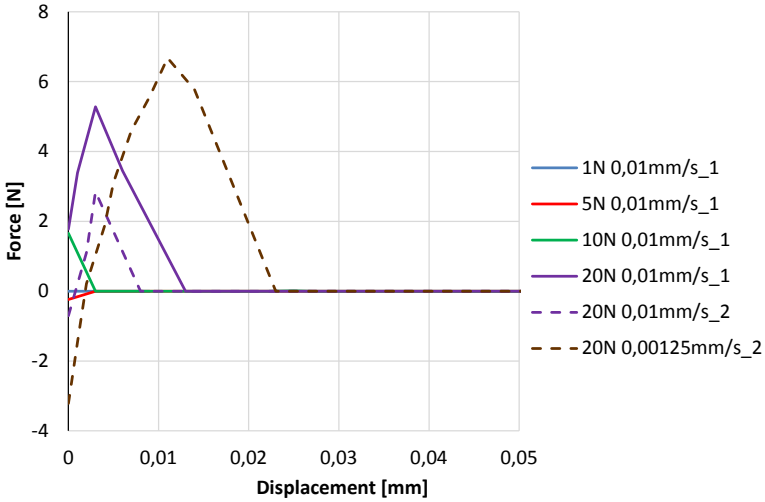

Figure 4.19 Force - displacement curves for all tensile tests on 10/20 while varying the assembly conditions.

The peak value for 20N_0,00125mm/s reported in Figure 4.19 has been obtained in a tensile test where a different strain rate was applied. In Figure 4.20 the healed strength for 10/20 for the different assembly conditions is plotted in comparison to the reference value. It should be noted that the variation of this reference value was very large as can be seen from the large intervals for the standard deviation. From the graph the following observations can be made. Also for this 10/20 binder both a higher assembly force and a lower assembly rate result in a higher healing strength. Next to this it is shown that for this binder an assembly force of 1 and 5 N does not even result in any detectable healing. As already mentioned, these results should be considered with care, due to the limited repetitions and the large variation in the values for the reference specimen.

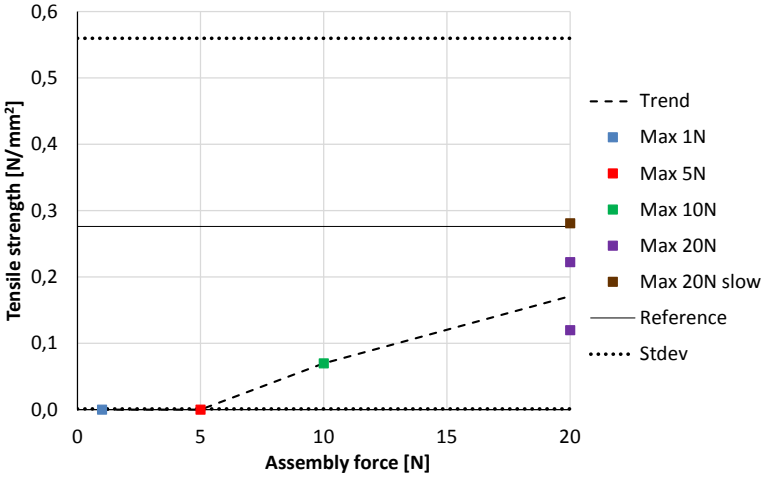

Figure 4.20 Reference, determined and corrected strength for the different assembly conditions for 10/20 bitumen.

4.6 DISCUSSION AND INTERPRETATION OF THE RESULTS

4.6.1 Impact of assembly conditions on instant healing strength

When the healed strength and the reference strength presented in the previous sections are compared, healing ratios can be calculated for different binders in relation to the applied assembly conditions. The graph relating healing ratios to assembly force for three binders; 70/100, 40/60 and 10/20, are shown in Figure 4.21. The impact of the deformation rate during the assembly phase on the healing ratio for two binders; 70/100 and 10/20 are shown in Figure 4.22. NB. In both graphs the error for 10/20 values is very large, as the strength of the reference specimen showed an extremely large variation. The results are presented to show that there is a trend in the healed strength for 10/20 specimen with respect to the applied assembly conditions.

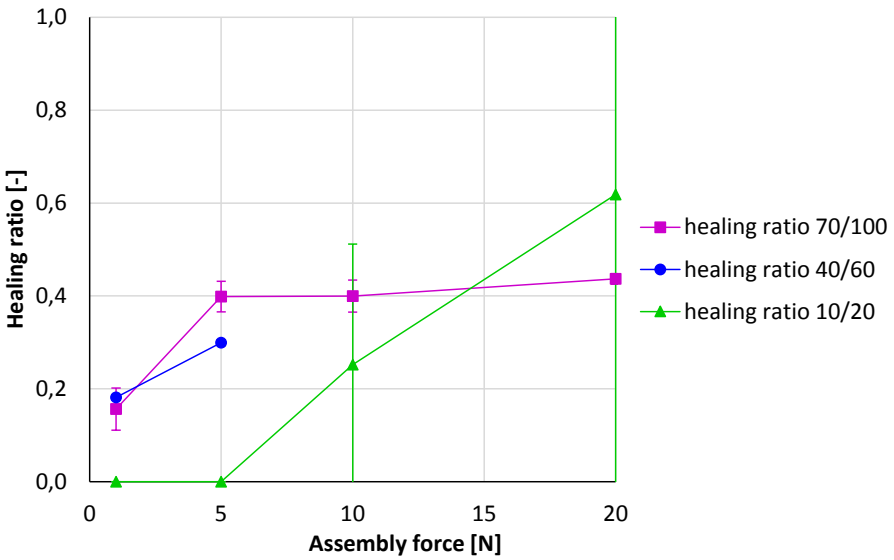

Figure 4.21 Healing ratios, just after the assembly phase is finished, for three types of bitumen correlated to assembly force, N.B. healing ratios are not comparable between binders as assembly rates differ per binder.

The results for the binders presented in Figure 4.21 & Figure 4.22 cannot truly be compared with one another; in the figure where the impact of assembly force is evaluated, the assembly speed varies per binder and vice versa. Nevertheless some information can be taken from these results. For all binders, the healing ratio increases with a higher assembly force and decreases with a faster assembly rate. It is also shown that that both soft and hard binders exhibit a certain amount of instant healing. However, soft binders show healing under a wider range of conditions, while the harder binders require a higher force perpendicular to the healing interface, or a slower the assembly rate to exhibit healing

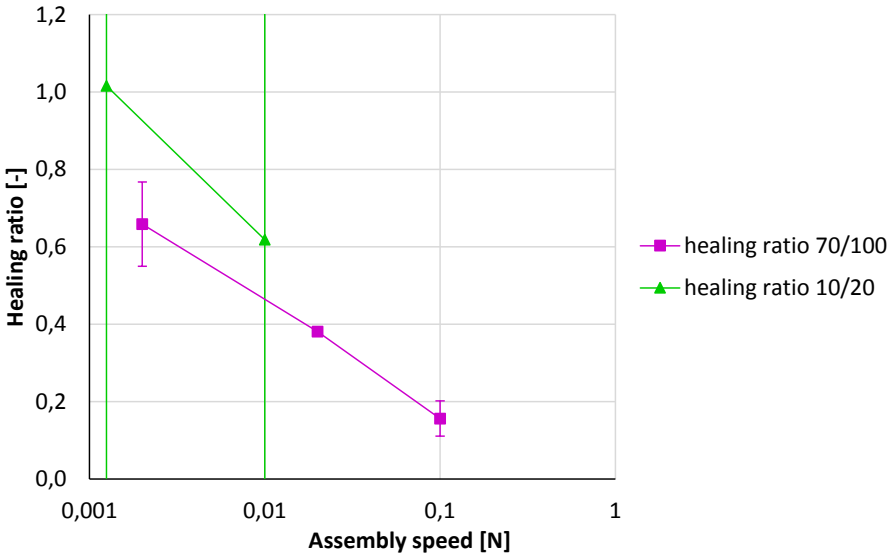

Figure 4.22 Healing ratios, just after the assembly phase is finished, for two types of bitumen in relation to assembly rate, N.B. healing ratios are not comparable between binders as assembly forces differ per binder type.

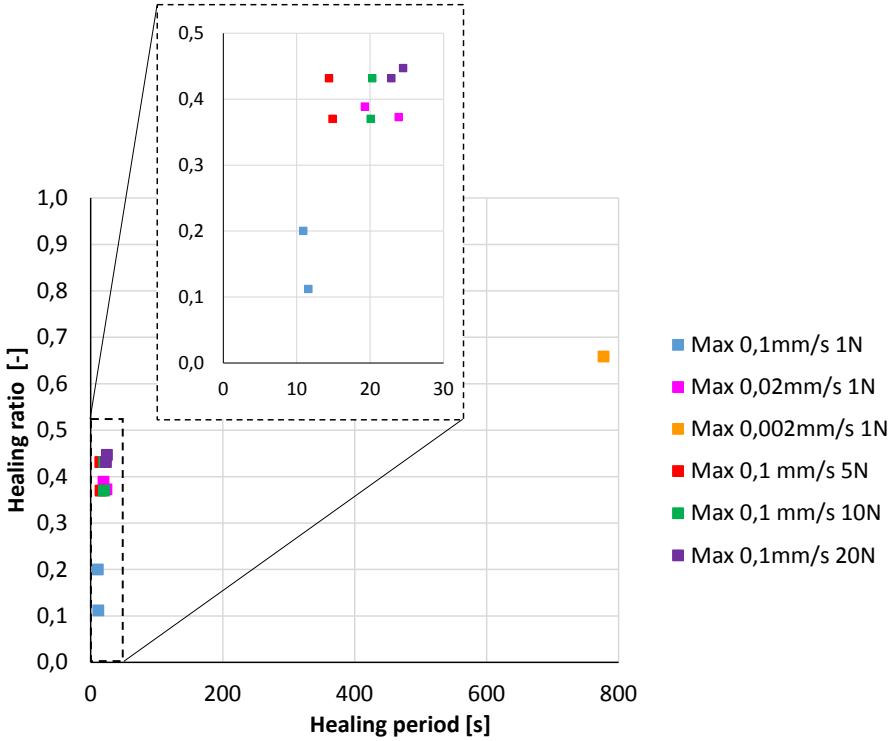

Figure 4.23 Healing ratio plotted versus healing period

behaviour. This suggests that the healing process of hard and soft binders is similar in nature, while the dynamics for harder binders require more favourable conditions.

As the healing periods were not the same for all presented results a check was done to assess the impact of the differences in healing period on the healing ratio, see Figure 4.23. From the figure it can be seen that there is no strong correlation between healing period and healing ratio. The next chapter (Chapter 5) focusses on the impact of healing time, in this chapter the impact of healing time will be studied in more detail.

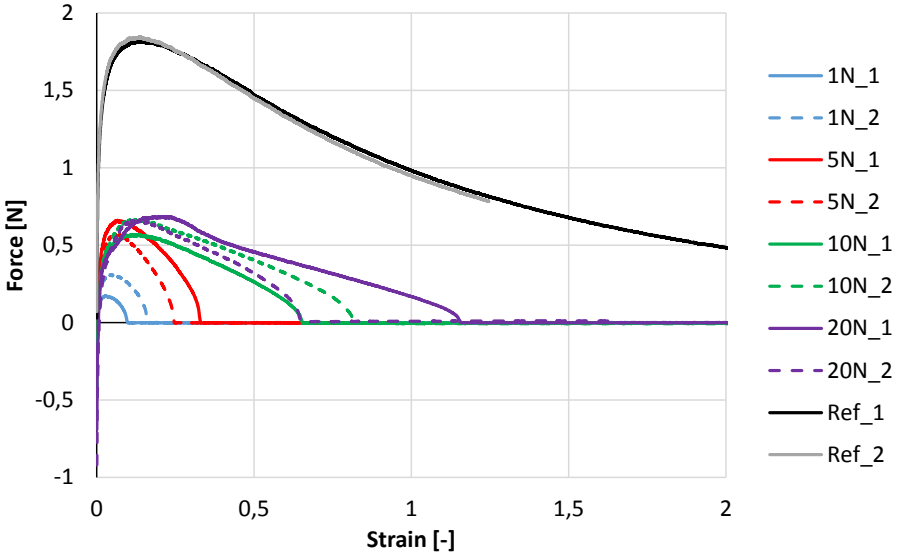

Figure 4.24 Force – strain graphs for 70/100 bitumen for both reference specimen and healed specimen subjected to different assembly forces.

4.6.2 Loss in toughness and apparent adhesive failure

It was noted that the assembly conditions also affected the toughness of the healed connection. The force strain diagrams for the healed specimen and the reference specimen force-strain graphs are presented in Figure 4.24 for 70/100 bitumen and Figure 4.25 for 40/60. In these graphs it can be seen that a higher healing force also has a positive influence on the post peak bearing capacity. It can also be observed that the healed connection of the harder 40/60 binder has less recovery of facture toughness compared to the softer 70/100 binder.

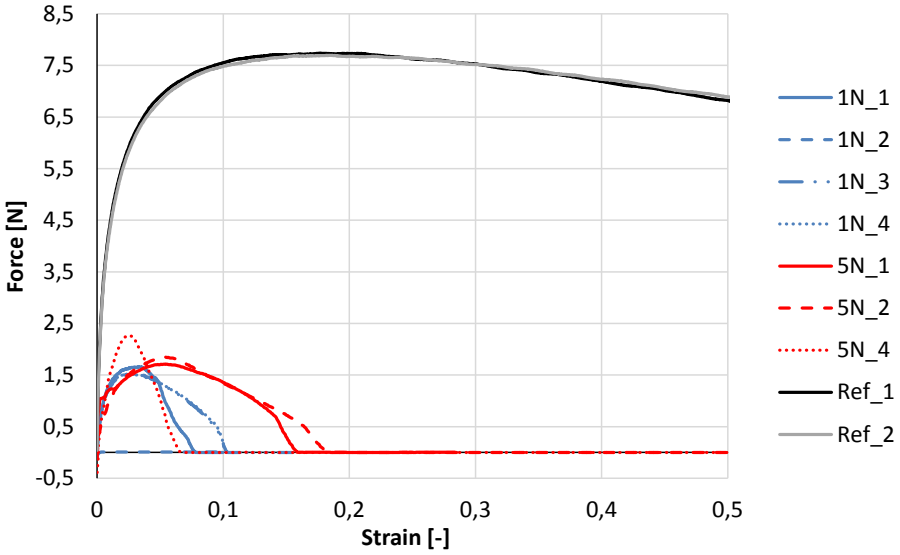

Figure 4.25 Force – strain graphs for 40/60 bitumen for both reference specimen and healed specimen subjected to different assembly forces.

4.6.3 Formulating a representative assembly protocol for a representative healing test

4.6.3.1 *Aim of the assembly procedure*

The second aim of the test series reported in this chapter was to formulate a general assembly protocol that can be used to compare the healing potential of different materials and different healing periods. The protocol aims to consistently bring a significant and comparable surface area into contact across different binder types, in a repeatable way. Consequently, following requirements are set for the assembly protocol;

- The assembly procedure results in a fixed amount of area in contact;
- The assembly protocol should be applicable to materials with a different stiffness and/or viscosity to be able to compare healing potential of different binder types;
- The assembly procedure is repeatable;
- The time period needed for the assembly phase is constant, to ensure one healing period.

4.6.3.2 *Guiding principles*

It is hypothesised that the assembly conditions control the amount of area in true contact for a specific material. Unfortunately, this hypothesis cannot be verified as there is no

good test method available to measure the amount of contact created. Therefore, at this stage, it's not possible to define an assembly procedure that guarantees an equal amount of true contact area.

As already mentioned in the introduction of this chapter, the only parameters that can be varied in the assembly procedure are the displacement rate during assembly and the force at which the displacement is stopped. The results presented in this chapter have shown that both the assembly force and the rate affect the healing ratio, although for some conditions a plateau level seems to be possible (70/100 above 10 N, at an assembly speed of 0,1 mm/s). Since the goal is to develop a procedure that compares different bitumen types, assembly force alone is unsuitable; harder materials yield less contact under the same force. Thus, a single force level cannot ensure comparable assembly conditions.

During execution of the test reported in this chapter, some limitations of the test set-up were uncovered. Firstly, for softer binders (40/60 and 70/100), large assembly forces or very low assembly rates caused excessive deformations. Since such specimens behave unpredictably in tensile tests, deformation during assembly should be limited to 1 mm to ensure reliable results. Additionally, the machine could not accurately apply deformation rates below 0,002 mm/s. Finally, when the imposed deformation is very small, sagging causes the actual contact area to fall below the intended 23,8 mm^2 (see Section 3.7.3). When formulating an assembly protocol all the situations mentioned above should be avoided.

4.6.3.3 *Approach*

In all healing results reported in this chapter, no material transfer between the healing surfaces was observed, indicating that healing occurred primarily through adhesion. According to the adhesion mechanism described in Section 2.7, adhesive healing is governed by interactions at the interface, which depend on both the intrinsic material properties (e.g., surface energy, viscoelastic behaviour) and the true contact area. In case that the binder type is constant, variations in adhesive healing strength can be attributed to differences in the effective contact area established during the assembly phase. This suggests that comparable healing responses imply similar interfacial contact areas, which is the first objective of the assembly protocol. Therefore for a single material, different parameters of the assembly conditions are compared to assess which combination has the best correlation with the observed healing.

The first approach assess the correlation between the amount of deformation applied during the assembly phase and the healing. As explained in Section 2.6, true contact between two surfaces is related to the local deformation of the surfaces. This local deformation or the amount of contact created could not be measured. However, since the total deformation during assembly is measured, and global stiffness likely correlates with local surface stiffness, it may serve as an indirect indicator of the contact area at

the healing interface. A second possible indicator of contact area is the energy applied during the assembly phase. For a given material, creating contact requires deformation, which in turn requires energy. Therefore, it is hypothesized that greater energy input during assembly leads to increased contact at the healing interface. The amount of energy spend during the assembly phase is determined by calculating the amount of work done during the assembly procedure using Equation 4.2, which implies calculating the area under the force-displacement curves of the assembly phase.

$$\boldsymbol{L = \int_{x_i}^{x_f} F(x)dx} \qquad (4.2)$$

Assessment of correlation of parameters with amount of contact

The correlation between healing ratio and both specimen deformation and assembly energy was analysed for the 70/100 bitumen, which underwent the widest range of assembly conditions. Figure 4.26 shows the healing ratio plotted against total specimen deformation during assembly. Figure 4.27 presents the relationship between the healing ratio and the work done during the assembly phase.

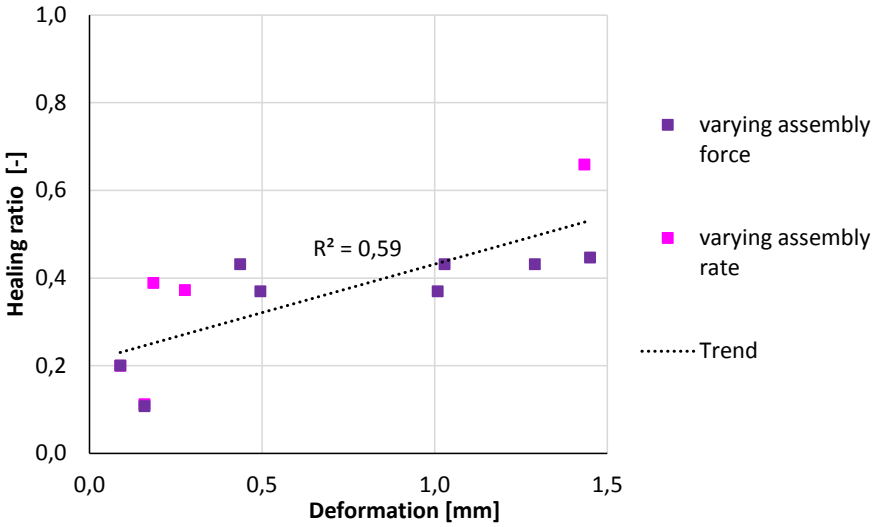

Figure 4.26 Correlation between displacement applied during the assembly phase and healing ratio for 70/100 binders that were tested for healing just after the assembly phase.

When Figure 4.26 is compared to Figure 4.27 it can be seen that there is a moderate correlation between the assembly displacement (R^2 = 0,59), while there is very weak correlation between the healing ratio and the energy invested in the assembly phase (R^2 = 0,13). It is concluded that based on the data in the graphs, the total amount of deformation applied during the assembly phase is an acceptable parameter to realize a similar amount of contact. Although it should be noted that this is only based on one material and therefore should be studied further.

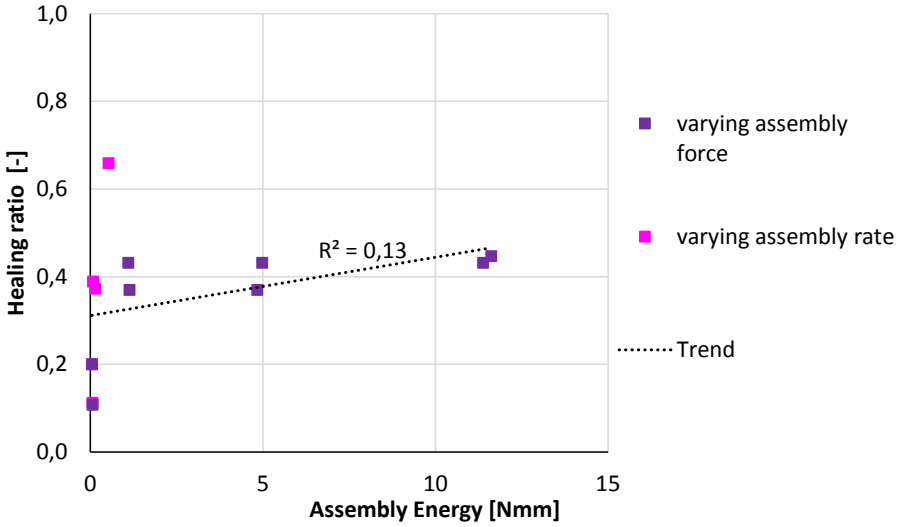

Figure 4.27 Correlation between assembly energy and healing ratio for 70/100 binders that were tested for healing just after the assembly phase.

4.6.3.4 *Advised assembly parameters*

Given the strong correlation between assembly phase displacement and contact area, it is recommended to apply a consistent deformation across a test series. To avoid excessive deformation, the applied displacement should not exceed 0,8 mm, while a minimum of 0,4 mm is advised to ensure sufficient contact.

Since displacement rate also affects the healing ratio, it is recommended to also use a consistent rate across all tests. When selecting this rate, it's important to avoid extremes. Very low rates prolong the assembly phase, which limits the feasibility of short healing periods and increases sensitivity to geometric variations between specimens. Very high rates reduce surface deformation, leading to smaller and more variable contact areas. Therefore, an assembly displacement rate between 0,01 and 0,1 mm/s is advised, ensuring the total assembly time does not exceed 30 seconds.

The total amount of deformation that should be applied during the assembly phase, cannot be used directly as input for the test protocol. Instead, a calibration test is needed to determine the appropriate combination of assembly force and displacement rate that produces the desired deformation. The calibration begins by selecting a displacement rate within the recommended range (0,01 – 0,1 mm/s). Using this rate and a high initial assembly force (e.g., 20 N), a test is performed to identify the force level at which the target deformation is achieved.

4.7 CONCLUSIONS AND RECOMMENDATIONS

The aim of this chapter was to answer RQ3; How does the creation of contact impact healing of bituminous binders? Next to this, an assembly protocol was needed for the planned research in the next chapter, which would ensure a proper starting point for the evaluation of the development of healing over time.

The results presented in this chapter demonstrate that the assembly conditions significantly affect the initial or instant healing ratio. This shows that even if the healing period and temperature are kept constant, the observed healing can strongly vary depending on boundary conditions at the healing interface; both a larger normal force or a slower displacement rate leads to a higher healing ratio. This implies that the boundary conditions at the healing interface have to be taken into account when designing and interpreting a healing test result. This provides a plausible explanation why the healing ratio can vary strongly between different test methods; as the nature of the set-up can strongly influence the boundary conditions at the healing interface.

The results show that the instant amount of healing that can be realized is quite significant. Depending on the assembly conditions and material the instant healing that is detected after seconds to minutes can be more than 50% of the original strength. The presented test results seems to indicate that the observed instant healing is correlated to the amount of surface area that has been brought into real contact. This also implies that adhesion plays a significant role in the recovery of strength. Although it should be noted that the support for this conclusion is based on indirect evidence and therefore requires further verification.

It has been demonstrated that softer binders require less favourable healing conditions compared to harder binders for a similar healing ratio. Although, it is very interesting that very hard binder (penetration grade 10/20), also shows a significant recovery of strength. Although, this does require very favourable boundary conditions at the healing interface; significant healing was only detected when the applied normal force during the assembly procedure was 10 times higher compared to bitumen with a penetration grade of 70/100.

The bond formed through healing is less tough than the original material. The effect is more pronounced in harder binders, as softer binders tend to regain more of their original toughness. This reduction in toughness may explain why healed specimens show lower fatigue resistance than fresh ones; cracks in healed specimen propagate faster due to increased brittleness.

For the healing test proposed in Chapter 3 an assembly procedure has been formulated which will allow to compare healing capacity of binders. This assembly procedure is based on fixing the amount of deformation that is applied during in the assembly phase, which should lie between 0,4 and 0,8 mm. Next to this, a fixed assembly rate should be used that is between 0,01 and 0,1 mm/s, while ensuring that the total assembly time stays below 30 s. Before a test series is conducted, a calibration test has to be

executed to select a combination of deformation rate and assembly force that meets the formulated requirements. It is recommended to verify the used of the total applied deformation during assembly as governing parameter for a uniform assembly procedure is verified for a wider range of materials.

5

DEVELOPMENT OF HEALING OF BITUMEN WITH TIME

DEVELOPMENT OF HEALING OF BITUMEN WITH TIME

The aim of this chapter is to obtain a more quantitative insight in the impact of time on healing of bitumen, by studying the development of healing with time. The direct tension two piece healing test presented in Chapter 3 is used to execute the work presented in this chapter. The specimens subjected to different healing periods have been assembled both in the testing machine and in the storage room. By using the combination of both assembly approaches, it is possible to study a variation in healing periods that spans several decades. Next to this, the combined effect of two different boundary conditions and healing periods is studied. This results in a more detailed view on the relevance of time in healing behaviour for different conditions.

In Section 5.1 the rationale is given behind the focus on the healing period when studying healing. In Section 5.2 the executed test program is presented. In Section 5.3 the healing results from tests performed on binders with different penetration grades are reported. Next, in Section 5.4 the healing results are presented for different binders of the same 70/100 penetration grade. Section 5.5 comments on the visual observations during testing, as these also provide some relevant insights. The chapter closes with conclusions (5.6) and recommendations (5.7).

5.1 INTRODUCTION

In most research done on healing, the healing period is identified as a key factor influencing the extend of healing, see Chapter 2. However, the correlation between time and healing has not been described extensively in a quantitative manner. Healing research has shown that the development of healing with time is not linear, but asymptotic; initially, longer healing periods significantly increase the amount of healing observed, however this effect diminishes with time and at very long time intervals no additional healing is observed. These observations are in line with the mechanisms that are believed to drive healing as described in Chapter 6. Both creation of surface contact and diffusion (driving homogenization of contact areas) show an asymptotic decline in further strength increase with longer healing periods.

To provide a more quantitative perspective on the development of healing with time, and obtain information on which time windows are most relevant for healing, the test program executed in this chapter studies the development of healing over several time decades. In order to assess the impact of a load perpendicular to the healing interface on healing, three binders with different penetration grades have been tested at different perpendicular load levels using both assembly in the storage room and assembly in the testing machine, as described in Chapter 5. Finally, to assess to what extend healing behaviour is dependent on the nature of the binder, the healing of three binders with the same penetration grade has been assessed.

5.2 TEST PROGRAM

5.2.1 Test temperature

For this part of the research a healing temperature of 14 °C was selected. This temperature was selected as to our current insights, this temperature is high enough for healing to occur, but also low enough to be able to follow the healing with time without excessive deformation of the specimen (see Chapter 3). Next to this, 14 °C is also a relevant temperature to study healing behaviour, as Dutch road structures have an average pavement temperature somewhere between 10 °C and 20 °C (J.H. Swart 1990). Therefore observations done on healing at 14 °C also have practical relevance. During the healing period samples were either placed in the storage room or inside the testing machine, depending on the location of assembly. The variation of the temperature in the storage room is slightly higher (14 °C +/- 1 °C) compared to the testing machine (14 °C +/- 0,2 °C).

To assess the extent of healing after the completion of a healing periods, specimens are tested in direct tension test using the two piece healing test presented in Chapter 3. The temperature during this direct tension test was 14 °C +/- 0,2 °C, although for a very limited number of cases a test temperature of 10 °C +/ 0,2 °C was used. The reason for this test temperature of 10 °C was to be able to compare the measured tensile strength with values reported in literature. These tests were executed in the initial stages of the research, at that time a representative tensile test executed at a common test temperature seemed the best option. However, as the research progressed and the option of assembly within the test machine was developed it became more logical to execute the tensile tests at the healing temperature, as there would be no time lost on chancing the temperature of the specimen to 10 °C. However, when this change was made no specimens remained of the first test series, therefore these tests were not executed at 14 °C as well.

5.2.2 Materials

The first part of this test program is executed using three binders with different penetration grades; a 70/100, a 40/60 and a 10/20. All binders originate from the same crude source (Q8) and are straight run bitumen. These are the same binders that also have been tested in Chapter 4. A penetration grade of 70/100 is regularly used in Netherlands for Porous Asphalt surface layers. Bitumen with a penetration grade of 40/60 is generally used for base and binder layers in the Netherlands. Bitumen with a penetration grade of 10/20 is not regularly used for the construction of pavements in the Netherlands. It is assumed that softer binders will show more healing, as this is reported in literature (Chapter 2). All three binders originate from a straight run refinery process with crude oil originating from the Middle East. Straight run bitumen are generally associated with good healing properties by the paving sector, although to the knowledge of the author this is not scientifically confirmed.

In a second test series three binders have been selected to study the impact of binder variations other than penetration grade. These three binders have the same penetration grade of 70/100 but are known to have a different origin. The three binders used are provided by different bitumen suppliers, more precisely Q8, Total and Nynas. The Q8 bitumen is the same that is used in the tests that focused on the impact of penetration grade and assembly conditions. There is no additional information on the background of the Total bitumen, however this is a bitumen that is frequently used in Netherlands. Nynas is another bitumen on the European market, which is known for its different appearance in AFM images, in which no multiphase system can be observed (Soenen et al. 2014).

5.2.3 Reference strength

In order to establish a healing ratio, reference specimen of 12 mm height are produced and tested two times to obtain a reference strength. The specimen were tested in tension, at a temperature of 14 °C, using a strain rate of 0,5 %/s.

5.2.4 Healing conditions for binders of different penetration grades

In order to study the impact of varying the stress states perpendicular to the healing interface, with different healing periods, a test series was carried out using different healing conditions. The difference in healing condition originates from the difference in assembly conditions, as specimen were assembled both in the storage room and inside the testing machine.

Table 5.1 provides an overview of the test program for specimens that were assembled in the storage room. Table 5.2 provides an overview of the specimens that have been assembled inside the testing machine. In both tables it can be seen that there is quite some variation in test conditions, this is mainly to address differences in material response. For instance the 70/100 specimens have not been stored with a load of 10.6 gram, as this extend of loading resulted in extreme deformation of the specimens. A similar situation holds for the applied load levels for machine assembly. Next to this, the 70/100 specimens have been tested to assess the tensile strength at 10 °C and not at 14 °C as already explained in Section 5.2.1. In the tables it is also visible that that for the 10/20 specimen many tests were only executed once. For this binder the test series evolved during execution, as the initial intended test conditions did not amount to any healing. Therefore during the series load conditions were expanded. However, as there were limited specimens available no specimens were left for repetitions. In spite of the lack of repetitions, it was decided to report the results anyway, as do provide some additional qualitative information.

For the specimen assembled inside the test machine. The reported healing period in the table corresponds to the total time that the surfaces were brought together, consisting of the assembly phase, the transition time needed by the machine and the applied healing period (which is zero for the first time step).

Table 5.1 Overview of test program of healing specimen assembled in the storage room

Binder type	Healing period [hours]	Load perpendicular to healing interface	Temperature during tensile test	Number of repetitions
70/100	0,1; 1; 24; 168	1,6 gram = 0,016 N	10 °C	3
40/60	1; 24; 168 1; 24; 168	1,6 gram = 0,016 N; 10,6 gram = 0,11 N	14 °C	2-3 2-3
10/20	16; 24; 168 24; 168	1,6 gram = 0,016 N; 10,6 gram = 0,11 N	14 °C	1 2-3

Table 5.2 Overview of test program of healing specimen assembled in the test machine

Binder type	Healing period [hours]	Load perpendicular to healing interface during assembly phase	Assembly rate	Temperature during tensile test	Number of repetitions
70/100	0,04; 0,06; 0,20; 1; 10; 100	1 N	0,01 mm/s	14 °C	2
70/100	0,006; 0,02; 0,06; 0,14; 0,56; 5,6; 56	1,5 N	0,04 mm/s	14 °C	2-3
70/100	0,006; 0,06; 0,56; 5,6; 16,7; 111	2,3 N	0,04 mm/s	14 °C	2
40/60	0,01; 1; 12 0,06; 24	1 N 5 N	0,005 mm/s	14 °C	2

5.2.5 Healing conditions for different binders with a penetration grade of 70/100

In order to investigate the impact of other binder aspects than penetration grade, the healing behaviour with time of three binders with the same penetration grade has been researched. In order to assess the rheological properties of the binder the complex modulus (G*) and phase angle (δ) are determined using the DSR.

The half-specimen are assembled at an assembly rate of 0,04 mm/s. Table 5.3 presents an overview of the healing periods applied when studying the three binders. In the table it can be seen that the test series span 3-4 decades of time, with healing periods ranging from 30 seconds up to 400.000 s (111 hours). The italic healing periods are used for all three binders. The Q8 binder was exposed to the longest healing period to investigate if this would lead to 100% healing. Most tests were repeated 3 times, except the Q8 series with a healing period of 111 hours. This test was repeated just two times, due to limited

availability of the test machine. As it has been shown in Chapter 3, that the repeatability of the test is quite reasonable.

Table 5.3 Overview of test program of healing specimen assembled in the test machine

Binder type	Healing period [hours]	Number of repetitions
Q8	*0,01; 0,06; 0,6; 6*; 17; 111	2
Total	*0,01; 0,06; 0,6; 6*; 55	3
Nynas	*0,01; 0,06; 0,6; 6*; 55	3

The intended strain rate during the tensile test was 0,5 %/s. However, as the series for Q8 originated from earlier series of measurements, the actual applied strain rate in this series was lower, more precisely 0,4 %/s. As before the fault originated from the loss in specimen height due to the assembly procedure, which was not taken into account when calculating the required displacement rate. As already presented in Section 4.2.5 the measured strength can be corrected to match a strain rate of 0,5 %/s using the correlation between strain rate and strength.

5.2.6 Corrections for applied strain rate

As in Chapter 4, the applied strain rate during the tensile tests of the healing specimen was often higher than the intended 0,5 %/s. This error in measured strength can be corrected using the correlation between strength and strain rate. This correlation is obtained within this research for Q8 70/100 and has been reported in Section 3.6. Equation 4.1 is based on these results and can be used to correct the measured strength to a representative value that matches the strain rate of the reference specimen of 0,5 %/s.

Even though this correlation is only available for Q8 70/100 bitumen, this value is used to correct all test results reported within this chapter also the ones were another binder was used. It was judged that the error using the wrong correction factor is smaller than not using a correction factor for the strain rate at all. However, for future research it is imported to recommended that the test program is set-up to ensure that these kind of corrections are not necessary.

Next to this, when calculation the healing ratio a correction is made to address the fact that the absolute value of the healing ratio cannot be larger than 1, following the approach presented in Section 3.7.4.

5.3 HEALING STRENGTH FOR BINDERS WITH DIFFERENT PENETRATION GRADES

5.3.1 70/100 bitumen, assembly in storage room at 14 °C, tensile test executed at 10 °C

For these test series there are no results reported for the assembly phase as this process is not monitored in the storage room. All the results of the tensile tests executed on both the reference and the storage healed specimen of this series are plotted in Figure 5.1. From the graph it can be seen that most of the half-specimen that were exposed to shorter healing periods of 0,1 and 1 hour come apart fully during the tensile test. This is visible in the graph as the moment when the curve jumps to zero quite abruptly. This type of failure was also observed manifold in the previous chapter where specimens were tested immediately after the assembly phase was completed. All specimen exposed to a healing period of 24 hours or longer did not come apart during the tensile test, demonstrating ductile failure trough out the tensile test.

The specimens that were exposed to a healing period of 168 hours (one week) had deformed quite significantly due to the permanent loading of the small weight. This had two undesirable consequences for the specimen geometry. In the first place the specimens are more likely to have an angular rotation. Due to this angular rotation, these specimens are more likely to break when they are fixed in the DSR for tension testing, as the clamps dictate an aligned geometry. In this test series two of the three test specimens that had healed for 168 hours failed during placement in the DSR, therefore only one result is reported for this healing period. The second consequence of these highly deformed specimen is that the whole surface of the silicon paper ring separating the half specimen comes into contact with the bitumen. Even though the bitumen doesn't stick very well to this paper, it still sticks a little. This can be seen from the high initial peak value for the specimen that has healed for 168 hours. For a short moment the full area of the paper ring is activated resulting in a stiff response and a high peak force. The paper doesn't stick well, therefore after a limited amount of deformation the specimen comes loose from the silicon paper and the response is again dominated by the contact of the two surfaces of the halve specimen. Consequently, when evaluating the results, the secondary is taken into account instead of the first high peak.

All peak values of the strength observed in the tensile tests and the amount of deformation observed after the healing period are reported in Table 5.4. As the specimens have deformed during the healing period, as a result of the weight that was placed on top, the specimen height and the total deformation are also reported in the table. As the reference specimen are not exposed to a load, these specimens have not deformed and no change in sample height is reported in the table.

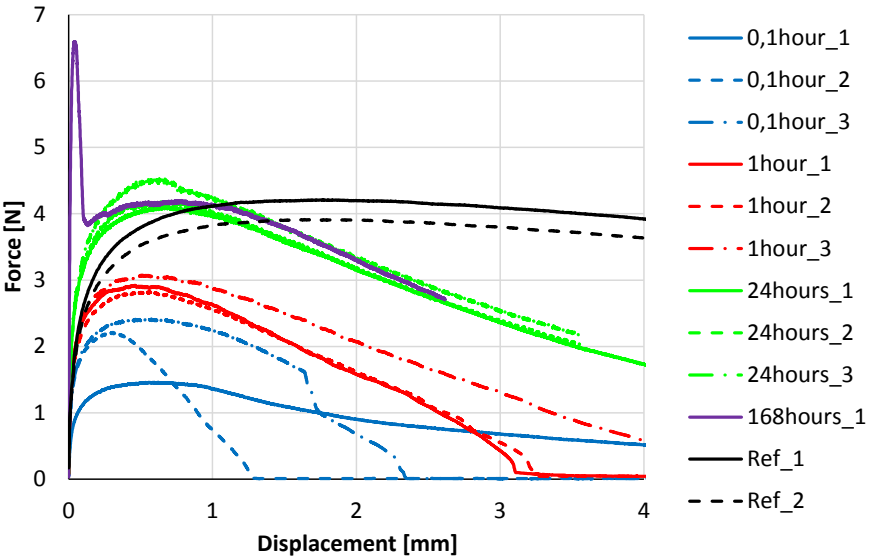

Figure 5.1 Force – displacement graph for all storage healed samples and reference samples of 70/100 bitumen healed at 14 °C and loaded in tension at 10 °C and a strain rate of 0,5 %/s.

Table 5.4 Overview of all peak forces and the amount of deformation during healing for all storage healed samples and reference samples of 70/100 bitumen healed at 14 °C and loaded in tensile at 10 °C.

Specimen	Peak force [N]	Strength [N/mm2]	Specimen height [mm]	Deformation during healing [mm]
0,1 hour 1	1,46	0,06	3,31	0,19
0,1 hour 2	2,21	0,09	3,11	0,39
0,1 hour 3	2,41	0,10	2,98	0,52
1 hour 1	2,92	0,12	2,90	0,60
1 hour 2	2,82	0,12	2,87	0,63
1 hour 3	3,08	0,13	2,66	0,84
24 hours 1	4,11	0,17	2,70	0,80
24 hours 2	4,19	0,18	2,34	1,16
24 hours 3	4,53	0,19	2,34	1,16
168 hours 1	4,20	0,18	1,80	1,70
Ref 1	4,21	0,15	-	-
Ref 2	3,91	0,14	-	-

All peak forces reported in Table 5.4 are plotted on both a linear and a logarithmic time scale and presented in Figure 5.2. The error bars in the graph represent the standard deviation. The result for a healing period of 168 hours doesn't show an error bar, as this point represents a single test result. From the figures some observations can be made. First of all, the linear graph clearly shows that healing does not develop linear with time, initially there is a strong increase with time which flattens for longer heeling periods. Another important observation is that the reference strength is lower compared to the healed strength. The high value for the healed specimen is most probably related to the difference in geometry, resulting in a higher strain rate for the healed specimen compared to the reference, as already has been explained in Section 3.7.3. The most remarkable observation that can be made from the graph is that the healed strength does not increase after 24 hours, which implies that this bitumen has fully healed within 24 hours under the imposed conditions.

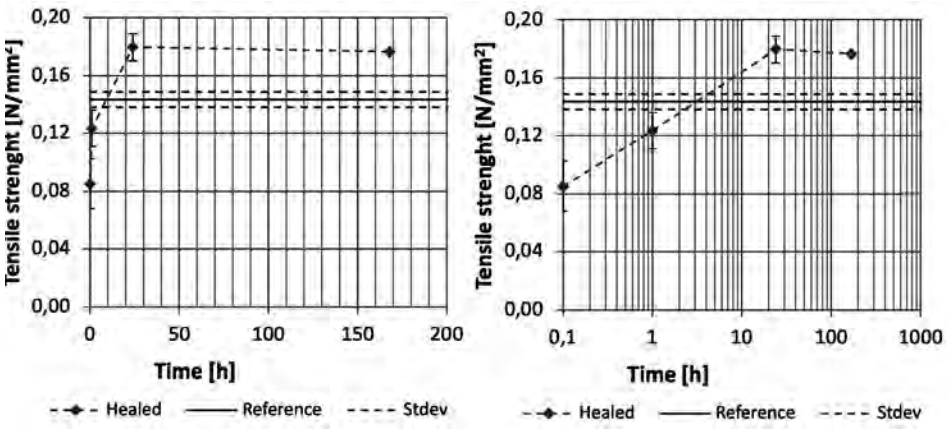

Figure 5.2 Observed healing strength and reference strength of 70/100 bitumen (Q8) healed at 14 °C and loaded in tensile at 10 °C on a linear (left) and a logarithmic time scale (right)

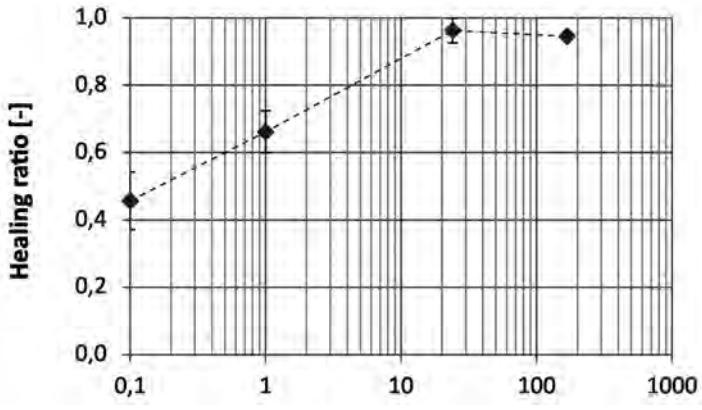

Figure 5.3 Healing ratio of 70/100 bitumen exposed to storage leaded with 1 gr and healed at 14 °C, after 0,1; 1; 24 and 168 hours of healing

Based on the reference and the healed strength the healing ratio with time can be plotted in Figure 5.3. To correct for the high healing value compared to the reference strength, the values are normalized using the approach presented in Section 3.7.4. From the graph is becomes clear that the largest part of the healing takes place within the first hours of healing, with more than half of the total healing taking place in the first 6 minutes.

5.3.2 70/100 BITUMEN. ASSEMBLY IN TEST MACHINE AT 14 °C, TENSILE TEST EXECUTED AT 14 °C

5.3.2.1 *Assembly force 1 N, assembly rate 0,01 mm/s*

The reference specimen were tested two times and the results are plotted in Figure 5.4. The numerical values for the maximum observed tensile strength are given in Table 5.5. The observed strengths are significantly lower compared the values for Q8 70/100 reported in Section 4.3. It is not clear what caused the difference in strength. It is most likely that this due to a difference bitumen batch or short term aging during the specimen preparation.

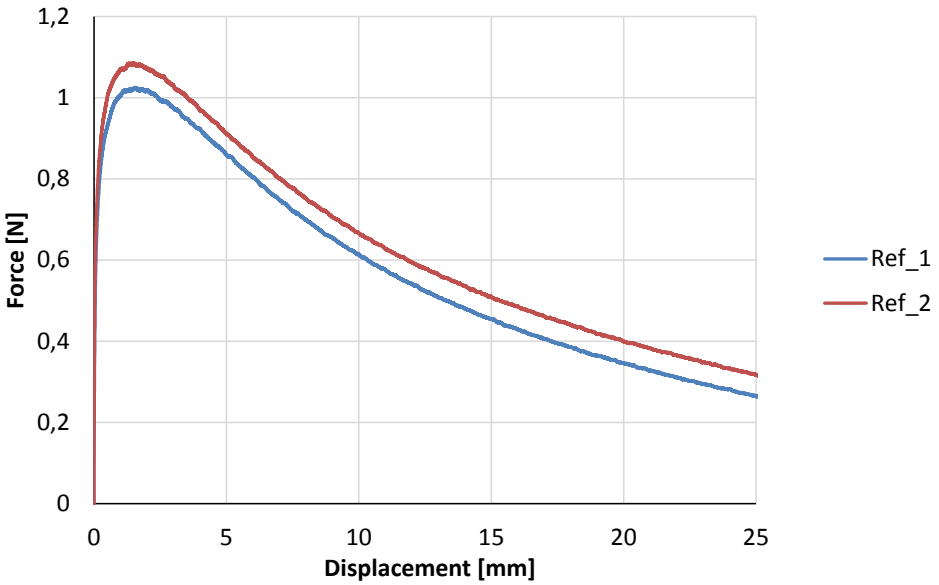

Figure 5.4 Force – Displacement graphs for reference specimen 70/100 at 14 °C

Table 5.5 Peak values for reference specimen taken at different moments in time

Specimen	Peak force [N]	Strength [N/mm2]
Ref_1	1,03	0,036
Ref_2	1,09	0,038
Average	**1,06**	**0,037**
Standard dev	**0,03**	**0,001**

During the assembly phase both the applied force and the resulting deformation are measured continuously. The force - displacement curves for all half-specimen that were assembled in this series are presented in Figure 4.2. From the graph it can be seen there is a more or less linear relation between the deformation an the detected assembly force, which can be interpreted as the stiffness of the material at this specific loading speed. However, there is also a significant variation in the amount of deformation that is required to achieve the prescribed force level of 1 N, from around 0,9 to 1,3 mm. This also results in a total applied deformation, which is slightly higher than the intended 0,8mm as formulated in Section 4.6.3. However, as the force-displacement curves do not show plateau values, it seems that the total applied deformation does match the requirements that were formulated for assembly phase. A final observation that can be done is that at the start of the assembly phase, for some specimens, the slight variation in the signal shows that there is some initialization effect.

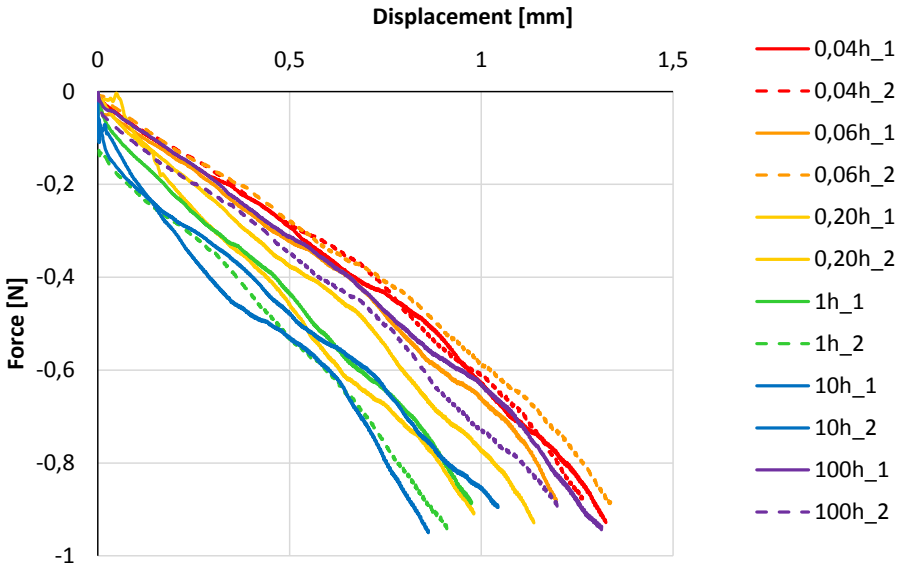

Figure 5.5 Force – displacement curve assembly phase for 70/100, assembly force 1 N and a rate of 0,01 mm/s

In Table 5.6 an overview is given of the numerical values of the applied displacement during the assembly phase, the time required for the assembly phase, the healing period and the consequential strain rate during the tensile test and. NB.

Table 5.6 Numerical values of assembly phase for 70/100, assembly force 1,0 N and a rate of 0,01 mm/s

Specimen	Assembly period [s]	Healing period [h]	Imposed displacement during assembly [mm]	Specimen height [mm]	Applied strain rate during tensile test [%/s]
0,04h_1	134	0,04	1,34	1,67	0,9
0,04h_2	128	0,04	1,28	1,72	0,9
0,06h_1	121	0,06	1,21	1,80	0,8
0,06h_2	136	0,07	1,35	1,65	0,9
0,2h_1	115	0,20	1,15	1,85	0,8
0,2h_2	99	0,20	0,99	2,01	0,7
1 hour_1	99	1,0	0,98	2,02	0,7
1 hour_2	93	1,0	0,92	2,08	0,7
10 hours_1	106	10	1,05	1,95	0,8
10 hours_2	88	10	0,87	2,13	0,7
100 hours_1	133	100	1,32	1,68	0,9
100 hours_2	122	100	1,21	1,79	0,8

All the results of the tensile tests while varying the healing time are shown in Figure 5.6. From the figure it can be seen that a longer healing period results in a higher peak strength. A second observation is that all the half-specimen in this series did not come apart during the tensile test. This deviates from the observations presented in Chapter 4. This is most probably the result of the larger imposed deformation applied during the assembly phase (average 1,1 mm) in this test series combined with the relatively slow assembly rate of 0,01 mm/s.

The tensile strengths are reported in Table 5.7. Using this information, the healing ratio with time is plotted in Figure 5.7 as a black line. From the graph is becomes clear that the largest part of the healing takes place within the first hours of healing, with more than half of the total healing taking place in the first 6 minutes.

Assembly force 1,5 N, assembly rate 0,04 mm/s; average deformation 0,4 mm.

The tensile test on the reference specimen is repeated three times. The results are plotted in Figure 5.8. The numerical values for the maximum observed tensile strength are given in Table 5.8.

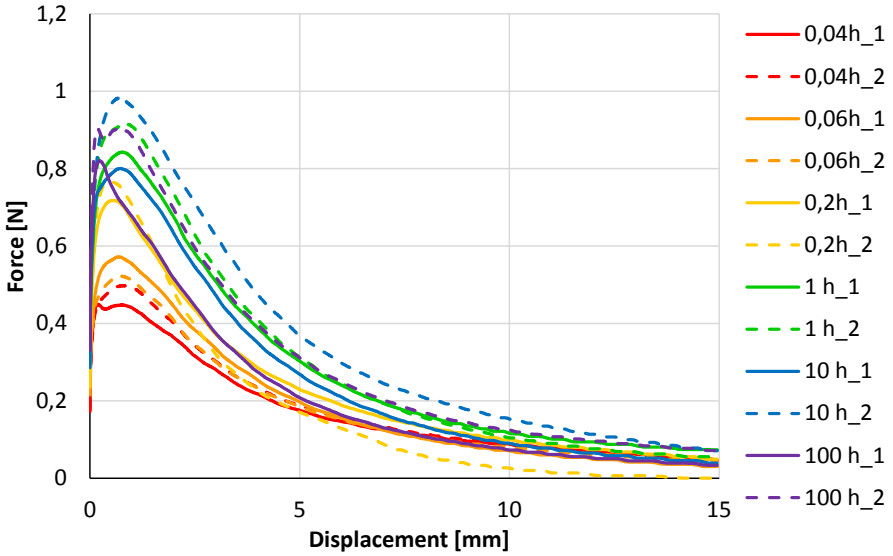

Figure 5.6 Force - displacement curves for all tensile tests while varying healing time for 70/100 bitumen

Table 5.7 The peak force and tensile strength for specimen with different healing times

Specimen	Healing period [h]	Peak force [N]	Strength [N/mm2]	Healing ratio [-]
0,04h_1	0,04	0,45	0,019	0,51
0,04h_2	0,04	0,50	0,021	0,56
0,06h_1	0,06	0,57	0,024	0,64
0,06h_2	0,07	0,52	0,022	0,59
0,2h_1	0,20	0,72	0,030	0,81
0,2h_2	0,19	0,77	0,032	0,86
1 hour_1	1,0	0,84	0,035	0,95
1 hour_2	1,0	0,92	0,039	1,03
10 hours_1	10	0,80	0,034	0,90
10 hours_2	10	0,98	0,041	1,11
100 hours_1	100	0,82	0,035	0,92
100 hours_2	100	0,90	0,038	1,02

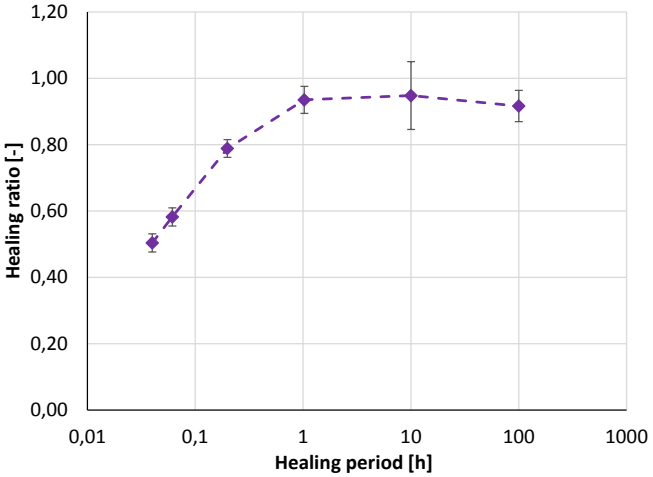

Figure 5.7 Healing ratio versus healing period for 70/100 bitumen assembled in the machine with a rate of 0,01 mm/s using an assembly force of 1 N and healed at 14 °C.

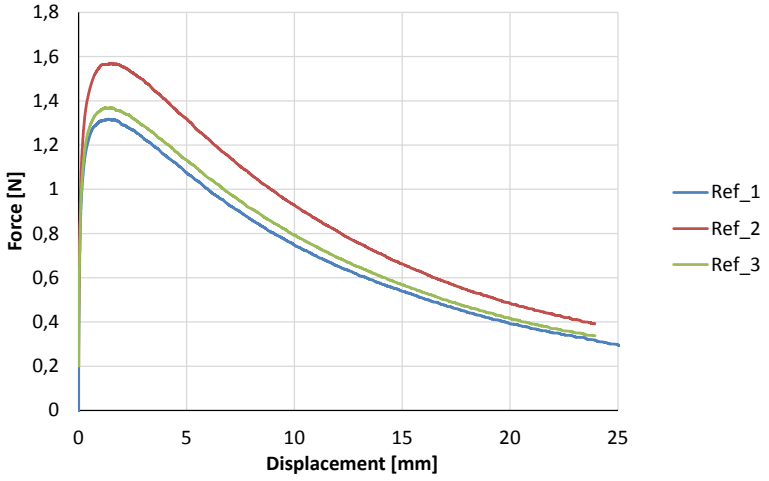

Figure 5.8 Force – Displacement graphs for reference specimen 70/100 at 14 °C

Table 5.8 Peak values for reference specimen for 70/100 bitumen taken in this series

Specimen	Peak force [N]	Strength [N/mm2]
Ref_1	1,32	0,047
Ref_2	1,57	0,055
Ref_3	1,37	0,048
Average	**1,42**	**0,050**
Standard deviation	**0,11**	**0,0038**

The intended deformation level for the assembly phase was 0,4 mm. During two initial calibration tests it was determined that this amount of deformation corresponded with an assembly force of 1,5 N. The forcedisplacement curves for the assembly phase of all half-specimen in this series are presented in Figure 5.9. From the graph it can be seen there is a more or less linear relation between the deformation an the detected assembly force, which can be interpreted as the stiffness of the material at this specific deformation speed. One specimen (0,006h_2) seems to have a deviating start of the assembly phase, it is not clear why this deviated. Most of the deformations are between 0,35 and 0,48 with outliers 0,3 and 0,55 mm.

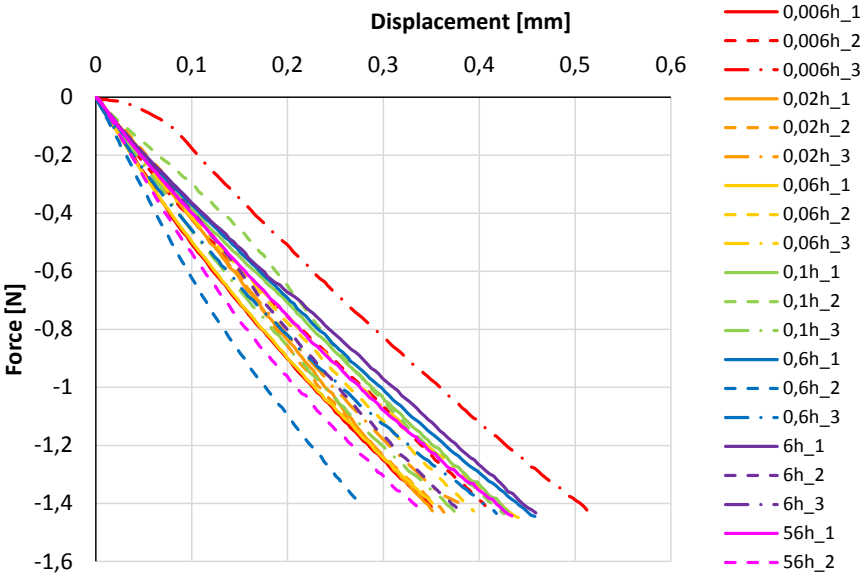

Figure 5.9 Force – displacement curve assembly phase for 70/100, assembly force 1,5 N and a rate of 0,04 mm/s

An overview of the displacement during assembly, the time needed for the assembly and the resulting strain rate during the tensile test is provided in Table 5.9.

Table 5.9 Numerical values of assembly phase for 70/100, assembly force 1,5 N and a rate of 0,04 mm/s

Specimen	Assembly time [s]	Actual healing period [h]	Imposed displacement during assembly[mm]	Specimen height [mm]	Applied strain rate during tensile test [%/s]
0,006h_1	9,4	0,005	0,37	2,63	0,38
0,006h_2	10,7	0,006	0,43	2,57	0,39
0,006h_3	13,6	0,007	0,54	2,46	0,41
0,02h_1	9,2	0,016	0,37	2,63	0,38
0,02h_2	9,5	0,017	0,38	2,62	0,38
0,02h_3	10,0	0,017	0,40	2,60	0,38
0,06h_1	9,2	0,058	0,37	2,63	0,38
0,06h_2	10,4	0,058	0,41	2,59	0,39
0,06h_3	11,6	0,059	0,46	2,54	0,39
0,1h_1	11,3	0,14	0,45	2,55	0,39
0,1h_2	11,2	0,14	0,45	2,55	0,39
0,1h_3	9,9	0,14	0,39	2,61	0,38
0,6h_1	12,0	0,56	0,48	2,52	0,40
0,6h_2	7,4	0,56	0,29	2,71	0,37
0,6h_3	11,0	0,56	0,44	2,56	0,39
6h_1	12,0	5,6	0,48	2,52	0,40
6h_2	10,0	5,6	0,40	2,60	0,38
6h_3	11,4	5,6	0,45	2,55	0,39
56h_1	11,4	56	0,45	2,55	0,39
56h_2	9,0	56	0,36	2,64	0,38

All the results of the tensile tests while varying the healing time are shown in Figure 5.10. From the figure it can be seen that a longer healing time results in a higher peak strength. A second observation is that contrary to the results reported in paragraph 6.3.2.1, for many of the shorter healing times the specimens have come apart fully, this is most probably the effect of a smaller assembly deformation resulting in less contact at the healing interface. One test (6h_1) was not valid as the clamps were not tightened properly consequently the specimen did not fail. The numerical values for the peak force, strength and calculated healing ratio are reported in Table 5.10. The resulting healing ratio with time is plotted in Figure 5.11. From the graph is becomes clear that the used conditions result in a less clear trend compared to the previous conditions. This could be caused by a less developed in the assembly phase.

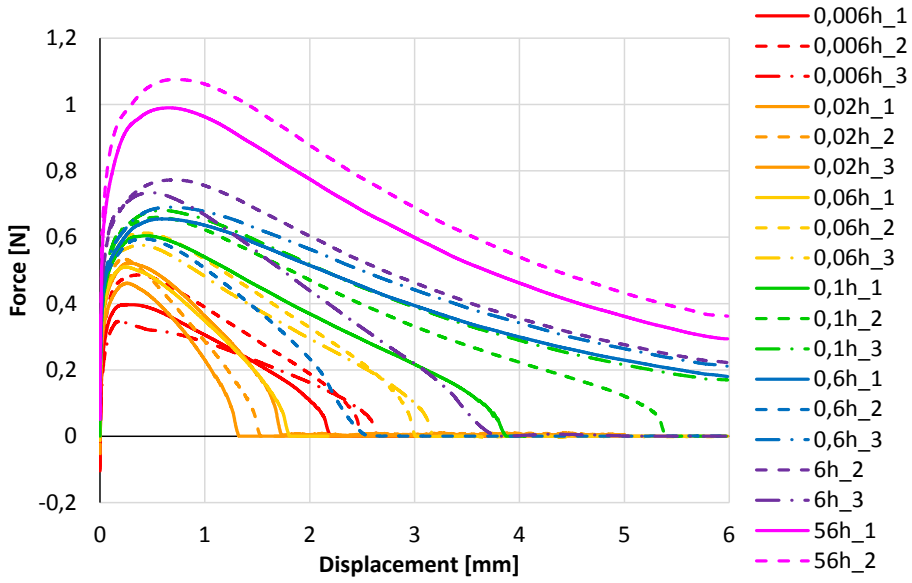

Figure 5.10 Force - displacement curves for all tensile tests with a rate of 0,04 mm/s and a force of 1,5 N while varying healing time for 70/100 bitumen

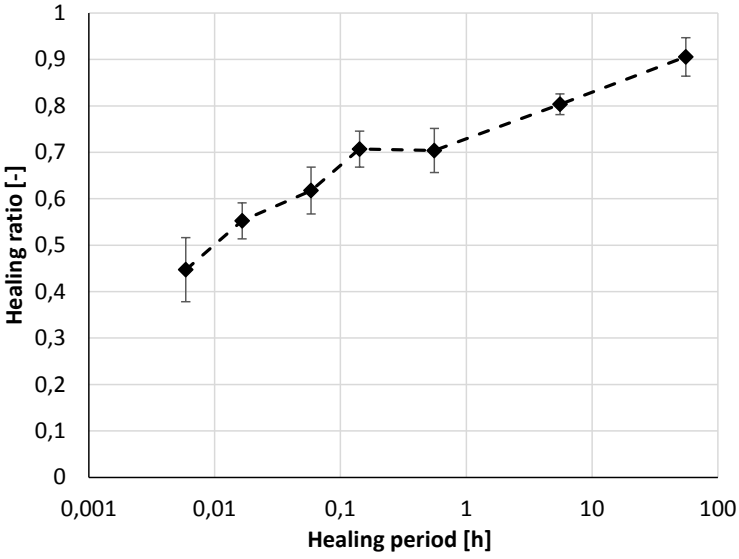

Figure 5.11 Healing ratio versus healing period for 70/100 bitumen assembled in the machine with a rate of 0,04 mm/s using an assembly force of 1,5 N and healed at 14 °C.

Table 5.10 The peak force and tensile strength for samples with different healing times, assembled with a rate of 0,04 m/s and at a force of 1,5 N

Specimen	Healing period [h]	Peak force [N]	Strength [N/mm2]	Healing ratio [-]
0,006h_1	0,0054	0,40	0,017	0,43
0,006h_2	0,0058	0,49	0,020	0,53
0,006h_3	0,0066	0,35	0,015	0,38
0,02h_1	0,016	0,52	0,022	0,57
0,02h_2	0,017	0,54	0,023	0,58
0,02h_3	0,017	0,46	0,019	0,50
0,06h_1	0,058	0,51	0,021	0,56
0,06h_2	0,058	0,61	0,026	0,67
0,06h_3	0,059	0,58	0,024	0,63
0,1h_1	0,14	0,60	0,025	0,66
0,1h_2	0,14	0,66	0,028	0,72
0,1h_3	0,14	0,68	0,029	0,74
0,6h_1	0,56	0,66	0,028	0,71
0,6h_2	0,56	0,59	0,025	0,65
0,6h_3	0,56	0,69	0,029	0,75
~~6h_1~~	~~5,6~~	-	-	
6h_2	5,6	0,77	0,033	0,82
6h_3	5,6	0,73	0,031	0,78
56h_1	55,6	0,99	0,042	0,87
56h_2	55,6	1,08	0,045	0,94

Assembly force 2,3 N, assembly rate 0,04 mm/s; average deformation 0,8 mm

The reference specimen that are used for this series are the same as the previous series using and assembly for of 1,5 N. The intended deformation level for the assembly phase was 0,8 mm. During two initial calibration tests it was determined that this amount of deformation corresponded with an assembly force of 2,3 N. The force - displacement curves for all half-specimen that were assembled in this series are presented in Figure 5.12. From the graph it can be seen there is a more or less linear relation between the deformation an the detected assembly force, which can be interpreted as the stiffness of the material at this specific loading speed. Nonetheless, there is also some variation in the amount of deformation that has to be implies to achieve the prescribed force level of 2,3 N, from around 0,55 to 0,9 mm. One specimen (0,008h_2) did not reach 2,3N during the assembly phase, due the an error in the machine setting, therefore the result of the specimen is not analysed.

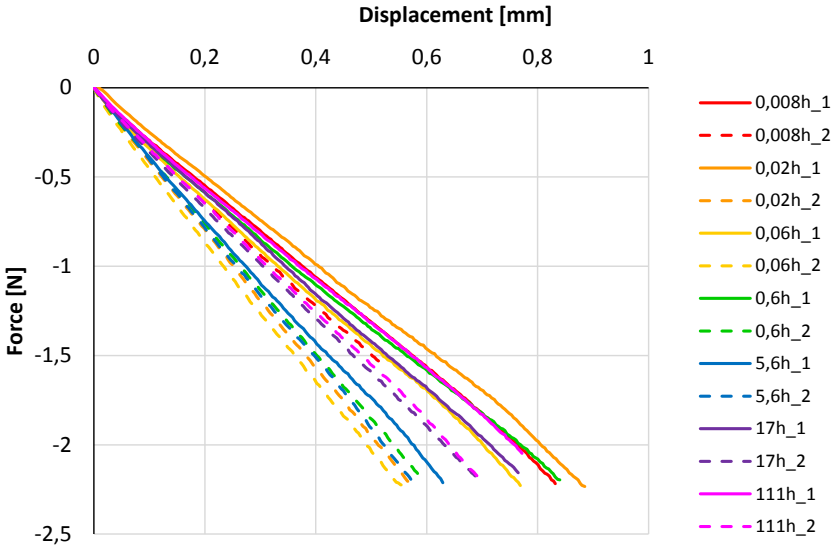

Figure 5.12 Force – displacement curve assembly phase for 70/100, assembly force 2,3 N and rate of 0,04 mm/s

An overview of the displacement during assembly, the time needed for the assembly and the resulting strain speed during the tensile test is provided in Table 5.11.

Table 5.11 Numerical values of assembly phase for 70/100, assembly force 2,3 N and rate 0,04 mm/s

Specimen	Assembly time [s]	Actual healing period [h]	Imposed displacement during assembly[mm]	Specimen height [mm]	Strain rate during tensile test [%/s]
0,008h_1	21,4	0,0087	0,9	2,15	0,38
~~0,008h_2~~	~~13,5~~	~~0,0065~~	~~0,5~~	~~2,46~~	~~0,33~~
0,02h_1	22,7	0,0202	0,9	2,10	0,39
0,02h_2	14,8	0,018	0,6	2,41	0,34
0,06h_1	19,8	0,061	0,8	2,21	0,37
0,06h_2	14,0	0,059	0,6	2,44	0,33
0,6h_1	21,6	0,56	0,9	2,14	0,38
0,6h_2	15,2	0,56	0,6	2,40	0,34
5,6h_1	16,3	5,56	0,6	2,35	0,35
5,6h_2	15,0	5,56	0,6	2,40	0,34
17h_1	19,7	16,7	0,8	2,22	0,37
17h_2	18,0	16,7	0,7	2,28	0,36
111h_1	19,9	111	0,8	2,21	0,37
111h_2	18,2	111	0,7	2,28	0,36

All the results of the tensile tests while varying the healing time are shown in Figure 5.13. From the figure it can be seen that a longer healing time results in a higher peak strength. A second observation is that less specimen are coming apart fully during the tensile test compared to the test series exposed to the lower assembly force of 1,5 N, reported in the previous paragraph. The numerical values for the peak force and tensile strength are reported in Table 5.12.

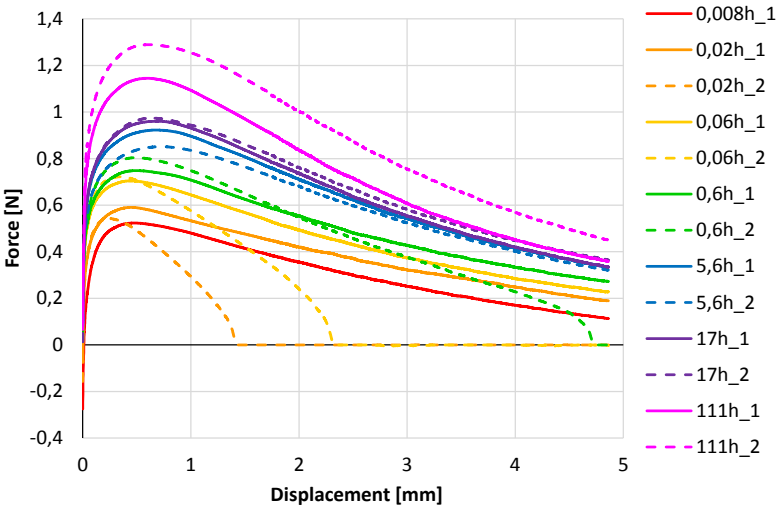

Figure 5.13 Force - displacement curves for all tensile tests assembled with a rate of 0,04 mm/s and a force of 2,3 N while varying healing time for 70/100 bitumen

Table 5.12 The peak force and tensile strength for samples with different healing times, assembled with a rate of 0,04 mm/s and at a force of 2,3 N

Specimen	Healing time [h]	Peak force [N]	Strength [N/mm2]	Healing ratio [-]
0,008h_1	0,008	0,5	0,022	0,49
0,02h_1	0,014	0,57	0,024	0,54
0,02h_2	0,014	0,54	0,026	0,57
0,06h_1	0,06	0,65	0,031	0,67
0,06h_2	0,06	0,66	0,035	0,76
0,6h_1	0,56	0,7	0,032	0,69
0,6h_2	0,56	0,74	0,038	0,83
5,6h_1	5,56	0,85	0,043	0,93
5,6h_2	5,56	0,78	0,040	0,87
17h_1	16,7	0,86	0,042	0,89
17h_2	16,7	0,89	0,044	0,93
111h_1	111	1,03	0,050	0,90
111h_2	111	1,14	0,058	1,05

The resulting healing ratio with time is plotted in Figure 5.14 as the red line. In this figure the healing ratio from the previous assembly conditions has also been plotted as these test series were executed on the same batch of material. It can be seen that a larger deformation during the assembly results in a higher initial healing ratio, which remains present while the healing period becomes longer. Although it should also be noticed that the differences are quite small. Both trends do not show a clear plateau value. The assembly displacement for both specimen was still less compared to the specimen that did show a plateau value. It is therefore plausible that the healing was not complete in the same time period, as the assembly phase did not result in full contact of the half specimen, therefore a longer healing period is required to establish contact.

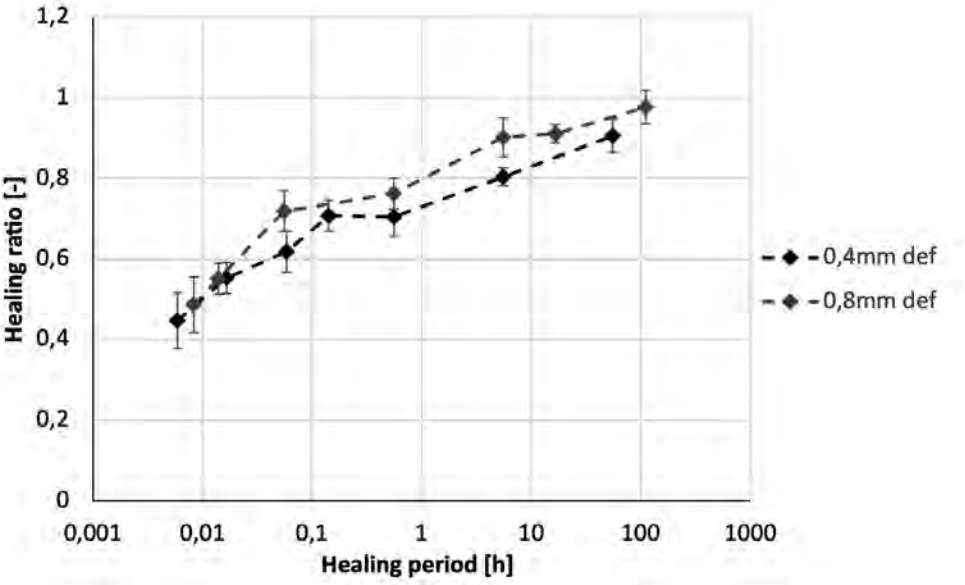

Figure 5.14 Healing ratio of 70/100 specimen assembled in the machine with a rate of 0,04 mm/s and a deformation of 0,4 mm in black (assembly force 1,5 N) and 0,8 mm in red (assembly force 2,3 N) healed at 14 °C.

5.3.3 Comparison of the healing ratio for the four 70/100 bitumen test series

All healing ratios for the 70/100 series with time are presented in Figure 5.15. The first observation that can be made is that even though all results report on a single material, tested at a single test temperature of 14 °C, there is not a unique healing trend with time. This proves again that healing is influenced by the assembly conditions influencing the created contact at the healing interface.

It can also be seen that the small but constant load present in the storage room, up until one hour results in a slower restoration of strength, compared to the shortly applied large assembly force inside the testing machine. However, after longer healing periods of 10 hours or more the restoration becomes larger.

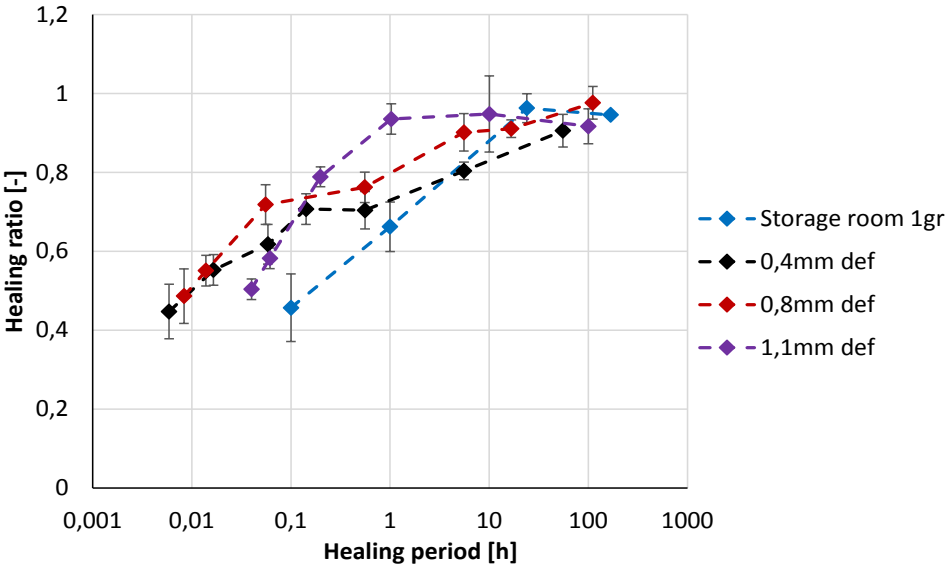

Figure 5.15 Overview of healing ratio trends with time for the various series of 70/100 bitumen test series on a logarithmic time scale.

Another observation that can be taken from the graph, is that all test series show an increase in healing ratio with time. This trend is not linear but asymptotic; initially additional healing time result in a significant increase in strength, however the positive impact of time diminishes fast. For all test series, the largest increase in healing occurs within the first 1 hour after assembly. The loss of the impact of time is illustrated in Figure 5.16, which is based on the trend for imposed deformation of 0,8 mm. The figure indicates that in the first time step of 0,05 hours (180 s) the healing increase is 20%, in the next time step of 0,5 hours (10 times longer ten the previous one) the increase in healing is only 15%, in the last 50 hours the increase in healing ratio is even less than 5%.

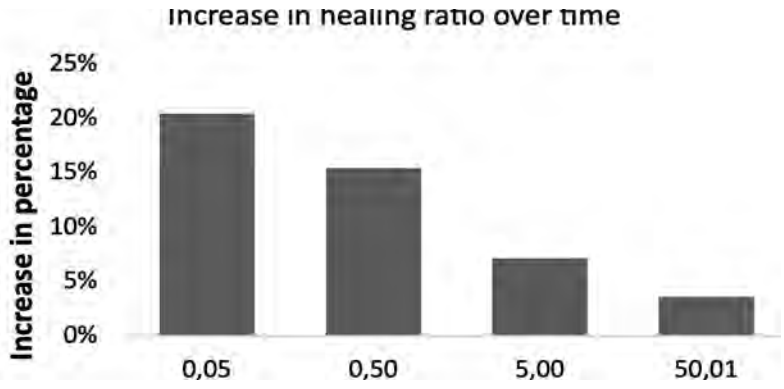

Figure 5.16 Schematic representation of the influence of healing period on healing strength for 70/100 bitumen at 14 °C, assembled inside the machine by an imposed displacement of 0,8 mm.

5.3.4 40/60 bitumen, assembly in storage room at 14 °C, tensile test executed at 14 °C

During storage healing half-specimens of 40/60 bitumen were loaded with a mass of 1 or 10 gram. During execution of the test it was noted that the weights in combination with the bit of room present in the storage moulds, could still result in a small misalignment or angular rotation between the top and the bottom half-specimen as was also noted for the 70/100 specimen (see Section 5.3.1). Due to the angular rotation and/or translation, these specimens are more likely to break just before tensile testing during fastening of the clamps of the DSR. As a result, multiple specimens broke when placing them in the DSR. As 40/60 is a harder bitumen, and consequently more brittle, this effect was stronger for the 40/60 specimen compared to the 70/100. Consequently, for several healing periods and loads there are only two test results instead of three.

The results of the tensile tests for both the reference and the storage healed specimen of 1 gram are plotted in Figure 5.17. From the figure, it can be seen that longer healing times result in higher healing strengths. Next to this, it can be seen that in most cases the half specimen come apart fully during the tensile test. In this it is unexpected that one specimen exposed to a healing period of 168 hours comes apart, while the ones that have healed for 24 hours don't. No plausible explanation can be provided for this.

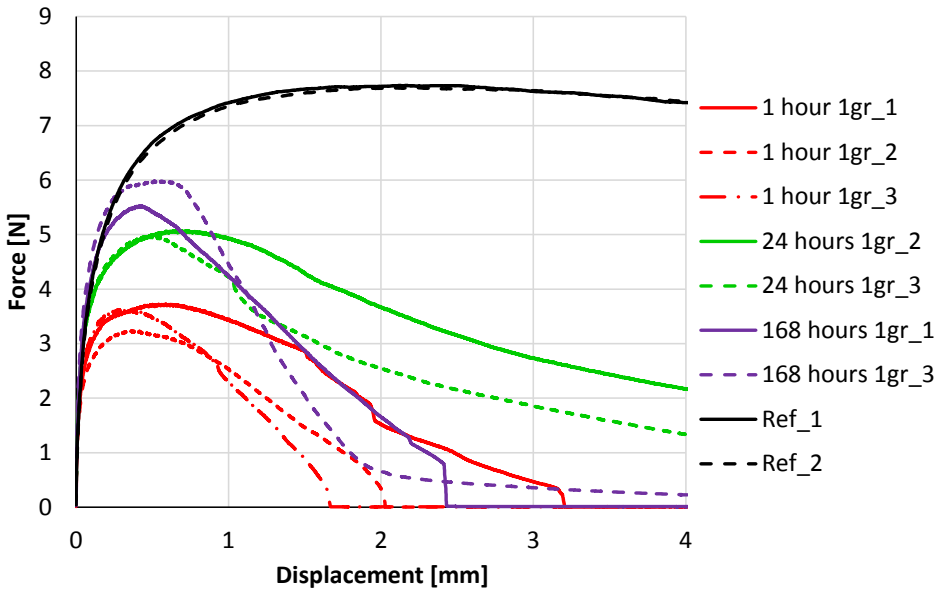

Figure 5.17 Force – displacement graph for storage healed samples loaded with 1gram and reference samples of 40/60 bitumen healed at 14 °C

The results of the tensile tests executed on both the reference and the storage healed specimen of 10 grams are plotted in Figure 5.18. In this test the shortest healing period (0,1 hour) is shorter compared to the 1 gram specimen (1 hour). Initially it was the intention to tests both series after a healing period at 0,1 hour, however when a weight of 1 gram was used, the healing for 40/60 bitumen was too small to be able to place the specimen in the testing machine to execute the tensile test, therefore for the 1 gram test series the shortest healing period was extended to 1 hour. In the test series with the larger weight, it was also seen that longer healing times result in higher healing strengths. Next, it can be seen that in most cases the specimens come apart fully during the tensile test. In this series the specimens that were exposed to a healing period of 168 hours while being loaded with a weight of 10 grams were quite deformed during the healing period, this could provide an explanation why these specimens show lower tensile strength values. The reference strengths reported in this graph are the same as the ones reported in Figure 5.17.

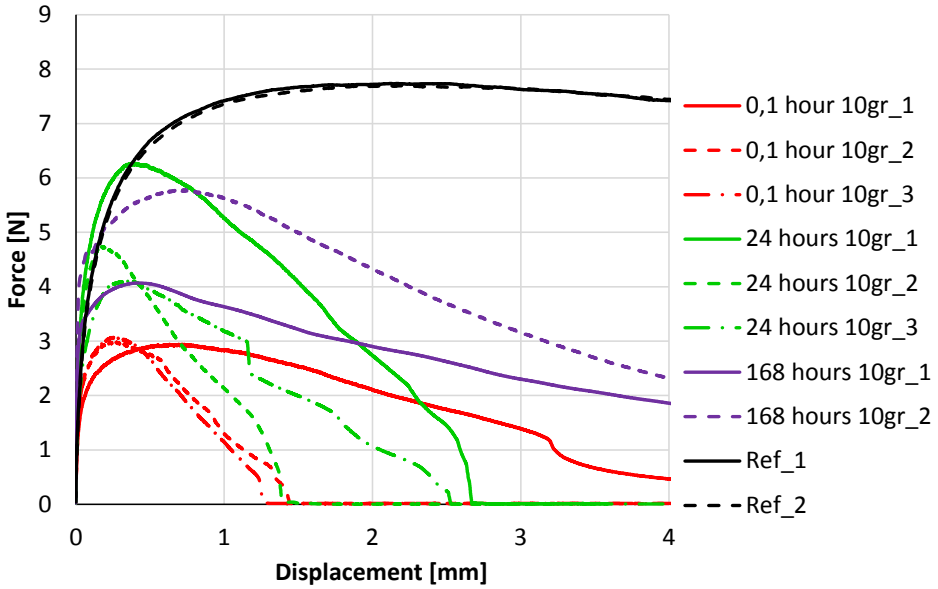

Figure 5.18 Force – displacement graph for storage healed samples loaded with 10 grams and reference samples of 40/60 bitumen healed at 14 °C

All peak values of the strength observed in the tensile tests and the amount of deformation observed after the healing period is reported in Table 5.13. In the table it can also be seen that the amount of deformation that the specimens have undergone during the healing phase for the specimens that have healed for 168 hours is very large compared to the intended applied deformation of maximum 1 mm.

Table 5.13 Overview of all peak forces and the amount of deformation during healing for all storage healed samples and reference samples of 40/60 bitumen healed and tested at 14 °C

Specimen	Peak force [N]	Strength [N/mm2]	Distance rings [mm]	Deformation during healing [mm]
1 hour 1gr_1	3,72	0,16	2,9	0,61
1 hour 1gr_2	3,24	0,14	3,0	0,52
1 hour 1gr_3	3,62	0,15	2,9	0,56
24 hours 1gr_2	5,07	0,21	2,9	0,6
24 hours 1gr_3	4,56	0,19	2,8	0,73
168 hours 1gr_1	5,07	0,21	1,8	1,7
168 hours 1gr_3	5,49	0,23	1,8	1,7
0,1 hour 10gr_1	3,24	0,14	2,7	0,61
0,1 hour 10gr_2	3,2	0,13	2,7	0,52
0,1 hour 10gr_3	3,31	0,14	2,7	0,56
24 hours 10gr_1	6,4	0,27	3,0	0,47
24 hours 10gr_2	5,41	0,23	2,7	0,76
24 hours 10gr_3	6,27	0,26	2,0	1,47
168 hours 10gr_1	4,24	0,18	2,0	1,5
168 hours 10gr_2	6,04	0,25	1,9	1,6
ref_1	7,78	0,28	-	-
ref_2	7,73	0,27	-	-

The resulting healing ratios for the strength of storage healed bitumen with a penetration grade of 40/60 are presented in Figure 5.19. From the graph it can be seen that the variation in test results is much higher for the specimens that were loaded with 10 grams. This is in line with the observations that these specimens were more deformed and placement in the testing machine could have affect the measured tensile strength. When the two healing conditions are compared it can be seen that a larger weight results in slightly more healing, although considering the error margins this difference is not statistically significant. The only significant difference is that after a healing period of 0,1 hours, only the specimens loaded with 10 grams demonstrated enough healing to be tested and are therefore, while the specimens loaded with 1 gram have not been tested and are therefore also not reported.

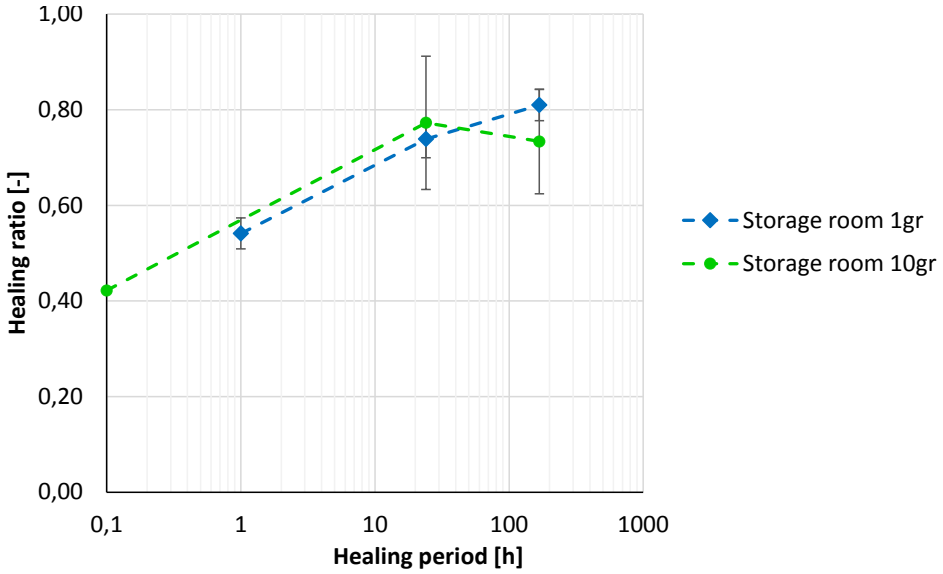

Figure 5.19 Healing ratio for strength of 40/60 bitumen exposed to storage healing loaded with 1 and 10 grams, healed at 14 °C

5.3.5 40/60 bitumen, assembly in tensile testing machine, tensile test executed at 14 °C

During the assembly inside the testing machine an assembly force of 1 or 5 N was used while an assembly rate of 0,005 mm/s was applied. A summary of the test conditions is given in Table 5.2. These tests were executed earlier in the research, therefore the assembly procedure was not calibrated to ensure a specified deformation level between 0,4 and 0,8 mm, as proposed in Section 4.7. Consequently the realized deformation for 1 N is less than would be advised to achieve full contact and for 5 N it is more.

The force displacement curves of the assembly phase for the 1 N series are shown in Figure 5.20. From the graph it can be seen there is a more or less linear relation between the deformation an the detected assembly force, which can be interpreted as the stiffness of the material at this specific loading speed. The total deformation applied for this condition 1 N and 0,005 mm/s varies quite significant and lies between 0,07 to 0,18 mm.

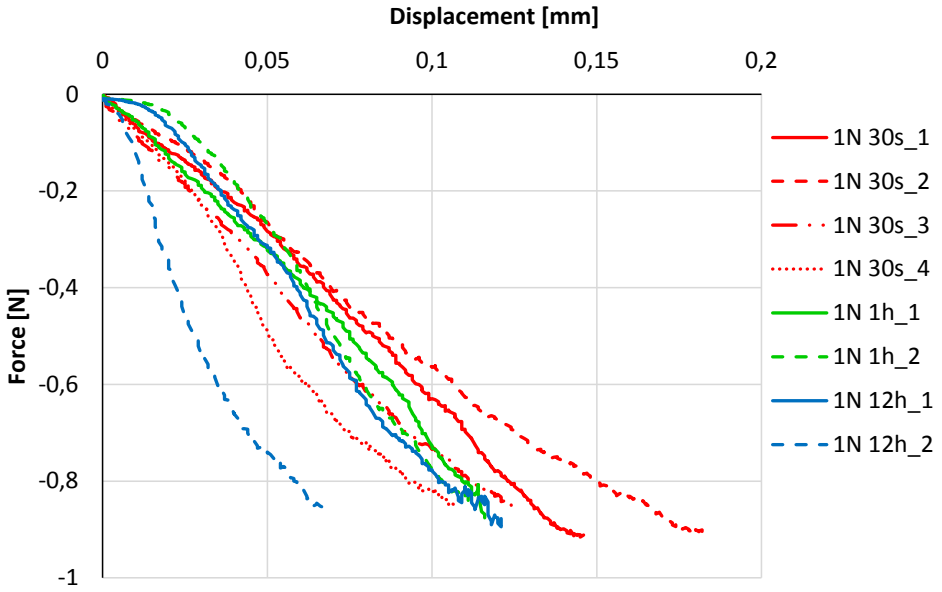

Figure 5.20 Force – displacement curve assembly phase for 40/60 bitumen at an assembly force of 1 N

The force displacement curves of the assembly phase of the 5 N series are shown as Figure 5.21. The graph, deviates from earlier graphs at it does not show a linear relation between the applied deformation and the assembly force. In most of the curves two different trends are visible and for some even three. Initially most curves have a steep inclination, which is followed by a less steep phase and for some of the specimen (5N 210s_1, 5N 210s_2 and 5N 24h_1) the assembly curve ends with again a steep phase. When the initial inclination is compared to the specimens assembled till 1 N, the inclination is the same, implying that this first phase of the response is consistently present for this material. A possible explanation for the loss in stiffness around an assembly force of 2 N could be the thixotropic nature of bitumen. As the assembly rate is rather slow, due to thixotropy the stiffness of the material could reduce with time. Although it should be noted that this explanation is rather speculative and not further validated. The following increase in stiffness for three of the specimens is observed between a deformation level of 0,8 to 1,3 mm. As at this deformation level it is possible that a larger part of the cross-section is activated, which could explain the increase in stiffness. The assembly graph also shows that something unusual has happened during the assembly of specimen 5N 24 hours_2; around an assembly force of -2,75 N, suddenly within one time step an assembly force of 5 N is detected. This is caused by a protruding part of the top clamp getting into contact with the bottom clamp. This specimen is therefore not included in any further analyses. The total deformation applied for this condition (5 N and 0,005 mm/s) varies quite significant and lies between 0,96 to 1,29 mm.

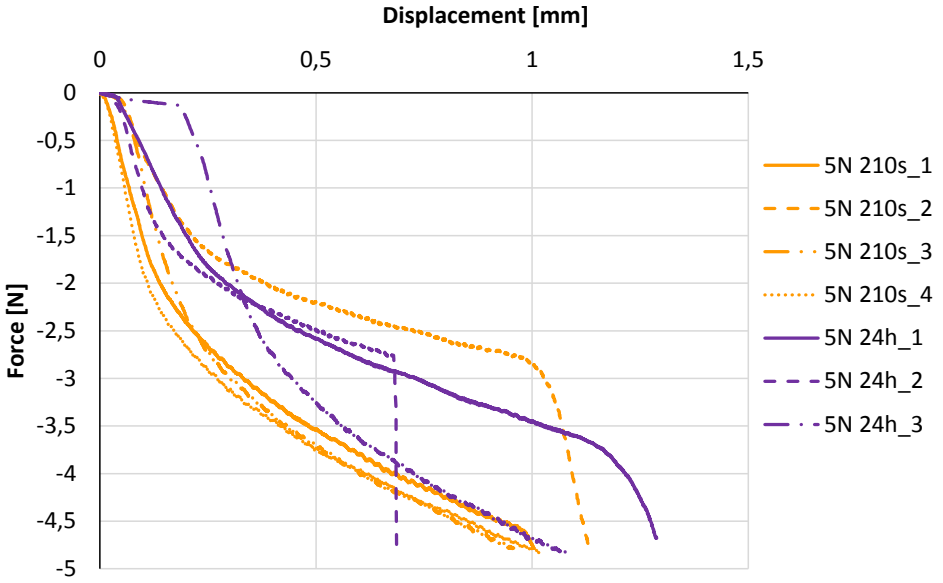

Figure 5.21 Force – displacement curve assembly phase for 40/60 bitumen at an assembly force of 5 N

An overview of the displacement during assembly, the time needed for the assembly and the resulting strain speed during the tensile test is provided in Table 5.14.

Table 5.14 Deformation during assembly and resulting strain speeds during tensile test

Specimen	Assembly period [s]	Healing period [h]	Imposed displacement during assembly[mm]	Specimen height [mm]	Applied strain rate during tensile test [%/s]
1N 30s_1	**30**	0,011	0,15	2,85	0,5%
1N 30s_2	**38**	0,013	0,19	2,81	0,5%
1N 30s_3	**27**	0,010	0,13	2,87	0,5%
1N 30s_4	**23**	0,009	0,11	2,89	0,5%
1N 1h_1	**24**	1	0,12	2,88	0,5%
1N 1h_2	**23**	1	0,12	2,89	0,5%
1N 12h_1	**25**	12	0,12	2,88	0,5%
1N 12h_2	**14**	12	0,07	2,93	0,5%
5N 210s_1	**197**	0,06	1,01	1,99	0,8%
5N 210s_2	**229**	0,07	1,14	1,86	0,8%
5N 210s_3	**193**	0,06	0,96	2,04	0,7%
5N 210s_4	**205**	0,06	1,02	1,98	0,8%
5N 24h_1	**260**	24	1,29	1,71	0,9%
5N 24h_3	**218**	24	1,08	1,92	0,8%

The results of the tensile tests executed on specimen assembled with both 1 and 5 N and the reference specimen are plotted in Figure 5.22. The test for specimen 5N 210s_3 was not executed properly, as the paper controlling the size of the contact had shifted over the contact area consequently reducing the amount of contact created and were therefore excluded from the results.

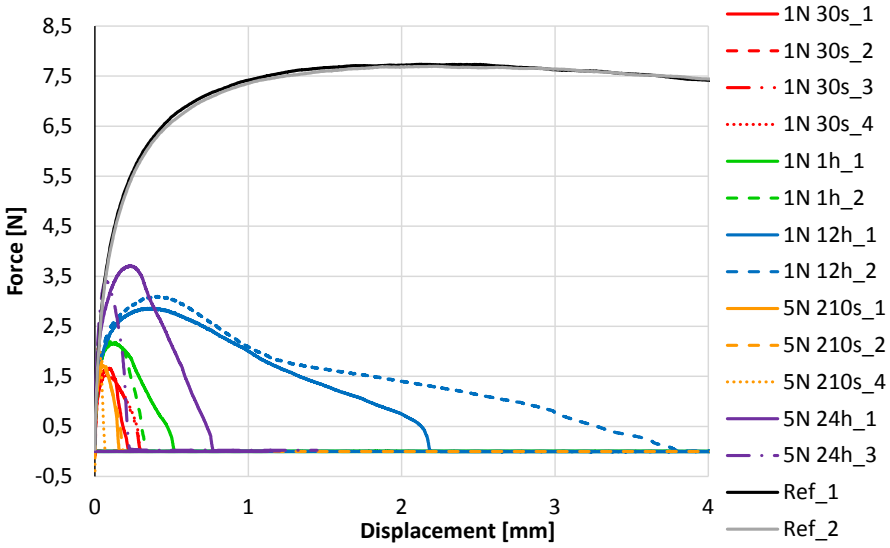

Figure 5.22 Force – displacement graph for specimen that healing inside the testing machine for 40/60 bitumen assembled at 1 and 5 N and kept in the machine for different healing times at 14 °C

From Figure 5.22 it can be seen that longer healing times, result in higher healing strengths. Next, it can also be seen that a higher assembly force leads to a higher healed strength for the same healing period. Finally, it can be observed that all specimen have come apart fully during the tensile test. The specimens that were loaded with 1 N and healed for 12 hours show the most ductile behaviour, while these do not have the highest peak strength and have not healed longest, nor have been exposed to the largest assembly force. No plausible explanation can be provided for this. All peak values of the strength measured in the tensile tests, the amount of deformation observed after the healing period and the resulting healing ratios are reported in Table 5.15.

Table 5.15 The peak force and tensile strength for 40/60 specimen with different healing

Specimen	Healing period [h]	Peak force [N]	Strength [N/mm2]	Healing ratio [-]
1N 30s_1	0,011	1,66	0,07	0,26
1N 30s_2	0,013	0,01	0,00	0,00
1N 30s_3	0,010	1,52	0,06	0,23
1N 30s_4	0,009	1,52	0,06	0,23
1N 1h_1	1	2,17	0,09	0,33
1N 1h_2	1	2,20	0,09	0,34
1N 12h_1	12	2,87	0,12	0,44
1N 12h_2	12	3,11	0,13	0,48
5N 210s_1	0,06	1,23	0,05	0,19
5N 210s_2	0,07	1,24	0,05	0,19
5N 210s_4	0,06	1,80	0,08	0,28
5N 24h_1	24	3,71	0,16	0,57
5N 24h_3	24	3,40	0,14	0,52
Ref_1		7,74	0,27	
Ref_2		7,70	0,27	

The resulting healing ratios for the strength of machine healed bitumen with a penetration grade of 40/60 are presented in Figure 5.23. From the graph it can be seen that a higher assembly force results in more healing, although the differences are small.

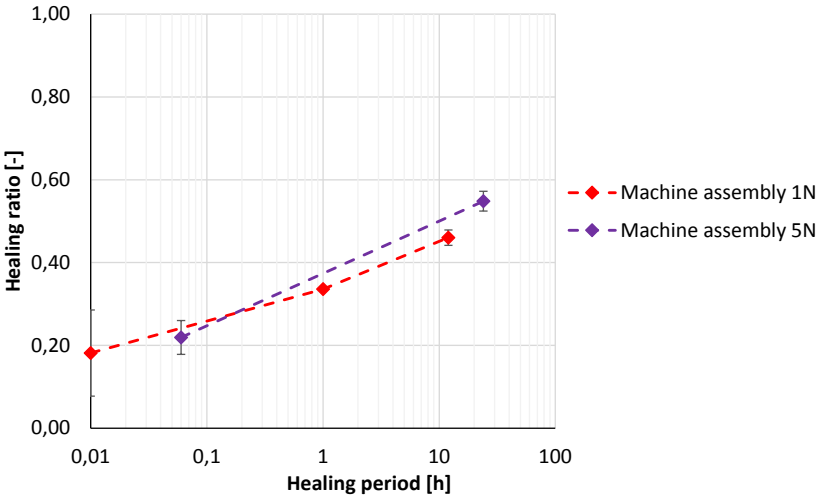

Figure 5.23 Healing ratio for strength of 40/60 bitumen exposed to machine healing loaded with 1 and 5 N, healed at 14 °C

5.3.6 Comparison of the healing ratio for the four 40/60 bitumen test series

In Figure 5.24 the healing ratios for both the 40/60 specimens that were assembled in the storage room (5.3.4) and inside the tensile machine (5.3.5) are presented with time on a logarithmic scale. From the graph it becomes clear that for all specimens the healing increases with time. The test series in which the specimens have been subjected to healing in the storage room show more healing. It seems that a small, but continuously present load (0,016 N and 0,11 N) is more effective in restoring contact compared to a larger load which is only present initially.

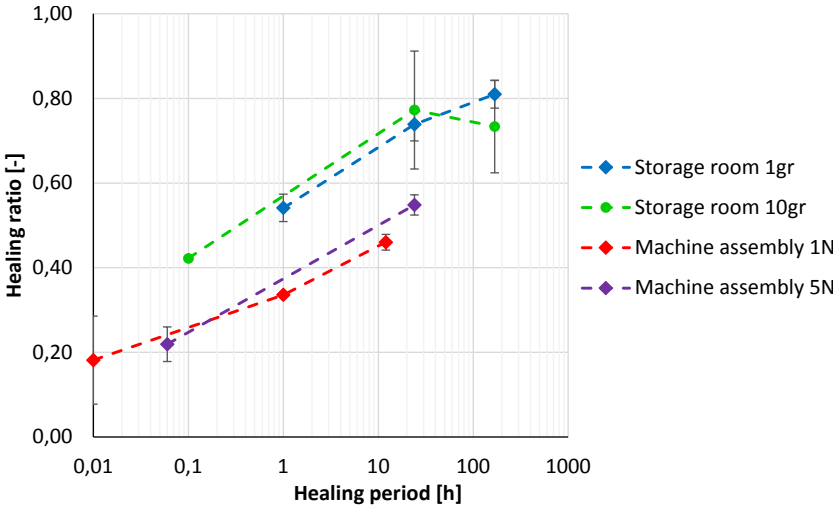

Figure 5.24 Healing of 40/60 bitumen assembled and stored under different conditions on a logarithmic timescale

5.3.7 10/20 bitumen, assembly in storage room at 14 °C, tensile test executed at 14 °C

The values for reference specimen are taken form Section 4.5.1. The applied strain rate of 0,5 %/s resulted in brittle fracture with a corresponding large variation in test results. The maximum observed tensile force of the specimens was 18,96 N, 0,34 N and 4,13 N, resulting in a strength of 0,67 N/mm^2, 0,01 N/mm^2 and 0,15 N/mm^2. The resulting average reference value for the tensile stress is 0.28 N/mm^2, with a standard deviation of 0.28! The extremely large variation indicates that the average value for the tensile strength has a very low reliability and any healing ratio calculated using this value is not realistic.

The test results of bitumen with penetration grade 10/20 that have healed in the storage room are presented in Figure 5.25. During the test phase more than half of the specimens broke prematurely. Sometimes specimens broke during handling, for instance when taking them out of the storage containers. However, most specimens failed during installation

in the testing machine. The 10/20 material is very stiff and brittle compared, therefore a slight misalignment already leads to failure when tightening the clamps around the rings. As a result, for most test conditions there are one or two test results reported instead of the desired three. For the specimen loaded with 1 gram, only 1 specimen was tested per healing period. For the test series loaded with 10 grams, more specimens survived, as such providing a qualitative indication that more resilient connections were created during the healing period as a result of the larger load.

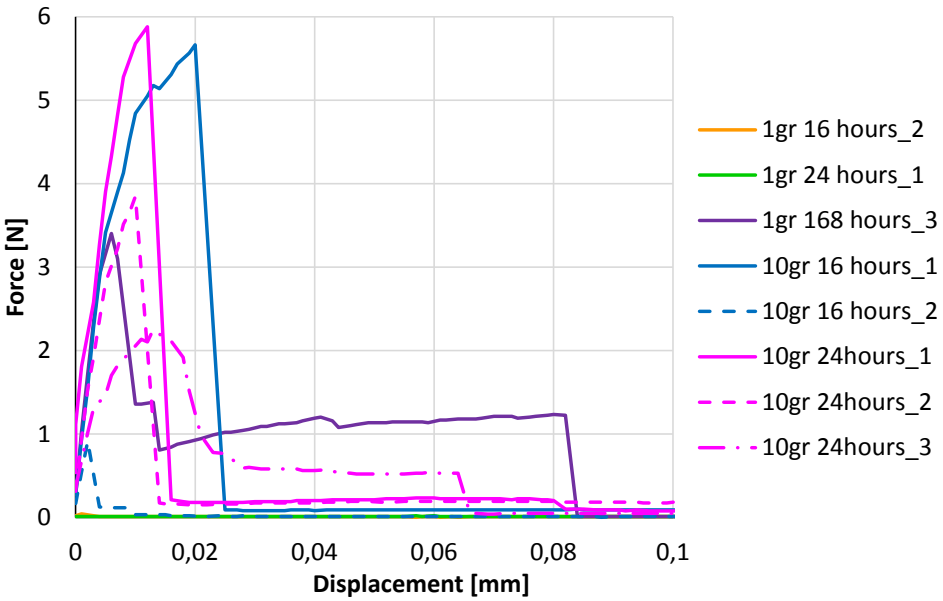

Figure 5.25 Tensile test results of 10/20 bitumen that has healed in the storage room for different time periods under different loading conditions and tested at a tensile strain of 0,5 %/s.

Figure 5.25 also shows that all executed tensile tests resulted in brittle failure, as was also the case for the reference specimen. Tensile tests resulting in a brittle failure, will by definition have a higher variation in measured force compared to ductile failures. Due to both the very small number of repetitions and the large variation, the reliability of the results for 10/20 bitumen is very low. However, in spite of their unreliability, it is decided to include the results in the thesis, as they do allow for some qualitative observations.

All peak values of the strength observed in the tensile tests and the amount of deformation observed after the healing period is reported in Table 5.16. In the table it can also be seen that the amount of deformation that the specimens have undergone during the healing phase for the specimens that have healed for 168 hours is very limited, especially in comparison to the 70/100 and 40/60 binder, showing that this binder is much stiffer.

Table 5.16 Overview of all peak forces and the amount of deformation during healing for all storage healed samples and reference samples of 10/20 bitumen healed and tested at 14 °C

Specimen	Peak force [N]	Strength [N/mm2]	Distance rings [mm]	Deformation during healing [mm]
1 gr 16 hours_2	0,041	0,00	3,11	0,39
1 gr 24 hours_1	0,052	0,00	3,15	0,35
1 gr 168 hours_3	3,402	0,14	3,37	0,13
10gr 16 hours_1	5,663	0,24	2,97	0,53
10gr 16 hours_2	0,913	0,04	3,15	0,35
10gr 24hours_1	5,882	0,25	3,35	0,15
10gr 24hours_2	3,848	0,16	3,03	0,47
10gr 24hours_3	2,252	0,09	2,95	0,55

Pictures have been taken of the surfaces of these 10/20 half-specimen after testing, see Figure 5.26, Figure 5.27 and Figure 5.28. NB. These pictures were only taken for the 10/20 series, as this type of observation could only be done on specimen that failed in a brittle manner. The pictures give an impression on the amount of surface area that has been involved in the healing process. Each picture shows a top and a bottom half of the specimen side by side, resulting in a mirror image of the damaged area on the two half-specimens. The glistering areas on the surface are typical for brittle fracture in bitumen. Therefore these glistering areas are interpreted as the areas where a healed connection was established, this connection is broken by the tensile test after healing. It can be seen that with longer healing periods and larger healing loads, larger areas of the surface are involved in the process of healing. A conclusion that can also be drawn based on these pictures, it that the failure in these specimens did not take place exactly at the healing interface, as a fresh fracture surface can be seen. This demonstrates that for 10/20 bitumen, the connection made at the healing interface is as strong as the bulk material. However, it is also clear that this only holds for the areas that were able to regain close contact. The pictures also show that for this very hard bitumen, an imprint of the roughness of the moulds is still visible in these specimen (where no connection was made). This imprint was not visible in the softer specimens.

In Figure 5.29 the observed healing ratio for the 10/20 series has been presented in time on a logarithmic timescale. The absolute values of this 10/20 tests series do not contain much information. The number of specimens in this series was low due to premature failure and the variation in the reference value is basically non sensical. However, if the healed values per lading conditions are compared some interesting trends can be seen. A first point to notice is that under favourable conditions healing can be observed for 10/20 bitumen, which also seems to increase with time. The images of the failed specimen (Figure 5.26, Figure 5.27 and Figure 5.28) also provide visible evidence that under a constant present small normal force, the amount of area in contact increases with time.

Figure 5.26 Surfaces of the top and the bottom half-specimens after tensile testing, storage healing, penetration grade 10/20, healing period: 16 hours, load: 1 gram, specimen 1, red circle indicates healed area.

Figure 5.27 Surfaces of the top and the bottom half-specimens after tensile testing, storage healing, penetration grade 10/20, healing period: 16 hours, load: 10 gram, specimen 2, red circle indicates healed area.

Figure 5.28 Surfaces of the top and the bottom half-specimens after tensile testing, storage healing, penetration grade 10/20, healing period: 168 hours (1 week), load: 1 gram, specimen 1, red circle indicates healed area.

5.3.8 Comparison of the healing behaviour of binders with three different penetration grades

In order to compare the healing behaviour between different penetration grades, first all the healing ratios of the strength for all three studied binders; 10/20, 40/60 and 70/100 are plotted together, see Figure 5.30. The red data corresponds to test series executed with 70/100 bitumen, the green data corresponds to the test series executed with 40/60 bitumen and the blue data corresponds to 10/20 bitumen. Later in this section the result will be compared per condition, however first all assembly conditions are presented in one plot. From the figure it can be seen that for all conditions the 70/100 bitumen is

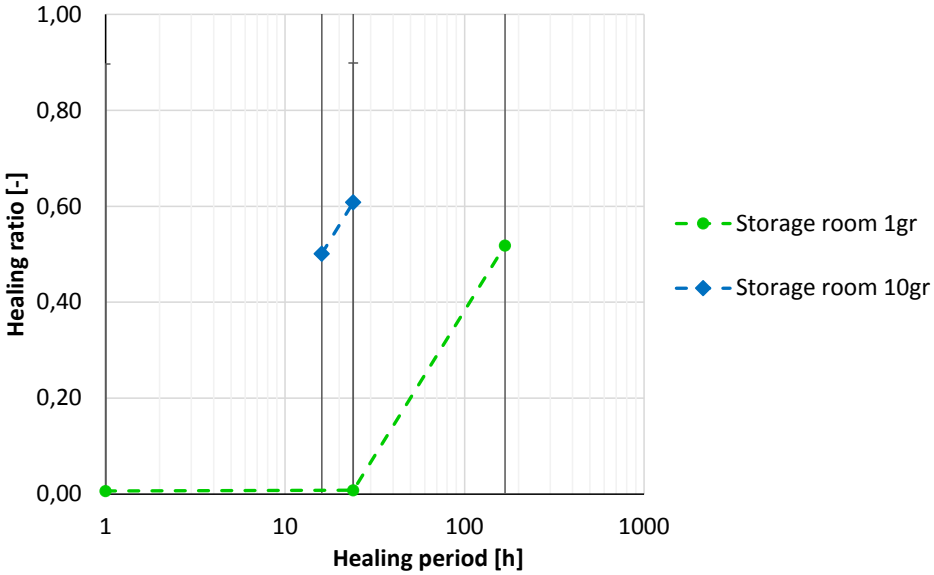

Figure 5.29 Healing ratio of 10/20 bitumen assembled in the storage room and stored under different conditions on a logarithmic timescale.

the better healer compared to 40/60 and 10/20, the healing develops faster and the maximum observed healing is larger. As mentioned, the limited test done on 10/20 bitumen should only be eventuated qualitatively, therefore these cannot really be judged here in comparison to the other binders.

In Figure 5.31 the impact of the penetration grade is shown even more clear, here the healing ratios are compared for the three binders where half-specimens are assembled using the same conditions; assembled in the storage room and loaded with a weights of 1 gram. After 24 hours the 70/100 specimen has healed for more than 90%, while the 40/60 specimen has healed for 70% and the 10/20 specimen does not show any healing at all.

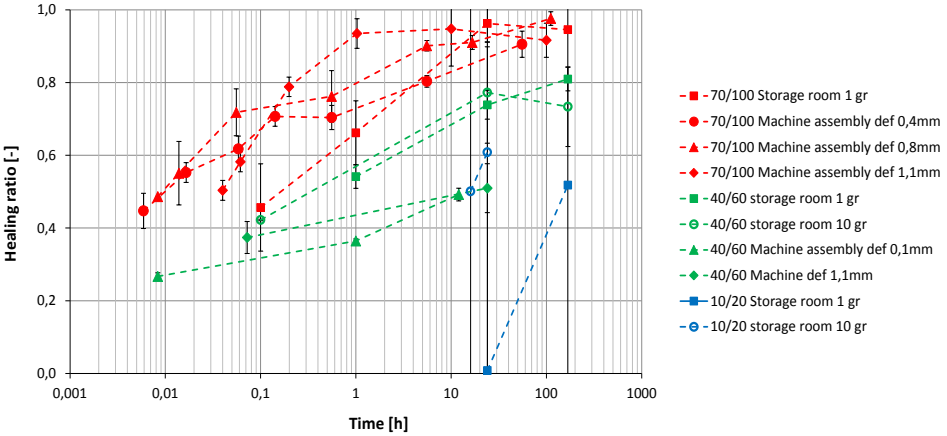

Figure 5.30 Healing ratios for the strength of all test series of binders with three different penetration grades on a logarithmic time scale.

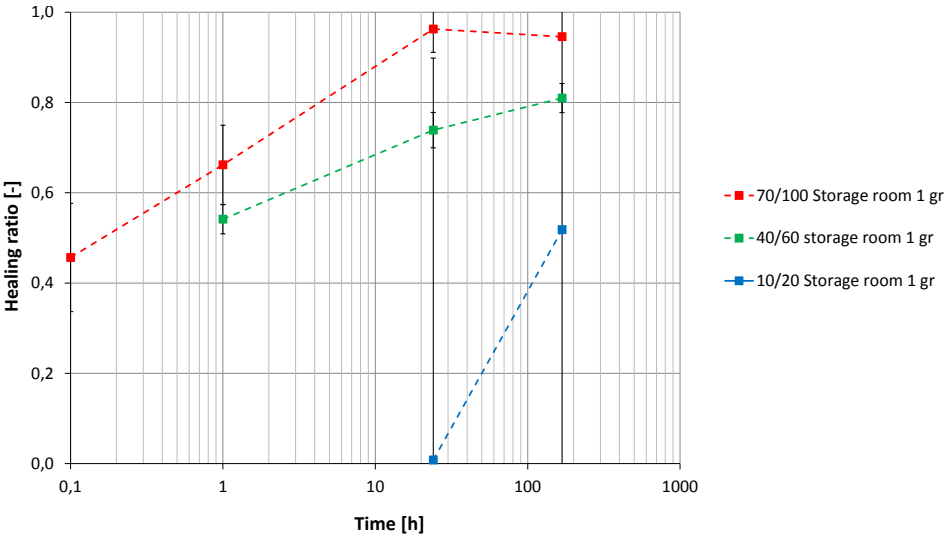

Figure 5.31 Healing ratios of binders with three different penetration grades subjected to assembly and healing in the storage room loaded with a weight of 1 gram

Another important difference that has been observed between the healing performance of the bitumen with different penetration grades was the difference in toughness of the healed connection. When the forcedisplacement curves of all tensile tests are compared under similar loading conditions, it can be seen that specimen made of harder binder more frequently come apart fully during tensile tests. An example of this is shown in Figure 5.32.

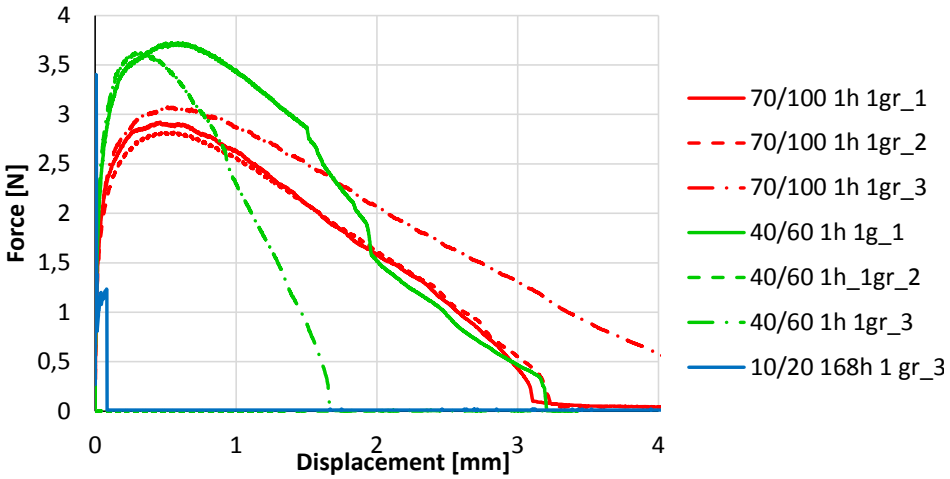

Figure 5.32 Force-displacement graphs for 3 types of binders, subjected to the same healing condition showing that harder binders come apart more often compared to softer binders

5.4 COMPARISON OF THE HEALING OF THREE DIFFERENT 70/100 BITUMEN

5.4.1 Introduction

In the previous section it has been shown that the penetration grade of the binder influences healing behaviour. In this section differences in healing behaviour between binders with the same penetration grade are studied. Therefore three different binders with the same penetration grade are studied using the two-piece healing test. Specimens are assembled inside the DSR, as this method results in less variation.

5.4.2 Assembly conditions

In this test series, a total deformation of 0,8 mm was applied during the assembly phase. For each material, a calibration test was conducted to determine the force required to achieve this deformation. The required assembly force varied slightly between them, as all materials have slight differences in stiffness, while the assembly rate was constant at 0,04 mm/s. The measured assembly forces were: 2,3 N for Q8, 2,1 N for Total and 1,9 N for Nynas. Indicating that Q8 is the stiffest material, followed by Total, with Nynas being the least stiff at this deformation rate.

As the both the deformation rate and the required deformation are the same for all specimens, the assembly phase requires on average 30 s for all specimen. Consequently, the shortest applied healing period in these test series is 30 seconds. Due to variation in specimens, there is variation in the actual applied deformation per specimen and the assembly period, which will be reported per specimen.

5.4.3 Healing corrections

As with the previous results a correction has been applied to address the geometrical error caused by sagging of the specimens during long healing periods following the approach presented in Section 3.7.4. During specimen preparation and handling, it was observed that the Nynas specimens were significantly more prone to sagging compared to those made with Total and Q8. This suggests that different correction parameters might be more appropriate for Nynas. However, since the extent of sagging was not quantitatively documented, there is no reliable basis for applying a different correction. As a result, the same correction parameters were used for all three binders.

5.4.4 Strength of reference specimens

Reference specimens have been produced to obtain a reference strength to be able to calculate the healing ratio. The test results of the tests run on the reference specimen are presented in Figure 5.33. In the figure all blue lines correspond to Q8, all red lines correspond to Total and all green lines to Nynas. The ranking of the tensile strength of the three binders is in line with the ranking of the stiffness observed during the assembly phase, with Q8 showing the highest tensile strength and Nynas the lowest. The peak values and the calculated corresponding tensile strength are given in Table 5.17.

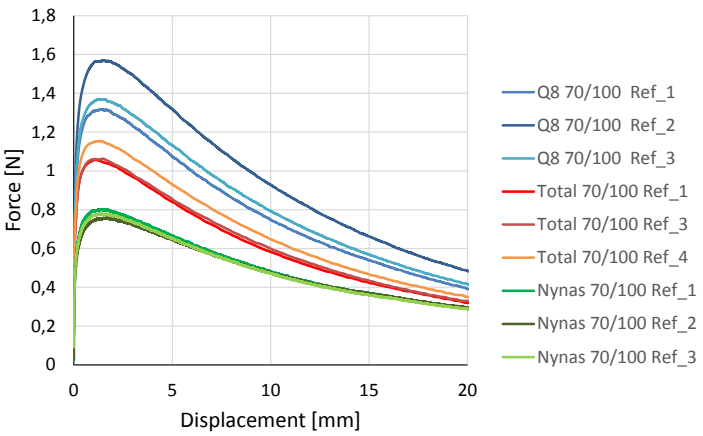

Figure 5.33 Force – displacement graphs of reference specimen tested at 0,5 %/s in tensile

Table 5.17 Peak force in tensile test and calculated strength

Specimen	Peak force [N]	Strength [N/mm2]
Q8 70/100 Ref_1	1,32	0,047
Q8 70/100 Ref_2	1,57	0,055
Q8 70/100 Ref_3	1,37	0,048
Q8 Average Fmax	**1,42**	**0,050**
Q8 Standard deviation	**0,11**	**0,004**
Total 70/100 Ref_1	1,06	0,037
Total 70/100 Ref_3	1,06	0,038
Total 70/100 Ref_4	1,15	0,041
Total Average Fmax	**1,09**	**0,039**
Total Standard deviation	**0,04**	**0,002**
Nynas 70/100 Ref_1	0,80	0,028
Nynas 70/100 Ref_2	0,76	0,027
Nynas 70/100 Ref_3	0,78	0,028
Nynas Average Fmax	**0,78**	**0,028**
Nynas Standard deviation	**0,02**	**0,001**

5.4.5 Results healing test Q8

The assembly and healing results of the Q8 70/100 test specimen, with this specific assembly rate and load, were also part of the test series presented in Section 5.3, where the impact of penetration grade was studied. Therefore these results of this test series is already presented in Section 5.3.2, this series has an assembly load of 2,3 N and an assembly rate of 0,04 mm/s.

5.4.6 Results healing test Total

The force - displacement curves for all Total half-specimen that were assembled in this series are presented in Figure 5.34. From the graph it can be seen there is a more or less linear relation between the deformation and the detected assembly force, which can be interpreted as the stiffness of the material at this specific loading speed. This observed stiffness varies slightly per specimen, resulting in a variation in the actual applied deformation from 0,5 to 0,8 mm. This will result in a difference in strain rate during the tensile tests for which the measured strength needs to be corrected.

All the results of the tensile tests with varying healing times for Total 70/100 are shown in Figure 5.35. From the figure it can be seen that a longer healing periods result in a higher peak strength. A second observation is that a limited number of specimens have come apart fully during the tensile test. Remarkably, none of the half specimens subjected to the shortest healing period of 30 s have come apart fully, while this did happen twice

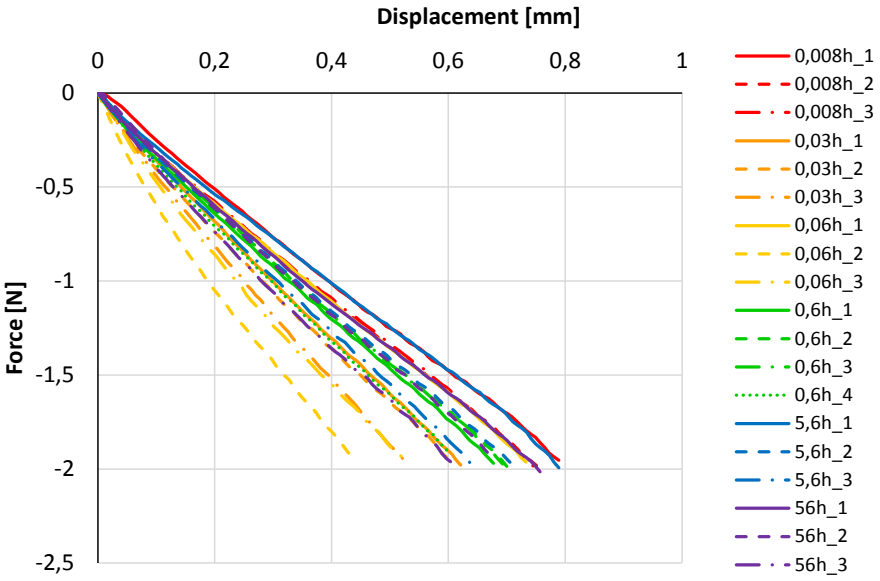

Figure 5.34 Force – displacement curve assembly phase for Total 70/100 bitumen with an assembly force of 2,1 N

An overview of the displacement during assembly, the time needed for the assembly and the resulting strain rate during the tensile test is provided in Table 5.18.

for specimens subjected to a healing period of 100 s and once for 200 s. This while the specimen subjected to a healing period of 30 seconds did show a lower tensile strength. This shows that it is possible to measure a higher healing strength while the specimens do come apart showing adhesive failure, showing that there is not direct connection between adhesive failure and strength. The observed peak force and corresponding tensile strength are reported in Table 5.19

5.4.7 Results healing test Nynas

The force - displacement curves for the assembly phase of all half-specimen that were made from Nynas binder are presented in Figure 5.36. From the graph it can be seen that the correlation between the deformation and the detected assembly force is more linear compared to the other two binders. The resulting stiffness varies slightly per specimen, resulting in a variation in the actual applied deformation from 0,72 to 0,89 mm. This variation is also a bit less compared to the variation observed for the Total and the Q8 specimen. An overview of the displacement during assembly, the time needed for the assembly and the resulting strain speed during the tensile test is provided in Table 5.20.

Table 5.18 Deformation during assembly and resulting strain rates during tensile test for Total 70/100

Specimen	Assembly time [s]	Healing period [h]	Imposed displacement during assembly[mm]	Specimen height [mm]	Strain rate during tensile test [%/s]
0,008h_1	20,6	0,008	0,82	2,18	0,52
0,008h_2	19,8	0,008	0,79	2,21	0,51
0,008h_3	19,6	0,008	0,78	2,22	0,51
0,03h_1	16,6	0,028	0,66	2,34	0,48
0,03h_2	16,0	0,028	0,64	2,36	0,48
0,03h_3	14,2	0,028	0,57	2,44	0,46
0,06h_1	19,4	0,056	0,77	2,23	0,50
0,06h_2	12,0	0,056	0,48	2,52	0,45
0,06h_3	14,2	0,056	0,57	2,44	0,46
0,6h_1	18,0	0,56	0,72	2,28	0,49
0,6h_2	18,6	0,56	0,74	2,26	0,50
0,6h_3	18,4	0,56	0,73	2,27	0,50
0,6h_4	16,2	0,56	0,65	2,36	0,48
5,6h_1	20,8	5,56	0,83	2,17	0,52
5,6h_2	18,8	5,56	0,75	2,25	0,50
5,6h_3	17,0	5,56	0,68	2,32	0,48
56h_1	20,0	55,6	0,80	2,20	0,51
56h_2	18,0	55,6	0,72	2,28	0,49
56h_3	16,2	55,6	0,65	2,36	0,48

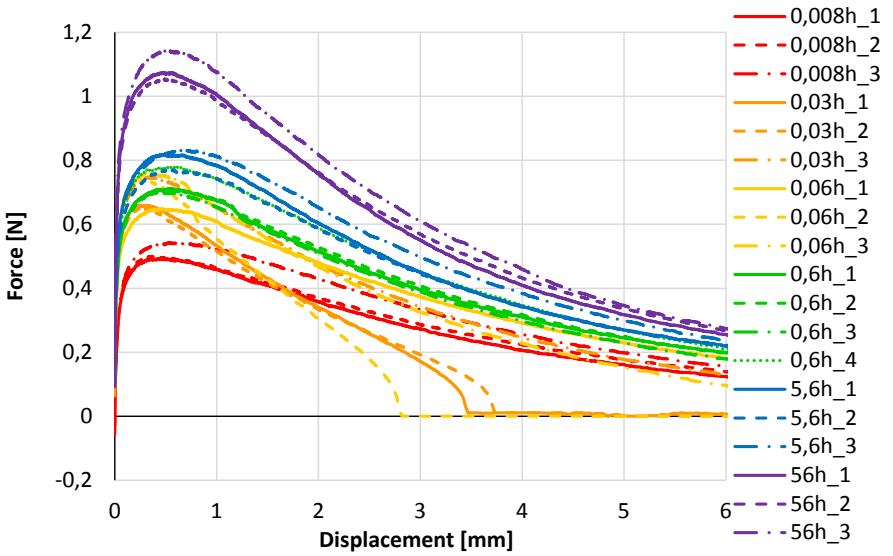

Figure 5.35 Force - displacement curves for all tensile tests while varying healing time for Total 70/100 bitumen

Table 5.19 The peak force tensile strength for Total 70/100 specimen with different healing periods

Specimen	Healing period [h]	Peak force [N]	Strength [N/mm²]	Average Strength [N/mm²]	St.dev [N/mm²]
0,008h_1	0,008	0,49	0,021		
0,008h_2	0,008	0,50	0,021		
0,008h_3	0,008	0,54	0,023	0,022	0,0009
0,03h_1	0,028	0,66	0,028		
0,03h_2	0,028	0,65	0,027		
0,03h_3	0,028	0,75	0,031	0,029	0,0018
0,06h_1	0,056	0,65	0,027		
0,06h_2	0,056	0,74	0,031		
0,06h_3	0,056	0,76	0,032	0,030	0,0021
0,6h_1	0,56	0,71	0,030		
0,6h_2	0,56	0,71	0,030		
0,6h_3	0,56	0,70	0,029		
0,6h_4	0,56	0,78	0,033	0,030	0,0014
5,6h_1	5,56	0,81	0,034		
5,6h_2	5,56	0,76	0,032		
5,6h_3	5,56	0,82	0,035	0,034	0,0011
56h_1	55,56	0,96	0,040		
56h_2	55,56	0,94	0,040		
56h_3	55,56	1,02	0,043	0,041	0,0014

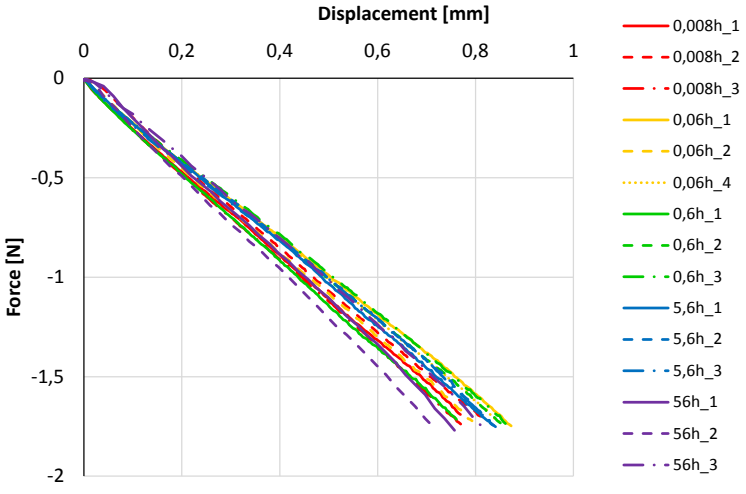

Figure 5.36 Force – displacement curve assembly phase for Nynas 70/100 bitumen with an assembly force of 1,8 N

Table 5.20 Deformation during assembly and resulting strain rates during tensile test for Nynas 70/100

Specimen	Assembly time [s]	Healing period [h]	Imposed displacement during assembly[mm]	Specimen height [mm]	Strain rate during tensile test [%/s]
0,008h_1	19,8	0,008	0,79	2,21	0,51
0,008h_2	21,1	0,008	0,84	2,16	0,52
0,008h_3	19,8	0,008	0,79	2,21	0,51
0,06h_1	22,4	0,056	0,89	2,11	0,53
0,06h_2	20,4	0,056	0,81	2,19	0,51
0,06h_4	21,9	0,056	0,87	2,13	0,53
0,6h_1	19,5	0,56	0,78	2,22	0,51
0,6h_2	21,9	0,56	0,87	2,13	0,53
0,6h_3	22,1	0,56	0,88	2,12	0,53
5,6h_1	21,6	5,56	0,86	2,14	0,53
5,6h_2	21,3	5,56	0,85	2,15	0,52
5,6h_3	21,5	5,56	0,86	2,14	0,52
56h_1	19,0	55,6	0,76	2,24	0,50
56h_2	18,0	55,6	0,72	2,28	0,49
56h_3	20,5	55,6	0,82	2,18	0,52

All the results of the tensile tests for Nynas 70/100 after applying different healing periods are shown in Figure 5.37. From the figure it can be seen that a longer healing periods result in a higher peak strength. A second observation that can be made from the graph is that four specimens came apart fully during the tensile test. This occurred for all specimens exposed to a healing time of 30 s and one specimen that was exposed to a healing period of 200 s. The result of one specimen, exposed to the largest healing period of 200.000 s, is not reported as the silicon paper had shifted and has reduced the area in contact. The observed peak force and corresponding tensile strength are reported in Table 5.21.

5.4.8 Discussion on comparison of healing trends with time for three 70/100 binders

The development of the healing ratio with time can be calculated for the studied Q8, Total and Nynas binder, using the observed tensile strengths and the reference strength, reported in the previous paragraphs. The results are presented in Figure 5.38.

The first interesting observation is that the trend in the healing behaviour for all three binders is more or less the same. For all binders the healing ratio at the shortest healing period of 30 seconds, or instant healing, is around 50% of the reference strength. The strength increase just after assembly phase is finished, during the first 200 s (~0,06 hour),

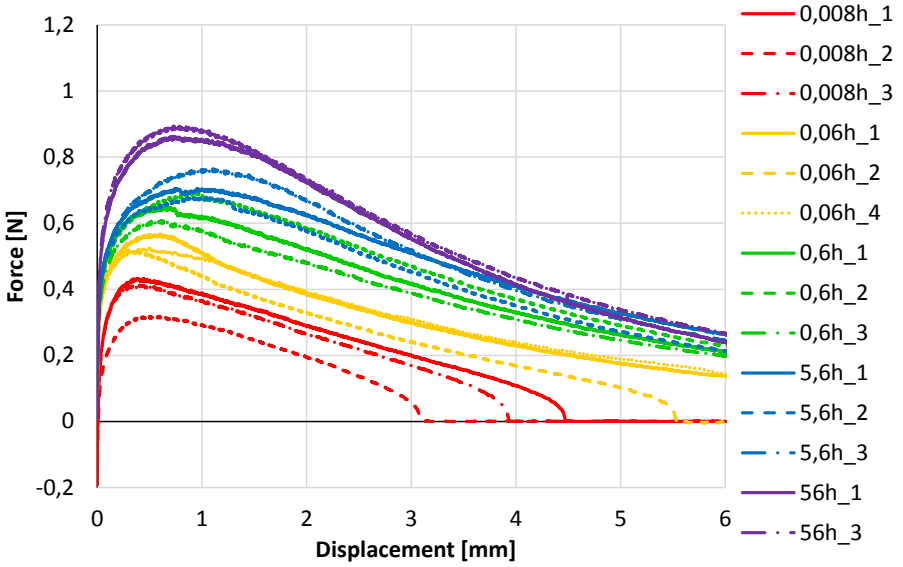

Figure 5.37 Force - displacement curves for all tensile tests while varying healing time for Total 70/100 bitumen

Table 5.21 The peak force and tensile strength for Nynas 70/100 specimen with different healing periods

Specimen	Healing period [h]	Peak force [N]	Strength [N/mm²]	Average Strength [N/mm²]	StDev [N/mm²]
0,008h_1	0,008	0,48	0,020		
0,008h_2	0,008	0,35	0,015		
0,008h_3	0,008	0,46	0,019	0,43	0,055
0,06h_1	0,056	0,62	0,026		
0,06h_2	0,056	0,57	0,024		
0,06h_4	0,056	0,58	0,024	0,59	0,024
0,6h_1	0,56	0,71	0,030		
0,6h_2	0,56	0,76	0,032		
0,6h_3	0,56	0,67	0,028	0,71	0,038
5,6h_1	5,56	0,77	0,032		
5,6h_2	5,56	0,74	0,031		
5,6h_3	5,56	0,83	0,035	0,78	0,039
56h_1	55,56	0,86	0,036		
56h_3	55,56	0,89	0,037	0,86	0,016

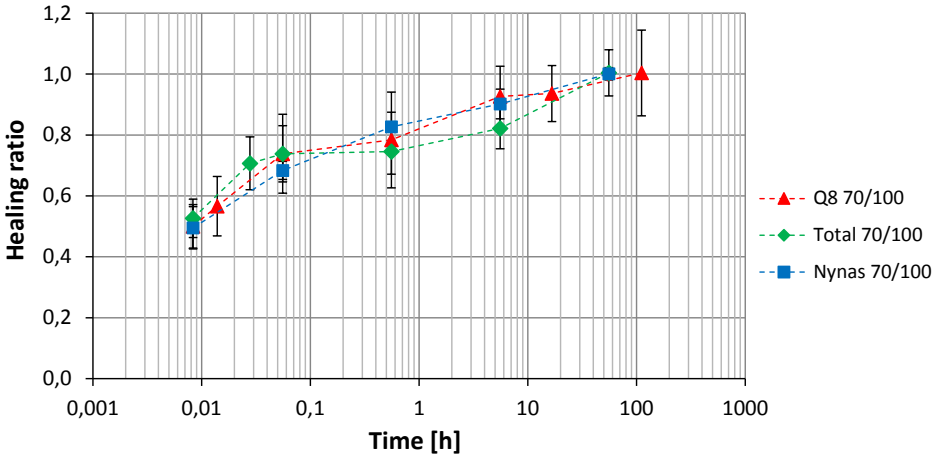

Figure 5.38 Healing ratios for three different 70/100 binders on a logarithmic timescale

is around 20% for all binders, which is relatively large compared to the increase in the following time steps. After 24 hours they have restored 90% of the strength. As was also reported from the other 70/100 results in Section 5.3.3, it can be seen that with each consecutive time step, the increase in strength is a little bit less, while the time steps increase by an order of magnitude.

In spite of the similarities in trends, some differences can also be observed between the binders. The trend for Total and Q8 shows a less smooth development with time. There is currently no data to explain why this happens. More research is needed to explain this behaviour and to assess if it related to healing or not.

5.5 VISUAL OBSERVATIONS DURING TESTING

Next to the measured values on healing, reported in the previous sections, some relevant insights into the healing behaviour can be taken from visual observations done while executing the healing tests. In this section the differences in the damage mechanisms between different healing conditions are evaluated using photographs of the healed specimens after tensile testing.

This section will describe an interesting observation which was done during the removal of the specimens from the tensile machine. During removal of the specimens from the machine after testing, the top clamp is moved upwards. The rate of deformation when dismounting the specimens is much higher, around 100 times faster, compared to the applied deformation rate during a tensile test. In many cases, the half-specimens that were still attached after the tensile test healing test, did come apart fully when the clamp was pulled up at high speed. Figure 5.39 shows an example of the situation before and

after the top clamp has been pulled up. The resulting failure interface is extremely flat, indicating a brittle failure. This failure plane coincides with the original healing interface. This type of behaviour, has been observed for healing periods up until 20.000 s (5,6 hours). The observed failure is distinctly different compared to the more ductile behaviour shown Figure 5.40, when the material is pulled into a thin thread. This more ductile behaviour was observed for longer healing periods or in case the specimens had warmed up to room temperature before removing. In Figure 5.41 more examples of brittle failures, after pulling the top clamp up fast are given for various materials and test conditions.

Despite the significant strength restoration, this brittle failure at high displacement rates for healing periods up to 5,6 hours suggests the healing interface remains the weakest connection. This indicates that healing interface is not fully homogenized. On the other hand, the ductile behaviour at longer healing periods as shown in Figure 5.40 indicates that homogenization does take place. Unfortunately, as this difference in behaviour was noticed after the execution of the test series was already in progress, the failure type is not systematically documented for all specimens. *Figure 5.39 a. Q8 bitumen healed for 5,6 hours at the end of tensile test. b. The same specimen after pulling the top clamp up at high speed.*

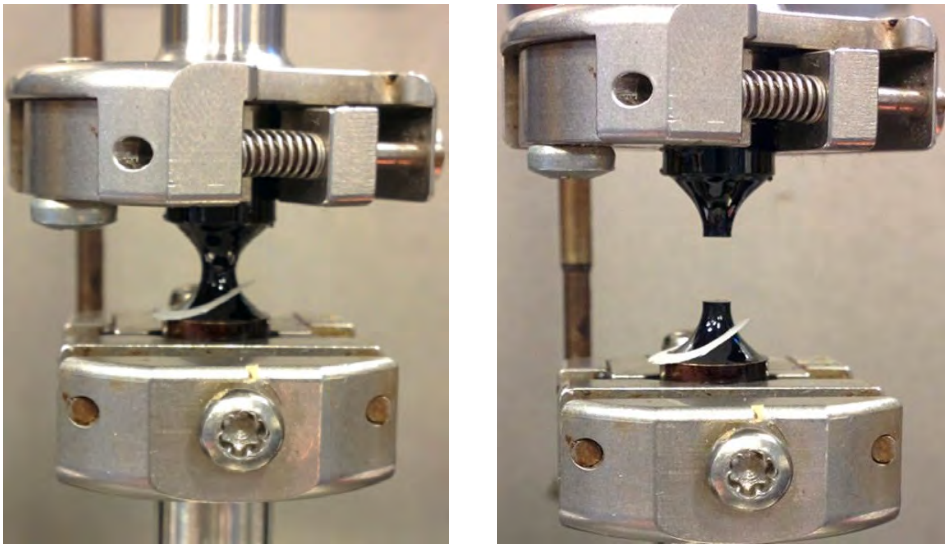

a. **b**.

Figure 5.39 a. Q8 bitumen healed for 5,6 hours at the end of tensile test. **b**. The same specimen after pulling the top clamp up at high speed.

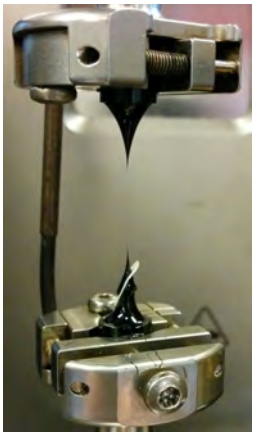

Figure 5.40 Nynas 70/100 specimen healed for 5,6 hours (Nynas70/100 5,6h_1), after a tensile test.

a

b

c

d

Figure 5.41 Specimens after tensile test; **a**. Total 70/100 specimen healed for 0,008h (Total 70/100 0,008h_1) **b.** Q8 70/100 specimen healed for 0,008h (Q8 70/100 0,008h_1) **c.** Q8 70/100 specimen healed for 0,06h (Q8 70/100 0,06h_2) **d.** Nynas 70/100 specimen healed for 0,6h (Nynas70/100 0,6h_2).

5.6 CONCLUSIONS ON THE IMPACT OF TIME ON HEALING

The results reported in this chapter provide answers to RQ4. The observed impact of time on healing is in line with previous research results reported (Bonnaure, Huibers, and Boonders 1982; Bhasin, Little, Bommavaram, and Vasconcelos 2008; Qiu 2012; Sun et al. 2018), as they show that performance recovery due to healing increases with time. This research provides a detailed perspective on healing behaviour by monitoring it over a broad time range, from seconds to several days. The results show that the rate of healing decreases rapidly over time, with the majority of healing occurring within the first few seconds to one hour. After this initial phase, the rate of improvement slows significantly, indicating that early-stage healing plays a dominant role in the overall recovery process.

As previously reported in the literature (see Section 2.9.1), healing in harder binders develops more slowly and to a lesser extent than in softer binders. Interestingly however, even the hardest binder studied with a penetration grade of 10/20, still demonstrated a significant amount of healing. Although healing of hard binders does require very favourable healing conditions. In this sense the observed healing for hard binders is more than was reported in previous research (De La Roche, Odeon, Simoncelli, and Spernol 1994; Qiu et al. 2009).

The research also demonstrated that the healed connection showed less post peak deformation capacity. At relatively short healing periods and more frequently for harder binders, the half specimens came apart fully during the tensile test at the end of the healing period. This tendency for healed surfaces to come apart, demonstrates that adhesion plays large role in strength recovery. It has been made assumable that for restoration of toughness, the healing interface has to be fully homogenized, which is observed for longer healing periods especially for the 70/100 binder. Within this it has been demonstrated that the recovery of strength proceeds faster compared to the recovery of toughness, which in turn would imply that the process of diffusion is slower compared to wetting.

The healing ability of three different 70/100 binders was assessed, using the same conditions. This demonstrates that for the same penetrations grade the trend in healing is quite similar. For all binders the healing ratio at the shortest healing period of 30 seconds, or instant healing, is around 50% of the reference strength, while 24 hours they all have restored 90% of the strength. This implies that for this group of binders, the hardness is a key parameter in healing, that is more important than the other differences in material characteristics between these binder. There are however small differences in healing performance, as the development over time was more smooth for Nynas compared to the other two binders.

The results indicate that binders exhibiting higher levels of instant healing also tend to show greater healing over time. If this trend holds across a broader range of binders, the two-piece healing test, applied with a short healing period, could serve as a rapid and effective method for ranking binder healing performance.

The test results of this chapter show that for healing inside the testing machine the following test conditions are suitable for long term healing tests:

- An assembly and healing temperature of 14 °C;
- An imposed deformation during the assembly phase of 0,8 mm;
- An assembly rate of 0,04 mm/s;
- A tensile rate of 0,5 %/s;

The test results of this chapter show that for healing test with assembly inside the storage room,

- An assembly and healing temperature of 14 °C;
- A weight of 1 gram for all materials;
- A tensile rate of 0,5 %/s;

5.7 RECOMMENDATIONS ON HEALING TESTING WITH TIME

It is recommended to further explore the effectiveness of the proposed test conditions inside the testing machine for harder binders, as this was non systematically studied during the executed research.

It is recommended to study if the healing trend over time is consistent for a wide range of binders, if so this implies that instant healing of a binder, measured just after the assembly phase is completed, can be used to rank healing ability of different materials. If this is the case, the presented two piece healing test could serve as a relatively easy and quick test to assess the healing capacity of a binder.

The results show that for shorter healing periods the surfaces can come apart fully showing no traces of homogenization of the surfaces, suggesting that all strength recovery is related to adhesion between surfaces. While research done on longer healing periods do show indications of homogenization. It would be interesting to focus a study on the moment of this transition and assess what parameters affect this transition. In this case photographs of specimens after testing should be an explicit part of the test program.

6

TRENDS AND PREDICTION MODELS FOR HEALING OF BITUMEN

6 TRENDS AND PREDICTION MODELS FOR HEALING OF BITUMEN

This chapter integrates new insights from the executed bitumen healing tests and supplements gaps with theoretical knowledge to refine and extend the existing healing model (RQ6). First, Section 6.1 presents preliminary test results on crack closure dynamics using a new image analysis technique known as Laser Speckle Imaging. Next, in Section 6.2, an expanded model for homogenization of the healing interface is presented. Section 6.3 presents the insights obtained from the twopiece healing test, by integrating the results from Chapters 4 & . Based on all this information an expanded qualitative model for healing is presented in Section 6.4. In Section 6.5 an augmented quantitative healing model is proposed, which expands on the existing healing model presented in Section 2.4.1, by proposing more elaborate equations which include all identified influencing parameters. Next, in Section 6.6 the time series obtained in Chapter 5 are fitted to a simplified version of the healing model to try and capture the observed behaviour in a simple equation, that can be used to predict healing. In Section 6.7 an attempt is done to look for correlations between the obtained healing parameter from Section 6.6 and rheological properties of bitumen. The chapter closes by summarizing the main findings.

6.1 ASSESSMENT OF PARTICLE DYNAMICS NEAR CRACKS USING LASER SPECKLE IMAGING

6.1.1 Introduction

In Section 2.9.3, it has been concluded that for asphalt to regain its original material properties, micro-cracks have to close and their interfaces need to homogenize. However, in literature there were no observations reported on the closure of cracks or the homogenization of the interfaces in bituminous materials. As part of this research, exploratory experiments on crack closure and bitumen dynamics using an innovative imaging technique called Laser Speckle Imaging (LSI) are executed at Wageningen University. The objective of these experiments is to study the dynamics in the material while the crack is closing.

LSI is a non-destructive technique aimed to study the dynamics of particles in soft matter. The technique is based on the illumination of a material surface using laser light and analysing patterns in the diffuse reflections. The laser light penetrates into the first molecule layers of a material and gets reflected by the molecules. The reflected light scatters in many directions. The scattered waves interfere with each other resulting in images with a random pattern of bright and dark spots, the speckle images. If the molecules don't move, the reflection is static, but if the molecules move as a result of diffusion or flow the spots on the images change resulting in something of a shimmer. By taking many images per second, and calculating differences in light and dark spots, the movement or dynamics of the particles can be quantified. The technique emerged in the

analyses of blood (Briers and Webster 1996), however has moved to analyse dynamics of other types of soft matter in the beginning of this century (Viasnoff, Lequeux, and Pine 2002). Since then, it has also been used to assess dynamics in self-healing of polymers (van der Kooij et al. 2017) (van der Kooij 2020).

6.1.2 Experimental set-up

6.1.2.1 *Introduction*

The aim of these experiments was to assess if this technique was able to capture the process of crack closure in real time and if these measurements could provide additional insights in the mechanism of the closure of cracks.

6.1.2.2 *Test method*

In Figure 6.1 a schematic impression of the set-up used is shown. It consists of a laser source. The power of the used laser was 1 Watt. This laser light is expanded, resulting into a wider beam of scattered laser light that can be cast on a surface. The laser light penetrates into the surface of the material and is partly reflected by the molecules it encounters. A camera is used to capture the reflected laser light. As the molecules in the surface move, the reflections captured by the camera changes with time. The changes in the reflections captured in the images over time are a reflection of the dynamics of the molecules in the material. The particle dynamics is defined as the two directional movement of a particle: Δr^2 or *d2*. This can be visualized by creating images with colour gradients for different particle movement intensities. Photos were taken over a period of maximum 18 hours. Experiments were terminated when no changes in particle dynamics were observed anymore.

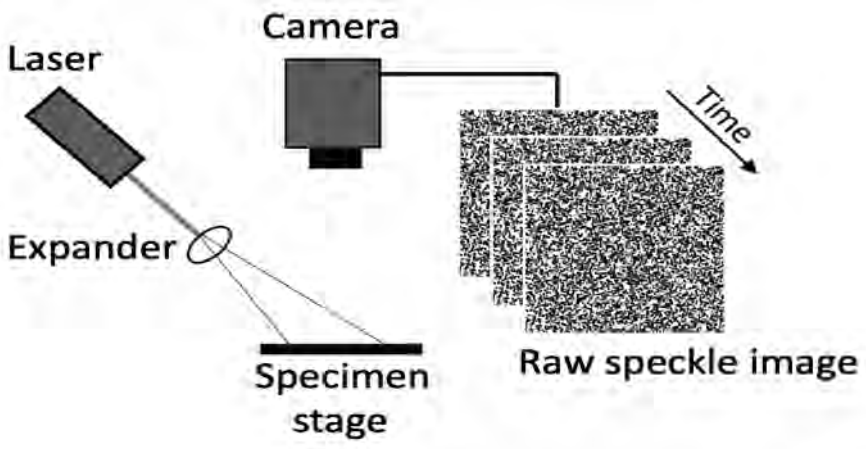

Figure 6.1 Schematic set-up of laser speckle measurement

6.1.2.3 *Test method Materials*

Two material were studied one bitumen and one mastic. The idea behind studying both bitumen and mastic, was that pure bitumen is expected to show the most dynamic behaviour providing an extreme situation, while mastic is expected to display material behaviour that is more close to an asphalt mixture. The bitumen was a straight run, unaged 70/100 bitumen. The mastic was made from the same bitumen; strain run, unaged 70/100 bitumen, which was mixed with an active filler in a 50:50 weight percentage.

6.1.2.4 *Test method Specimen design*

In order to mimic a crack, disc shaped specimens with a notch were designed. The disc has a diameter of 24 mm and a thickness of 1 mm, see Figure 6.2. The specimens were produced in a rubber mould, in which the notch was already present. The bitumen and the mastic was heated till 165 °C and then poured into the rubber mould. During the test, the specimens are placed horizontally on a piece of microscopy glass. During the first set of experiments, the particle dynamics at the notch was studied in detail. In a second experiment a mortar specimen was broken in two pieces, as shown in Figure 6.2 to study the dynamics of the closure of a full crack. The crack was created by placing a specimen in a freezer at 18 °C for one night and consequently breaking it, resulting in a brittle crack starting at the notch. Immediately after breaking the specimen, the pieces are put together and the experiment is started.

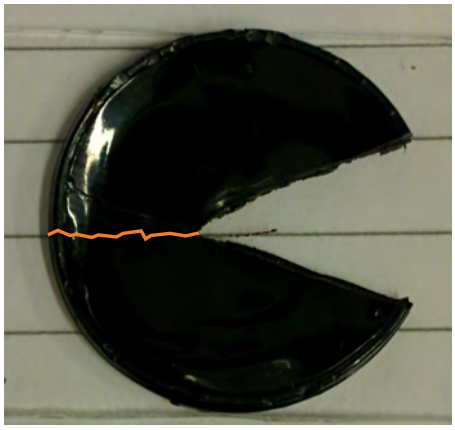

Figure 6.2 Specimen geometry showing the notch and in red the crack that was made to study crack closure

6.1.3 Observed particle dynamics at the tip of the notch

A first observation when conducting the experiment, was that bitumen is a challenging material to study with this specific technique. As bitumen is extremely black, almost all the light from the laser is absorbed and only a very small fraction is reflected. This

results in two challenges, in the first place the specimen heats up significantly; during the experiment the specimen temperature exceeded 60 °C, secondly the amount of reflected light on which the experiment is based, is very limited. As these issues are directly related to the used measurement principle, they cannot be resolved easily. A very effective cooling stage and/or a very sensitive light sensor in the camera could create a more controlled test set-up. However, these adjustments were not attainable for this exploratory research. Therefore, when interpreting the result these shortcomings should be taken into account.

One effect of the intense heating was that the bitumen specimen actually really melted. This can be seen from the deformed shape of the specimen at the end of the experiment in Figure 6.3b. The location where the laser light hit the surface has also significantly changed. This melting did ensure that the material in the specimen flowed, resulting in the closure of the notch.

The closure of the notch with time is displayed in Figure 6.3 c1 to c3. NB. note that these imaging are magnified by a factor 20 compared to the photo of the specimen in a. In the images, a lighter colour is correlated to a higher particle movement intensity, indicating that the particle movement is most intense at the tip of the notch. In c1, the tip of the notch is visible at the top of the image, c2 and c3 are made 40 and 80 seconds later. The consecutive images show how the notch moves downwards as it closes. Initially the speed at which the notch moves in the bitumen specimen is around 0,01 mm/s, this speed reduces as the notch grows wider.

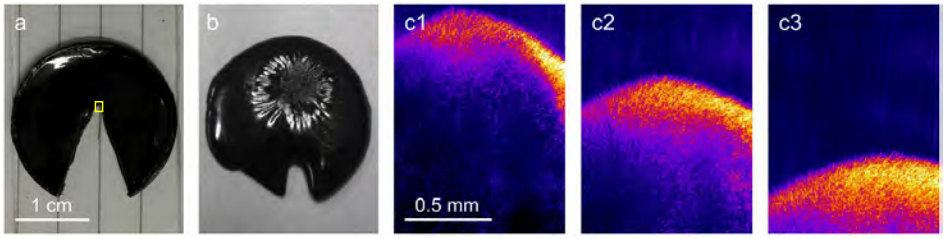

Figure 6.3 Using LSI to assess crack closure. (a) Bitumen specimen prior to an LSI measurement, with in yellow the focus area of c1 to c3. (b) Bitumen specimen after illumination of the notch tip with a 1 Watt laser beam for 18 hours. (c1–c3) images showing the 2d parameter when the bitumen flows downward closing the notch, with time steps between the images of 40 s (van der Kooij 2020).

Based on the theory introduced in paragraph 2.6.3.2, this local particle movement intensity at the tip, can be explained by the additional surface energy that is gained by molecules at the crack tip, due to the “loss” of surface area and the consequential gain in energy.

A comparison of the dynamics of the pure bitumen at the notch and at the bulk is presented in Figure 6.4. From the graph, with a local time parameter (τ) on the horizontal axis and

two directional movement on the vertical axis (Δr^2), it can be seen that the movement near the notch (blue dots), is significantly more intense compared to the movement in the bulk (black squares). In laser speckle imaging, the slope of the Δr^2 parameter to τ is used to assess whether the observed particle movement is dominated by flow or diffusion; if the slope have a value of 1, the dynamics is dominated by diffusion if the slope has a value of 2, it is dominated by flow. Based on this definition it is concluded that the particle movement near the crack tip is dominated by flow, both for the case of the mortar and pure bitumen. After the notch is closed, the material comes into a state of equilibrium and the observed dynamics of the particles correspond to the process of diffusion. The crack closure was roughly four times slower for mastic compared to bitumen.

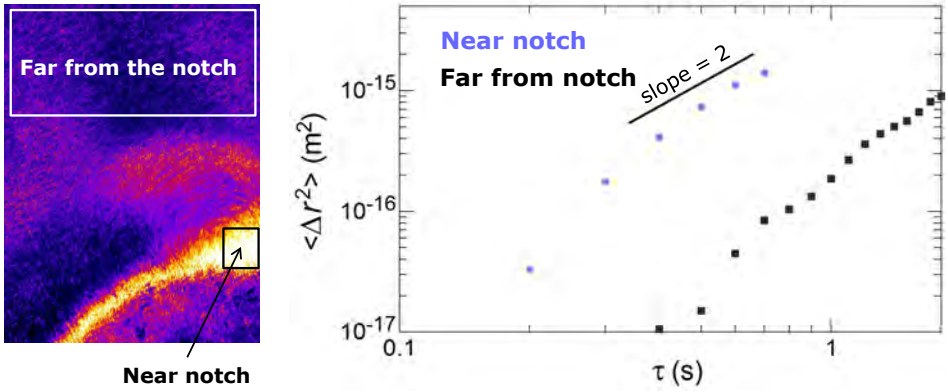

Figure 6.4 Quantified analyses of particle movement near and further away from the notch.

6.1.4 Observed particle dynamics at the closure of a crack in mortar

The particle dynamics near the crack of the fully broken mortar specimens are presented visually in Figure 6.5. In this figure, from top to bottom, consecutive timesteps are shown for particle dynamics at same location. Again the lightest colour is used for the highest particle dynamics. In the image, the crack runs horizontally over the middle of the image. The scale of the image indicates that the crack width is initially around 200 µm. If the images from different time steps are compared, it can be seen that initially there is a high particle movement intensity at the healing interface. Over time the intensity at the healing interface reduces, as contact between the two surfaces is established. After 1000 s seconds (~ 17 minutes) all particle dynamics has stabilized. Like previous experiment where the movement at the notch was followed, the particle dynamics is most intense when the crack is closing and contact is reestablished. Like the closing notch a zip like motion in the closure of the crack can be observed, were the crack is closing from left to right.

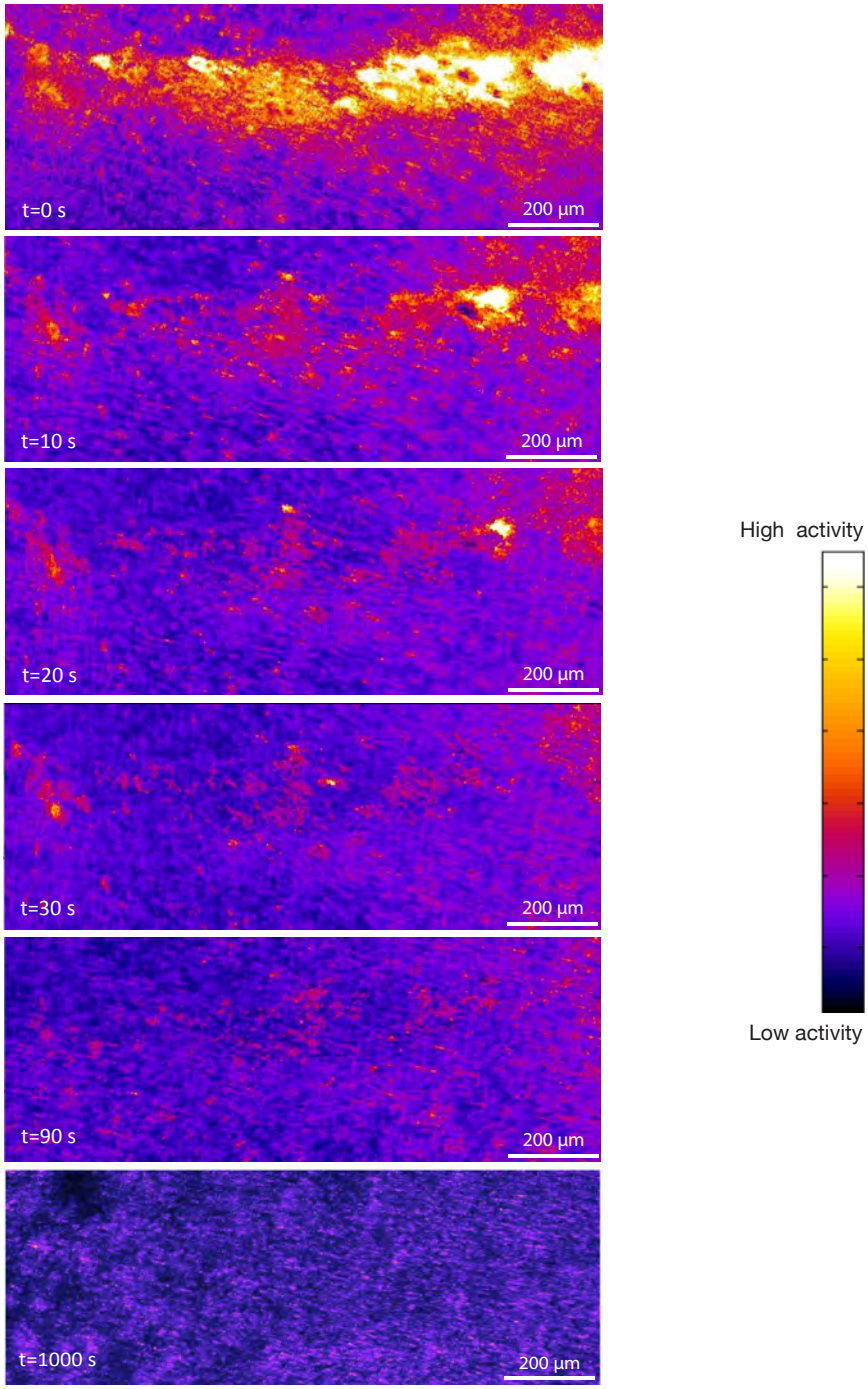

Figure 6.5 Closing of a brittle fracture in mortar, value of ***d2*** (activity parameter) over time determined using LSI

6.1.5 Conclusions and recommendations on the use of LSI for asphaltic materials

The results of the preliminary tests demonstrate that the particle or molecular movement of bitumen and mastic intensifies around the healing interface and normalizes after contact has been established. These experiments confirm the concept that surface energy is an important driver for the regeneration of contact, making it likely that the amount of area in contact during a rest period will increase with time. As such the experiments underpin the relevance of surface energy for healing of bitumen.

The presented work also demonstrates that LSI has potential to identify particle dynamics in bitumen, which might lead to new interesting insight on differences in dynamics under different conditions. However, it is recommended that the technique is optimized for the use on bituminous materials, as the heating of the specimen in the preliminary experiment was too intense to study the material under conditions that are present in the pavement. More quantitative measurements require temperature control of the specimen during the experiment. This might be done by placing the specimen on a platform that can extract heat fast, a so called heat sink. Next to this, laser light with different wave lengths could be tried, as the absorbance might be wavelength dependent. Although, it is not unlikely that bitumen absorbs all wave lengths equally.

6.2 MATERIAL MODEL FOR HOMOGENISATION OF THE HEALING INTERFACE

6.2.1 Introduction

In the healing model introduced in Section 2.4, diffusion is identified as the key process that drives homogenization of contact areas. Following up on this, Section 2.8 provided more details on diffusion in bitumen. Equation 2.8, from this section, describes the governing parameters for diffusion; time, concentration difference, travel speed and travel distance of molecules. If all these parameters would be known, the equation provides the amount of time needed for homogenisation of the healing interface. This section tries to provide substantiated assumptions on key parameters for bitumen diffusion, with the goal of making a theoretical best guess to the required time period that is needed for full homogenization of the healing interface. Section 6.2.2 describes the assessment of the expected differences in chemical composition at the healing interface. Section 6.2.3 aims to identify which process in homogenization is the slowest and is therefore expected to dominate the homogenisation behaviour. In Section, 6.2.4, assumptions are provided for the other parameters in the equation, which is followed by a result of the theoretical assessment of required time period for homogenization.

6.2.2 Differences in bitumen composition at the healing interface and the bulk

The material at both sides of the healing interface is the same. However, as a result of

the presence of an interface, there are differences in arrangement and composition of the material at the healing interface in comparison to the bulk, as has been already observed in literature, as discussed in paragraph 2.6.3.5. For the material to regain its original properties, homogenisation of these differences is required. Therefore in this section, information obtained from literature described in Chapter 2 is interpreted to propose the three most important differences in chemical composition at the healing interface that will drive homogenisation.

The first difference is that a **larger average distance** between molecules can be expected at the healing interface, compared to the bulk. This larger distance is caused by the fact that, just after the two surfaces have wetted each other and are in very close contact, molecules at the healing interface need time to rearrange themselves into the most energy favourable constellation. At the interface parts of larger molecules are sticking out, as a result the molecules of the other side are slightly hindered in their approach resulting in a slightly larger average distance between molecules. Over time, as a result of both thermal energy in the molecules, triggering vibration and rotation (see paragraph 2.5.4.3) and surface energy (see Section 2.7.2 and Section 6.1), the molecules at the surface will reorient themselves to obtain a more favourable energy position and consequently the average distance will become smaller.

The second difference at the interface is **a difference in chemical composition**, due to surface energy optimization at the crack surfaces. As already mentioned in paragraph 2.6.3.5, at a newly created surface, molecules will reorient themselves to lower the amount of free surface energy. Therefore, at the crack surface there will be relatively more molecules with a relatively low surface energy. In bitumen molecules will have less surface energy if they are smaller and less polar (Redelius and Soenen 2015). The degree of the difference in molecular composition, depends on the age of the crack, and the mobility of the molecules, as time is required to achieve the most energy favourable condition. The principles of surface energy indicate that the most plausible situations is that there is single layer of molecules with a lower surface energy, as the energy gain in the second layer of molecules is very limited compared to the first (Kendall 2001). At the moment the crack is closed, the energy advantage of low energy molecules at the healing interface is lost. Consequently, the low energy molecules will redistribute over the whole bitumen body due to Brownian motion ensuring homogenisation. As the low energy molecules are assumed to be the smaller molecules, their travel speed will be slightly higher compared to asphaltenes.

The third difference between the healing interface and the bulk is that there are **no molecules bridging the interface**. It is assumed that molecules bridging the interface will add to the toughness of the crack, as during loading molecules have to be pulled out from the interface to reopen the crack (Wool and O' Connor 1981). This pulling out of molecules requires sliding action, adding toughness to the connection, as mentioned in paragraph 2.5.4.3. It is said that asphaltenes are the essential components that

build viscosity in bitumen (Read and Whiteoak 2003; Hofko et al. 2016; Redelius and Soenen 2015). Therefore, there is consensus that to fully restore the material properties, asphaltenes have to bridge the healing interface. Asphaltenes are large enough to physically bridge the interface. However, as asphaltenes are the largest molecules in bitumen, they experience the most spatial hinderance and therefore move relatively slow.

These three differences at the healing interface that require homogenisation to restore properties are schematically visualized in Figure 6.6. In the left image, the interface of the healing interface is shown at $t = 0$, showing a relatively large distance between the molecules, different and smaller molecules at the interface and no molecules bridging the interface. To achieve homogenization the as presented in the right image, molecules need to travel. The expected travel distance and speed and the resulting required time will be discussed in the next section.

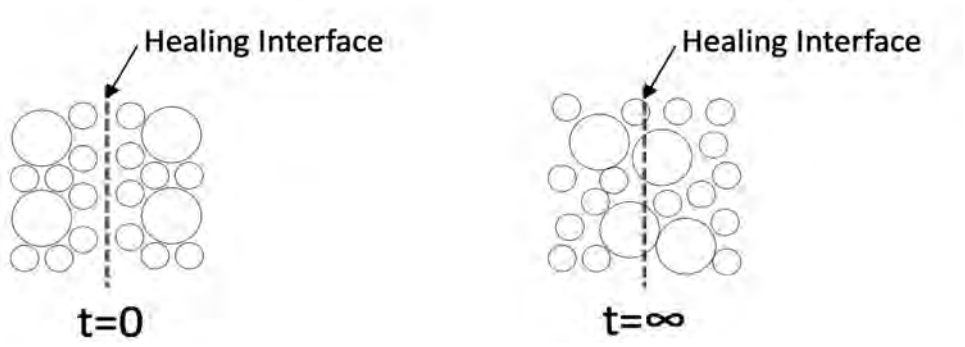

Figure 6.6 Schematic image of differences in molecular arrangement at the healing interface before and after homogenization.

6.2.3 Governing processes controlling the homogenization rate

Using the concept of travel speed of molecules (diffusion coefficient *D*) and travel distance (*x*) following Equation 2.8, the rate of homogenization for the three types of inhomogeneity identified in Section 6.2.2 can be compared. This is relevant as the slowest process will ultimately determine the homogenization rate.

The first type of inhomogeneity described, was the large average distance between molecules at the healing interface. To even out this inhomogeneity, molecules need to travel a very short distance as they only need to approach each other a little closer. Next to this, the larger molecules do not necessarily need to travel in absolute sense, as the average distance can be reduced by smaller molecules arranging themselves more closely around the larger molecules. Therefore the diffusion coefficient for this process is not the average self-diffusion coefficient of the bitumen, instead the diffusion coefficient of the smaller molecules is more appropriate, which is a little higher. When

these parameters are brought into Equation 2.8, it can be concluded that this aspect of homogenization will be relatively fast, as the travel distance *x* is relatively small and the diffusion coefficient *D* is relatively large.

The second type of inhomogeneity are low energy molecules at the healing interface, which need to travel away from the interface into the bulk. The travel distance of these molecules is larger compared to the first type of inhomogeneity, as the molecules need to travel the same distance as their own size to move to the bulk. The travel speed of these molecules is expected to be higher compared to the average diffusion speed of bitumen. In the first place because the relative small size of the molecules. Next to this, these molecules are less polar and therefore have less interaction with surrounding molecules, which increases the travel speed (Bhasin, Bommavaram, Greenfield, and Little 2011). As a result, it can be concluded that the travel of low energy molecules away from the interface will require more time compared to reducing the average distance between molecules at the interface.

The third type of inhomogeneity is the lack of molecules bridging the gap. To realize bridging, the largest molecules (asphaltenes) need to move from the bulk to the centre of the interface. Looking at Figure 6.6, is can be estimated that this implies a distance consisting of half their own size plus the size of the small molecules that are present at the interface. As the asphaltenes are the largest and most polar molecules in bitumen, their diffusion speed will be slower compared to the average self-diffusion of bitumen. This means that compared to the other two processes, the movement of asphaltenes from to bulk towards the healing interface results in the largest travel distance (*x*) and the slowest travel speed (*D*). It is therefore assumed that this process will govern the rate of homogenization at the healing interface.

6.2.4 Derivation of governing parameters for diffusion controlling homogenization

3.2.3.1 *Estimated parameters*

In the previous section it has been argued that it is very likely that the total time needed for homogenization is governed by the time needed for an asphaltene molecule to travel to the centre of the healing interface. In this section an attempt is done to quantify the parameters for Equation 2.8 for this specific case, which means that estimates will be formulated for the travel distance of an asphaltene (*x*), the diffusion coefficient of asphaltenes (D_A), the concentration of asphaltenes at the bulk C_{A0} and at the interface C_{Ax}.

3.2.3.2 *Estimated concentration of asphaltenes*

The first assumption needed is the concentration of asphaltenes in the bulk (C_{A0}). The concentration of asphaltenes is different for each bitumen but will be somewhere between 5 and 20% (Read and Whiteoak 2003; Eberhardsteiner et al. 2015). An assumption for the

concentration of asphaltenes in the bulk is taken at 15%, this is somewhere between the upper and the lower bound. The second assumption needed is the initial concentration of asphaltene molecules at the healing interface (C_{Ax}). As discussed in paragraph 2.6.3.5, asphaltene molecules are expected to travel from a bituminous surface to optimize surface energy. Therefore the amount of asphaltenes is assumed to be zero at the healing interface. The last assumption that is needed is the concentration asphaltenes at the healing interface, at which the homogenisation is considered to be complete. As Equation 2.8 describes an asymptotic process, really achieving 100% concentration at the healing interface requires an extremely long time, while at 95% the material behaviour will be very close to 100%. Therefore in chemistry often 95% of the original concentration is considered as full homogenization.

3.2.3.3 *Estimated travel distance of asphaltenes*

The travel distance of asphaltene molecules from the bulk to the healing interface has to estimated. As already mentioned this is about half their own size, plus the size of the surface molecules. In paragraph 2.5.3.2 the largest size of an asphaltene molecule is estimated to be 2 nm. The size of the molecules at the surface are expected to be smaller than a typical asphaltene molecule, however the exact size is not known. An estimate of the size of the small molecules near the surface is made by taking the smallest molecule size in bitumen, which is around 300 amu (see paragraph 2.5.3.2). It is not trivial to assess the size of a bitumen molecule of 300 amu, as amu is based on the weight of a molecule, which can have a range of shapes. An approach to estimate the size can be based on the size of an asphaltene molecule. A molecule of 300 amu is about 3 times lighter compared to an asphaltene molecule, which is estimated to be about 1000 amu. As the molecule has a 3D shape, while weight has one dimension, the difference in size is an a power root of 3 of the size, resulting is a reduction in size in one dimension of about 70%. Therefore it is reasonable to assume that the small molecules are 70% of the size of the large molecules, resulting in an estimated size of 1,4 nm.

Consequently, the travel distance for an asphaltene to realized homogenisation is estimated to be 2,4 nm (1 nm representing half the size of the asphaltene molecule, plus 1,4 nm from the thickness of surface layer at the interface). It should be noted that this assumption does not take into account that agglomerations of molecules could be present, which would result in significantly larger travel distances. The proposed 2,4 nm is significantly smaller than the distance of 10 nm that Bhasin, Bommavaram, Greenfield, and Little (2011) used as molecular travel distance in their molecular dynamics analyses to study healing over a crack interface. In their paper they do not clarify why they use this distance, however as it is the only reference in literature found on this topic, it is assumed to be relevant and is therefore used as an upper bound value for the travel distance of an asphaltene molecule in further calculations.

3.2.3.4 *Estimated diffusion speed of asphaltenes*

The last parameter from Equation 2.8 for which an estimate is needed is the diffusion coefficient. All molecules in bitumen have a different mobility based on their size and their molecular interaction potential (Karlsson and Isacsson 2003). This means that there is not one value for the self-diffusion coefficient for bitumen, there is a wide range of diffusion speeds that can be observed in bitumen. For this specific case the diffusion coefficient of asphaltene molecules is required. Within this research three possible approaches are used to obtain an estimate of the diffusion speed of asphaltenes in bitumen. For all three methods the diffusion coefficient at 25 ºC is determined.

The first approach is based on the use of the Stokes-Einstein Equation presented as 6.1, this equation can be used to calculate a diffusion coefficient based on the viscosity of a liquid.

$$D = \frac{RT}{6\pi N_A \eta r} \tag{6.1}$$

With R being the gas constant 8,31 kgm^2/s^2Kmol; T the absolute temperature; N_A being Avogadro constant $6{,}02*10^{23}$ mol^{-1}; η being the viscosity of the material and r the radius of the diffusing particle. At a temperature of 25 °C, assuming a viscosity of $1*10^7$ Pa·s (Read and Whiteoak 2003) and a particle size of an asphaltene of 2 nm. This equation results in $D = 1*10^{-20}$ m^2/s.

The second approach uses a technique called molecular dynamic simulations (Zhang and Greenfield 2007; You et al. 2020). In these type of calculations all molecular interactions that can develop between molecules are calculated and from the sum of all interactions conclusions can be drawn on material properties. One of the properties is the diffusion coefficient. As already mentioned in Paragraph 2.5.3.2 bitumen contains too many different molecules to be able to include all molecule types in a calculation. Therefore, calculations are performed on a simplified, artificial bitumen which only contains a limited number of molecules aimed to mimic the key molecular groups in bitumen. Zhang and Greenfield (2007) were one of the first to try and calculate the diffusion coefficient using three types of molecules and they reported a diffusion coefficient of $1*10^{-12}$ m^2/s at 25 °C. A more recent study which used 12 types of molecules found a significantly lower value for the diffusion coefficient of $7{,}04*10^{-14}$ m^2/s at 25 °C (You et al. 2020). As the work on molecular dynamics has developed strongly over recent years, the more recent value is expected to be more accurate. However, the reliability of this value still has to be considered with care as these simulations have not been verified by experiments on the actual material and they do they do not include the presence of an microstructure which is often reported in bitumen, see also Paragraph 2.6.2.4.

The third approach uses experimental measurements performed on bitumen. There are very limited reports on experiments aimed to determine the self-diffusion properties of bitumen. Instead, most research focusses on describing how different substances

travel through bitumen. The best data originates from Filippova et al. (2000), who have performed NMR measurements on bitumen. They report a value for self-diffusion for the asphaltenes of $4*10^{-12}$ m^2/s at a temperature of 120 ºC. This value can be transformed in a value for 25 ºC using Equation 6.1, which results in a diffusion factor of $1*10^{-17}$ m^2/s. This manipulation should be considered with care, as it is known that the microstructure of bitumen significantly changes over this temperature range (Soenen et al. 2014). At 120 ºC bitumen has no microstructure and behaves like a liquid, while at room temperature bitumen is expected to have some kind of microstructure. The presence of a microstructure is expected to hinder molecular movement reducing molecular motion and consequently the diffusion coefficient.

3.2.3.5 *Estimates for homogenization times*

In this section the assessed parameters are implemented into Equation 2.8 to calculate possible homogenisation periods. The previous paragraphs have shown for both the travel distance and especially for the diffusion coefficient, there is a wide range in plausible values, which will result in an even wider range for the calculated homogenization periods.

Figure 6.7 presents the extend of homogenization of the healing interface versus time, for the three determined values for diffusion coefficient ($D_{moleculardynamics}$:$7*10^{-14}$ m^2/s; $D_{experimental}$;$1*10^{-17}$ m^2/s and $D_{stokes\text{-}einstein}$;$1*10^{-20}$ m^2/s at 25 ºC) and the upper and lower value of the travel distance (2,4 nm and 10 nm). In Table 6.1 an overview is provided on the time required in seconds to realized 95% homogenisation at the healing interface for each of the combinations. From the figure and the table, it can be seen that homogenization for both the diffusion coefficient from molecular dynamics and experimental data occurs very fast; 95% homogenisation requires respectively 0,1 and 100 s for 2,4 nm. Only the Strokes-Einstein approach produces a homogenization process that takes a significant amount of time, more precisely 100.000 s (≈28 hours) for x = 2,4 nm and 1.000.000 s (≈11 days) for x = 10 nm.

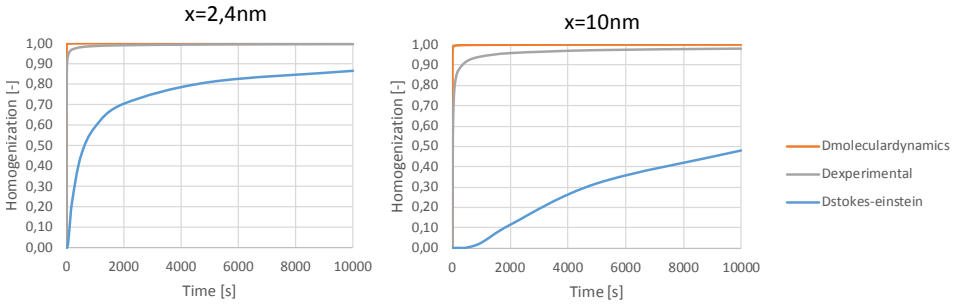

Figure 6.7 The relative concentration of asphaltenes at the healing interface at different moments in time, assuming x = 2,4 nm and 10 nm, with $D_{moleculardynamics}$ = $7*10^{-14}$ m^2/s; $D_{experimental}$ = $1*10^{-17}$ m^2/s; and $D_{Stokes\text{-}Einstein}$ = $1*10^{-20}$ m^2/s at 25 ºC.

Table 6.1 Time needed in seconds for homogenization for different values for homogenization distances and diffusion coefficients at 25 ºC

	$D_{moleculardynamics}$ $7*10^{-14}$ m²/s	$D_{experimental}$ $1*10^{-17}$ m²/s	$D_{stokes\text{-}einstein}$ $1*10^{-20}$ m²/s
2,4 nm	0,1 s	100 s	100.000 s
10 nm	1 s	1000 s	1.000.000 s

In order to narrow the band width in homogenization times, arguments can be considered to prefer one estimation method over the other, especially with respect to the diffusion coefficients as these have the largest bandwidth. The diffusion coefficient obtained using molecular dynamics is considered to be least reliable, as this value is not experimentally validated and the composition of bitumen is extremely simplified. The experimentally obtained value stems from a real observation in bitumen and has therefore most connection to reality, although it should be taken into account that it has been obtained at 120 °C, a temperature were bitumen has no microstructure. Therefore this value should be considered as a upper bound value. If based on this reasoning the experimental value is seen as an upper bound value, the time required for homogenization most likely lies somewhere between the grey and the blue lines of Figure 6.7. The resulting homogenisation time is now between 100 s (x = 2,4 nm and D = $1*10^{-17}$ m²/s) and 11 days (x = 10 nm and D = $1*10^{20}$ m²/s) at a temperature of 25 °C. This is still a very wide range, however it is interesting to see that the highest value is in the range days and not weeks or years, if this is true, this implies that healing periods that are present in pavements are in the range that they have effect. As a lot of assumptions were needed to arrive at this point, this insight should considered as the start of a debate, not the end conclusion.

6.3 INSIGHT OBTAINED FROM THE TWO-PIECE HEALING TESTS

6.3.1 Introduction

The two piece healing test in direct tension was developed with the aim to understand more about the mechanisms behind healing. This section describes what new insights have been obtained by varying stress at the healing interface and by studying healing over a wider time range from seconds to days. These insights are clustered for each identified parameter that has been identified by the two piece healing method to influencing healing.

6.3.2 The relevance of the amount of area in true contact at the healing interface

The literature presented in Chapter 2 has demonstrated that the first step in the process

of healing is the creation of contact between the two surfaces at the healing interface. An important parameter when studying the creation of contact is the amount of area brought into contact. Here a distinct difference should be made between the apparent amount of contact and the true amount of contact. The apparent amount of contact refers to the projection of the two surfaces at the healing interface. The true contact is the area that is in true molecular contact, implying that molecules are in the same range of each other as they were before the damage occurred. However, while executing the two-piece healing tests in this research it turned out to be practically not feasible to determine the amount of area brought in true contact. Therefore when interpreting the results of the two-piece healing tests, the amount of true contact area created was inferred from other parameters.

The results presented in Section 4.6.1 show that for two completely separated surfaces (complete damage) of a single material, brought together and exposed to a short healing period in the order of seconds, at a single temperature, more healing was observed when a larger assembly force (Figure 4.21) or a slower assembly rate (Figure 4.22) was applied. Considering the parameters influencing healing, as identified in Section 2.9.1, this implies that the only plausible explanation for more healing, is a larger surface area that has come into true contact. Next to this, it was demonstrated in Section 4.6.3 that the total amount of deformation applied during assembly phase correlates with the amount of healing detected. Also for this case it seems most plausible that, the reason that more healing is detected is caused by a larger area in contact true contact in the case where the surfaces are pushed together more intensely by applying a larger deformation.

Therefore, even though not directly proven, it can be concluded that the results presented in this research, point towards the strong importance of the amount of true area in contact for healing. Therefore the amount of true contact area should be an explicit parameter in a healing model. A secondary advantage of making the true area in contact an explicit parameter in a healing model, is that it might trigger future research to study this parameter in more detail.

6.3.3 The impact of stress state at the healing interface

In Chapter 3 two different test approaches were presented to assess healing. In the first approach specimens were brought into a storage room, for assembly and healing for a period of 6 minutes to a week, during the whole healing period the healing interface was subjected to a very small stress perpendicular to the healing interface of 0,0002 to 0,0044 N/mm^2. In the second approach specimens were assembled and left to heal inside the testing machine. In this case the stress perpendicular to the healing interface was significantly higher; between 0,04 and 0,84 N/mm^2. However, in this approach the stress was only applied during the assembly phase, which took between 10 to 200 seconds, during the consecutive healing period no stress was applied. The difference between the applied conditions is nicely illustrated in Figure of Section 3.2.3.

The impact of the different assembly conditions is investigated by plotting two specific results from Chapter 4 in one graph, see Figure 6.8. From the graph it can be seen that, after a healing period of one hour, a similar healing ratio can be observed for specimens that where either subjected to an initial high assembly stress (0,1 N/mm^2) or a constant low stress (0,0007 N/mm^2). Apparently these two very different conditions resulted in a similar amount of contact area. This type of behaviour can be expected from a viscous material like bitumen, as the response of the material is time dependent.

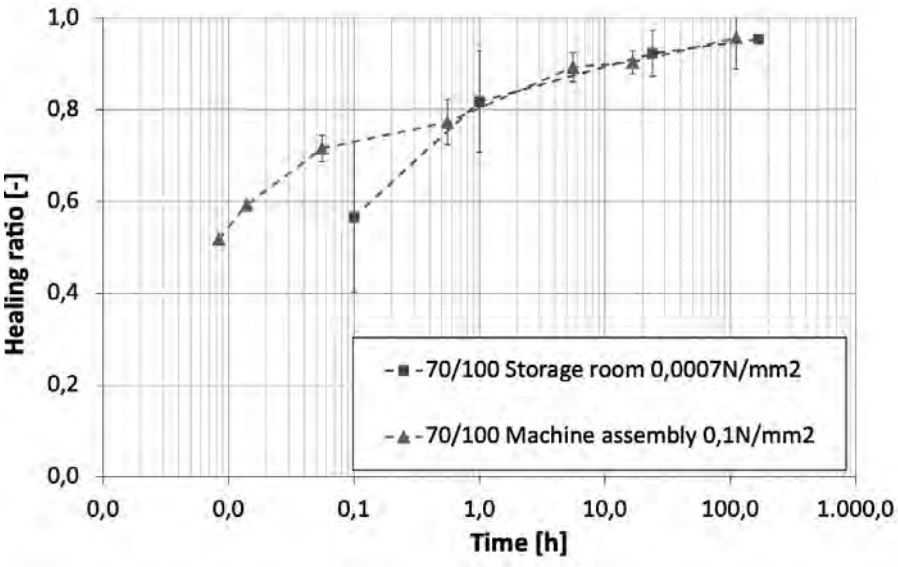

Figure 6.8 Comparison of healing between 70/100 specimen assembled in the storage room and the testing machine

The results for the two different type of healing conditions are also compared for harder binders in Figure 6.9. For the storage room stress the same weights were used for 10/20 bitumen and 40/60 bitumen, while in machine assembly a larger stress was applied for 10/20 bitumen compared to the 40/60 bitumen. It can be observed that the storage room conditions resulting in a significant amount of healing for 40/60 bitumen, also for shorter healing periods, compared to the 10/20 bitumen. The 10/20 bitumen that could be stresses strongly inside the tensile machine in a controlled way, did demonstrate a significant amount of healing. Even though the loading conditions are not really comparable, these results do show that that for harder bitumen more stress is needed perpendicular to the healing plane to establish contact. If enough force is applied to establish contact, healing can be observed.

The results show that for all three binders tested, the stress state at the healing interface influences the observed healing and therefore is a key element of healing model.

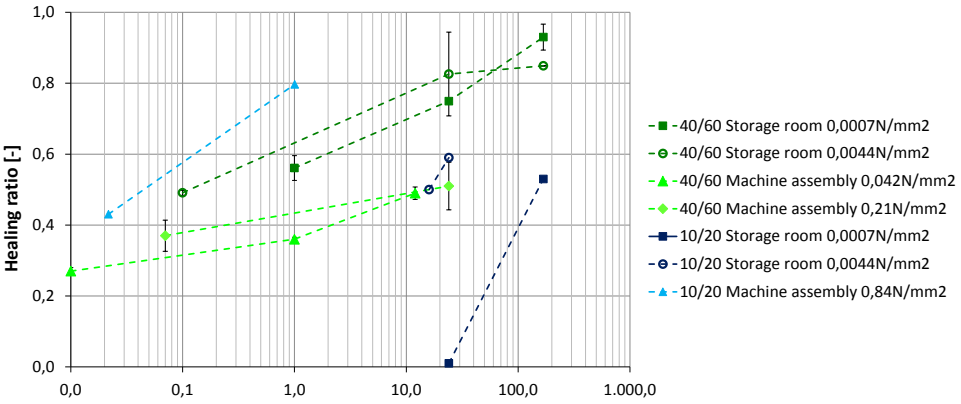

Figure 6.9 Comparison of healing ratios between 40/60 and 10/20 binders assembled in the storage room and the testing machine

6.3.4 The role of adhesion in healing

The healing theory presented in Section 2.7 suggests that the observed healing can partly attributed to the adhesion between asphaltic surfaces. In Chapter 4 it is argued that the initial healing, seconds to minutes after contact, is most likely related to adhesion, as there is no visible evidence of material exchange between the two surfaces at the healing interface. If this conclusion is combined with the results presented in Chapter 5, it can be concluded that the amount of healing that can be attributed to adhesion is significant. For soft 70/100 binders, the instant healing was around 40% to 50% of the healed strength after several days, see Figure 5.15. As adhesion strength could also contribute to the further strength increase after longer healing periods, this implies that for soft binders at least 50% of the healing can be attributed to adhesion. For the harder binders the amount of instant healing, with no visible evidence for material transfer was lower, ranging from 0 to 40%. This could indicate that for these harder binders the contribution of adhesion is less, however it could also indicate for these harder binders the assembly force applied during the experiments was not high enough to create a similar amount of area contact as for the 70/100 specimen. This is not unlikely considering the impact of stress during the healing phase as presented in the previous section. It is therefore concluded that adhesion plays a significant role in healing. As such, the result confirm that adhesion should be included in a healing model.

It is important to note that in Chapter 4 it is also concluded that a connection based on adhesion is less ductile compared to the original connection. As toughness is an important quality of asphalt pavements, this loss of toughness might prove to be important and needs further attention when researching healing.

6.3.5 The impact of time on strength and toughness of the healing interface

In Chapter 5 the influence of time on healing is studied in detail. The results show that the impact of time on healing is not linear. An example is the observed trend in healing of 70/100 bitumen as shown in Figure 6.10. In the figure it can be seen that at short healing periods the effect of time on healing strength is quite strong. In the first 300 seconds after assembly the healing ratio increases with 0,25. However, this impact of time on healing diminishes fast, because in the following 3300 (ten times longer) the healing ratio increases less with 0,18. A similar trend is discussed in Section 5.4.8 for the other 70/100 binders studied. This demonstrates that even though time influences healing significantly a short healing periods, the influence of time on healing strength becomes small and possible even insignificant for long healing periods. This also becomes very apparent when the results are plotted on a linear scale, as has been done in the right graph of Figure 6.10.

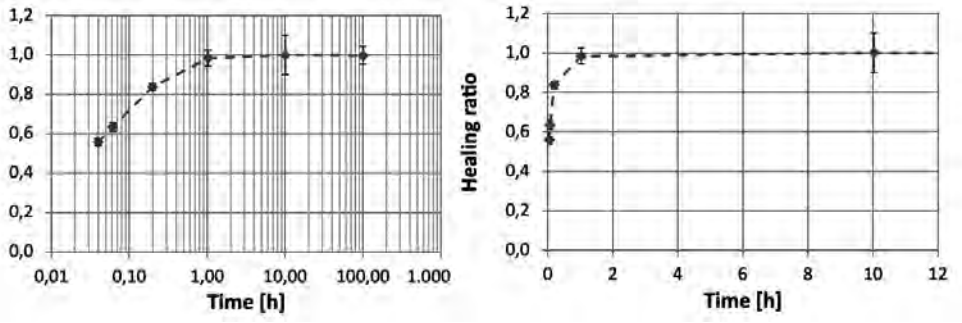

Figure 6.10 Development of healing ratio with time for 70/100 bitumen assembled inside the testing machine, on the left on a logarithmic scale and on the right on a linear scale (based on results presented in paragraph 6.3.2.1)

It should be noted however that Chapter 5 also concluded that longer healing periods do restore toughness. As the toughness is an important material property contributing to the pavement performance, this aspect should be studied further.

6.3.6 Adhesive failures and diffusion

Section 6.3.4 discusses that at short healing periods of seconds to minutes as used in Chapter 4 adhesive failure can be observed. There is no visual evidence of material transfer of one side of the healing interface to the other. This implies that in these short times the total amount of molecules that bridge the two surfaces is very small. Indicating that the diffusion of the large molecules, which are able to bridge the distance between the two surfaces, is very limited during these healing periods. The results reported in Chapter 5 are not conclusive on the longest healing period for which adhesive failure is still observed, as the occurrence of adhesive failure also depends on the used assembly conditions. However, adhesive failures are reported for some specimens subjected to healing periods of 50, 100, 200, 2000 s and 1 hour. It is interesting to combine these

observations on adhesive failures with the obtained insights from Section 6.2. The diffusion scenarios presented in Figure 6.7 shown that it is likely that during a healing period of 2000 seconds some diffusion of the largest molecules over the interface has occurred, as it was said that is was most likely that actual diffusion rates are somewhere between the blue and the grey line. The lack of any visible evidence of diffusion could indicate two things, either there is something limiting the initial speed of diffusion or the process of diffusion is actually even slower than the slowest variant suggested in Figure 6.7.

A slow initial diffusion rate may result from surfaces being close enough for measurable adhesion but too far for diffusion. Surface roughness may explain the significant physical distance between the bitumen surfaces. In Paragraph 2.6.2.4 is has been illustrated that bitumen containing waxes have a certain surface roughness, caused by different phases in its microstructure. It has also been illustrated in this paragraph how surface roughness reduces the total surface area in molecular contact. The typical surface roughness detected by the AFM for a bitumen containing waxes is around 50 nm. As explained in Section 2.7.2, adhesion forces are present if surfaces are 50 nm apart, the this distance will create a barrier for diffusion. The Nynas bitumen used in this research does not contain waxes and is therefore expected to have significantly less surface roughness compared to the other specimen.

This distance due to roughness is not expected to persist at the healing interface as there are mechanisms that will reduce the roughness over time. Already at the moment that the surfaces are brought together, the roughness will reduce. At this moment it is likely that the stiffer *catana* domains, instead of deforming are pushed down into the softer *para* surroundings. If this happens these domains become local zones with where the area has less molecular contact. The literature reported in Paragraph 2.6.2.4 suggests that surface roughness decreases over time, allowing adhesion to gradually pull the surfaces fully together over time to create full molecular contact. As such providing a plausible explanation for a delay in the start of the homogenisation process.

Using the two-piece healing test, experiments have been executed on bitumen containing waxes, more specifically Total and Q8 and a bitumen that do not contain wax more specifically Nynas. The chart showing the healing trends over time is reproduced below, as Figure 6.11. If roughness would impede the creation of contact and the consequent homogenization, Nynas is expected to be the better healer as this bitumen has significantly less roughness. The results show that Nynas has a more consistent increase over time. However, the differences between the binders are also relatively small, so the lack of material transfer could also still be caused by a smaller diffusion coefficient compared to the estimations put forward in Section 6.2. It is therefore recommended to execute further research on how the surface roughness of bitumen affects healing, along with improved estimates for asphaltene diffusion coefficients within bitumen.

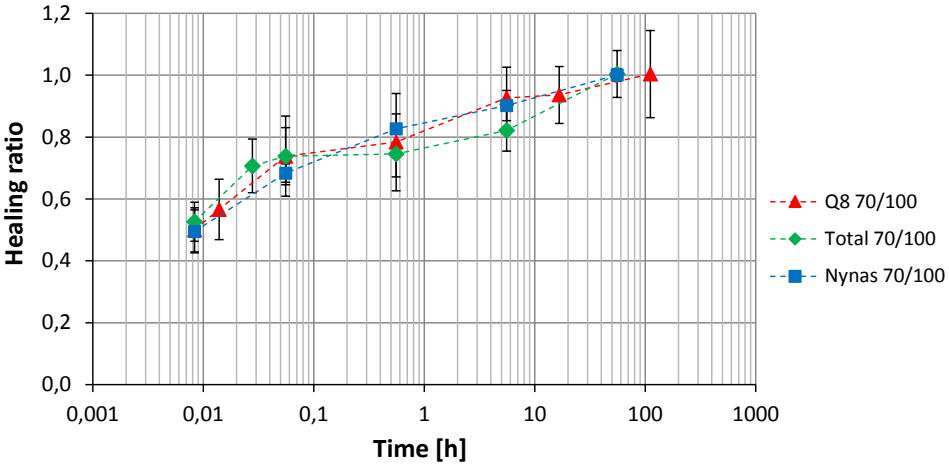

Figure 6.11 Healing ratios for three different 70/100 binders on a logarithmic timescale

6.4 QUALITATIVE HEALING MODEL

6.4.1 Processes in healing

The observations described in Section 6.1 to 6.3 can be brought together to create an improved qualitative material model for healing of asphaltic materials. This model is illustrated in Figure 6.12. In order to describe the mechanisms playing a role in healing, three healing situations are distinguished, which will be described in more detail below;

a) initial healing with a sub-optimal contact at the healing interface,

b) initial healing with an optimal contact at the healing interface and

c) complete healing showing a fully homogenised healing interface.

In healing situation **a**, there are only several small areas of the total contact zone (A_0) that are in full molecular contact (A_t), while most of the surface area is just close enough to experience some adhesive interactions. This is schematically shown in the left image of Figure 6.12. As the areas with full molecular contact are spatially spread and the areas in between have some adhesive interaction, the entire cross section is activated when the healing interface is subjected to a tensile test, resulting in a strong recovery of stiffness. However, as only limited areas are close enough to have strong adhesive interactions, the recovery of strength is limited and a small force can already break the relatively weak connection. Due to the significant spatial barrier for most of the healing interface and the short healing period, diffusion of molecules over the interface is limited, resulting in hardly any recovery of toughness.

In healing situation **b**, where full contact at the healing interface is realized shortly after the healing period has started, the interaction between the surfaces is different. In this

case almost the whole healing interface is close enough to experience intense adhesive attraction ($A_0 = A_t$). As the whole healing interface is in strong adhesive contact, the entire cross-section is activated when a deformation is applied resulting in a fully restored stiffness. As the surfaces have not homogenised yet, the average distance between molecules is larger at the healing interface, resulting in less molecular interaction compared to the bulk. As a result, the strength is not fully restored in this situation. Observations reported in Chapter 4 indicate that the strength is expected to be at least 50% of the original strength. The recovery of toughness is still small for this situation, as molecules have not diffused over the healing interface, bridging the gap and thus creating more ductile behaviour.

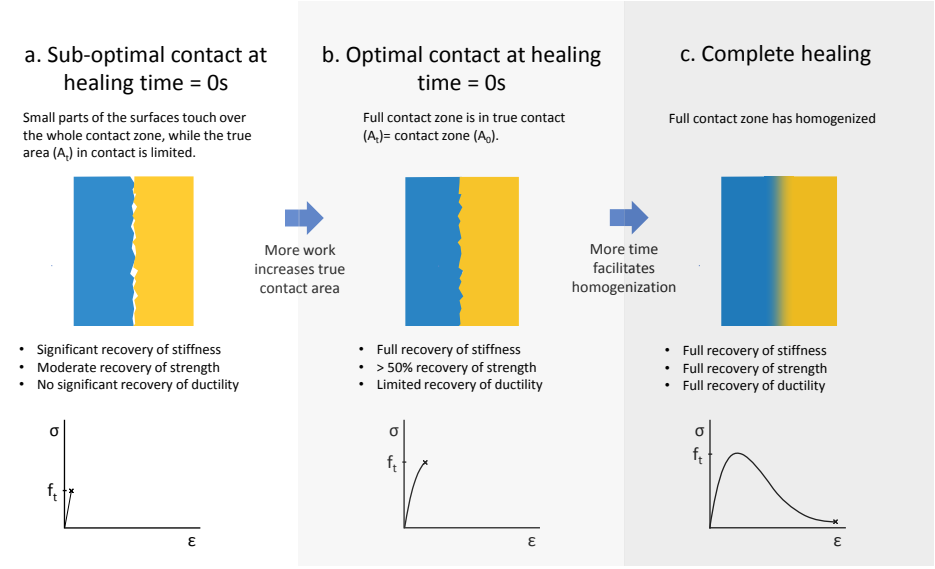

Figure 6.12 Qualitative model on healing of asphalt surfaces, showing three situations for healing.

When enough time has passed healing situation **c** will be achieved, where the contact will be fully restored. Once full molecular contact is present, with time, diffusion will ensure homogenization of the material at the healing interface. In this case the original tensile strength is fully restored. Next to this, the process of homogenization will also restore the toughness of the material, ensuring post-peak bearing capacity.

6.4.2 Time period required to achieve complete healing

An important question is how much time is needed to achieve complete healing (situation c). As discussed in Section 6.2, estimating homogenization time theoretically is challenging due to large uncertainties in variable selection. While Section 6.3.6 also made clear that microroughness will influence the amount of surface area in true contact. Another approach to estimate the time needed to achieve situation c, is use the test

results from the two-piece program as a starting point. While this will not yield to a single solution, these results can define an upper and lower bound for the time period needed.

To determine a lower bound, the longest healing period when adhesive failure was observed is taken. Section 5.5 reports that adhesive failures are observed for unaged 70/100 bitumen for healing periods up to 20.000 s (5,6 hours). Next to this, specimen of 40/60 bitumen demonstrated adhesive failure up to a healing period of one week. This indicates that the lower bound of complete healing depends on the type of binder, where it requires more than 5,6 hours for fresh 70/100 bitumen and 1 week for 40/60 bitumen. For these cases, the assembly conditions were not comparable, therefore it is very likely that the amount of contact created is different. Therefore, these lower bounds should be considered to be a very rough indication.

To determine an upper bound, the healing period is taken when a healing ratio of 1 is first observed. Based on the reported test results in Chapter 5, this can happen from 1 hour till 168 hours for the 70/100 binders. The largest value aligns with an upper bound, indicating a 168-hour upper limit for complete healing of 70/100 binders. The other binders studied in this research have not reached a healing ratio of 1. Therefore no upper bound value can be estimated for these binders.

6.4.3 Influencing parameters on healing performance

Results obtained with the newly developed test method seem to indicate that the ranking in healing performance is the same for the initial healing detected at $t = 0$ (healing situation a&b) and the healing after long healing periods (situation c). This could be interpreted as an indication that the initial healing determined with the two piece healing test is indicative for the relative healing potential of a binder compared to other binders. This should be validated with a wider range of binders which are representative for the Dutch market.

In this qualitative model, higher penetration-grade binders heal more easily as their surfaces deform and reconnect faster. Next to this their homogenisation will also proceed faster as their self-diffusion rate is expected to be higher due to a higher molecular mobility, see also Section 6.2. While healing may be slower, even very hard binders exhibit some healing ability. However, achieving healing situation b is more challenging with harder binders. Actual conditions in practise will determine if situation b is likely to occur in practise. To be able to predict if hard binders are expected to demonstrate healing behaviour, it is desirable to obtain more information on actual stresses and strains in pavements near a micro crack.

6.4.4 Application of qualitative healing model to open questions in healing

6.5.4.1 *Quick stiffness recovery with limited elongation of fatigue life*

Section 2.2.1 reports that fatigue-based healing tests show rapid stiffness recovery

during rest periods, but only slight improvement in load cycles to failure. A hypothesis to explain this effect is formulated based on the qualitative healing model presented in Section 6.4. In Figure 6.13 schematically illustrates a four-point bending fatigue test on asphalt beams. The specimen undergoes sinusoidal loading, alternately pushing down and pulling up. Research (Erkens 2002) indicates asphalt is weakest under tension, leading to invisible microcracks at the top and bottom where tensile forces are highest.

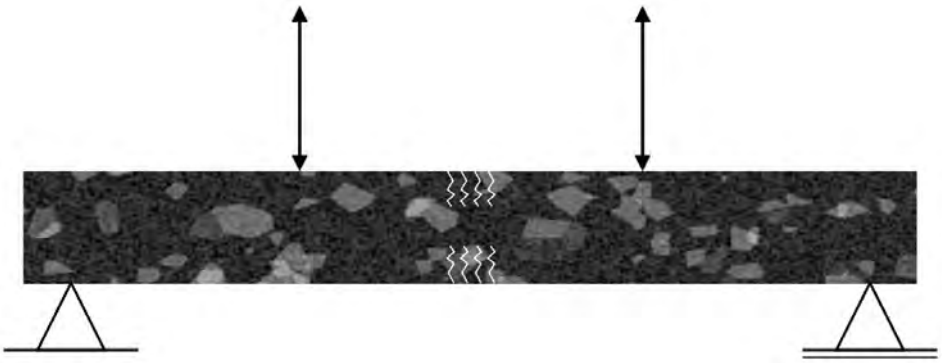

Figure 6.13 Loading configuration of a 4 point bending test for fatigue

During a fatigue test the observed stiffness is reduced. As already explained a significant part of this stiffness reduction is caused by biasing effects. But is small part is also caused by the creation of microcracks, which reduces the height of the specimen. Since stiffness is proportional to the cube of specimen height, a 10% loss in specimen height (a zone of 2,5 mm microcracks at the top and the bottom) leads to a 27% stiffness reduction. During rest periods the specimen is kept in the neutral position, resulting in a very limited force perpendicular to the healing plane. As a result, the surfaces microcracks of the microcracks have some ability to regenerate contact, although the amount of true contact is expected to be limited, resulting in healing situation a from Figure 6.12. This implies that for the first loading cycles the full cross-section is activated, resulting in a high stiffness. However, as the bond between the surfaces is weak, the contact is already lost after a small number of load cycles. Thus explaining why the stiffness recovery can be almost 100%, while the fatigue life sees little improvement.

6.5.4.2 *More healing in force controlled healing tests*

The qualitative model explains why force-controlled fatigue tests show more healing than deformation-controlled tests, as observed in past research (see Section2.3.3). During a fatigue test, cyclic loading is applied, resulting in alternating compressive and tensile stresses. As said, microcracks are created as a result of tensile loading, as the material is weaker in tensile mode. The compression part of the loading cycle brings the crack surfaces together again, facilitating healing. During a deformation controlled test, the

deformation is kept constant while the cracks grow, while in a force controlled test the deformation increases. Therefore, during a force controlled test, the surfaces are brought together with more intensity, resulting in a larger true contact area at the healing interface, facilitating more healing.

6.5.4.3 *Positive effect of expansion of the binder on healing*

The qualitative model also results in an interesting combination with the recent findings on the role of temperature expansion on healing as has been observed by Grossegger and Garcia (2019). In their research the authors have studied healing of porous asphalt surface layers using induction heating. Their studies originally aimed to identify the optimal temperature for asphalt healing. Instead, they discovered that the rate of temperature change mattered more than the absolute temperature. When trying to explain this, they realized that expansion of the binder due to a change in temperature was actually driving the recovery of strength, instead of the flow that was triggered by increased viscosity. This observation aligns well with the suggested qualitative healing model. Apparently binder expansion is more effective to reunite surfaces, compared to the flow of warm bitumen, demonstrating that bringing surfaces together is key in healing. If this theory holds, testing at a single temperature may overlook the effect of this mechanism, as binder expansion coefficients vary between binders.

6.5.4.4 *Healing of innovative binders*

The presented healing model implies that, as long the surfaces at a healing interface can regenerate their contact, the material in contact can generate adhesion and the transport of material over this contact is possible, restoration of properties is possible. This perspective could also be projected on innovative binders. This implies that both the hardness of a binder and its mobility are the parameters influencing the healing, while it does not matter if this hardness is the result of a combination of a rejuvenator and an aged binder or a fresh binder, provided that all components are fully blended. If modifications are added to binders that reduce their ability to regenerate contact on the short or long term this will have a negative effect on the healing ability of binders. It is recommended to execute additional tests with the two-piece healing test on different type of innovative binders to assess their short and long term performance and verify these assumptions.

6.5 AUGMENTED QUANTITATIVE HEALING MODEL

6.5.1 Additional variables for a healing model

In Section 2.4 existing material models for healing are presented. These are based on the concept that two processes are essential in healing; the regeneration of contact and the homogenization of this contact. These processes are sequential at an individual spot at

the healing interface. Since the entire surface does not come into contact simultaneously, both processes occur parallel, both contributing to the overall healing performance. In this section some additional components and variables will be added to this model.

The first variable that has to be added to the existing healing model is the normal stress perpendicular to the healing interface. The larger the normal stress and the longer it remains present, the more healing will occur. A larger normal stress increases the amount of initial contact created and it increase the rate with which the amount of contact area increases over time, as also mentioned in paragraph 2.6.2.3. For a viscous material, the amount of contact created as a result of the normal stress depends on the complex modulus, therefore the amount of contact created should depend on the product of the applied normal stress (σ_h) and the complex modulus (G^*).

A second additional parameter, that has to be incorporated into the material model, is the surface roughness, see paragraph 2.6.2.4 and Section 6.3.6. As a surface is never ideally flat, instant true contact over the whole healing interface is not a realistic assumption. Therefore, the surface roughness will have an effect on the creation of contact.

A third aspect that has to be added to the model is surface energy as a driver for wetting or regeneration of true contact area. This concept has been described in Section 2.6.3 and implies that surface energy triggers the material near the healing interface to flow in order to create true contact. The LSI experiments, described in Section 6.1, confirm this concept, as it is demonstrated that bituminous material actively flows to cracks to reinstall surface contact. It should be noted that in Section 2.7.2 it has been stated this effect does require surfaces to be less than 100 nm apart.

6.5.2 Mathematical representation of augmented healing model

This concept of healing as the sum of two processes has already been expressed in a mathematical equation by Wool and O' Connor (1981), presented as Equation 2.5 in Paragraph 2.4.2.2 and repeated below as Equation 6.2. The additional model parameters discussed in the previous section, should be incorporated into this mathematical model, to provides more detail in the equations for contact area growth ($A(\tau)$) and strength development the area in contact (R_h).

$$\boldsymbol{R = \int_{\tau=0}^{\tau=t} R_h(t-\tau)\frac{dA(\tau)}{d\tau}d\tau} \qquad (6.2)$$

An equation for surface contact developing over time $A(\tau)$ has been presented by Bommavaram, Bhasin, and Little (2009) as Equation 2.6, which is repeated below as Equation 6.3 for more clarity.

$$\boldsymbol{I_h(t) = I_0 + (1 - I_0)(1 - e^{-qt^r})} \qquad (6.3)$$

In Section 2.6.4, Equation 2.7 is presented to provide a 2D representation of area growth, which is repeated as Equation 6.4. In Equation 2.7 parameter k, expresses the rate of spreading.

$$\rho(t_h) = 1 - e^{-kt_h^m} \quad (6.4)$$

F Equation 6.3 and 6.4 are combined with the concept that the rate of spreading (parameter *k*) is dependent on viscosity, surface energy and the normal stress that is applied during the healing period (σ_{ht}) and the nucleation parameter *m*, is related to the roughness of the material, Equation 6.5 can be formulated.

$$A(\tau) = A_0 + (1 - A_0) \times (1 - e^{-k*t^m}) \quad (6.5)$$

with

A_0= the initial contact area

k = spreading parameter, dependent on viscosity, surface energy and σ_h

m = nucleation parameter, dependent of surface roughness

At this point in time, insights are lacking on how the parameters on nucleation and growth are exactly related to the more fundamental material parameters, this requires more experimental work.

A_0, the initial contact area in Equation 6.5 also has to worked out in more detail to show the impact of the applied normal stress during assembly (σ_{h0}) and the complex modulus (G^*). This can be addressed by dividing the stress at assembly σ_{h0} over the dynamic modulus G^* and while adding a factor for the material roughness, see Equation 6.6.

$$A_0 = \alpha \times A_p \times \frac{\sigma_{h0}}{G^*} \quad ((6.6)$$

with

A_0= the initial contact area

α = factor related to roughness

A_p = the total potential contact area

σ_{h0} = the applied normal stress during assembly

G^* = the dynamic modulus

Next, a more detailed equation has to be constructed for R_h that expresses that there is an instant adhesion strength plus an additional strength which develops over time as a result of homogenisation through diffusion (see Equation 2.8). This results in Equation 3.3.

$$R_h = R_0 + (1 - R_0) \times \left(1 - \mathrm{erf}\left(\frac{x}{2\sqrt{D \times t}}\right)\right) \quad (6.7)$$

with

R_0 = adhesion strength

x = travel distance of asphaltenes to centre of the healing interface

D = the diffusion coefficient of asphaltenes in bitumen

t = time period that the healing interface is in true contact

Next, Equations 6.5 & 6.7 have to be inserted in the in the convolution Equation 6.2 to provide one integral equation, presented as Equation 6.8. In this equation healing is defined as the ratio between the performance of a healed sample, and the original undamaged performance, therefore the value of R lies per definition between 0 and 1. Equation 6.6 is not integrated in the equation to keep it readable.

$$R = \int_{\tau=0}^{\tau=t} \left(R_0 + (1 - R_0) \times \left(1 - erf\left(\frac{x}{2\sqrt{D(t-\tau)}}\right)\right) * \left(\frac{d\left(A_0 + (1-A_0)(1-e^{-k*t^m})\right)}{d\tau}\right) d\tau \qquad (6.8)$$

with

R = overall healing ratio

R_0 = adhesion strength

x = travel distance of asphaltenes to centre of the healing interface

D = the diffusion coefficient of asphaltenes in bitumen

t = total healing period

τ = time

A_0 = the initial contact area, following Equation 6.6

k = spreading parameter, dependent on viscosity, surface energy and σ_{ht}

m = nucleation parameter, dependent of surface roughness

To get more insight into the possible outcome of this equation, a possible solution of both contribution parts (Contact area growth $A(\tau)$ and the performance of the contact area R_h) and their convolution are presented in Figure 6.14. $A(\tau)$ represents the growth of the amount of true contact area over time if the initial contact is 0. In this example 95% of the area achieves true contact after 5 hours. R_h represents the performance of the contact area, for the case that the immediate performance is 50% of the final performance. R_h is a dimensionless parameter which can be strength, stiffness or toughness. In this example, a period of 10 hours is assumed to result in 95% homogenization. This assumption is based on the lower and upper limits of the healing period as determined in Section 6.3.5. R is the total value of the healing performance based in the integral of $A(\tau)$ and R_h.

From Figure 6.14 is can be seen that for the presented case, when the full area is in true contact (after 5 hours ~18.000 s), the total observed healing R is almost the same as R_h, the process of homogenisation. While initially the curve for the development of contact

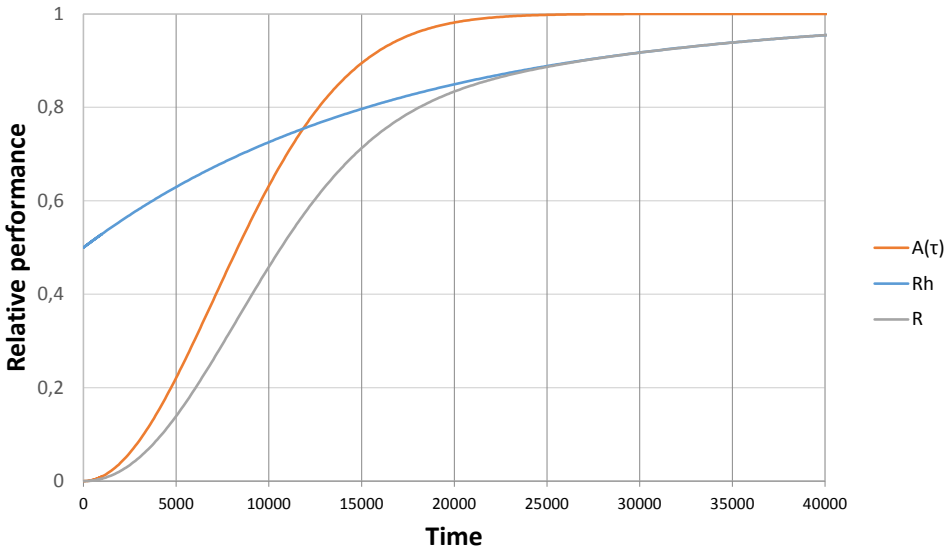

Figure 6.14 Graph demonstrating one possible outcome of the development of the healing over time (***R***), based on the combination of the contribution of $\boldsymbol{R}_h$ (the performance of areas in contact) and ***A***(***τ***) (the amount of area in true contact).

area is quite similar to that of total healing. This implies that the relative speed of the two processes will determine which of the processes is dominant at what timeframe. It could be interesting for future research to design experiments where one of the two processes is deliberately fast or very slow, as this will create the opportunity to study the processes individually. However, literature has already shown that this might be challenging to achieve, see 2.4.3; Bommavaram, Bhasin, and Little (2009) intended to realize instant full contact with their two piece healing set-up, however Qiu (2012) showed that this condition was actually met and both processes were still influencing the observed healing.

Next to this, it can also be taken from the graph that if the process of regenerating contact and the strength of this contact cannot be measured separately, it is challenging if not impossible, to discern which part of the observed healing should be attributed to which of the two processes. An attempt can only be successful if many data points over time are taken. Next to this, special attention has to be paid on the moment that contact is created. In most experimental set-ups A_0 does not start at 0 as the situation projected above, as either the specimen is not fully broken or surfaces are actively brought together as is the case for the two-piece healing test.

6.5.3 Healing trends development of stiffness, strength and toughness over time

In this section quantitative trend lines for the total healing ratios for stiffness, strength and toughness over time are proposed. In these trendlines the instantly detectable healing (R_0) is reported and the time dependant part (R_t). They are based on the healing model proposed in the previous section, the qualitative healing model from Section 6.4 and the time related experiments reported in Chapter 5. The proposed trend lines are presented in Figure 6.15. In this figure the three material properties are presented on the same time axis, one above the other, to demonstrate similarities and differences in the healing ratios. These are constructed from the perspective of bitumen, however the trends for asphalt will be similar, however the development over time is expected to be slower.

In the top image presents the recovery of stiffness. For stiffness the amount of instantly detectable healing R_0 is relatively high compared to strength and toughness. The observed instant stiffness depends on the amount of area that close enough to experience adhesion. This depends on the conditions bringing the surfaces together, the roughness and the viscos-elastic properties of the surface. Over time more area will be close enough to experience adhesive contact, consequently resulting in full recovery of the stiffness.

The middle trend shows the recovery of the strength. The strength is determined by the total amount of surface area that is in full molecular contact (A_t), as in this case adhesive forces are strongest, and the extend of homogenisation. The initial healing ratio will be higher if more area is in true contact. As with the stiffness, the initial amount of area in

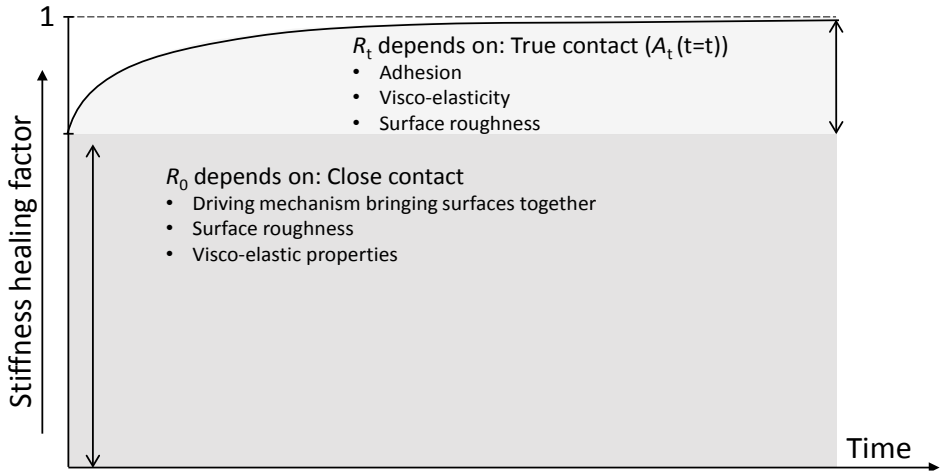

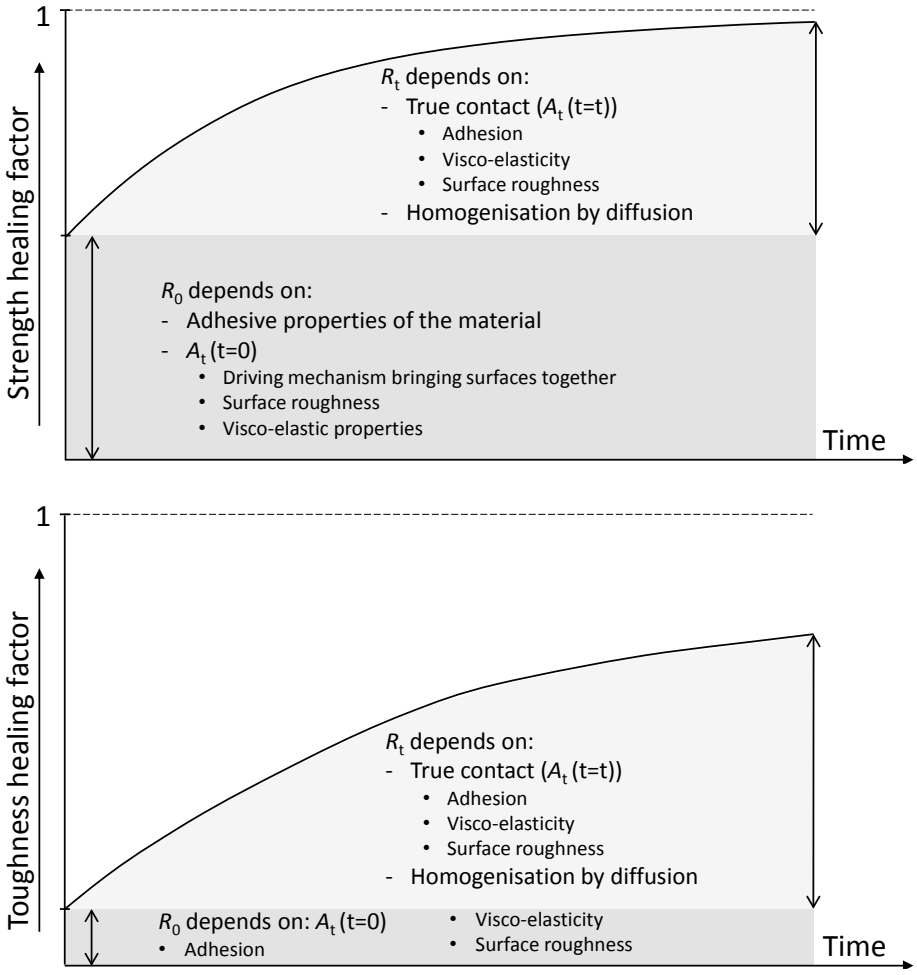

Figure 6.15 Healing trends for stiffness (top), strength (middle) and toughness (bottom) of bitumen with time

true contact depends on the conditions that bring surfaces together, the roughness and the viscos-elastic properties of the surface. The true contact area (A_t) will increase with time, as surfaces gain energy by achieving full molecular contact. Homogenisation is not present at t = 0, however the most important step to recover strength, is reducing the average distance between molecules at the healing interface, which is relatively fast as described in Section 6.2.3.

The bottom image shows the recovery of the toughness. This recovery is slower compared to strength and much slower compared the stiffness. The most important recovery is related to the transport of large molecules over the healing interface. However, even at the shortest healing periods, when surfaces come apart fully at a tensile test, there a

certain amount of post peak strength capacity for both 40/60 and 70/100 binders. NB. For 10/20 binders no post peak behaviour was observed, this is not different compared to the unhealed specimen. Toughness without homogenisation can be explained by the ductile deformation of the zones next to healed interface that are also activated when specimens are pulled apart. Therefore the initial recovery of toughness is not zero, but close to zero. With time the toughness increases, true contact facilitates the process of homogenization, ensuring full recovery of the toughness as molecules at the interface get intertwined again, ensuring much toughness. However, full recovery requires more time compared to strength and stiffness.

6.5.4 Relevant healing periods from a practical perspective

It is important to consider which rest periods, are most relevant for the performance of a pavement in practice. Two mechanical loading cycles are most important for pavements. The first one is related to the passing of vehicles, each heavy vehicle implies a small load on the pavement and the sum of millions of vehicle passing's results in fatigue failure. The second one is related to temperature change, where due to temperature variations during the day, stresses can build up in longitudinal direction of the pavement. Their durations differ significantly.

The healing factor used in the design phase is aimed to address healing that is relevant for fatigue loading imposed by heavy vehicles. Dutch highways experience heavy use, with short intervals between vehicle loads; based on 24-hour data, 0,5 to 5 heavy vehicles pass per minute, varying by highway (Rijkswaterstaat 2022). This implies that rest periods between vehicle loads in highways are quite short, between 12 seconds to 2 minutes on average. This means that the shortest healing periods studied in this research might actually be the most relevant for this type of healing behaviour. Implying that creating contact and adhesion is key for healing that occurs in between of the passing of heavy vehicles and the slower process of homogenization is less relevant for this aspect of healing.

However, healing behaviour of asphalt can also influence another process occurring in pavements. When asphalt expands as a result of heating of the pavement during daytime, this could also be the driving mechanism bringing surfaces of (micro) cracks together. The results presented in Section 6.3.3 demonstrated that a small normal force present for a longer time period can be very effective in establishing contact at the healing interface. Therefore an assessment has been made on the magnitude of normal forces that could be present in Dutch base layers as a result of thermal expansion. Data on temperatures in Dutch pavements was obtained from a previous study (J.H. Swart 1990). This study reports temperatures at the asphalt surface and at a depth of 190 mm. A representative temperature variation of a 24 hour period at a depth 190 mm is presented in Figure 6.16. From the figure it can be seen that with a 50 mm ZOAB surface layer (a porous asphalt,

standard for Dutch highways), at a depth of 190 mm, the temperature rises during the day with 2,5 °C per 6 hours, or 0,4 °C per hour.

In order to calculate the amount of stress that can build up as a result of this temperature variation, assumptions need to be made on the linear expansion coefficient and the stiffness of the pavement. In Section 2.1.7 a range of values for linear expansion for asphalt are given. To avoid overestimating expansion, calculations use the lower bound

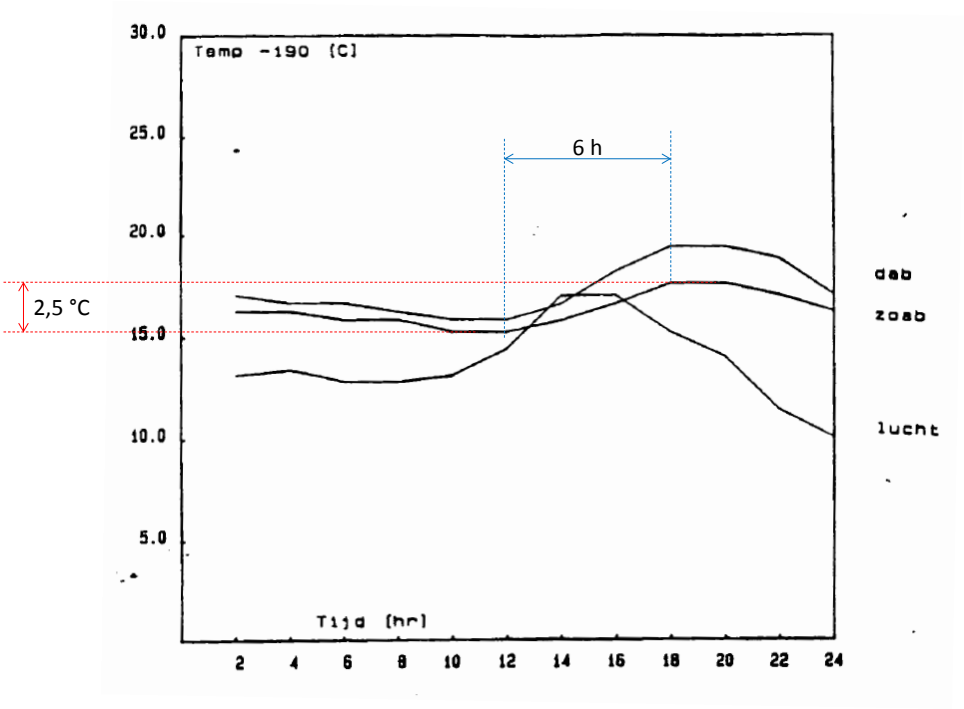

Figure 6.16 Temperature measured during a 24 hour period in a pavement construction at a depth of 190 mm, at Lexmond Netherlands on August 2nd 1987 (J.H. Swart 1990)

value, which is $2 \cdot 10^{-5}$ /°C. The stiffness of a pavement depends on the temperature and the design, however 10 GPa at 20 °C is a common value for new pavements in Netherlands. In this example, the temperature of the pavement is slightly lower (between 15 °C and 17,5 °C), consequently the actual stiffness of the asphalt will be a bit higher, by taking the value for the stiffness at 20 °C again a lower bound assumption is taken.

If the stresses in the pavement don't relax, the parameters above, amount to a compression force in the of around 0,4 x $2 \cdot 10^{-5}$ x $10 \cdot 10^{3}$ = 0,08 N/mm^2 after one hour, at depth of 190 mm. Of course the assumption of no relaxation is absolutely not realistic for asphalt. However, tests in this research showed that a normal force a 100 times smaller (0,0007 N/mm^2) resulted in a significant impact on the observed healing, see also 6.3.3. This means that if 99% of the stresses would relax, the resulting stress would

still be large enough to result in healing. In the experiments 1 hour of healing under a continuous compression force of 0,0007 N/mm^2 resulted in a healing ratio of 80% for 70/100 and 50% for 40/60. For the harder 10/20 binder more force was needed, in this case 0,84 N/mm^2 resulted in a healing ratio 80%. However, asphalt made with these harder binders will also relax much less, therefore the normal force for these binders will automatically be higher. This calculation suggests temperature stresses can generate sufficient compressive force to close cracks from traffic loading and aid healing. Future research should measure and model stresses in pavement from traffic and temperature in more detail to validate this hypothesis.

6.6 FITTING TWO-PIECE HEALING DATA TO THE HEALING MODEL

6.6.1 Introduction

This section aims to fit healing data from the two-piece test to the healing model, focusing on strength development at the interface over time. Since healing strength progression is nonlinear, only test series with at least four data points are used to ensure meaningful trend analysis.

6.6.2 Simplified healing model

The inputs of the model are the healing period, material properties and the condition at the healing interface. The output of the model is the healing ratio with respect to strength over time, see Figure 6.17.

Healing time was monitored closely in this research and serves as the first model input. The most interesting data points are at values at the extremes, in this case at $t = 0$ and $t = \infty$. In order to retrieve information at both the extremes, the test series aimed to test healing at the shortest and the longest possible healing period. Due to practical

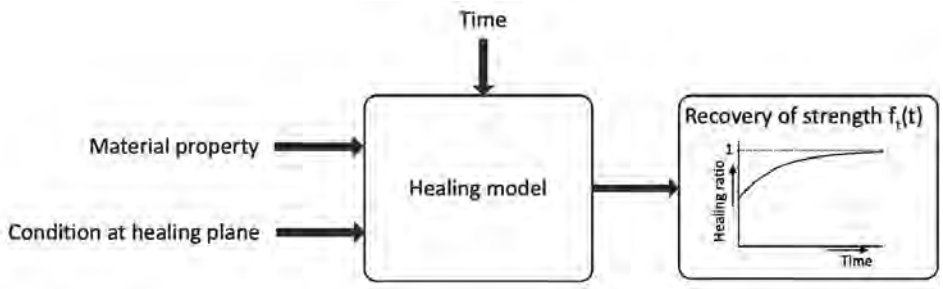

Figure 6.17 Schematic set-up for the healing model for strength including in- and output

limitations, the shortest test period that is used in this fitting exercise is $t = 30$ s, the longest period was 111 hours (or roughly 4,5 days or 400.000 s). This time span covers a significant part of theoretical time span required for homogenisation of the healing interface as reported in Section 6.2.

As only three different materials were tested, the model only contains one parameter to predict the impact of the material on the healing ratio. With respect to the condition at the healing interface, the amount of deformation during the assembly phase is seen as the most suitable parameter, as has been illustrated in Section 4.6.3. This parameter is interpreted as the amount of area brought into contact.

In Section 6.5.2 a mathematical equation has been presented that addresses most relevant parameters in healing of a bituminous material, see Equation 6.8. As this model was designed to contain all the known parameters, it contains more than 10 parameters. Many of these parameters have not been controlled or registered in the executed experiments. For instance there is an estimate with an extremely wide range for the self-diffusion coefficient of the largest molecules. Next to this roughness of surfaces is not measured and only theoretical estimates can be provided for the travel distance of molecules to realize homogenisation. If the small amount of data from the two-piece healing set-up would be fitted to this complex equation, the solution space for the parameters presented in the equations is infinite. This will therefore not result in any additional insight or understanding of the healing mechanism. Therefore, it is decided that it is more effective to use a simple empirical equation to try and fit the data. This equation is based on the sigmoidal shape, which is used for most proposed healing models, but it has only has two coefficients p and q to match the total amount of input parameters available and is presented as Equation 6.9.

$$R(t_h) = 1 - e^{-pt_h{}^q} \qquad (6.9)$$

With

R = healing ratio [-]

t_h = healing period [s]

p = model parameter [-]

q = model parameter [-]

6.6.3 Fit of the different materials exposed to similar assembly conditions

This section investigates whether the experimental data can be adequately described by Equation 6.9. Additionally, it evaluates whether the material type influences can be related to either of the two parameters within this equation. The input data consists of healing times series from three different 70/100 bitumen; Total, Q8 and Nynas, subjected to the same assembly conditions, as presented in Figure 6.18. The applied assembly condition consists of bringing two half specimens together until a total deformation of 0,8 mm, while applying an assembly rate of 0,04 mm/s at a temperature of 14 °C.

In Figure 6.18 every dot represents the average value of the test results obtained at that moment in time. Each colour represents a different material. The left graph shows fitted curves where both coefficients in Equation 6.9 can vary freely. Next, one parameter is fixed to tests its potential to represent the specific assembly condition applied in these test series, while the other parameter correlates with the intrinsic healing ability of the material. It is chosen to fix coefficient *q* at the median value, as this results in one graph staying the same, providing a clearer refence to compare the impact of fixing one parameter to the quality of the fit. The right graph shows the fitted curves for the case that coefficient *q* is the same for all three binders. The matching parameter values with the presented fits in the graphs are presented in Table 6.2. As could be expected, the fitted curves follow the data more closely when both coefficients are free to take any value, which can also be seen from the higher R^2 values. However, by fixing *q* the ranking of the healing ability of the three binders is not affected; in both situations Nynas is the fastest healer of the three, with Q8 performing slightly better compared to Total. In case *q* is fixed, the R^2-values are still quite reasonable. From this it can be taken that coefficient *q* from Equation 6.9 could potentially correlate with the assembly conditions, while coefficient *p* correlates with the material, with a higher value of *p* indicating a material with more healing potential. Although, it should be realized that the goodness of fit could also originate from the fact that the healing behaviour of these three binders is quite similar. To verify if *q* could really be a material parameter, a wider range of binders should be tested and statistical significance should be checked explicitly.

6.6.4 Fit of the same material exposed to two different assembly conditions

This section investigates whether the experimental data can be adequately described by Equation 6.9. Additionally, it evaluates whether the assembly method can be related to either of the two parameters within this equation. The data used comes from test series where three different assembly conditions were used on a single material; Q8

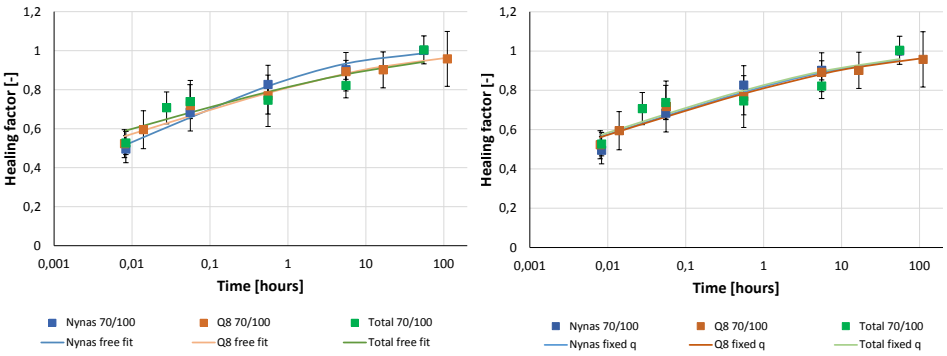

Figure 6.18 Healing test result of three different 70/100 bitumen, subjected to similar assembly conditions; a displacement of 0,8 mm; on the left free fit of ***p*** and ***q*** to Equation 6.9, on the right ***q*** is fixed at 0,15 while ***p*** can vary.

70/100 bitumen. Two test series were assembled inside the test-machine, with an imposed displacement during assembly of either 0,8 mm or 1,1 mm, a third test series was assembled inside the storage room. The healing ratios over time of all three series are shown in Figure 6.19. In the figure the squares represent the average value of the test results at a specific healing time, with each colour representing one of the test series. In the left graph three fits are plotted, corresponding to the situation where both coefficient p and q from Equation 6.9 can vary freely.

This time *p* is fixed to tests its potential to represent the intrinsic healing capacity of the material, while *q* is assumed to correlate with the intrinsic healing ability of the material. It is chosen to fix coefficient *q* at the median value, as this resulted in the highest R^2 values. Parameter *p* is fixed at the value that was used in Section 6.6.3 for this material (Q8). The resulting graphs with *p* fixed are presented in the right graph The values of *p* and *q* for all fits are given in Table 6.3. The fit with *p* fixed for the series with an assembly displacement of 1,1 mm (dark red) is rather poor, as also can be seen from the R^2-value while the other two fits are reasonable. As one of the fits with a fixed *p* value is judged to be poor, it is concluded that, either *p* is also affected by the assembly conditions and therefore not strictly correlated to the type of material, or that more parameters are needed in this model to define the impact of assembly condition. As the research has demonstrated the large impact of assembly conditions on the observed healing, it is actually rather likely that this behaviour is controlled by more than one coefficient. If more data would be available Equation 6.10 would be a logical option for adding a second coefficient.

Table 6.2 Coefficients corresponding to the various fits presented in Figure 6.18

	Fit	p	q	R^2-value
Nynas	free	1,92	0,20	0,968
Q8	free	1,67	0,15	0,970
Total	free	1,68	0,13	0,978
Nynas	*q* fixed	1,71	0,15	0,892
Q8	*q* fixed	1,67	0,15	0,970
Total	*q* fixed	1,57	0,15	0,977

$$H(t_h) = 1 - re^{-pt_h{}^q} \qquad (6.10)$$

H = healing ratio

t_h = healing period

r = coefficient related to assembly conditions

q = coefficient related to assembly conditions

p = coefficient related to material

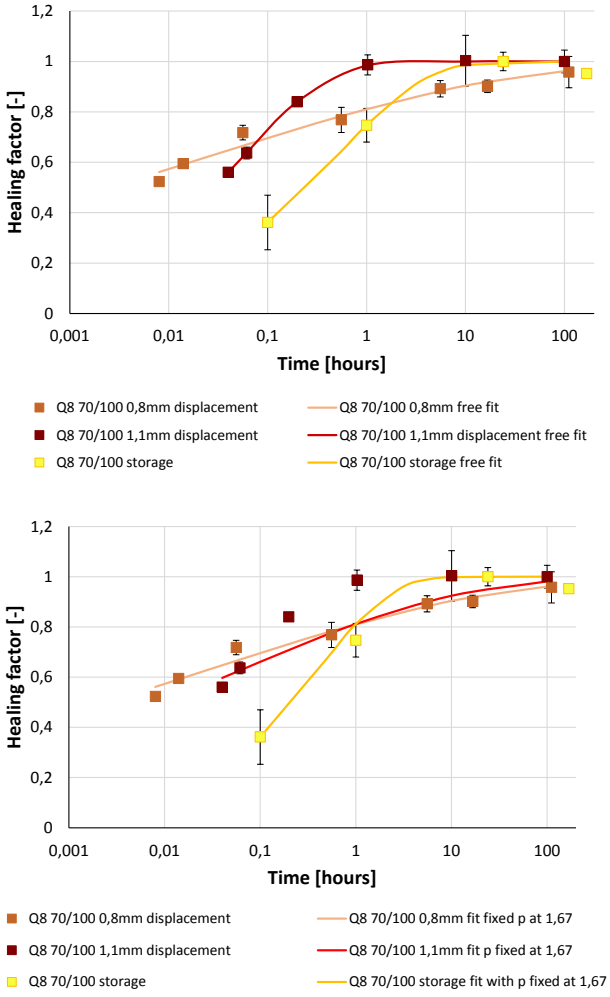

Figure 6.19 Healing test results of one bitumen type subjected to different assembly conditions; with a free fit to Equation 6.9 on the left and a fit with a fixed value for coefficient ***p*** of 1,67 on the right.

Table 6.3 Coefficients corresponding to the various fits presented in Figure 6.19

	Fit	*p*	*q*	R^2**-value**
Q8 70/100 0,8mm displacement	free	1,67	0,15	0,970
Q8 70/100 1,1mm displacement	free	4,13	0,50	0,9999
Q8 70/100 storage room	free	1,37	0,49	0,991
Q8 70/100 0,8mm fit	*p* fixed	1,67	0,15	0,970
Q8 70/100 1,1mm	*p* fixed	1,67	0,19	0,714
Q8 70/100 storage	*p* fixed	1,67	0,57	0,97

This fitting exercise has demonstrated that even though a simple Avrami equation with two parameters is able to capture the healing behaviour of a single test series, it is not possible to prove that either of these parameters is connected to a real physical parameter. Based on the correlation found in 6.6.3 it is possible that coefficient *p* is related to the intrinsic healing ability of a material, however the correlation might very well also be coincidental, as the material behaviour of the three binders quite similar as all binders used to find this correlation have the same penetration grade.

6.7 CORRELATING HEALING TO RHEOLOGICAL PROPERTIES

6.7.1 Introduction

This section explores correlations between healing behaviour and rheological properties. The starting point is the assumption that coefficient *p* as determined in subsection 6.6.3 for the case were *q* is fixed is the material parameter for healing. This in implies that the values for *p* as reported in the last three rows of Table 6.2 are correlated to the intrinsic healing performance of the material. If this is really the material parameter, this parameter might be correlated to other material parameters of the binder.

As already pointed out in Section 6.6.3, the amount of data substantiating this correlation is very limited. Therefore, the exercise described in this section should be seen as a recipe for a possible approach, while limited conclusions should be based on the outcome. The bitumen parameters that are checked for their correlation with parameter *p* with respect to healing behaviour are the penetration grade and a rheological parameter derived by a master curve obtained from DSR measurements.

6.7.2 Correlation between healing and penetration value

The penetration value is traditionally used as the most important indicator for the performance of bitumen. Within this research the penetration value of the binder was not determined. However, it is calculated using a previously determined correlation between *G** determined with the DSR and the penetration (Saal and Labout 1940). The used correlation is reproduced as Equation 6.11 and describes a relation between the *G** at 25 °C and 0,4 Hz with the penetration value.

$$\log\left(G^*_{0.4Hz;25°C[MPa]}\right) = 2.923 - 1.9 * \log\left(Pen_{25°C[dmm]}\right) \qquad (6.11)$$

The found penetration values for the different binders are reported in Table 6.4. NB. It can be noted that the reported values are on the low side, considering the binder grade (70/100).

6.7.3 Correlation between healing material parameter p and DSR derived parameters

6.8.3.1 *Master curves*

Master curves are determined to describe the rheological behaviour of the used binders, see Figure 6.21. The tests and the constructed curve are for 14 °C, matching the healing measurements executed in Chapters 4 & . The test is performed twice and the average result is presented.

From the figure it can be seen that there are only slight differences in rheological behaviour,

Table 6.4 Calculated penetration values based on observed rheological performance using Equation 6.11.

	Pen-value
Q8	66
Total	72
Nynas	75

The correlation between the penetration values calculated above and coefficient *p* is visualized in Figure 6.20. It can be seen that the correlation between *p* and the calculated penetration value is present, with a R^2 of 0,82.

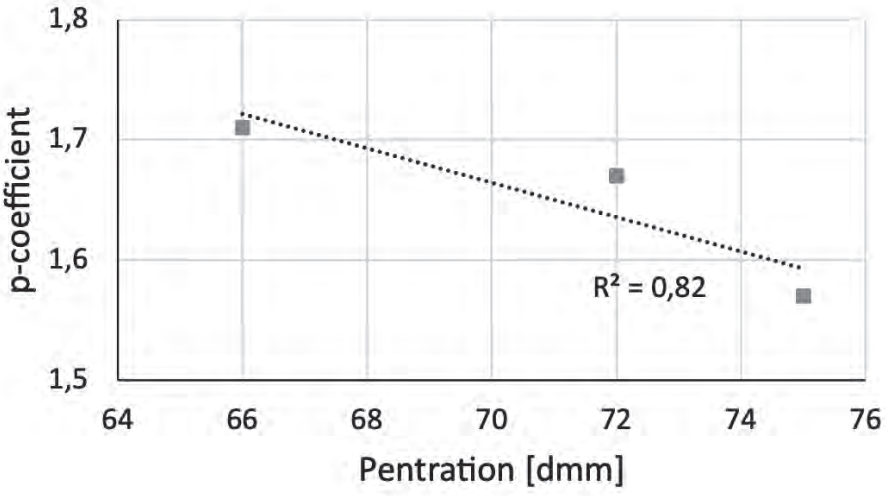

Figure 6.20 Correlation between calculated penetration value and healing parameter p

which could be expected as the three binders have the same penetration grade. However, there are some small differences in behaviour that will be discussed here. The complex modulus at fast loading rates is almost exactly the same for all binders. However, at lower loading frequencies the differences are a bit larger; Q8 has the highest stiffness, followed by Nynas, while Total shows the lowest stiffness. When evaluating the figure it should be kept in mind that the G^* is plotted on a log scale, which makes the differences in stiffness look smaller than they actually are; at the lowest loading frequency, the stiffness of Q8 is around 45% higher compared to the stiffness of Total. When evaluating the phase angle

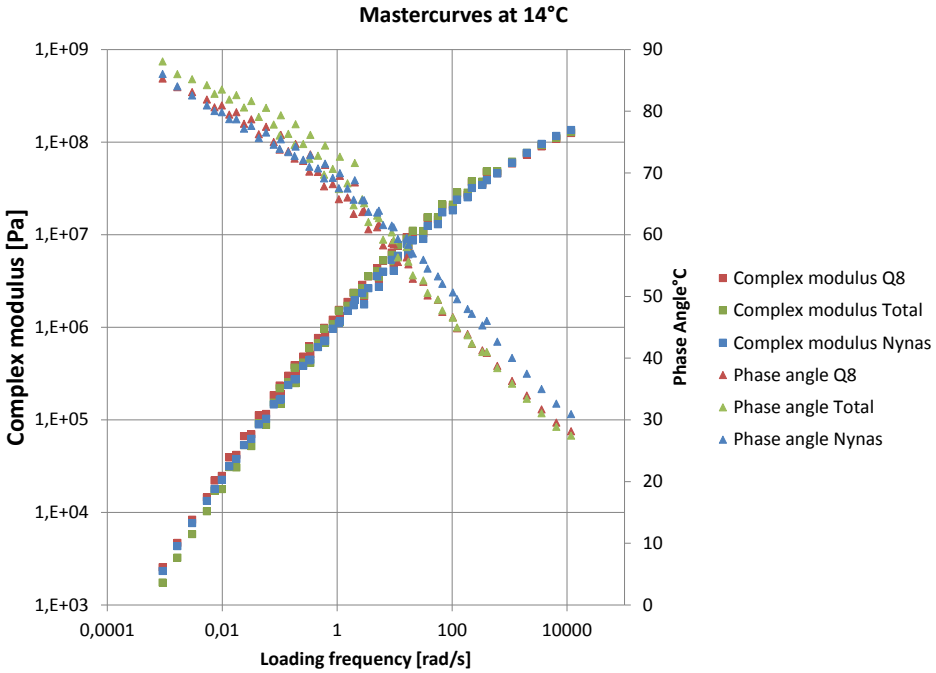

Figure 6.21 Complex modulus and phase angel determined at 14 °C for Q8, Total and Nynas binders all 70/100

(which is not on a logarithmic scale), it can be noticed that Nynas has a significantly higher phase angle at fast loading rates, compared to Total and Q8. At slow loading rates the phase angle of Total is slightly higher.

As the name indicates a master curves describe a range of values. A correlation to the healing material parameter p, requires a single value. This means that a single value has to be distilled from the master curve which is indicative for healing performance. However, in the literature review (Chapter 2), is was already pointed out that there is not one single value from the master curve that is indicative for healing. In this section two possible single values from the master curve, which have been suggested by other researchers, will be studied.

6.8.3.2 *Correlation between healing and Log G*/δ*

The healing model presented in Section 6.4 indicates that the creation of contact is essential for healing. Section 2.6 described the relevance of different processes in that influence the creation of contact, showing that surfaces with a lower stiffness, which deform more easily, accelerate the creation of contact. When these concepts are projected on the master curve, a better healer is expected to have a lower complex modulus and a higher phase angle. A lower complex modulus will result in more deformation under the same load, resulting in more contact area and consequently more healing. A higher phase angle indicates that the material has more ability to flow, this property will also ensure a more efficient contact growth at a healing interface, resulting in more healing. Therefore, it is expected that a parameter that combines the complex modulus (G^*) and the phase angle (δ) has potential to correlate with the healing parameter p. The design approach from the United States, called Super Pave, has already proposed a parameter to combine G^* and δ, using the log of G^* divided by δ (AASHTO 2001), see Equation 6.12.

$$\alpha = Log\,(G^*)/\delta \qquad (6.12)$$

In the Super Pave design approach, parameter α is used to judge if a binder has enough resistance against rutting. To ensure the pavement is stiff and elastic enough to minimize the risk of permanent deformation, a minimum value is required at a relatively high temperature. As said above, the requirements for good healing performance are a low stiffness combined with a high deformation ability, therefore better healing should correlate with a low value for parameter α at the used test temperature 14 °C. To calculate the correlation between α and the healing parameter p, a frequency for determining α must be chosen. The research presented in Chapter 5 indicates that changes is healing performance are strongest at healing periods of seconds to minutes, pointing towards a frequency of 0,01Hz to 1 Hz. However, as different processes occur, which might have their own frequencies as shown in Section 6.4.4, it is not known which frequency is most appropriate to determine α. Therefore, the correlation between α and p is investigated for a range of frequencies, presenting a trend line for each frequency, see Figure 6.22. From the figure, it can be seen that the correlation between α and p is dependent on the loading frequency.

At low loading frequencies, which are expected to be relevant for healing behaviour, there is hardly any influence of the α-parameter on the material healing coefficient p. At higher loading frequencies the influence increases, but the correlation is not strong. Based on this data, the α-parameter does not seem relevant for the healing behaviour.

6.8.3.3 *Correlation between healing and crossover frequency*

Another parameter based on the master curve is the so called crossover modulus. This is the value of the complex modulus G^* at the frequency where the storage modulus (G') equals the loss modulus (G''), i.e., when the material exhibits equal elastic and viscous behaviour. Normally this point is determined at a relatively high temperature, however

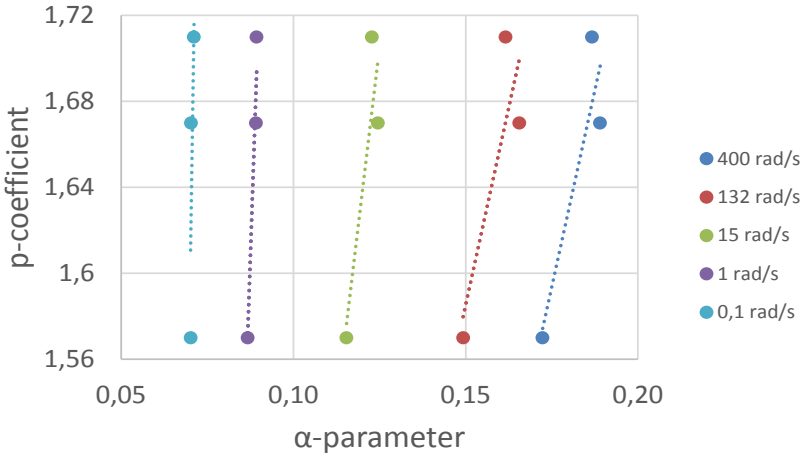

Figure 6.22 Correlation between the rheological parameter ***α*** at different loading frequencies at 14 °C and the healing coefficient ***p***

for this case it is determined at 14 °C. The values for the cross over modulus and the *p* value for the different binders are presented in Table 6.5. The correlation between these parameters is presented in Figure 6.23. From the R^2value shown in the figure, the correlation between the two parameters is Quite good.

Table 6.5 Crossover modulus at 14°C for three binders

	Cross-over Modulus [Pa]	p [-]
Q8	2,91E+07	1,71
Total	3,01E+07	1,67
Nynas	4,38E+07	1,57

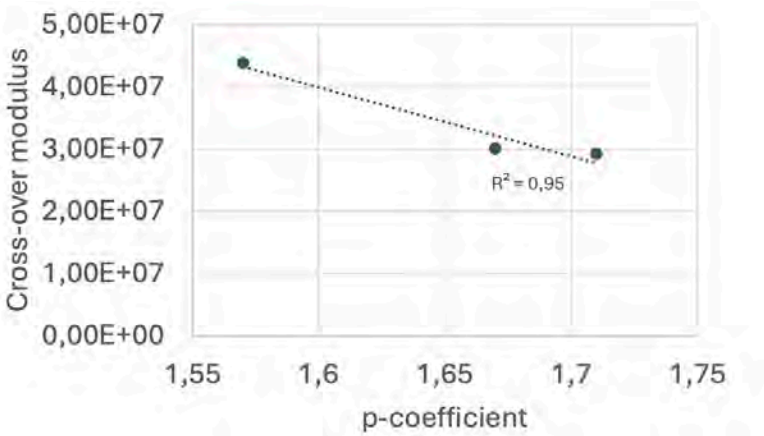

Figure 6.23 Correlation between crossover modulus at 14 °C and healing parameter p

6.7.4 Conclusions on correlations between healing and other rheological parameters

Of all parameters, the study found the best correlation between the cross-over frequency and the healing material parameter *p*. However, as there are only three datapoints, the chance of a coincidental correlation is rather high. Next to this, as mentioned in the introduction it is already questionable if parameter *p* is really the material parameter for healing. Therefore no further correlations were sought and it is recommended to execute more healing research with a wider variety of binders, before looking for any correlation to other material parameters.

6.8 CONCLUSIONS

Preliminary tests using Laser Speckle Imaging (LSI) have shown that this technique has potential for assessing bitumen particle dynamics, making it possible to discern between diffusion and flow in closure of cracks. The technique should be optimized further, however the executed tests could already demonstrate that surface energy gain was the driving force, for crack closure in the zip like motion in bitumen and mastic.

Based on a number of assumptions, a theoretical estimate has been made for the time that is needed to homogenize the healing interface at 25 °C resulting in a period between 100 s and 11 days. The executed tests with the two piece healing tests did show adhesive failure up until 20.000 s (~5,6 hours) indicating that homogenization requires more time than this theoretical lower bound. Resulting in an estimate for full homogenization between 5,6 hours and 11 days.

A qualitative healing model is developed, offering a more detailed explanation of healing processes. It reveals that surface contact is not strictly binary, as adhesion occurs even before homogenization. This suggests healing can happen almost instantly if surfaces reconnect. The model also explains why stiffness and strength recover faster than toughness, which requires significantly longer healing periods for full restoration. This model can already be used to address some of the open questions in healing of asphalt to propose hypotheses on the mechanism behind these phenomena.

As the creation of contact is the first step in healing, the characteristics of the surface also play an important role in healing. Both roughness and inhomogeneities in composition will affect the ease with which contact is established.

A more elaborate quantitative healing model is formulated, which adds several key parameters to the existing material model for healing; the normal force perpendicular to the healing interface; the surface roughness and the surface energy. However, it has also been made clear that it is quite challenging to deduce the contribution of these different parameters from one integral healing test. To fully understand their effects, each parameter must be examined separately.

An attempt is made to correlate the healing behaviour with time to another rheological parameter. This resulted in a reasonable correlation between the cross-over frequency at 14 °C and the observed healing in the two-piece healing test. Since the correlation is based on only three datapoints within a narrow data range, further research on a broader selection of binders is needed for verification.

7

CONCLUSIONS AND RECOMMENDATIONS

CONCLUSIONS AND RECOMMENDATIONS

This thesis has explored the phenomenon of healing in bituminous materials, with a particular focus on bitumen as the binding agent in asphalt pavements. The main goal was to advance the theoretical understanding of the phenomenon, to help guide the development of assessment methods for healing ability of innovative and traditional binders. This is done through a combination of literature review, the development of a novel experimental set-up, the execution of a test program using this set-up. The thesis attempts to bring all insights together by augmenting the existing healing model. The main conclusions of this work are summarized in this chapter, with a focus on the newly developed two piece healing test (Section 7.1.1), the novel insights into healing (Section 7.1.2) and the augmented healing model (Section 7.1.3). The chapter closes with recommendations for further research in healing theory (Section 7.2.1) and for practical implementation of the two piece healing test (Section 7.2.2).

7.1 CONCLUSIONS

7.1.1 Advantages of the new two-piece tensile healing test

The two-piece healing test in direct tension developed in this research has proven to be a robust and discriminative method for evaluating binder healing. It captures both the immediate adhesion resulting from contact formation and the time-dependent healing associated with interface homogenization. As such, it offers a practical and comparative tool to rank the healing performance of different binders.

The assembly conditions used in the two-piece healing test, specifically the normal force and displacement rate, have a significant impact on the healing ratio. This demonstrates that boundary conditions at the healing interface play a critical role in healing assessment. This observation also provides a possible explanation why previous healing studies reported a large variation in healing behaviour depending on the test setup, as different test configurations inherently alter the stress and imposed displacement at the healing interface. Therefore, careful control and documentation of stresses and displacements at the healing plane increase insights when interpreting healing test results. Within the research, a laboratory protocol has been produced that includes guidelines for suitable boundary conditions.

The results indicate that binders exhibiting higher levels of instant healing also show more healing over time. If this trend remains present for a broader range of binders, the two-piece healing test, applied with a short healing period, has promising potential to serve as a rapid and effective method for ranking binder healing performance.

7.1.2 Novel insights into healing behaviour of bitumen

The research has shown that the regeneration of contact and the resulting adhesive force

at the healing interface, contributes significantly to the restoration of strength. As the adhesive part of healing only requires surfaces to be in contact, this part of healing can occur almost instantly, if healing surfaces are brought together effectively. The instant restoration of strength, ranges from 40 to 60% for 70/100 penetration grade binders and from 20 to 30% for 40/60 binders.

The strong influence of assembly conditions, particularly the resulting contact area, on the measured healing response might help to explain why past studies have reported widely varying healing outcomes. It is possible that differences in how damaged surfaces are brought into contact, across different healing test setups, significantly affect the observed healing, underscoring the importance of controlling boundary conditions in healing experiments.

As the creation of contact is the first step in healing, the characteristics of the surface also play an important role in healing. Both roughness and inhomogeneities in composition at the surface will affect the ease with which contact is established.

This research provides a detailed perspective on healing behaviour over time, by monitoring the strength development over a broad time range, from seconds to several days. The results show that the rate of healing decreases rapidly with time, with the majority of healing occurring within the first few seconds to one hour. After this initial phase, the rate of improvement slows down significantly, indicating that early-stage healing plays a dominant role in the overall recovery process.

The results show that toughness is the slowest property to recover during healing. Since pavements rarely experience rest periods long enough to allow full toughness recovery, complete healing is unlikely to occur in practice. This suggests that the instant component of healing, driven by initial contact and adhesion, may be more relevant to real-world pavement performance than long-term healing processes.

Preliminary tests using Laser Speckle Imaging (LSI) have shown that this type of set-up is able to assess particle dynamics in bitumen, making it possible to discern between diffusion and flow in closure of cracks. These tests also show how cracks close in a zip like motion, which can be attributed to surface energy pulling surfaces together.

7.1.3 Additions to existing healing models

The research has confirmed that within crack healing of bitumen there are two important processes, the regeneration of contact area and the homogenization of this contact area. Based on additional insights from the test results and the literature review, the healing model has augmented providing more insight on how restoration of damage influences the overall response of the material, see Figure 7.1.

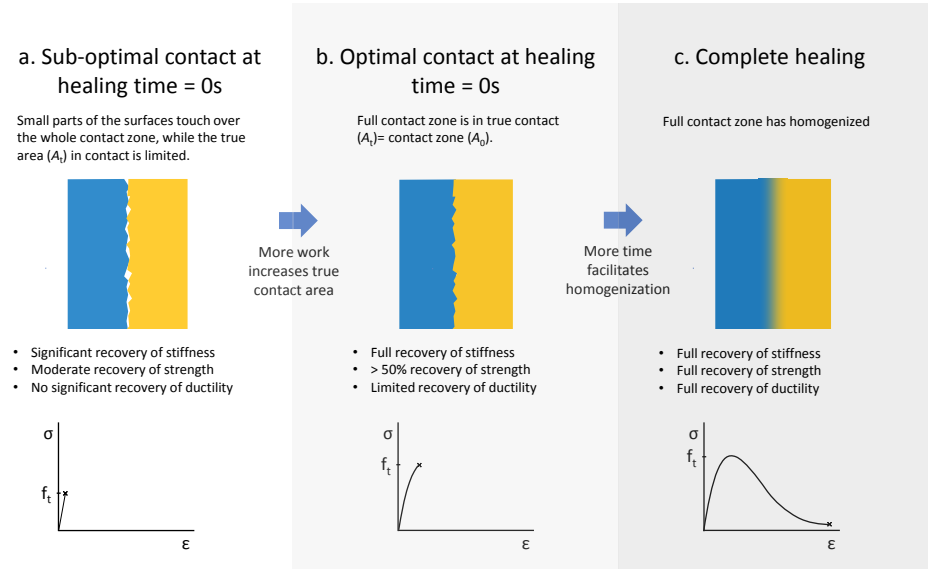

Figure 7.1 Two processes in crack-healing of bitumen and asphalt and their impact on the response of the material.

The existing quantitative healing model was extended to include key parameters such as normal force, surface roughness, and surface energy. However, as not all of these parameters were studied in the experimental part of this research, it was not possible to validate these additions to the model.

7.2 RECOMMENDATIONS

7.2.1 Further enhancement of our insights in healing of bitumen and asphalt

Laser Speckle Imaging (LSI) has shown promising potential for investigating the closure of cracks in asphaltic materials. The technique is able to distinguishing whether flow or diffusion is the governing transport mechanism behind the observed crack closure. As heating of the specimen during the experiment was intense, it is recommended to further optimize LSI for the use in asphaltic materials, by integrating a temperature-controlled specimen stage with cooling ability. This would enable more precise and versatile testing, allowing for instance exploration into healing mechanism in bitumen, mortar and asphalt at different temperatures.

To better understand the influence of surface characteristics and composition on healing, it is recommended to analyse specimen surfaces in detail before and after the two-piece healing test. Techniques such as Atomic Force Microscopy (AFM) or Laser Scanning Confocal Microscopy (LSCM) could provide valuable insights into the microroughness and possibly also stiffness or chemical composition, before and after testing and could help to determine their impact on the observed healing behaviour.

To directly observe the development of true contact during healing, innovative experimental methods should be explored. With the increasing availability of advanced instrumentation, one promising approach is to conduct assembly and healing tests within a micro-tomograph. This would allow in-situ visualization of contact regeneration at the healing interface, offering deeper insight into the underlying mechanisms.

The recommendations above could be used to validate the additional proposed parameters to the healing model.

7.2.2 Enhancing the Two-Piece Healing Test for Binder Evaluation

Both the repeatability and the reproducibility of the two piece healing test, using both assembly methods, should be studied in more detail. This should result in the quantification of the variation with a description of contribution of various sources of variation.

The results show that the actual contact area between specimen surfaces was not consistently controlled, despite the intended setup. To improve reliability, the amount of contact formed under different assembly conditions should be verified more thoroughly, and the test protocol should be refined to minimize sources of error.

Based on the findings of this research, the instant healing measured by the two-piece direct tension test appears to be a reliable and efficient indicator of overall binder healing performance. To confirm its broader applicability, this approach should be validated across a wider range of binders, including innovative types such as rejuvenated and warm mix binders, to determine whether their healing behaviour aligns with that of traditional binders.

The two-piece healing test is an assessment method on binder level. To confirm its relevance for practice, it should be verified that binder healing determined with this test has predictive power for healing of asphalt concrete.

While this research highlights the slow recovery of toughness during healing, the current test method doesn't provide an tailored approach for its quantitative assessment. It is therefore recommended to optimize the test protocol to accurately capture toughness restoration, enabling more detailed investigation of this critical performance parameter.

REFERENCES

REFERENCES

- AASHTO. 2001. “Specification for Performance Graded Asphalt Binders M320.” In.
- Adamson, Arthur W, and Alice Petry Gast. 1967. *Physical chemistry of surfaces* (Interscience publishers New York).
- Avrami, Melvin. 1939. ‘Kinetics of phase change. I General theory’, *The journal of chemical physics*, 7: 1103-12.
- Ayar, Pooyan, Fernando Moreno-Navarro, and Mª Carmen Rubio-Gámez. 2016. ‘The healing capability of asphalt pavements: a state of the art review’, *Journal of Cleaner Production*, 113: 28-40.
- Baaj, H. 2025. ‘STAR report on crack healing in print’.
- Baaj, Hassan, Hervé Di Benedetto, and Pierre Chaverot. 2005. ‘Effect of binder characteristics on fatigue of asphalt pavement using an intrinsic damage approach’, *Road Materials and Pavement Design*, 6: 147-74.
- Baglieri, Orazio, Hassan Baaj, Francesco Canestrari, Chao Wang, Ferhat Hammoum, Lucia Tsantilis, and Fabrizio Cardone. 2022. “Testing methods to assess healing potential of bituminous binders.” In *Proceedings of the RILEM International Symposium on Bituminous Materials: ISBM Lyon 2020 1*, 55-62. Springer.
- Bahia, Hussain U, Huachun Zhai, K Onnetti, and S Kose. 1999. ‘Non-linear viscoelastic and fatigue properties of asphalt binders’, *Journal of the Association of Asphalt Paving Technologists*, 68.
- Bazin, P, and J Saunier. 1967. “Deformability, fatigue and healing properties of asphalt mixes.” In *Intl Conf Struct Design Asphalt Pvmts*.
- Bhasin, Amit, Rammohan Bommavaram, Michael L Greenfield, and Dallas N Little. 2011. ‘Use of molecular dynamics to investigate self-healing mechanisms in asphalt binders’, *Journal of Materials in Civil Engineering*, 23: 485-92.
- Bhasin, Amit, Veronica T Castelo Branco, Eyad Masad, and Dallas N Little. 2009. ‘Quantitative comparison of energy methods to characterize fatigue in asphalt materials’, *Journal of Materials in Civil Engineering*, 21: 83-92.
- Bhasin, Amit, Dallas N Little, Rammohan Bommavaram, and Kamilla Vasconcelos. 2008. ‘A framework to quantify the effect of healing in bituminous materials using material properties’, *Road Materials and Pavement Design*, 9: 219-42.
- Bizarro, Diana Eliza Godoi, Zoran Steinmann, Isabel Nieuwenhuijse, Elisabeth Keijzer, and Mara Hauck. 2021. ‘Potential carbon footprint reduction for reclaimed asphalt pavement innovations: Lca methodology, best available technology, and near-future reduction potential’, *Sustainability*, 13: 1382.
- Blom, Johan, Hilde Soenen, Antigoni Katsiki, Niko Van den Brande, Hubert Rahier, and Wim van den Bergh. 2018. ‘Investigation of the bulk and surface microstructure of bitumen by atomic force microscopy’, *Construction and Building Materials*, 177: 158-69.
- Blom, Johan, Hilde Soenen, and Niko Van den Brande. 2021. ‘New evidence on the origin of ‘bee structures’ on bitumen and oils, by atomic force microscopy (AFM) and confocal laser scanning microscopy (CLSM)’, *Fuel*, 303: 121265.
- Bommavaram, Ramamohan Reddy, Amit Bhasin, and Dallas N Little. 2009. ‘Determining Intrinsic Healing Properties of Asphalt Binders: role of the dynamic shear rheometer ‘, *Transportation Research Record: Journal of the Transportation Research Board*, 2126: 47-54.

- Bonnaure, FP, AHJJ Huibers, and A Boonders. 1982. 'A laboratory investigation of the influence of rest periods on the fatigue characteristics of bituminous mixes', *Journal of the Association of Asphalt Paving Technologists*, 51: 104-28.
- Briers, J David, and Sian Webster. 1996. 'Laser speckle contrast analysis (LASCA): a nonscanning, full-field technique for monitoring capillary blood flow', *Journal of biomedical optics*, 1: 174-79.
- Carpenter, Samuel H, Khalid A Ghuzlan, and Shihui Shen. 2003. 'Fatigue endurance limit for highway and airport pavements', *Transportation Research Record*, 1832: 131-38.
- Carpenter, Samuel H, and Mark Jansen. 1997. "Fatigue behavior under new aircraft loading conditions." In *Aircraft/Pavement Technology In the Midst of ChangeASCE, Air Transport Division, Airfield Pavement CommitteeAmerican Society of Civil Engineers*.
- Carpenter, Samuel H, and Shihui Shen. 2006. 'Dissipated energy approach to study hot-mix asphalt healing in fatigue', *Transportation Research Record: Journal of the Transportation Research Board*, 1970: 178-85.
- Cheng, Dingxin. 2002. 'Surface free energy of asphalt-aggretate system and performance analyses of aphalt concrete based on surface energy ', Texas A&M.
- Claessen, AIM, JM Edwards, P Sommer, and P Uge. 1977. "Asphalt pavement design--the shell method." In *Volume I of proceedings of 4th International Conference on Structural Design of Asphalt Pavements, Ann Arbor, Michigan, August 22-26, 1977*.
- Climate, Uinted Nations. 2015. "The paris agreement." In.
- Cocurullo, A, GD Airey, AC Collop, and C Sangiorgi. 2008. "Indirect tensile versus two-point bending fatigue testing." In *Proceedings of the institution of civil engineers-transport*, 207-20. Thomas Telford Ltd.
- Shell International Petroleum. 1978. *Shell pavement design manual : asphalt pavements and overlays for road traffic*.
- D. Williams, D.N. Little, R.L. Lytton, Y. R. Kim, and Y. Kim. 2001. "Microdamage healing in asphalt and asphalt concrete, volume II: Laboratory and field testing to assess and evaluate microdamage and microdamage healing." In.
- Daniel, J. S., and Y. R. Kim. 2001. 'Laboratory evaluation of fatigue damage and healing of asphalt mixtures', *Journal of Materials in Civil Engineering*, 13: 434-40.
- Das, Prabir Kumar, Niki Kringos, Viveca Wallqvist, and Björn Birgisson. 2013. 'Micromechanical investigation of phase separation in bitumen by combining atomic force microscopy with differential scanning calorimetry results', *Road Materials and Pavement Design*, 14: 25-37.
- de Gennes, Pierre-Gilles, Francoise Brochard-Wyart, and David Quere. 2004. *Capillarity and Wetting Phenomena: Drops, Bubbles, Pearls, Waves* (Springer Science & Business Media).
- De La Roche, Chantal, Hugues Odeon, Jean-Pierre Simoncelli, and Alexandra Spernol. 1994. 'Study of the fatigue of asphalt mixes using the circular test track of the laboratoire central des Ponts et Chaussées in Nantes, France', *Transportation Research Record*.
- Delgadillo, Rodrigo, Dong Woo Cho, and Hussain Bahia. 2006. 'Nonlinearity of Repeated Creep and Recovery Binder Test and Relationship with Mixture Permanent Deformation', *Transportation Research Record*, 1962: 2-11.
- Di Benedetto, H., De La Roche, C., Baaj, H., Pronk, A., & Lundström, R. 2004. 'Fatigue of bituminous mixtures.', *Materials and Structures*, 37: 202-16.
- Di Benedetto, Hervé, Quang Tuan Nguyen, and Cédric Sauzéat. 2011. 'Nonlinearity, heating, fatigue and thixotropy during cyclic loading of asphalt mixtures', *Road Materials and Pavement Design*, 12: 129-58.

- Eberhardsteiner, Lukas, Josef Füssl, Bernhard Hofko, Florian Handle, Markus Hospodka, Ronald Blab, and Hinrich Grothe. 2015. 'Influence of asphaltene content on mechanical bitumen behavior: experimental investigation and micromechanical modeling', *Materials and Structures*, 48: 3099-112.
- Einstein, Albert. 1905. 'On the motion of small particles suspended in liquids at rest required by the molecular-kinetic theory of heat', *Annalen der physik*, 17: 549-60.
- EN-12697-24. 2012. "Bituminous mixtures—Test methods for hot mix asphalt. Part 24: Resistance to fatigue." In.: European Standards.
- Erkens, Sandra Maria Johanna Grada. 2002. 'Asphalt concrete response (acre): determination, modelling and prediction'.
- FHWA. 2008. "ARC Consortium Quaterly Technical Pogress Report." In *QuarterlyReport_April-June*. FHWA.
- Filippova, AG, LG Kirillova, NA Okhotina, NK Dvoyashkin, AV Filippov, SI Vol'fson, AG Liakumovich, and Ya D Samuilov. 2000. 'Viscosity of polymer–bitumen binders', *Colloid Journal*, 62: 755-58.
- Francken, L. 1979. 'Fatigue performance of a bituminous road mix under realistic test conditions', *Transportation Research Record*.
- Francken, Louis. (ed.)^(eds.). 1998. *RILEM Report 17: Bitumious Binders and Mixes* (London).
- Gaestel, Ch, R Smadja, and KA Lamminan. 1971. 'Contribution à la connaissance des propriétés des bitumes routiers', *Rev. Gentile. Routes et Aérodromes*, 466: 85-94.
- García, Álvaro. 2012. 'Self-healing of open cracks in asphalt mastic', *Fuel*, 93: 264-72.
- García, Álvaro, Erik Schlangen, and Martin Van de Ven. 2011. 'Properties of capsules containing rejuvenators for their use in asphalt concrete', *Fuel*, 90: 583-91.
- García, Álvaro, Erik Schlangen, Martin van de Ven, and Quantao Liu. 2009. 'Electrical conductivity of asphalt mortar containing conductive fibers and fillers', *Construction and Building Materials*, 23: 3175-81.
- Gauthier, Gilles, Didier Bodin, Emmanuel Chailleux, and Thibaud Gallet. 2010. 'Non linearity in bituminous materials during cyclic tests', *Road Materials and Pavement Design*, 11: 379-410.
- Gibson, Lorna. 2016. "Edx MOOC MIT: Mechanical behavior of materials." In.
- Greenwood, James A, and JB Pl Williamson. 1966. 'Contact of nominally flat surfaces', *Proceedings of the royal society of London. Series A. Mathematical and physical sciences*, 295: 300-19.
- Groenendijk, ir. J. 1998. 'Accelerated Testing and Surface Cracking of Asphaltic Concrete Pavements. Proefschrift, Technische Universiteit Delft', TU Delft.
- Groenzin, Henning, and Oliver C Mullins. 1999. 'Asphaltene molecular size and structure', *The Journal of Physical Chemistry A*, 103: 11237-45.
- Grossegger, D, and A Garcia. 2019. 'Influence of the thermal expansion of bitumen on asphalt self-healing', *Applied Thermal Engineering*, 156: 23-33.
- Hammoum, F, C de La Roche, JM Piau, and C Stefani. 2002. "Experimental investigation of fracture and healing of bitumen at pseudo-contact of two aggregates." In *9th international conference on asphalt pavements*.
- Healroad. 2018. Accessed 16/06/2018.
- Hofko, B, L Eberhardsteiner, J Füssl, H Grothe, F Handle, M Hospodka, D Grossegger, SN Nahar, AJM Schmets, and A Scarpas. 2016. 'Impact of maltene and asphaltene fraction on mechanical behavior and microstructure of bitumen', *Materials and Structures*, 49: 829-41.

- Huurman, Rien M, Liantong Mo, and Milliyon F Woldekidan. 2010. 'Unravelling porous asphalt concrete towards a mechanistic material design tool', *Road Materials and Pavement Design*, 11: 583-612.
- Isailović, Ivan, Michael P Wistuba, and Augusto Cannone Falchetto. 2017. 'Influence of rest period on asphalt recovery considering nonlinearity and self-heating', *Construction and Building Materials*, 140: 321-27.
- J.H. Swart, E. Vos, L.J.M. van Baal en J.C. Maessen. 1990. "Temperatuurinetingen in zeer open asfaitbeton en dicht asfaitbeton en effect op ditnensionering en op wintergiadheid." In.: Rijkswaterstaat.
- Jahanbakhsh, Hamid, Mohammad M Karimi, Hamed Naseri, and Fereidoon Moghadas Nejad. 2020. 'Sustainable asphalt concrete containing high reclaimed asphalt pavements and recycling agents: Performance assessment, cost analysis, and environmental impact', *Journal of Cleaner Production*, 244: 118837.
- Ji, Xiaoping, Yueqin Hou, Haiwei Zou, Bo Chen, and Yingjun Jiang. 2020. 'Study of surface microscopic properties of asphalt based on atomic force microscopy', *Construction and Building Materials*, 242: 118025.
- Jing, R. 2019. 'Ageing of bituminous materials: Experimental and numerical characterization', Delft University of Technology.
- Johnson, KL, K Kendall, and AD Roberts. 1971. "Surface energy and the contact of elastic solids." In *Proceedings of the Royal Society of London A: Mathematical, Physical and Engineering Sciences*, 301-13. The Royal Society.
- Karlsson, Robert, and Ulf Isacsson. 2003. 'Laboratory studies of diffusion in bitumen using markers', *Journal of materials science*, 38: 2835-44.
- Kendall, Kevin. 2001. *Molecular adhesion and its applications: the sticky universe* (Springer).
- Kim, Y Richard, Dallas N Little, and Fred C Benson. 1990. 'Chemical and mechenical evaluation on healing mechanism of asphalt concrete', *Journal of the Association of Asphalt Paving Technologists*, 59.
- Kim, Yong-Rak, DN Little, and RL Lytton. 2003. 'Fatigue and healing characterization of asphalt mixtures', *Journal of Materials in Civil Engineering*, 15: 75-83.
- Kim, Yong Rak, Dallas N Little, RL Lytton, John D'Angelo, Richard Davis, Geoffrey Rowe, Gerald Reinke, Mihai Marasteanu, Eyad Masad, and Reynaldo Roque. 2002. "Use of dynamic mechanical analysis (DMA) to evaluate the fatigue and healing potential of asphalt binders in sand asphalt mixtures." In *Asphalt Paving Technology: Association of Asphalt Paving Technologists-Proceedings of the Technical Sessions*, 176-206. Association of Asphalt Paving Technologist.
- Kliewer, Julie E, Chris A Bell, and Dan A Sosnovske. 1995. 'Investigation of the relationship between field performance and laboratory aging properties of asphalt mixtures', *Engineering properties of asphalt mixtures and the relationship to their performance*, 44: 3.
- Kose, Sadi, Murat Guler, Hussain U Bahia, and Eyad Masad. 2000. 'Distribution of strains within hot-mix asphalt binders: applying imaging and finite-element techniques', *Transportation Research Record*, 1728: 21-27.
- Lee, Hyun-Jong, and Y Richard Kim. 1998. 'Viscoelastic continuum damage model of asphalt concrete with healing', *Journal of Engineering Mechanics*, 124: 1224-32.
- Leegwater, Greet, Amir Taboković, Orazio Baglieri, Ferhat Hammoum, and Hassan Baaj. 2020. "Terms and definitions on crack-healing and restoration of mechanical properties in bituminous materials." In *RILEM International Symposium on Bituminous Materials*, 47-53. Springer.

- Lesueur, Didier. 2009. 'The colloidal structure of bitumen: Consequences on the rheology and on the mechanisms of bitumen modification', *Advances in Colloid and Interface Science*, 145: 42-82.
- Little, D. N., A. Bhasin, and M. K. Darabi. 2015. 'Damage healing in asphalt pavements: Theory, mechanisms, measurement, and modeling. theory, mechanisms, measurement, and modeling.' in, *Advances in Asphalt Materials: Road and Pavement Construction*.
- Little, Dallas N, David H Allen, and Amit Bhasin. 2018. 'Chemical and mechanical processes influencing adhesion and moisture damage in hot mix asphalt pavements.' in, *Modeling and design of flexible pavements and materials* (Springer).
- Little, DN, RL Lytton, D Williams, and CW Chen. 2001. "Microdamage healing in asphalt and asphalt concrete, Volume I: Microdamage and microdamage healing, Project summary report." In.
- Liu, Q, HEJG Schlangen, and G Van Bochove. 2013. 'The first engineered self-healing asphalt road: How is it performing?'.
- Liu, Quantao, Erik Schlangen, Martin van de Ven, and Álvaro García. 2010. 'Healing of porous asphalt concrete via induction heating', *Road Materials and Pavement Design*, 11: 527-42.
- Lu, Xiaohu, Hilde Soenen, and Per Redelius. 2003. "Fatigue and healing characteristics of bitumens studied using dynamic shear rheometer." In *Proc. 6th RILEM Symposium PTEBM*, 408-15.
- Lundström, Robert, Jonas Ekblad, and Ulf Isacsson. 2004. 'Influence of hysteretic heating on asphalt fatigue characterization', *Journal of Testing and Evaluation*, 32: 484-93.
- Lyne, Åsa Laurell, Viveca Wallqvist, and Björn Birgisson. 2013. 'Adhesive surface characteristics of bitumen binders investigated by atomic force microscopy', *Fuel*, 113: 248-56.
- Lyne, Åsa Laurell, Viveca Wallqvist, Mark W Rutland, Per Claesson, and Björn Birgisson. 2013. 'Surface wrinkling: the phenomenon causing bees in bitumen', *Journal of materials science*, 48: 6970-76.
- Maillard, S, C de La Roche, F Hammoum, L Gaillet, and C Such. 2004. "Experimental investigation of fracture and healing at pseudo-contact of two aggregates." In *3rd Euroasphalt and Eurobitume Congress, Vienna*.
- Maillard, Samuel, Chantal de La Roche, Ferhat Hammoum, Christian Such, and Jean Michel Piau. 2004. 'Bitumen healing investigation using a specific fracture test', *Road Materials and Pavement Design*, 5: 45-63.
- Mangiafico, S, C Sauzéat, H Di Benedetto, S Pouget, F Olard, and L Planque. 2015. 'Quantification of biasing effects during fatigue tests on asphalt mixes: non-linearity, self-heating and thixotropy', *Road Materials and Pavement Design*, 16: 73-99.
- Mangiafico, Salvatore, Cédric Sauzéat, Hervé Di Benedetto, Simon Pouget, François Olard, and Luc Planque. 2016. "Biasing effects (non-linearity, self-heating, thixotropy) occurring during fatigue tests on bituminous mixtures." In *6th Eurasphalt & Eurobitume Congress, Prague, Czech Republic*, 13.
- Masson, J-F, V Leblond, and J Margeson. 2006. 'Bitumen morphologies by phase-detection atomic force microscopy', *Journal of microscopy*, 221: 17-29.
- Mensink, Liz, Aikaterini Varveri, Panos Apostolidis, Milliyon Woldekidan, Hans Hendrikse, Joop Groen, and Bert Jan Lommerts. 2024. "CIRCUROAD: Collaboration Towards Non-petroleum Binders in the Netherlands." In *The International Workshop on the Use of Biomaterials in Pavements*, 103-08. Springer.

- Mewis, Jan, and Norman J Wagner. 2009. 'Thixotropy', *Advances in Colloid and Interface Science*, 147: 214-27.
- Molenaar, AAA. 2018. "Design of flexible pavement, update 2018." In *Delft University of Technology, The Netherlands*.
- Monismith, Carl L, Robert Louis Alexander, and Kenneth E Secor. 1966. "Rheologic behavior of asphalt concrete." In *Assoc Asphalt Paving Technol Proc*.
- Moreno-Navarro, F, and MC Rubio-Gámez. 2016. 'A review of fatigue damage in bituminous mixtures: Understanding the phenomenon from a new perspective', *Construction and Building Materials*, 113: 927-38.
- Moreno-Navarro, Fernando, Miguel Sol-Sánchez, and M Carmen Rubio-Gámez. 2015. 'Exploring the recovery of fatigue damage in bituminous mixtures: the role of healing', *Road Materials and Pavement Design*, 16: 75-89.
- Nahar, SN. 2016. 'Phase-Separation Characteristics of Bitumen and their Relation to Damage-Healing'.
- Nahar, SN, AJM Schmets, A Scarpas, and G Schitter. 2013. 'Temperature and thermal history dependence of the microstructure in bituminous materials', *European Polymer Journal*, 49: 1964-74.
- Nahar, SN, AJM Schmets, G Schitter, and A Scarpas. 2014. "Quantitative nanomechanical property mapping of bitumen micro-phases by peak-force atomic force microscopy." In *12th ISAP Conference on*.
- Palvadi, Sundeep, Amit Bhasin, and Dallas N Little. 2012. 'Method to Quantify Healing in Asphalt Composites by Continuum Damage Approach', *Transportation Research Record: Journal of the Transportation Research Board*, 2296: 86-96.
- Paris, Paul C, Hiroshi Tada, and J Keith Donald. 1999. 'Service load fatigue damage—a historical perspective', *International Journal of Fatigue*, 21: S35-S46.
- Pauli, AT, RE Robertson, CM Eggleston, JF Branthaver, and W Grimes. 2001. 'Atomic force microscopy investigation of SHRP asphalts', *PREPRINTS-AMERICAN CHEMICAL SOCIETY DIVISION OF PETROLEUM CHEMISTRY*, 46: 104-10.
- Peng, Keyu. 2024. 'Evaluating the Fatigue and Healing Performance of Asphalt Binders in Base Course Mixtures Using Various Test Protocols', Technical University Delft.
- Petersen, JC, RE Robertson, JF Branthaver, PM Harnsberger, JJ Duvall, SS Kim, DA Anderson, DW Christiansen, and HU Bahia. 1994. 'Binder characterization and evaluation: Volume 1', *Rep. No. SHRP-A-367, Strategic Highway Research Program, National Research Council, Washington, DC., Google Scholar*.
- Phillips, MC. 1998. "Multi-step models for fatigue and healing, and binder properties involved in healing." In *Eurobitume workshop on performance related properties for bituminous binders, Luxembourg*.
- Pipintakos, Georgios, Johan Blom, and Hilde Soenen. 2021. 'Coupling AFM and CLSM to investigate the effect of ageing on the bee structures of bitumen', *Micron*, 151: 103149.
- Pronk, AC, and PC Hopman. 1991. 'Energy dissipation: the leading factor of fatigue.' in, *Highway research: Sharing the benefits* (Thomas Telford Publishing).
- Qiu, Jian. 2012. 'Self-Healing of Asphalt Mixtures ', Technical University Delft.
- Qiu, Jian, A AA Molenaar, Martin FC van de Ven, and Shaopeng Wu. 2012. 'Development of Autonomous Setup for Evaluating Self-Healing Capability of Asphalt Mixtures', *Transportation Research Record: Journal of the Transportation Research Board*, 2296: 15-23.

- Qiu, Jian, Martin van de Ven, and Andre Molenaar. 2013. 'Crack-healing investigation in bituminous materials', *Journal of Materials in Civil Engineering*, 25: 864-70.
- Qiu, Jian, MFC Van de Ven, S Wu, J Yu, and AAA Molenaar. 2009. 'Investigating the self healing capability of bituminous binders', *Road Materials and Pavement Design*, 10: 81-94.
- Raithby, KD, and AB Sterling. 1970. "THE EFFECT OF REST PERIODS ON THE FATIGUE PERFORMANCE OF A HOT-ROLLED ASPHALT UNDER REVERSED AXIAL LOADING AND DISCUSSION." In *Association of Asphalt Paving Technologists Proc*.
- Read, John, and David Whiteoak. 2003. *The Shell bitumen handbook* (Thomas Telford).
- Redelius, Per, and Hilde Soenen. 2015. 'Relation between bitumen chemistry and performance', *Fuel*, 140: 34-43.
- Rijkswaterstaat. 2011. "Specificaties Ontwerp Asfaltverhardingen." In.--- 2022. 'INtensiteit WEgVAkken (INWEVA) 2022', Accessed 24-05-2023. https://maps.rijkswaterstaat.nl/dataregister/srv/api/records/f58eacc9-ca69-487a-a53b-11efad0bbbd1.
- Saal, RNJ, and JWA Labout. 1940. 'Rheological Properties of Asphaltic Bitumen', *The Journal of Physical Chemistry*, 44: 149-65.
- Sandra Erkens, Arthur van Dommelen, Dave van Vliet, and Greet Leegwater. 2012. 'Healing van asfaltmengsels, onderzoek naar een pragmatische proefmethode'.
- Santagata, Ezio, Orazio Baglieri, Davide Dalmazzo, and Lucia Tsantilis. 2009. 'Rheological and chemical investigation on the damage and healing properties of bituminous binders', *Asphalt Paving Technology-Proceedings*, 28: 567.
- Santagata, Ezio, Orazio Baglieri, Lucia Tsantilis, and Davide Dalmazzo. 2013. 'Evaluation of self healing properties of bituminous binders taking into account steric hardening effects', *Construction and Building Materials*, 41: 60-67.
- Schapery, RA. 1984. 'Correspondence principles and a generalizedJ integral for large deformation and fracture analysis of viscoelastic media', *International Journal of Fracture*, 25: 195-223.--- 1989. 'On the mechanics of crack closing and bonding in linear viscoelastic media', *International Journal of Fracture*, 39: 163-89.
- Schmets, A. J. M. A. A. J. M. 2009. 'First-principles investigation of the multiple phases in bituminous materials: The case of asphaltene stacking', *Adv. Testing Charact. Bituminous Mater.*, 1: 143-50.
- Schmets, AJM, Nicole Kringos, A Scarpas, C Duif, G Schitter, and T Pauli. 2009. 'First-principles investigation of the multiple phases in bituminous materials: the case of asphaltene stacking', *Advanced testing and characterisation of bituminous materials*, 1: 143-50.
- Schmets, AJM, SN Nahar, B Dillingh, H Fischer, A Scarpas, and S Erkens. 2012. 'Vergelijkend AFM Onderzoek: Microstructuur van bitumen in relatie tot healing', *IQ-2011-59*.
- Soenen, Hilde, Jeroen Besamusca, Hartmut R Fischer, Lily D Poulikakos, Jean-Pascal Planche, Prabir K Das, Niki Kringos, James RA Grenfell, Xiaohu Lu, and Emmanuel Chailleux. 2014. 'Laboratory investigation of bitumen based on round robin DSC and AFM tests', *Materials and Structures*, 47: 1205-20.
- Song, Injun, Dallas N Little, Eyad A Masad, and Robert Lytton. 2005. 'Comprehensive evaluation of damage in asphalt mastics using X-ray CT, continuum mechanics, and micromechanics (with discussion)', *Journal of the Association of Asphalt Paving Technologists*, 74.
- Speight, James G. 2014. *The chemistry and technology of petroleum* (CRC press).
- Stegeman, René. 2020. 'Analysis of asphalt concrete fatigue through energy methods'.

- Sun, Daquan, Tianban Lin, Xingyi Zhu, Yang Tian, and Fuliang Liu. 2016. 'Indices for self-healing performance assessments based on molecular dynamics simulation of asphalt binders', *Computational Materials Science*, 114: 86-93.
- Sun, Daquan, Guoqiang Sun, Xingyi Zhu, Alvaro Guarin, Bin Li, Ziwei Dai, and Jianming Ling. 2018. 'A comprehensive review on self-healing of asphalt materials: Mechanism, model, characterization and enhancement', *Advances in Colloid and Interface Science*, 256: 65-93.
- Van den Bergh, W. Van de Ven, MFC. 2012. 'The Influence of Ageing on the Fatigue and Healing Properties of Bituminous Mortars', *Procedia-Social and Behavioral Sciences*, 53: 256-65.
- Van den Bergh, Wim. 2011. 'The effect of ageing on the fatigue and healing properties of bituminous mortars'.
- van der Kooij, Hanne M. 2020. 'Let there be light: Quantitative imaging of nanoscale dynamics in polymer materials', Wageningen University and Research.
- van der Kooij, Hanne M, Arijana Susa, Santiago J García, Sybrand van der Zwaag, and Joris Sprakel. 2017. 'Imaging the Molecular Motions of Autonomous Repair in a Self-Healing Polymer', *Advanced Materials*, 29: 1701017.
- Van Dijk, W. 1975. 'Practical fatigue characterization of bituminous mixes', *Journal of the Association of Asphalt Paving Technologists*, 44: 38-72.
- Van Dijk, W, H Moreaud, A Quedeville, and P Uge. 1972. "The fatigue of bitumen and bituminous mixes." In *Presented at the Third International Conference on the Structural Design of Asphalt Pavements, Grosvenor House, Park Lane, London, England, Sept. 11-15, 1972.*
- Van Dijk, W, and W Visser. 1977. "Energy Approach to Fatigue for Pavement Design." In *Association of Asphalt Paving Technologists Proc*.
- Van Lent, DQ. 2014. 'Interfacial interactions and mass transfer at the interfacial region of bituminous hydrocarbon mixtures', TU Delft, Delft University of Technology.
- Verstraeten, J, V Veverka, and L Francken. 1982. "Rational and practical designs of asphalt pavements to avoid cracking and rutting." In *Proceedings, Fifth International Conference on the Structural Design of Asphalt Pavements*, 45-58.
- Viasnoff, Virgile, Francois Lequeux, and DJ Pine. 2002. 'Multispeckle diffusing-wave spectroscopy: A tool to study slow relaxation and time-dependent dynamics', *Review of scientific instruments*, 73: 2336-44.
- Westera, GE. 1993. "Healingonderzoek deelrapport I evaluatie van zeven healingonderzoeken [in Dutch]." In. Twello, The Netherlands: DWW Rijkswaterstaat.
- Westera. 1994. "Deelrapport 2 nadere beschouwing van het fenomeen healing bij asfalt [in Dutch]." In. Twello, The Netherlands: DWW Rijkswaterstaat.
- Westera, Pelgröm. 2002. "Review healing." In *CROW Wegenbouwkundige Werkdagen*.
- White, Scott R, NR Sottos, PH Geubelle, JS Moore, M_R Kessler, SR Sriram, EN Brown, and S Viswanathan. 2001. 'Autonomic healing of polymer composites', *Nature*, 409: 794-97.
- Wöhler, Alfred. 1870. Über die festigkeitsversuche mit eisen und stahl (Ernst & Korn).
- Wool, R.P., and K.M. O' Connor. 1981. 'A theory crack healing in polymers', *Journal of Applied Physics*, 52: 5953-63.
- Wu, Dong Yang, Sam Meure, and David Solomon. 2008. 'Self-healing polymeric materials: a review of recent developments', *Progress in Polymer Science*, 33: 479-522.
- You, Lingyun, Theodora Spyriouni, Qingli Dai, Zhanping You, and Ashok Khanal. 2020.

'Experimental and molecular dynamics simulation study on thermal, transport, and rheological properties of asphalt', *Construction and Building Materials*, 265: 120358.

- Zhang, Liqun, and Michael L Greenfield. 2007. 'Relaxation time, diffusion, and viscosity analysis of model asphalt systems using molecular simulation', *The journal of chemical physics*, 127: 194502.
- Zwaag, Sybrand. 2008. *Self healing materials: an alternative approach to 20 centuries of materials science* (Springer Science+ Business Media BV).

APPENDIX A

LABORATORY PROTOCOL TWO PIECE HEALING TEST IN DIRECT TENSION FOR BITUMEN

APPENDIX A: LABORATORY PROTOCOL TWO PIECE HEALING TEST IN DIRECT TENSION FOR BITUMEN

A.1 Objective / Purpose

The goal of the experiment is to assess the healing ability of a bituminous binder.

A.2 Background

A.2.1 *General test set-up*

Within this experiment two pieces of the same asphalt binder are brought together under controlled conditions. The aim of the experiment is to assess how the interaction at the area in contact develops, as a result of specific assembly conditions and the healing period. The interaction between the two pieces of binder is hypothesized to be correlated to the situation where two sides of a crack regain contact.

Within the experiment description, the pieces of bitumen are called 'half specimen', while an assembled specimen is called 'specimen'. The healing interface, is the area were the two half specimen are in contact and interaction occurs. The amount of interaction at this healing interface is assessed by performing a tensile test, after the half specimens are brought together and left for a specific healing period. The result of this tensile test can be compared to a reference specimen. This reference specimen consists of a single piece of the same bitumen, which represents the undamaged material behaviour.

The test consists of three phases. A schematic impression of the assembly procedure is presented in Figure A.1. Phase 1 is the assembly phase, where the two pieces of bitumen are brought together, under controlled conditions, using a certain force. Phase 2, is the healing phase, during which the assembled specimen is subjected to a specific healing period. Phase 3 consist of a tensile test, that assesses the amount of restoration that has occurred at the healing interface as a result of Phase 1 & 2. A piece of silicon paper with a hole of Ø5,5 mm is placed between the two half-specimen to ensure that the contact area during assembly and healing is limited.

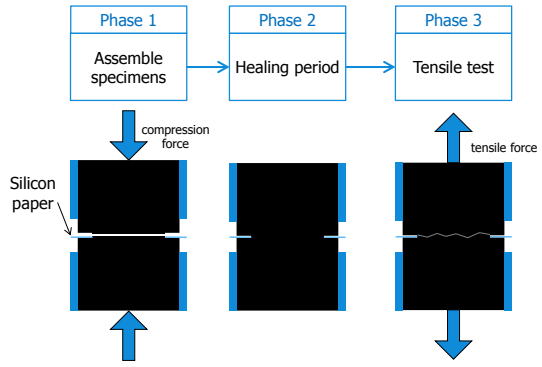

Figure A.1 Schematic impression of assembly, healing and testing of specimens

A2.2 *Two assembly methods*

Phase 3 has to be executed inside a tensile test machine. Phase 1 & 2 can be executed either inside a testing machine or inside a temperature chamber. If Phase 1 & 2 are executed inside a testing machine, this is named ‘machine assembly’. When Phase 1 and 2 are executed in a temperature controlled room this is named ‘storage room assembly’. The biggest difference between the two assembly conditions is the stress at the healing interface during both the assembly and healing phase. In case of assembly inside the test machine, the initial stress is large, but only present for a short time to ensure contact. In case of assembly inside the storage room, the stress at the healing interface is much smaller, as it is applied by use of a small weight, however it is present during the total healing period. The applied stress during the assembly and healing period is schematically presented in Figure A.2. The grey areas in the figure indicate when forces and displacement are recorded by the tensile test machine.

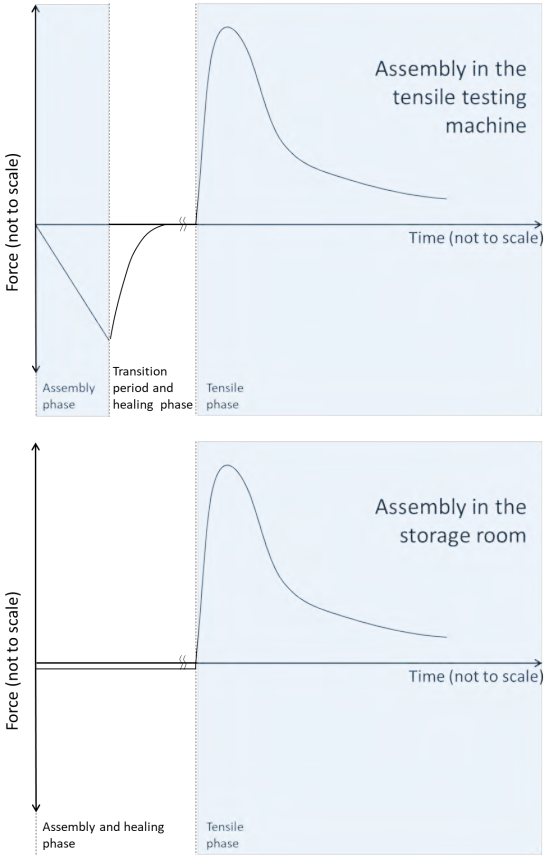

Figure A.2. The normal force in the healing specimen, for the case of machine assembly (above) and storage room assembly (below), in grey the time period is indicated when forces and deformations are recorded.

The smallest load that can be applied in the storage room is 0,6 gram (0,06 N), corresponding to the self-weight of the top half-specimen. 10 gram is the largest weight that still fits on a specimen, resulting in a load of 10,6 grams (or 0,11 N). The resulting stress at the healing interface is 1 to 2 orders of magnitude smaller compared to the assembly stress used in the machine.

A.3 SPECIMEN DESIGN AND PRODUCTION

A.3.1 Geometry half specimen

The half specimen consist of bitumen poured in a stainless steel ring. This ring controls the geometry of the half-specimen and enables fixation in a tensile testing machine. To control the amount of area brought into contact, the specimen has an elevated contact area with a diameter of Ø 5,5mm (23,8 mm^2). The geometry of the half-specimen with the contact area is shown in Figure A.3.

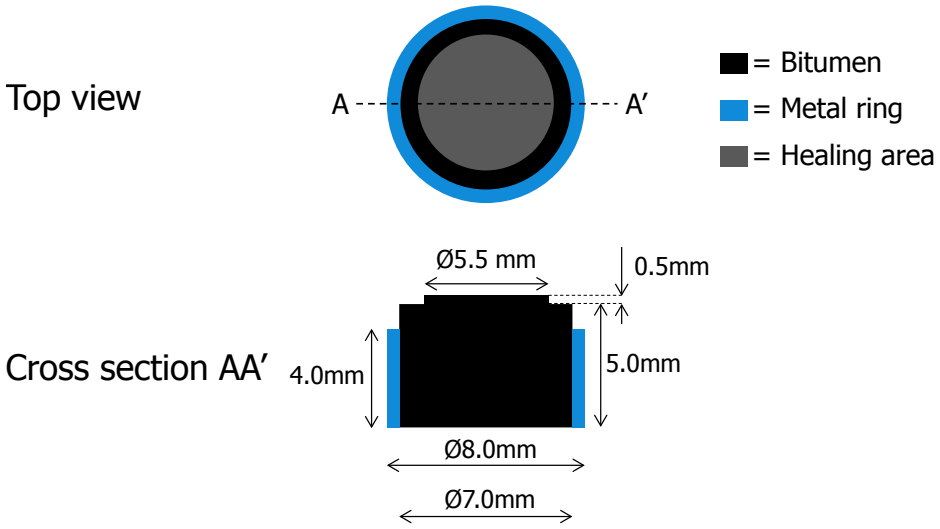

Figure A.3. Top view and cross section of one half-specimen, indicating dimensions and material use.

The half-samples are made upside down, in a specially designed rubber mould that contains eight repetitions of the counter form of the half specimen, see Figure A.4. Before pouring the bitumen into the mould, the stainless steel rings are placed in the holes in the mould.

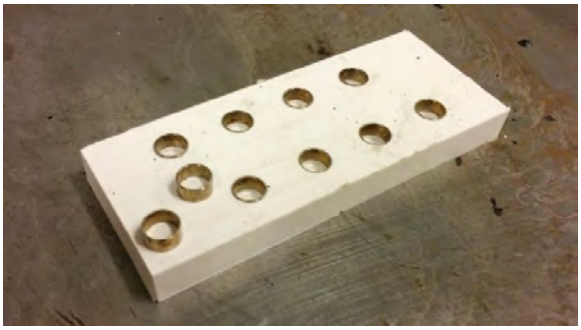

Figure A.4. Silicon rubber mould to produce 8 half specimen, with stainless steel rings in place and two loose rings on top for reference

The rubber mould is made of a two component silicon rubber poured into a contra mould. The contra mould is custom made of Teflon with a precision of +/-0,1 mm. This design of the contra mould is presented in Figure A.5. This contra mould can be used to create a multitude of silicon rubber moulds.

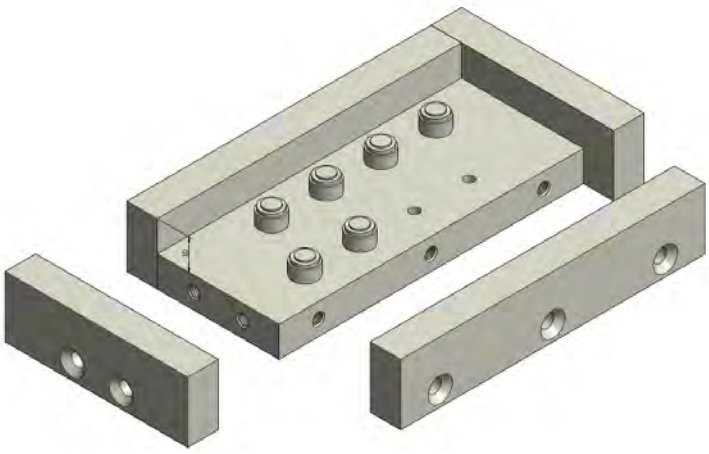

Figure A.5. Contra mould for casting of the silicon rubber moulds

A.3.2 Geometry reference specimen

The reference specimen is a column with a height of 12 mm and a diameter of 6 mm. The ends are enclosed with the same stainless steel rings as the half-specimen, allowing for fixation and handling, see Figure A.6. This shape is adopted from previous research executed at the TU Delft (Huurman, Mo, and Woldekidan 2010).

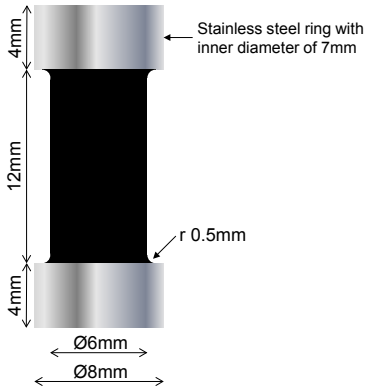

Figure A.6. Shape and dimensions of reference specimen, consisting of a column of bitumen with stainless steel rings on the top and the bottom to be able to clamp the specimen in the testing machine (Huurman, Mo, and Woldekidan 2010).

A.3.3 Specimen production

- The bitumen can and the silicon mould, including the metal rings, are placed in an oven for one hour at 165 °C to ensure that both the bitumen and the mould are 165 °C.
- The hot bitumen is poured into the mould.
- A slight excess of bitumen is used, to ensure that after temperature shrinkage, the metal ring is completely filled with bitumen.
- The mould with half-specimen is left to cool for 30 minutes at room temperature.
- The mould is placed in the freezer at -24 °C for 1 hour.
- The mould is taken from the freezer and the excess of bitumen on top of the metal ring is removed using a heated knife.
- The half-specimens are removed from the mould.
- The half specimens are placed in a temperature controlled room (14 °C +/-1 °C) and left for 48 hours to cure.

A.4 MATERIALS AND EQUIPMENT

For the execution of the uniaxial tensile test (Phase 3) a DSR or DMA is required with a minimum tensile capacity of 40 N, e.g. Anton Paar, EC Twist 502. This test machine should be equipped with a temperature control chamber with high precision control (+/-0,2 °C) with a range of at least -10 to 40 °C. Accessories are available to fix cylindrical specimens with a diameter of 8 mm.

Round silicon papers Ø8 mm, with a hole in the middle of Ø5,5 mm are needed to control the contact area during and after assembly.

In case the option is chosen to assemble half-specimens inside the testing machine, see Section 0, the software controlling the machine has to facilitate programming of several consecutive steps in a single test run, ensuring a quick transition between the assembly, healing and tensile phase.

In case the option is chosen to assemble specimen inside a temperature chamber, the following equipment is needed:

- A temperature chamber where specimens can be assembled and stored.
- Small calibrated weights of 1 and 10 grams for loading during the assembly and healing phase.
- Stainless steel tubes, with an inner diameter of 8,5 mm, to ensure vertical alignment of the half-specimens during the assembly and healing phase.
- Silicon paper to cover the inside of the stainless steel tubes to prevent any excess of bitumen from sticking to the tube.
- A device to measure the distance between the rings after the healing period.

A.5 SAFETY PRECAUTIONS

The preparation of specimens requires high temperatures, therefore laboratory certified oven gloves are required.

Binder had to be removed from all equipment using chemical solvents. A fume cup board is required to safely work with solvents.

A.6 PROCEDURE

As mentioned in Section 0, two assembly procedures can be followed. Both procedures will be prescribed below. For both set-ups three repetitions are required. In case of storage room assemble spare specimens should be prepared in case a specimen fails prematurely as a result of transport and handling.

A.6.1 Machine assembly

In case that the Anton Paar testing machine is used, there are only two parameters that can be varied during the assembly phase; the displacement rate that brings the half-specimens together and the magnitude of the normal force that triggers the end of the assembly phase. These parameters are referred to as ‘assembly rate’ and ‘assembly force’, respectively. The goal of the assembly phase is to create good contact, while the

specimen shape remains intact. During an initial test an assembly rate can be selected, while a high assembly force chosen, to determine at which assembly force good contact is created without excessive deformation, for this specific assembly rate.

The following steps are taken during the assembly phase for the machine assembled specimens:

- A half-specimen is placed in the top clamp of the testing machine.
- A half-specimen is placed in the bottom clamp of the testing machine.
- A round piece of silicon paper, with a hole in the middle of Ø5,5 mm is placed over the bottom specimen.
- The temperature chamber is closed.
- The temperature in the test chamber is kept at the required assembly temperature for 15 minutes to allow for temperature equilibrium of the half-specimen.
- The top specimen and the bottom specimen are brought towards each other using a constant displacement rate, during this assembly phase the displacement and the force are measured. When the two half specimens touch a normal force builds up, the machine stop at the predefined assembly force, determined in an initial test.

The healing phase the machine assembled specimens, is as follows:

- During the healing phase, the distance between the specimens remains constant at the point where the assembly phase concluded.
- No force is applied.
- Residual stress from the assembly phase can relax during this period.

The healing period starts when the two surfaces first come into contact during the assembly phase and a force starts to build up. The duration of the assembly phase depends on the selected assembly conditions. After the assembly phase is finished, the machine needs 10 seconds to transition from compression mode to the tensile mode, which is required for Phase 3. Therefore, the shortest healing period that can be applied is the assembly period from the moment surface touch plus 10 seconds. The longest healing period that can be applied depends on the availability of the test machine and the total research periods available.

The tensile phase for the machine assembled specimens, is as follows:

- At the end of the healing phase, the specimen assembled in the machine is ready for testing, it is at an equilibrium temperature of 14 °C and the clamps are fixed.
- The specimen is pulled apart with a strain rate of 0,5 %/s; the required displacement rate is already known from the experimental design and is given as input before the assembly phase is started.

- The force and the displacement are recorded during the tensile test to determine the performance of the healed interface.

A.6.2 Storage room assembly

The assembly procedure for the storage room assembled specimen, is as follows;

- A piece of silicon paper is placed inside the alignment tube to cover its surface to prevent the half specimens from sticking to it.
- All alignment tubes are placed on tray or petri dish covered with silicon paper, to prevent the specimens from stick to it.
- Any excess bitumen on the outside of the stainless steel rings of the half-specimens has to be removed using a solvent, to ensure that the specimens fit inside the alignment tubes.
- A half-specimen is placed on the bottom of the in a storage tube, with the contact area facing upward.
- A round piece of silicon paper, with a hole in the middle of Ø5,5 mm is placed over the bottom specimen.
- A second half-specimen is placed inside the tube, on top of the first sample, with the contact area facing downwards.
- An additional weight can be placed on top of the specimen for a higher normal force at the healing plane. A piece of a silicon paper has to be placed in between the specimen and the weight, to prevent sticking, see Figure A.7.

In this set-up the normal force perpendicular to the healing interface is determined by the self-weight of the top specimen and if present the weight placed on the top half specimen.

Figure A.7. An assembled test specimen with a weight of 1 gram placed on top.

The healing phase is for the storage room assembled specimen is as follows:

- The healing period starts when the top half specimen is placed in the alignment tube.
- After the prescribed healing period has ended, the weight is removed.
- To minimize healing after the healing period has ended and the weight is removed, the healed specimen is placed in a horizontal position in a fridge a temperature of 0 °C +/- 2 °C. The specimens remain under this conditions until the moment of testing, which is no more than 24 hours later.

The tensile phase for the storage room assembled specimen consists of the following steps:

- The healed specimen is taken from the fridge.
- The specimen is carefully taken from the alignment tube.
- The distance between the rings of the two half-specimen is measured.
- Based on the distance between the rings, the displacement rate, matching a strain rate of 0,5 %/s is calculated and used as input for the tensile test.
- The specimen is placed in the bottom clamp of the testing machine, see Figure 3.12.
- The top clamp is fully opened to ensure enough space for the top ring.
- The top clamp is moved down slowly, until it encloses the top ring.
- The top clamp is fixed carefully, as at this moment small misalignments between the rings can result in stresses at the healing interface and premature failure. A slow fastening of the clamp will allow any resulting stresses to relax before they lead to failure.
- Before starting the tensile test, the specimens are kept in the temperature chamber at the desired test temperature for 15 minutes to ensure temperature equilibrium of the specimen.
- A tensile test is executed at a strain rate of 0,5 %/s.
- The force and the displacement are recorded during the tensile test.

A.6.3 Reference specimen

In order to establish a healing ratio, tensile tests are executed on reference specimen to obtain a reference strength. This test is executed two times and the average value is taken as the reference strength. The temperature history of these specimen is kept as similar as possible to the healed specimen.

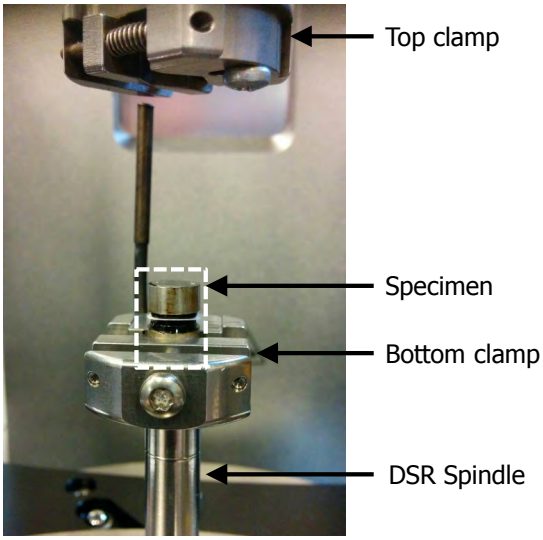

Figure A.8 Specimen including silicone paper ring fixed in bottom clamp in DSR.

The test procedure is as follows:

- The specimen is taken from the fridge.
- The specimen is placed in the bottom clamp of the testing machine.
- The top clamp is fully opened to ensure enough space for the top ring.
- The top clamp is moved down slowly until it encloses the top ring.
- The top clamp is fixed carefully. At this moment small misalignments between the rings can result in stress inside the specimen and premature failure. A slow fastening of the clamp will allow any resulting stresses to relax before they lead to failure.
- Before starting the tensile test, the specimens are kept in the temperature chamber at the desired test temperature for 15 minutes to ensure temperature equilibrium of the specimen.
- A tensile test is executed at a strain rate of 0,5 %/s.
- The force and the displacement are recorded during the tensile test.

A.7 DATA COLLECTION

When the specimen is assembled inside the machine, the force and displacement are recorded at least each second during the assembly phase. This information is helpful to check if the assembly phase has been executed according to plan.

During the tensile test the force and displacement are recorded at least each second. These values are plotted in a force displacement curve to assess the interaction at the healing place, an example of such a curve is presented as Figure A.9.

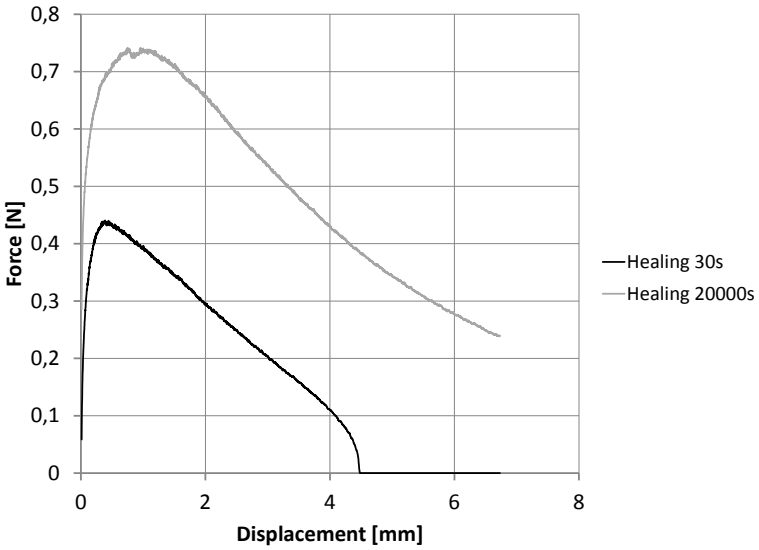

Figure A.9. Force-displacement curve of a tensile test for a short and a longer healing period, for healing at 14 °C.

A.8 OBSERVATIONS

After the tensile test of the healed specimen is finished the specimens have to studied visually, to assess interaction at the healing interface. The following details should be noted:

- When the temperature chamber is opened, it should be recorded if the halfspecimens came apart fully during the tensile test, see Figure A.10.a&b.
- In case the specimens came apart the surfaces of the specimens should be studied using a magnifying glass to look for traces of material transfer from one side to the other (e.g. appearance of fibrils or scratches on the surface). If possible a photograph should be taken.

A.9 CALCULATIONS

Different aspects of the tensile test and the resulting force displacement curve can be used to assess the extent of healing. The most obvious parameter to assess healing is the peak force. However, it is also possible to determine the stiffness, the deformation

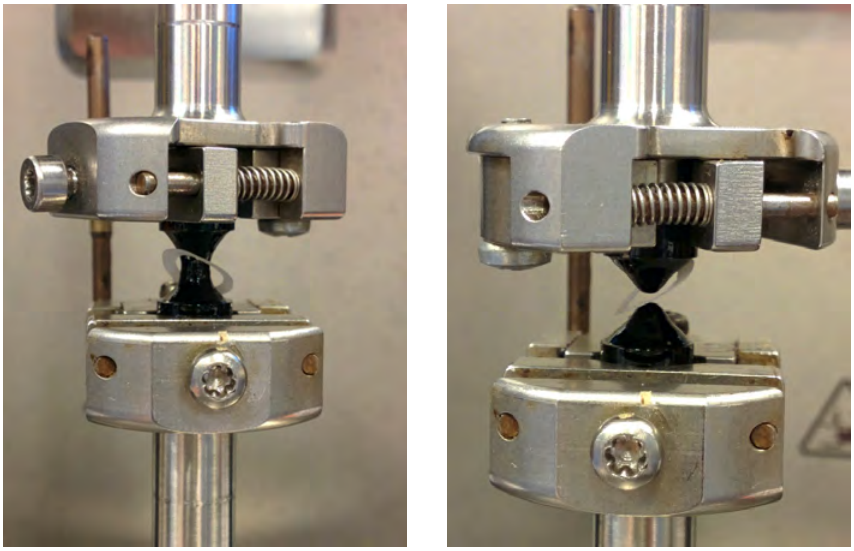

Figure A.10. Pictures taken from healed specimens after a tensile test; a. specimen after a healing period of 30 s, where the healing interface has come apart during the tensile test; b. specimen after a healing period of 20.000 s where the specimen has remained in one piece.

capacity or the amount of work that is required for a certain amount of deformation. To be able to properly assess the deformation capacity or the amount of work, the total applied deformation for the different healing periods should be the same, using the same measurement interval.

Healing is the restoration of performance after damage relative to the original performance, which can be expressed using the healing ratio, see Equation 9.1. Therefore to calculate the healing in each specimen, the performance measured on the assembled specimen in terms of strength or deformation capacity has to be divided over the original performance obtained from the reference specimen.

$$Healing\ ratio = \frac{f_{healed}}{f_{original}} \times 100\% \tag{A.1}$$

A.10 RESULTS

The result of the experiment is a healing ratio for a specific asphalt binder exposed to imposed assembly and healing conditions.

A.11 REFERENCES

Huurman, Rien M, Liantong Mo, and Milliyon F Woldekidan. 2010. 'Unravelling porous asphalt concrete towards a mechanistic material design tool', Road Materials and Pavement Design, 11: 583-612.